warwick.ac.uk/lib-publications

THE BRITISH LIBRARY DOCUMENT SUPPLY CENTRE

TITLE

BUCKLING IN CONTINUOUS COMPOSITE BEAMS

AUTHOR

Chun Keung Roger Fan

**INSTITUTION
and DATE**

University of Warwick 1990

cms

CAM. 1

<u>BUCKLING IN CONTINUOUS COMPOSITE BEAMS</u>

by

Chun Keung Roger <u>Fan</u> BSc, MSc, DIC
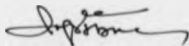
A thesis for the degree of
Doctor of Philosophy,
submitted to the University of Warwick

Department of Engineering,
University of Warwick, England
May, 1990

Declaration

The work described in this dissertation was carried
out by the candidate between September 1986 and December
1989 in the Department of Engineering at the University
of Warwick under the supervision of Professor R. P.
Johnson. Unless otherwise where reference is made
to the work of others, this dissertation describes
the original work of the author. It has not been
submitted for a degree at any other University.

C. K. R. Fan

University of Warwick,
Coventry,
England.

Summary

Two aspects of the buckling behaviour of continuous composite beams of steel and concrete are considered. The first part relates to the study of moment redistribution in braced slender beams (Class 3 draft Eurocode 4) due to local buckling in the hogging moment regions. The second part describes the experimental work to investigate the ultimate load behaviour of unbraced compact beams (Classes 1 and 2 draft Eurocode 4) in the hogging moment regions.

For a braced continuous slender composite beam, local buckling at an internal support allows a redistribution of bending moment from the hogging regions to the sagging regions, in addition to material nonlinearity. This effect was studied by a computer simulation on two-span beams. The program takes into account not only the effect of local buckling, but also material nonlinearity and residual stresses, on moment redistribution. The ultimate loads designed to the less conservative method for Class 3 beams in the draft Eurocode 4 were used as a datum in the parametric study. The simulation then gave an independent assessment of the appropriateness and safety of these loads at the ultimate limit state. It is shown that the design method is slightly conservative. Residual stresses have very little effect on the ultimate carrying capacity. Furthermore, in design to the draft Eurocode 4, unpropped construction is more restrictive than propped construction, and hence the results are also more conservative.

Lateral buckling of continuous unbraced composite beams in the hogging moment regions can only occur in a distortional mode, and is most unlikely to happen in practical building or bridge structures using hot-rolled steel sections of span up to about 30m. Various design methods based on numerical studies now exist to predict the ultimate strength of continuous composite beams affected by distortional lateral buckling, but few experimental results are available to validate their theoretical assumptions and accuracy. Tests at realistic scale on two T-beams and two inverted U-frames at the Class 2-3 interface, in accordance with the draft Eurocode 4, are reported. Their results are compared with predictions by five design methods, four of which are satisfactory for the beams tested except BS5400:Part 3. Due to premature fracture of reinforcing fabric in one of the U-frame tests, it is recommended not to include their contribution in moment resistance, when the composite cross-section is plastic and a design requires a large amount of rotation capacity in the hogging moment regions. Based on limited test results, a tentative method is proposed to provide a quick check, whether distortional lateral buckling needs to be considered or not, for continuous composite beams with Class 1 or 2 cross-sections.

Contents

List of Tables

List of Figures

List of Plates

Notation

B, b	breadth of steel section
b_0	outstand of flange in compression or breadth of steel section
D, h_a	overall depth of steel section
t, t_w, w, TW	thickness of web of steel section
d	clear depth of steel web between flanges
t	thickness of flange of steel section (Chapters 3 and 4 only)
ε_c	compressive strain of bottom fibre
ϕ', ϕ	hogging and sagging curvatures
M', M	hogging and sagging moments at an internal support and midspan
M_p', M_y'	plastic and first yield hogging moments of resistance for a composite cross-section
M_p, M_y	plastic and first yield sagging moments of resistance for a composite cross-section
R	rotation capacity
θ_a, θ_p	available and plastic rotations in hogging moment region (Fig. 2.2)
χ	ductility parameter for composite beams
λ_{LT}	lateral torsional buckling slenderness parameter (BS5400: Part 3)
σ_{li}	limiting design compressive stress
δ, Δ	lateral deflection of unrestrained bottom flange or linear displacement
L	length of a member or span of a beam
P_{cr}	elastic critical buckling load
E, E_s	Young's modulus for structural steel
G	shear modulus for structural steel
J	St.Venant torsion constant for steel section

l_e	effective length
z_p	plastic section modulus of steel or composite section
z_{xc}, z_{xt}	elastic section moduli of steel or composite section with respect to compressive and tensile fibres
λcr	critical load factor
σ_{cr}, f_{cr}	elastic critical buckling stress
β	modified buckling slenderness parameter for composite beams
f_y	yield stress of reinforcement or structural steel
β_l, β_d	local and distortional buckling slenderness parameters
β_f, β_w	flange and web slenderness ratios for a composite beam
σ_y	yield stress of structural steel
r_y	radius of gyration of bottom flange about minor axis of steel section
y_t	maximum tensile fibre distance from elastic neutral axis
k	web flexural stiffness, N/mm
$[K]$	elastic stiffness matrix
$[G]$	stability matrix
υ	Poisson's ratio for steel
αd, $\alpha'd$	depths of web in compression using elastic and plastic theories
N, N_o	applied and critical compressive forces to bottom flange due to bending moment for a continuous beam
I	second moment of area for steel section
$\beta 1$	dimensionless modulus for web flexural stiffness
$\underline{\lambda}$	dimensionless slenderness for buckling
k_{eq}	equivalent elastic foundation stiffness

I_y	second moment of area for steel section about minor axis
L_{cr}	critical buckling length
M_{cr}	elastic critical buckling moment for a composite beam
n, C_4	slenderness correction factors for shape of bending moment diagram
v_t	slenderness correction factor for torsional effect, web distortion and position of shear centre, etc
χ_{LT}	lateral torsional buckling slenderness factor (draft Eurocode 4)
L_o, L_{o1}, L_{o2}	distance between an internal support and point of contraflexure for a continuous beam, or length of a cantilever
r_{cp}	radius of gyration of portion of web and bottom flange in compression below plastic neutral axis about minor axis of steel section
A_r, A_{rt}	total area of slab longitudinal reinforcement
b_c, h_c	breadth and depth of concrete slab
f_{cu}	characteristic cube strength of concrete
I_c, I_u	cracked and uncracked second moments of area for composite cross-section
$M_m{}'$	peak hogging moment in cantilever test
V	maximum applied shear force
V_{pl}, V_p	shear capacity = $\sigma_y dw/\sqrt{3}$
w_1, w_2	design loads for a two-span beam
L_1, L_2	span lengths of a two-span beam
γ_m, γ_M	partial safety factor for a material
γ_f, γ_F	partial load factors
θ'	total rotation at the end of a cantilever or at a point of contraflexure

$\theta_b{}'$ irreversible rotation of a quasi-cantilever in a continuous beam when $M' = M_y'$

$\theta_{bc}{}'$ irreversible rotation of a cantilever when $M' = M_y'$

$\theta_e{}'$ elastic rotation

$\theta_i{}'$ irreversible rotation

ε_ϕ strains corresponding to curvature ϕ

ε_r residual strains

σ_s longitudinal stresses across steel section

A_s cross-sectional area of steel section

σ_{rt} longitudinal stress in reinforcement

λ load factor

λ_b, λ_f buckling and failure load factors

α ratio of cracked to uncracked flexural stiffness for a composite cross-section

α_e modular ratio

ξ tolerance limit for convergence

g, q characteristic dead and imposed loads

f_u ultimate stress for steel or reinforcement

E_r secant modulus of elasticity at 0.1% strain for reinforcement or fabric

t_{tf}, TF   thickness of top flange of steel section

t_{bf}, TB   thickness of bottom flange of steel section

θ experimental beam rotation for a double cantilever

θ_c, θ_s transverse rotations of concrete and bottom steel flange

$\varepsilon_c, \varepsilon_b$ compressive and bending strains

WT, WB   breadths of top and bottom flanges of steel section

Δ_c, Δ_s	lateral displacements of concrete and bottom steel flanges in U-frame tests
ϕ	diameter of reinforcing bars or fabric (Chapter 9)
A_T, A_B	areas of top and bottom reinforcement per metre strip of concrete slab
d_s	distance between top slab and centroid of reinforcement (Fig. 10.1)
I_s	second moment of area of concrete or composite slab per metre strip
B', a	distance between two adjacent steel sections in an inverted U-frame
h_s	distance between shear centres of flanges
M_s	elastic critical buckling moment for steel section
C_θ, k_s	torsional spring constant for slab transverse bending and web distortion

CHAPTER 1

INTRODUCTION

1.1 Preamble

In recent years composite construction has become a
popular fast-track method of construction in U.S.A. and
Western Europe. For the past five years over 50% of the
new commercial steel buildings in these areas are either
composite or semi-composite. This rapid growth is a
result of continuous innovations in the design and
construction of composite structures, and also encourages
further research and development. Two new codes of
practice for design in composite construction, Eurocode
4[1] and BS5950 : Part 3.1 [2], both in draft form, are
now available for public comments.

Composite beams are vital components in a composite steel
structure, and have been a subject of research since the
1950's. The composite beams considered here are made up
of unstiffened steel I-sections, welded stud shear
connectors, and insitu concrete slabs above, with or
without metal decking. In current practice composite
beams are usually designed as simply-supported, but at
longer spans, their deflections due to service loads
would probably govern the design rather than the
strength, that might lead to the use of deeper steel
sections. This is undesirable not only because the

design does not make use of the strength of the beam economically and increases the material cost, but also there will be a reduction in the effective floor zone. An alternative approach to improve the economy and to limit excessive deflections is to design composite beams as continuous.

This project forms part of a long-term study into the ultimate behaviour of continuous composite beams in the region of an intermediate support. Many problems have been tackled previously including the effect of local buckling, ultimate moment of resistance, ultimate shear capacity, partial shear connections, design of semi-rigid joints in composite frames, redistribution of moments, cracking, and more recently distortional lateral buckling of the bottom flange. In hogging moment regions, buckling is one of the structural problems facing designers as far as the stability of the beam is concerned. If it has a slender cross-section and is braced laterally, part of the web and the bottom flange under compression are prone to local buckling [3], that might reduce its hogging moment of resistance and rotation capacity. For beams with long unbraced hogging regions, the steel bottom flange may be susceptible to distortional lateral buckling [4,5,6], often associated and interacting with local buckling adjacent to an intermediate support, causing a decline in its bending stiffness.

Composite beams are classified into four classes according to both draft Eurocode 4 and BS5950 : Part 3.1, depending on the flange and web slenderness ratios of the steel section. The classification system is explained briefly in Chapter 2 and this project adopted the terminology and rules given by draft Eurocode 4 closely in terms of classification of cross-sections. The work reported here consists of studies of two aspects of the ultimate behaviour of continuous composite beams affected by buckling in the hogging regions: (i) a parametric study to investigate the amount of moment redistribution for braced beams with Class 3 (slender) cross-section that occurs due to local buckling; and (ii) an experimental study to investigate the effect of local buckling and distortional lateral buckling as well as their interaction, and their influence on the ultimate moment of resistance, for unbraced beams with Class 2 (compact) cross-section. The scope of the project applies to the design of both building structures and medium span viaducts, but excludes long span (over 30 m) highway bridges.

In this thesis, the first chapter describes the objectives of the project. The next chapter gives a review of literature and previous work related to moment redistribution and distortional lateral buckling in

composite beams, and also presents the current design
procedures regarding the latter. This is followed by the
report of the numerical work on moment redistribution for
Class 3 continuous composite beams. The first part
(Chapter 3) describes the computer program used in the
study and the second part (Chapter 4) presents the
results of the parametric study and conclusions. The
experimental work on distortional lateral buckling is
reported in three parts. The first (Chapters 5 and 6)
describes the tests on two double cantilevers (T beam)
labelled as T1 and U1, and the second (Chapters 7,8 and
9) describes the tests on two inverted-U frames acting as
double cantilevers labelled as U2 and U3. Results and
discussions are given in Chapters 6 and 9 for each series
respectively. In Chapter 10, all the experimental
results are then discussed and compared with theoretical
predictions from various design methods described in
Chapter 2. Finally conclusions and tentative design
recommendations for distortional lateral buckling are
also given in Chapter 10.

The Système Internationale (S.I.) units are used for
measurement throughout this thesis. In all the figures
linear dimensions are in mm unless otherwise stated.

1.2 Objectives of the project

1.2.1 Redistribution of moment

In braced continuous composite beams, redistribution of
bending moment occurs from the hogging regions to the
sagging regions as a result of concrete cracking,
material yielding and local buckling. This makes a
significant departure between the true distribution of
moments and that expected from elastic analysis. By
satisfying the compatibility requirements imposed by the
boundary conditions, the amount of redistribution can be
determined by a numerical simulation using realistic
inelastic moment-curvature relationships and
characteristic moment-rotation curves of the hogging
regions due to local buckling. Previous research [7] had
been carried out on beams with Class 1 or 2 cross-section
to justify the use of the simple plastic collapse design
method, and to identify the limitations of its
application. The research described here is concerned
with the design of uniform continuous composite beams
with Class 3 cross-section, and the amount of moment
redistribution permitted within which a beam can still
resist the design load prior to failure.

In design to draft Eurocode 4 (EC4) [1], there are two
design methods given with regard to the elastic global

analysis of Class 3 continuous beams. Apparently one method is less conservative than the other, and it allows up to 20 per cent redistribution of hogging moments determined by elastic cracked analysis, in the belief that local buckling can provide sufficient increase in rotation capacity in the hogging regions, without causing a rapid decline of the hogging moment of resistance, to shed at least this amount of bending moment to the mid-spans before collapse occurs. The objective of the work was to identify the margin of safety of this less conservative method by a computer study, using realistic material properties and the limited test data on the post-local-buckling behaviour of cantilevers with Class 3 cross-section, over a wide range of beams with practical dimensions. In the parametric study, it was assumed that complete shear connection was provided, and that the bottom flange of the beams was braced against lateral-torsional buckling.

1.2.2 Experimental work on distortional lateral buckling

For continuous composite beams the steel bottom flange
will normally be in compression over a length between the
two points of contraflexure adjacent to an internal
support. If the beam is unbraced, the bottom flange in
the hogging regions may be vulnerable to lateral-
torsional buckling, sometimes initiated by local buckling
adjacent to an internal support, depending very much on
the geometrical proportions of the web and the bottom
flange. This instability impairs the ultimate load
carrying capacity of the beam, and so sometimes bracings
are required in order to achieve an economic design
solution. BS5400: Part 3[8] and draft BS5950 : Part
3.1[2] give the requirements for bracing provision to
bridge girders and building beams respectively.

However, for beams with stocky cross-section (Class 1 or
2), such as hot-rolled universal beam sections used in
buildings and viaducts, it is widely believed that the
provision of lateral bracings is inconvenient, costly and
unnecessary. For a multi-beam floor system, the
torsional stiffness of the reinforced concrete slab is
much stiffer than that of the steel section, and it seems
logical to assume that, depending on the flexural
stiffness of the web, it should be able to transfer to

the bottom flange the lateral and torsional restraints provided to the top flange by the slab. Unfortunately there is not sufficient experimental evidence to substantiate this view. The composite beams of greatest research interest have been those with Class 2 webs and flanges in accordance with EC 4.

The scope of the present work is therefore limited to composite beams with unstiffened web within the Class 2 limit. Although instability of the bottom flange could undermine the ultimate strength of continuous composite beams, little research had been done to tackle the problem, both theoretically and experimentally. Until recently a number of design methods, which use different conceptual models and are mainly based on numerical methods, have been proposed, and they are discussed in detail in Chapter 2. The relevant conceptual model is the continuous inverted-U frame, with at least two parallel beams attached to the common slab by shear studs, which may be either of reinforced concrete or a composite slab with profiled steel decking. Tests have been done on specimens of realistic scale to study the buckling behaviour of composite beams in the hogging moment region. The objectives of these tests were to provide guidance regarding assumptions and modelling for theoretical work, and also data on the ultimate hogging moment of resistance for Class 2 unbraced beams.

Since a generally accepted method of assessing the susceptibility of the hogging region to distortional lateral buckling is not yet available. The test results have been used to provide spot checks on their predictions and appropriateness of various methods described in Chapter 2. The buckling phenomenon in composite beams is rather complex, because it is dependant upon many parameters, such as the geometrical and material properties of the steel I-section, the transverse bending stiffness of the concrete slab attached to the steel top flange, the amount of shear connection, the type and position of the applied loads, and the boundary conditions. The experimental work also sought to identify the most significant design parameters and the appropriate slenderness limits for unstiffened and unbraced continuous composite beams within Class 2 in accordance with EC 4, which are not affected by distortional lateral buckling as far as the plastic moment of resistance is concerned.

CHAPTER 2
PREVIOUS RESEARCH AND THEORETICAL MODELS

2.1 Introduction

There are two main areas of research in this project, and
so this chapter is divided into two parts, one devoted to
each piece of work. The first part gives a review of
research on local buckling in composite beams, and
explains its effect on redistribution of moments. Then
follows a discussion of the current design philosophy for
Class 3 continuous composite beams in accordance with the
draft Eurocode 4 [1]. The background for the present
research is then given.

The second part of this chapter is concerned with an
experimental study of distortional lateral buckling of
continuous unbraced composite beams using hot-rolled
sections in the hogging moment region. To begin with, a
review of literature related to this instability problem
is given. Many design recommendations addressed to this
practical problem have recently been proposed by
different research workers, and a few of the more
appropriate of these, are discussed in greater detail.
The existing British codified methods for the design of
beams susceptible to lateral-torsional instability, in
particular the U-frame approach of BS5400 : Part 3 [8],

are also given and comments are made on their appropriateness. Very little experimental work on U-frame action in composite steel and concrete beams has been reported, thus calibration of the predictions from various design methods against experimental results cannot be achieved. This deficiency has led to the present experimental investigation aimed at understanding the distortional lateral buckling behaviour of composite beams subjected to hogging moment gradient.

2.2 Local buckling

Assuming lateral-torsional buckling is not a controlling factor, the ultimate carrying capacity of a beam is closely related to the critical compressive stress which instigates local buckling at critical cross-sections. When an I-beam has a very thin web and flanges, it will buckle locally at stresses well below the yield point of the material. On the contrary, when the web and flanges are stocky, the local buckling stress is well above the yield point and the buckle will be plastic. The transition between these two extremities is not yet well defined due to the fact that local buckling occurs in the inelastic range (material partially yielded), which is reflected by the scatter of experimental results [9]. Variations in residual stresses of the test specimens also increase the scatter. Local buckling of thin-walled steel sections has been researched extensively over the past forty years because of its prominent influence on the strength of beams and columns, and there is a well established basic literature [10,11,12]. For composite steel and concrete beams, local buckling does not occur in the steel top flange attached to the concrete slab, when the beam is subjected to sagging bending. This problem arises only when a composite beam is designed as continuous, so part of the web and bottom flange are subjected to compression in the hogging moment regions due to static loading. Hence local buckling normally

occurs close to an internal support. Local buckling behaviour is very similar in bare steel beams and in composite beams, but generally the composite beam is more vulnerable to local buckling if the same size of steel section is used in both cases as shown in Fig. 2.1. This is because the neutral axis in the composite cross-section is shifted towards the slab due to the tensioning of longitudinal slab reinforcement, and as a result the compressive strains in the web and bottom flange are proportionally higher.

Van Dalen [13] tested seventeen composite double cantilevers in negative bending and produced evidence of severe local buckling in composite beams using hot-rolled steel sections. Then a systematic research on local buckling in composite beams was conducted by Climenhaga [14] and his main objective was to classify composite cross-sections which are suitable for the use of plastic design as adopted in steel structures. He concluded that the web slenderness limit for composite beams should be more restrictive than that for steel beams to allow the use of plastic design because of the effect of local buckling.

Hamada and Longworth [15] also carried out a study on buckling of composite beams in negative bending. They concluded that the ultimate moment capacity of composite beams in negative bending is affected by local flange

buckling unless the compression flange is stiffened by a cover plate, and the bending resistance decreases significantly with increase in the flange width-thickness ratio. Bradford [16] presented a finite strip method of analysis for the inelastic local buckling of composite beams in negative bending, which includes non-linear material behaviour and residual stresses. Other research [17,18] was more related to the carrying capacity of continuous composite beams affected by local buckling rather than buckling behaviour alone.

If a continuous composite beam is designed plastically, its ultimate strength depends on whether sufficient rotation capacity in the hogging regions is available to enable the formation of a collapse mechanism. Rotation capacity is defined as the ability to deform and to rotate at critical cross-sections while maintaining the predicted moment of resistance, which is not necessarily the plastic moment of resistance. However for the application of plastic hinge theory, large rotation capacity is required to redistribute bending moments in the hogging regions to the sagging regions, that cannot be achieved without the presence of plastic deformations. These deformations are concentrated in a short segment of beam containing the critical cross-sections, which is often visualised as a plastic hinge. Local buckling affects not only the ultimate moment of resistance but also the formation of plastic hinges in the hogging

region.   More   recent   studies   [19,20,21,22,23]
concentrated on plastic rotations in composite beams and
their influence on the design of continuous composite
beams.

2.3 Classification of cross-sections

From previous discussions, the resistances of cross-sections and their ability to deform are therefore closely related to the slenderness of the web and flange in compression. Codes of practice in many countries give limitations on these slendernesses and classify beams with various cross-sections into groups for the purpose of assessing the bending resistance as well as choosing the most appropriate method of structural analysis. In the early 1970's, the introduction of limit state design philosophy into codes of practice for design of structures began to take place in Europe and North America, which encouraged the development of plastic design especially in buildings. In U.K., classification of cross-sections in steel structures first appeared in BS5400 : Part 3 [8]. Cross-sections are defined as either compact or non-compact by meeting several slenderness provisions. From definition, compact sections are restricted to those which can develop the full plastic moment before, and maintain it after, the onset of local buckling. The more recent codes of practice [1,2,24,25] have taken one step further than BS5400 in the classification of cross-sections, by dividing them into four classes, depending on the level of susceptibility to local buckling. Eurocode 4 is more relevant to the present work and the definitions for each class are extracted as follows:-

Class 1 - plastic cross-sections are those which can develop a plastic hinge with sufficient rotation capacity to allow full redistribution of bending moments in the structure.

Class 2 - compact cross-sections are those which can develop the plastic moment capacity of the section although local buckling and/or crushing of concrete limits rotation at constant bending moment.

Class 3 - semi-compact cross-sections are those in which the stress in the extreme compression fibres of the structural steel should be limited to yield because local buckling would prevent development of the plastic moment capacity of the section.

Class 4 - slender cross-sections are those liable to local buckling of the structural steel by compressive stresses less than the yield stress.

From Eurocode 4 the four classes of cross-section are defined by the limiting width-thickness ratios for steel flanges and webs given in Table 4.2 of draft Eurocode 4, and the background is given in the commentary on the draft Eurocode 4 [26]. Implications of this classification system for the design of composite buildings have been discussed by Johnson [27] and by Brett et al [28,29].

The relation between the classification and the rotation capacity is shown diagrammatically in Fig. 2.2. In the

case of a Class 1 or 2 beam, rotation capacity is defined by

$$R = \frac{\theta_a}{\theta_p} - 1 \qquad (2.1)$$

as illustrated in Fig. 2.2.

Kemp [30] has given detailed discussions on the rotation capacity requirements in the design of continuous composite beams in relation to their classification for local buckling. He made comparisons between these requirements and the available rotation capacities observed in tests on plain steel sections, and concluded that there is no strong evidence to support a difference in classification of local buckling for Classes 1 and 2 between EC 3 [25] (steel) and EC 4 [1] (composite).

2.4 Moment redistribution

Like steel beams, composite beams also show ductile behaviour because the steel section is made of elastic-plastic material. When a continuous composite beam is loaded, a redistribution of moments occurs in relation to the distribution of moments calculated from elastic analysis. This is due to the fact that moment-curvature relationships in both the hogging and sagging moment regions are no longer linear at high loads. As expected, the amount of moment redistribution is closely related to the ductility (rotation capacity) in both hogging and sagging regions. The main causes of limitation in rotation capacity are local buckling of the steel section in a hogging region and crushing of the concrete in a sagging region. To enable plastic design, large amount of rotation capacity in the hogging region is often required, as the plastic moment of resistance at the support can be less than 50% of that at midspan.

Most of the early research works were related to the application of plastic design to composite beams. Barnard et al [31,32,33] and Yam et al [34] have conducted research to study the ultimate behaviour in the sagging region, and verified the validity of using simple plastic theory for the design of simply supported composite beams by computer tests. Barnard [33] also presented a method for estimating the curvature of a cross-section in sagging bending.

The moment-rotation characteristic affected by local buckling in the hogging region was a subject of research by Climenhaga [14] both theoretically and experimentally. In his tests, the hogging region of a continuous beam was modelled as a double cantilever. From the tests he identified four types of cross-section behaviour, and proposed a set of slenderness rules for unstiffened I-sections suitable for the application of plastic design.

A more comprehensive background on the research of ultimate strength of continuous composite beams before 1974 has been given by Hope-Gill [35]. He also used the research results on moment-rotation or moment-curvature characteristics from Barnard [33] and Climenhaga [14] for sagging and hogging regions respectively, to conduct a computer study to determine the conditions under which continuous composite beams will reach their plastic design loads. This work was complimented by tests on three three-span continuous composite beams [17], and published by Johnson and Hope-Gill [7]. Hope-Gill [36] subsequently extended his work on redistribution of moments to cover composite beams of slender cross-section which cannot be designed plastically.

A detailed cross-sectional analysis of composite beams in relation to the moment-curvature characteristics in sagging bending was presented by Rotter and Ansourian [19]. A ductility parameter χ was defined as the ratio

of the limiting neutral axis depth to the conventional neutral axis depth at ultimate strength. From test and numerical results, Ansourian [20,21] concluded that for continuous composite beams having a compact steel section the available rotation capacity in the hogging regions is usually adequate to shed moments to the sagging regions, and with a minimum value of χ equal to 1.4, simple plastic design using full plastic moment values may be confidently used under conditions of severe rotation requirement in the sagging regions, for the worst combinations of spans and loading.

2.5 Design of class 3 continuous composite beams

In current practice class 3 beams are not allowed to have
a design moment of resistance higher than the first yield
moment, M_y', to avoid premature local buckling in the
hogging region. The ultimate strength of a uniform
continuous beam is dependent on how much support moments
can be redistributed to the mid-span before collapse
rather than the attainment of maximum moment of
resistance at the support. When the cross-sections at
the support are Class 3, there is limited post-local
buckling rotation capacity in the hogging region; whilst
the cross-sections at mid-span are Class 1 or 2, there is
always surplus in bending strength in comparison to the
elastic moment distribution. These two conditions allow
moment redistribution to take place.

In order to achieve better economy in the design of Class
3 continuous beams, the draft Eurocode 4 [1] has proposed
a quasi-elastic method allowing up to 20% redistribution
of support moments to midspans in addition to the
conventional elastic analysis. This new method given in
Clause 4.4.3.2 of the draft EC 4 is based on the
assumption that the post-local buckling rotation capacity
in the hogging region can be relied on to shed at least
this amount of bending moment before collapse occurs, in
the belief that the hogging moment of resistance of the
cross-sections at the support does not fall so sharply
due to local buckling. The midspan regions are required

to remain elastic (which is rarely a constraint in uniform Class 3 composite beams), as any inelastic sagging curvature would increase the demand on the limited rotation capacity available near the internal supports.

A design example for a two-span uniform Class 3 composite beam (Appendix B) shows that the less conservative method of the two given in the draft EC4 allows the beam to carry loads 40% more than that determined by the traditional elastic analysis without redistribution.

Apparently the new method, which allows substantial moment redistribution, was thought to be too liberal . A numerical analysis, reported here, has been carried out to check on the safety of this method, and to validate its application, using the post-local buckling moment-rotation characteristic in the hogging region observed from double cantilever tests and realistic moment-curvature relationships including non-linear material response for the hogging and sagging regions. The ultimate carrying capacity of a beam is determined numerically by satisfying the kinematic condition, which requires a continuity of moment and rotation along the beam. This work has been published [37] and a copy is enclosed in Appendix A. The development of the computer program and the parametric study were carried out by the present author.

2.6 Theoretical studies on distortional lateral buckling

At the internal support of a continuous beam instability
may determine its carrying capacity; local buckling may
occur in the hogging regions depending on the web and
flange slenderness ratios of the steel cross-section, and
if the beam is unbraced, overall buckling of the bottom
flange may take place depending not only on the
slenderness ratios of the cross-section, but also the
shape of the bending moment distribution along the beam.
Local buckling has been discussed in section 2.2, and the
common practice to take into account its effect in design
is to impose strict geometrical limits. The overall
lateral buckling of the bottom flange for continuous
unstiffened (except at the support) and unbraced
composite beams is now discussed.

Lateral buckling of the bottom flange between laterally
restrained supports is a complex problem, which can
either occur alone, or interact with local buckling as a
coupled mode of overall buckling. For composite beams
using hot-rolled sections and of practical dimensions,
some degree of interaction between local and lateral
buckling usually exists at collapse. In contrast to
plain steel beams, the top steel flange is connected to a
concrete slab by means of shear connectors, and so the
composite top flange is effectively restrained against
any possible lateral displacement. The bottom flange is
restrained partially from lateral displacement by the

web, but the level of restraint is dependent largely on the flexural stiffness of the web. Lateral buckling of the bottom flange is only possible when the web distorts out of its plane associated with excessive lateral displacements of the bottom flange as shown in Fig. 2.3. The parameters most likely to influence this type of buckling are the web and the bottom flange slenderness ratios, the ratio of length of the hogging region to the flange width, the moment distribution along the beam, and the torsional stiffness of the bottom flange.

There exists a well established research literature on the elastic lateral-torsional buckling of steel beams (38,39,40,41), which are laterally unrestrained between the end supports, but very little on composite beams. Yet web distortion is seldom considered in the previous studies. Since composite beams are closely akin to plain steel beams, previous research on the latter is first discussed, and is then extended to composite beams, with emphasis on the theoretical treatments of various design methods available. The fundamental analytical techniques in solving buckling problems between the two are indeed very similar.

2.6.1. Plain steel beams

Beams in the medium range may buckle after the spread of
some plasticity in the section, therefore inelastic
overall buckling has also been studied extensively
[42,43,44,45,46]. There is less research [47,48,49,50]
on the lateral-torsional buckling of continuous steel
beams probably because the interaction between adjacent
segments during lateral buckling and the corresponding
effect on the buckling load are rather difficult to
predict. Lateral buckling of I-beams restrained on the
top flange by purlins or profiled sheeting has also been
studied [51,52,53], but again the analysis does not
include web distortion that may occur in practice. Since
lateral bracings can enhance the buckling strength of I-
beams, some research [54,55] has been conducted to
provide design guidances.

Before the last decade,there was relatively little research
on distortional lateral buckling of steel I-beams
(lateral-torsional buckling coupled with web distortion),
although it is a practical problem for the design of
unstiffened and unbraced plate girders. Web distortion
is more significant in plate girders with slender
unstiffened webs (Class 3 or 4) than in hot-rolled I-
sections with comparatively stocky webs (Class 1 or 2).
This effect would reduce the effective torsional
resistance of the beam against lateral-torsional
buckling, and therefore the buckling load is lower than

that using classical rigid web theory [56]. Research on the subject before 1983 has been covered in reviews by Bradford [57]. Distortional buckling was first considered by Nylander [58] in 1943. Until the early 1970's, elastic stability problems were tackled mostly by either using energy methods or solving the governing differential equations [10,56]. In the treatment of web distortion, the strain energy stored in the web due to flexural bending is added to the total strain energy of the system, and then the usual variational approach is used to find the minimum buckling load [10]. Most modern theoretical treatments of buckling problems are numerically based, and the commonly used methods are the finite element method [59] and its variation, the finite strip method [60].

Rajasekaran and Murray [61] presented an elastic finite element analysis of coupled local buckling in wide-flange beam-columns. They concluded that the model gives good results for coupled local flange buckling with overall lateral-torsional buckling but does not represent web buckling. The effect of initial imperfections and inelastic material response was not considered. Johnson and Will [62] later developed a three dimensional assemblage of thin plate elements having both membrane and bending stiffnesses, a more powerful method than the one dimensional element suggested by Rajasekaran and Murray. Plate elements were used for web and flanges,

and therefore the cross-section was allowed to distort freely. However its merits are outweighed by computational effort due to a considerable number of degrees of freedom. Akay, Johnson and Will [63] then refined this rather complex procedure into a two dimensional analysis, taking the advantage of symmetry about the mid-surface of the web for I-sections, and hence reduced the computional effort significantly. But both methods cannot take into account of the effect of initial imperfections and material non-linearity.

In 1978 Hancock published a paper [64], which gives a better understanding about distortional lateral buckling of I-beams in the elastic range. He used the finite strip method to study the interaction between local and lateral buckling in I-beams. A similar approach was also suggested by Plank and Wittrick [65]. More research [66,67,68] using the finite strip method has been carried out in Australia to study web distortion and overall buckling in I-beams systematically. In general, the results indicated that for determinate hot-rolled I-beams the effects of web distortion are small, so that their buckling loads are close to those calculated by the classical rigid web method. Although elastic analyses of distortional lateral buckling of determinate I-beams are now well established, very little research has been done to investigate distortional lateral buckling of continuous beams especially in the inelastic range. In

continuous beams local buckling may occur at critical cross-sections prior to overall buckling of the member. The possibility of premature local buckling causing subsequent flexural buckling has only been considered by a few researchers [69,70,71,72] using the effective width concept for the buckled regions. Obviously the solution is approximate because a real beam does not have effective cross-sections as assumed in the analysis.

Experimental work investigating distortional lateral buckling coupled with local buckling in hot-rolled I-beams has been very sparse, probably because of the complexity of its nature. However, on a few occasions web distortion was observed and reported in related tests [73,74] using slender plate girders.

Most of the earlier research could not accommodate geometrical and material non-linearity, but a few attempts have been made to study distortional lateral buckling in the inelastic range. Bradford [75] represented a finite element method of analysis to investigate inelastic distortional buckling of determinate, hot-rolled I-beams. Dowling et al [76] described the use of a non-linear finite element program to study the overall stability of plate girders, which are used to construct tapered frames for industrial buildings. They claimed that both geometrical and material non-linearity have been included in the analysis, therefore a better insight into the combined

effects of local buckling, lateral buckling and distortion can be made. However this work is restricted to plate girders.

2.6.2 Composite beams

Compared to its counterpart , research on distortional lateral buckling of continuous composite beams is less well documented. An isolated composite I-beam in a structure rarely exists, and normally it is a part of a slab/deck-multi-beams system - a typical example is a continuous inverted U-frame consisting of two or more adjacent steel beams and the slab to which they are attached (Fig. 8 in BS5400 : Part 3 [8]). Therefore it is virtually impossible for the beam to buckle as a whole laterally, so if overall lateral buckling is to occur, excessive lateral deflections of the bottom flange coupled with web distortion has to take place no matter how stocky is the web, assuming that no failure occurs in the slab or the shear connection. However a rigid web may be sufficient to transfer the positional restraint given to the top flange through shear connection by the slab to the bottom flange, and intuitively the bending moment of resistance may not be impaired by premature overall buckling, dependent on the cross-section slenderness ratios and beam geometry. Previous research on this subject tried to explore the potential benefit of

U-frame action in stabilizing unstiffened and unbraced
beams, hoping that costly and fatigue prone bracing
systems could be wholly or partially displaced in bridge
structures, whilst in buildings unnecessary bracings to
the compressive flange could be eliminated so as to
improve economy. A summary of the development of
continuous composite construction in buildings and
bridges has been given by Brett et al [28,29] and Weston
[77]. Different approaches in dealing with the design
against distortional lateral buckling in continuous
composite beams are now discussed in detail .

2.6.2.1 Codified methods in U.K.

In the draft building code for composite beams, BS5950 :
Part 3.1 [2], for checking the lateral stability of the
bottom flange in negative moment regions it is
recommended to follow Appendix G of BS5950 :Part 1 [2],
or BS5400 : Part 3 [8] regarding torsional restraint by
the concrete slab, or to refer to specialist literature.
The design provisions of Clauses G.2 and G.3 of Appendix
G in BS5950 : Part 1 are based mainly on the works by
Horne and Ajmani [78], and Horne and Singh [51,53]. This
work was originally carried out to check the stability of
stanchions and rafters in steel portal frames restrained
by equally spaced purlins. The analytical model is
elastic and does not include any rotational restraint

contributed by the purlins; also the analysis assumes buckling to occur by twisting of the entire section about a longitudinal axis passing through the centres of the purlins at a fixed distance above the top flange without web distortion. To allow for intermediate loads on the member between restraints, such as a composite beam, a 'five moment' formula is suggested in Clause G.3.6.1, however this formula is entirely empirical. It was checked numerically using an energy method for a limited number of examples, and proved to be conservative. With short hogging moment regions and relatively stocky webs, the predictions from this method may be unrealistic.

In the checking of lateral-torsional buckling for beams, BS5400 : Part 3 requires the calculation of the beam slenderness parameter, λ_{LT}, which is similar to the well-known slenderness parameter for a strut; the limiting design compressive stress, σ_{li}, is then obtained from Fig. 10 corresponding to this λ_{LT} value. This design curve is deduced using the Perry-Robertson method to take into account the effects of initial geometrical imperfections, residual stresses and material yielding with respect to the experimental results on overall buckling of steel beams. Details concerning the construction of this graph are given elsewhere [77]. BS5400 recognises the fact that the bridge deck can stabilise laterally unrestrained flanges in compression, and therefore allows the use of U-frame action as a mean

of stabilising the compressive part of the bottom flange.
Design of beams continuously restrained by a deck is
given in Clause 9.6.6. The compressive flange is assumed
to be restrained by the webs and the concrete deck as a
continuous series of inverted U-frames as shown in Fig.
2.4. The slenderness parameter λ_{LT} is a function of the
effective length for lateral torsional buckling, le,
which in turn depends on the lateral deflection of the
unrestrained flange, δ, corresponding to the flexibility
of the U-frame defined in Fig. 2.4. The joints in the U-
frame are assumed to be rigid for the calculation of δ.

In this model, the bottom flange is idealised as a strut
on elastic foundation of modulus $1/\delta$. From elastic
buckling theory for the strut [56], the elastic buckling
load for a strut of length, L, with a single curvature
sine wave buckle, is given as:

$$P_{cr} = (\pi . E . I_c / L) + (L / \pi . \delta) \qquad (2.2)$$

where I_c is the second moment of area of the compression

flange about its centroidal axis parallel to the
web

Differentiation of P_{cr} with respect to L and equating to
zero to get the minimum buckling load gives:

$$L = (E . I_c . \delta)^{0.25} \qquad (2.3)$$

Substituting L in Eqn.(2.3) into Eqn.(2.2), gives:

$$P_{cr} = 2 (E . I_c / \delta)^{0.5} \qquad (2.4)$$

The Euler load for a strut is defined as:

$$P_{cr} = \pi . E . I_c / l_e^2 \qquad (2.5)$$

Combining eqns. (2.4) and (2.5), gives an expression for the effective length:

$$l_e = (\pi/\sqrt{2}) (E.I_c.\delta)^{0.25} \qquad (2.6)$$

The effective length is given in Clause 9.6.6.2 as:

$$l_e = 2.5 (E.I_c.\delta)^{0.25} \qquad (2.7)$$

Equation (2.7) is slightly more conservative than equation (2.6). Instead of using the design curves for struts, BS5400 adopted an unified approach for both cases - plain steel beams and composite beams designed as U-frames; and defines the slenderness parameter as (Clause 9.7.2):

$$\lambda_{LT} = (l_e/r_y) . k_4\eta v \qquad (2.8)$$

where

l_e is the effective length for lateral torsional buckling

r_y is the radius of gyration of the whole steel beam section about its minor axis

k_4 is a buckling parameter to take account of the torsional effect derived from different types of cross-section, = 1.0 for composite beams

η is a factor to allow for the shape of the bending moment diagram, = 1.0 for beams restrained by U-frames

v is a cross-section slenderness factor dependent on the shape of the beam, and for beams of uniform section it can be obtained from table 9 in BS5400 : Part 3 using the parameters:

$\lambda_F = (l_e/r_y).(t_f/D)$ and $i = I_c/(I_c+I_t)$

where

t_f is the mean thickness of the two flanges
of an I section

D is the overall depth of the beam measured from
the bottom flange to level of tension
reinforcement

I_c and I_t are the second moments of area of the
compression and tension flanges respectively,
about the minor axis of the I-section.

Equation (2.8) is derived using the elastic lateral
torsional buckling theory for steel beams and some
approximations of the cross-sectional properties commonly
used in practice.   Apparently BS5400 assumes that the
effective length, obtained from buckling analysis of the
bottom flange, is also valid for the whole beam.   The
method becomes very conservative, for reasons discussed
in depth by Johnson [79] and Weston [77].   It should be
pointed out that the departure between the real and code
results is largely affected by the way that the effective
length in Eqn. (2.7) is calculated, because:

1.   The bottom flange as a strut is assumed to be
subject to uniform compression, and therefore the effect
of moment gradient along the beam is being ignored.

2.   The buckling shape is unlikely to take the form as a
half sine wave between the two lateral restraints, but

rather to include more terms in the Fourier series, depending on the flexibility of the web.

3. The spring stiffness of the elastic foundation is higher in regions closer to the supports, and hence greater lateral restraint is given to the bottom flange in those regions than elsewhere in the beam.

4. Warping and torsional restraints to the bottom flange at the support are neglected, but they have significant contribution to stabilise the bottom flange from moving laterally.

To complicate the situation further, in the calculation of the beam capacity BS5400 introduces a $D/2y_t$ factor, the ratio of half the beam depth to the maximum tensile fibre distance from the elastic neutral axis, to correct the limiting compressive stress for non-compact beams (Clause 9.8.3), after the limiting buckling stress has been obtained from Fig. 10. The background for this factor has been discussed briefly by Chaterjee [80], and the appropriateness of using this factor for composite beams has been discussed by Johnson [79] and Weston [77]. The following paragraph is a summary of their findings.

In the derivation of the curve for σ_{li} in Fig. 10, the plastic section modulus, Z_p, of beams for both equal and unequal flange sections were used in the calculations. Hence the conversion of this limiting stress to moment

capacity should use the plastic modulus for all kinds of sections. However, in practice elastic section moduli, Z_{xc} and Z_{xt}, with respect to the extreme compression and to the extreme tension fibre respectively, are commonly used for the design of non-compact beams, and to avoid confusion of presenting a method for them in terms of the plastic section modulus, the $D/2y_t$ factor is an empirical adjustment to allow the use of the elastic section moduli. For composite beams subject to hogging bending, Z_p is usually greater than Z_{xc} but less than Z_{xt}. The $D/2y_t$ factor will be greater than 1.0, and in this case the apparent elastic moment capacity, $\sigma_{li}Z_{xc}$, is being increased to give a better prediction with respect to the true moment capacity, $\sigma_{li}Z_p$, assumed in Fig. 10. The accuracy of the $D/2y_t$ factor is dependent on how good is the approximation to the shape factor, Z_p/Z_{xc}, for the section under consideration.

Despite all the confusion and irritation to designers using Clause 9.8.3, it is important to note that Fig. 10 was derived for plain steel beams only against lateral-torsional buckling - a mode combining both lateral and twisting displacements of the whole cross-section. It is not valid for composite beams restrained by U-frame action, because lateral movement of the top flange is virtually impossible, and the overall buckling mode must be distortional provided that there are no secondary failures such as shear connection.

2.6.2.2 Distortional buckling analysis as a bifurcation problem

Many design rules for steel beams against lateral
torsional buckling are based on the Perry-Robertson
method, which requires the knowledge of the elastic
critical load or stress of the beam, to take account of
the real beam behaviour. The schematic behaviour of a
beam subjected to static loading is shown in Fig. 2.5,
and the critical load is at point A, "point of
bifurcation". This elastic buckling or critical load is
usually obtained from an eigenvalue analysis by
optimising the total potential energy of the system.
Kapur and Hartz [81] developed an eigenvalue analysis
suitable for studying the stability of plates using the
finite element method. Based on the same principle,
Johnson and Bradford [4] presented an elastic finite
element analysis to determine the critical load for
unstiffened, fixed-ended, composite bridge beams buckling
in a distortional mode. Each beam was modelled as an
inverted-T section, which consists of only the web and
the bottom flange, with the top of web fully prevented
from lateral and rotational movement. This model is
slightly unconservative because the top flange can rotate
in a real situation. To allow for continuity of the
bottom flange over a support in the case of a continuous
beam, at the fixed end of the beam the boundary
conditions were relaxed, so that rotation of the bottom
flange about a vertical axis is allowed. The action of

shear and longitudinal bending stresses for each element along the beam were calculated using statics for a fixed-ended beam subjected to uniformly distributed loads.

The critical load factor λ_{cr} for a given initial stress distribution was obtained by solving the eigenvalue equation in the form:

$$| [K] - \lambda_{cr} [G] | = 0 \tag{2.9}$$

where

[K]   is the elastic stiffness matrix that represents the resistance of the beam against lateral-torsional buckling with web distortion

[G]   is the stability matrix that represents the tendency of the stress distribution in the beam to trigger distortional buckling taking into account second order plate deformations.

The critical stress at the bottom flange, σ_{cr}, is associated with the lowest root of λ_{cr} in the determinantal equation, Eqn. (2.9).

A parametric study was carried out by varying the following parameters:-

i)   The web depth/thickness ratios, d/t, ranging from 39 to   100.

ii)   The flange width/thickness ratio, B/T, ranging from 9.6   to 15.

iii) The span/flange width ratio, L/B, ranging from 48 to 90, with spans up to about 30 m.

iv) The breadths of the concrete flange of 220 mm in depth, b, ranging from 2 m to 4 m, and the ratios of total reinforcement area to slab area, r, ranging from 1% to 2%.

The results showed that the critical compressive stress, σ_{cr}, was influenced predominantly by the web slenderness ratio, d/t, and the rest of the variables had minor influences. Based on the Perry-Robertson method in relation to the critical stresses as used by BS5400, a modified slenderness parameter, β, was proposed for the design of unstiffened composite beams against distortional buckling. The proposed formula for β is given as,

$$\beta = 3.4 \ (\ d/t \ )^{0.7} \tag{2.10}$$

$$\text{and} \quad \lambda_{LT} = \beta \ . \ (\ 355/f_y \ )^{0.5} \tag{2.11}$$

The limiting compressive stress, σ_{li}, can then be obtained from Fig. 10 in BS5400 : Part 3 by knowing λ_{LT}. The beam capacity is obtained in the usual way as outlined in the code. This approach assumes that there are no differences between distortional buckling of composite beams and lateral-torsional buckling of steel beams in terms of initial geometric imperfections, residual stresses and plasticity.

Equation (2.10) is only valid for distortional buckling, that excludes the effect of local buckling in the support region and its possible interaction with distortional

lateral buckling. For beams with high elastic distortional buckling stress, well above yield, due to the spreading of plasticity near an internal support inelastic local buckling of the bottom flange and part of the web under compression may occur and interact with distortional lateral buckling in a way not considered in the preceding analysis (Eqn.(2.9)). To investigate the effect of local buckling on the beam's strength, Bradford and Johnson [5] subsequently presented a finite strip method of inelastic analysis for local buckling moments of composite beams with the presence of residual stresses. From the results of a parametric study on 11 beams of non-compact proportion in accordance with BS5400, it was found that inelastic local buckling preceded distortional buckling in composite beams with a non-compact compression flange with spans less than 40 m. A tentative design method for predicting the ultimate strength of continuous composite beams, which takes into account both the effect of local and distortional buckling in the hogging regions, was proposed. This method is more general than the preceding proposal using equation (2.10) alone, and involves the calculation of two buckling slenderness parameters, β_1 and β_d, for local and distortional buckling respectively. The geometry of the composite cross-section is shown in Fig. 2.6. The method is summarized as follows:-

i) Calculate the flange and web slenderness ratios as,

$$\beta_f = (b_o/T) (f_y/355)^{0.5} \quad (2.12)$$

and $\beta_w = (\alpha d/t) (f_y/355)^{0.5} \quad (2.13)$

ii) Calculate the shape factor S for the steel compression flange as,

$$S = Z_{ph} / Z_{xc} \quad (2.14)$$

where

Z_{ph} is the plastic section modulus of the composite section in hogging bending

Z_{xc} is the elastic section modulus for the steel compression flange of the composite section in hogging bending

iii) Calculate β_l and β_d as,

$$\beta_l = 3.5 (\beta_f \beta_w)^{0.5} \quad (2.15)$$

and $\beta_d = 3.1 (S_f f_y/355)^{0.5} (d/t)^{0.7} \quad (2.16)$

where S_f is taken as the shape factor S in Eqn. (2.14) and 0.87S for compact and non-compact cross-sections respectively.

Then take β as the higher of β_l and β_d, and use Eqn. (2.11) to obtain λ_{LT}.

iv) Find σ_{li}/σ_y from Fig. 10 of BS5400 : Part 3

v) To avoid the confusion of using the $D/2y_t$ factor as discussed in section (2.6.2.1) above, this factor is replaced by 0.87S. Therefore the limiting compressive stress, σ_{lc}, is taken as the limiting buckling stress, σ_{li}, for a   compact section

or as $0.87S\sigma_{li}$ for a non-compact section, but not
higher than σ_y. The bending resistance is
calculated in the same way as Part 3 using
Clause 9.9.

Although this method seems rather sophisticated, it is
worth noting that it still treats local and distortional
lateral buckling as two separate events. In order words,
the interaction between these two modes of buckling has
not been considered in the numerical analysis.   In
addition the moment distribution is obtained by assuming
a fixed-ended beam subjected to uniformly distributed
loads, thus the hogging regions are always shorter than
the sagging region. This assumption does not much affect
the local buckling, but may be unconservative if the
length of the hogging region becomes longer, regarding
the effect of distortional buckling. Nevertheless, for
bridge beams of practical dimensions, the predictions are
likely on the safe side because there are degrees of
conservatism built into the model in the treatment of
material   nonlinearity,   geometric   imperfections   and
residual stresses for distortional buckling. This method
gives resistance moments that are typically double those
given by the design in accordance with BS5400 : Part 3.

2.6.2.3 Non-linear large deflection analysis

A more elaborate way of investigating the interaction
between local and distortional buckling in continuous
unstiffened and unbraced composite beams has been carried
out recently by Weston [6,77], who used a modified
version of a large deflection non-linear finite element
program originally developed by Crisfield [82,83]. This
program is suitable for the analysis of assemblies of
thin, rectangular, stiffened plates, and was previously
used to study the collapse behaviour of stiffened box
girder diaphragms, serving a check on the Merrison design
rules [84]. Ivanov's yield criterion [85] was used in
the program to simulate the spread of plasticity rather
than the usual Von Mises yield criterion. Similar to the
approach by Johnson and Bradford discussed earlier, only
fixed-ended beams subjected to uniformly distributed
loads were studied. The composite cross-sections in the
hogging and sagging moment regions were transformed into
two types of steel cross-section as shown in Fig. 2.7 as
equivalent steel cross-sections.

In the finite element analysis, the top and bottom
flanges of the mono-symmetrical I-beam were treated as
stiffeners, which attached to the adjacent web plate
elements. In fact a segment of the flange and part of
the web were combined to form a stiffened web plate
element, therefore the behaviour of the flange
(stiffener) was described in terms of the same

displacement variables used for the adjoining web plate
element. The flange under compression buckles locally in
a torsional mode with short wave length, so this
stiffened web plate element cannot simulate the flange
local buckling very well, unless a finer division of
elements adjacent to the support is made. But this is
usually onerous and cost ineffective. The program also
allowed for the effects of initial geometric
imperfections and residual stresses, but the torsional
rigidity of the flange (stiffener) was assumed to be
elastic throughout the analysis. The latter may be
unconservative because the torsional resistance of the
bottom flange could be overestimated due to the spreading
of plasticity near the support, which could increase
deformations at a lower load level. In the analysis the
top flange was fully prevented from lateral displacement,
and twist along the members was restrained by a degree
appropriate to the slab stiffness, but at the fixed-ended
support the boundary condition permitted the bottom
flange to rotate about a vertical axis, that is, the same
condition as adopted by Johnson and Bradford.

A parametric study was carried out and 19 beams with
spans ranging from 23 m to 33 m were analysed. It was
found that varying the form of initial longitudinal bow
of the bottom flange from anything between one and six
half-sine waves had only a small influence on the
collapse load, less than 5 per cent generally. This was

due to the fact that the destabilising region was always located close to the support. In contrast to the findings by Johnson and Bradford, the results indicated that the slenderness of the bottom flange is also an important parameter to determine the critical load for distortional lateral buckling; generally for beams with a fixed span and constant depth, the ultimate capacity increases as the flange slenderness ratio, B/T, increases by keeping the web slenderness ratio, d/t, unchanged. Therefore it seems that Bradford and Johnson method's regarding distortional buckling may give unsafe predictions for girders of unusual shape with a narrow and thick bottom flange, as the flange slenderness ratio is not a design parameter.

Based on the numerical results, a new slenderness parameter, β, was proposed as,

$$\beta = 1.28 \ (\ L/r_y \ )^{1/2} \ (d/t)^{1/3} - 29 \qquad (2.17)$$

where

    L   is the beam span

    r_y is the radius of gyration of the bottom flange about the minor axis of the steel section

, to be used in conjunction with Fig. 10 of BS5400 : Part 3 to obtain the limiting compressive stress for distortional buckling. The beam capacity is then calculated following the same procedures as in BS5400.

A comparison between these two methods suggested by Bradford et al and Weston respectively has been made in Fig. 2.8, where β_ℓ and β_w are defined in eqns. (2.12) and (2.13). It is clear from Fig. 2.8 that the two methods agree closely when the combined slenderness is less than 18, but above that Bradford and Johnson (B & J) method becomes unsafe. The discrepancy is getting higher as the slenderness increases. Not surprisingly, Weston concluded that B & J method gave unsafe predictions for girders, which have the ratio L/r_y of the bottom flange higher than 350. Nevertheless it is worth noting that the points with $\sqrt{\beta_\ell \beta_w}$ higher than 18 in Fig. 2.8 are obtained using Weston's specimens, which have the bottom flange width-to-thickness ratios outside the practical range and rather long spans. So Weston has used specimens outside the intended scope of the B & J method.

However both methods suffer the same drawbacks, neglecting the effect of variation of moment gradient other than the case of fixed-ended beams, and the restraining effect from the adjoining members to the span under consideration with respect to torsional and warping constraints at the supports. The former is likely to give a lower buckling load for a beam with a less steep moment gradient, but the latter on the contrary may be beneficial. Both studies concentrated on beams of non-compact cross-section, however most of the composite beams using hot-rolled section have compact cross-section

- Class 1 or Class 2 beams, and a review of literature reveals that there is very little work on the subject related to distortional buckling of compact composite beams. For this type of beams, extensive yielding coupled with inelastic local buckling in the support region may influence the overall stability of the bottom flange, hence reduce the ultimate capacity of the beam.

2.6.2.4 Strut on elastic foundation

Svensson [86] has adopted a more classical approach to examine distortional lateral buckling. The bottom flange of a continuous composite beam was idealised as a column subject to a varying axial force, which arises from the distribution of bending moment along the beam, between two supports, bearing against an elastic foundation with Winkler modulus k, which is represented by the flexural stiffness of the web per unit length as

$$k = Et^3/4(1-v^2)d^3 \qquad (2.18)$$

The model is shown in Fig. 2.9, and the buckling load can be obtained by the following governing differential equation with the boundary conditions.

$$EI \frac{d^4w}{dx^4} + \frac{d}{dx}\left(N(x)\frac{dw}{dx}\right) + kw = 0 \qquad (2.19)$$

$$x = 0 \quad : \quad w = 0 \text{ and } d^2w/dx^2 = 0$$

$$x = l \quad : \quad w = 0 \text{ and } d^2w/dx^2 = 0$$

where w is the lateral displacement

N(x) is the axial force at position x (compression +ve)

l is the length of the column

Galerkin's method was used to solve the above equations in non-dimensional form. Different types of axial force distribution $N(x) = N_o n(x)$ represented by a second order polynomial have been tried, and the results for the lowest buckling load, N_o (critical), were presented in design tables and graphs with respect to the dimensionless modulus, βl, which is defined as,

$$\beta l = (k l^4 / E I)$$ (2.20)

Combining eqns. (2.18) and (2.20) for $u = 0.3$, βl becomes,

$$\beta l = 1.35 \ (t^3 l^4 / d^3 TB^3)^{0.25}$$ (2.21)

The derivation of the foundation stiffness Eqn. (2.18) ignores the flexibility of the concrete slab, so the foundation is slightly over-stiff. Weston [77] has demonstrated that for typical bridge girders the error is unlikely to exceed 4%. Svensson also suggested that the limiting compressive stress at the bottom flange can be obtained from one of the ECCS strut design curves [87] by using the dimensionless slenderness $\underline{\lambda}$, which is given as,

$$\underline{\lambda} = (f_y / \sigma_{cr})^{0.5}$$ (2.22)

where σ_{cr} is the elastic buckling stress of the bottom
flange for a particular case of moment
distribution along the beam

According to the first draft Eurocode 3 [87], the bending
resistance can be taken as the first yield moment only
when σ_{cr} is higher than $2.3f_y$ from equation (5.3.16) for
$E = 205$ kNmm^{-2}. Substituting this value into Eqn.
(2.22), it gives $\underline{\lambda} = 0.66$. It seems to indicate that
distortional lateral buckling would not occur when the
dimensionless slenderness is less than 0.66, even though
yielding has already started in the most critical cross-
sections. The second draft Eurocode 3 [25] changes the
maximum value of $\underline{\lambda}$ from 0.66 to 0.4.

It is useful to know the critical value of $\underline{\lambda}$, such that
yielding of the cross-section would not affect the
lateral stability of beams of compact cross-section,
because the bending resistance is then solely governed by
inelastic local buckling of the compression flange.

Williams and Jemah [88] studied the same problem as
Svensson using a different approach. The elastic
buckling loads for distortional buckling were obtained by
using a computer program VIPASA [89], which is based on
the Von Karman thin-plate theory and is capable of handling
any prismatic assembly of flat uniformly longitudinally
compressed rigidly connected plates. In the analysis,
the web and the bottom flange were divided into 5 equal

and 2 equal segments respectively. It was found that the results from VIPASA were lower than those obtained by Svensson. To achieve a closer agreement between the predictions from the plate theory and the equivalent strut concept, it was suggested that it would be safer to add 15% of the web area to the flange area, when finding σ_{cr} by treating the bottom flange as an elastically supported column. Also more comprehensive design curves were given including fixed-ended beams and cantilevers.

More recently Goltermann and Svensson [90] presented a refinement of the column on elastic foundation method, which includes the effect of rotational restraint at the top flange, passing on to the bottom flange. The model (Fig. 2.10) adds 15% of the web to the free flange, and replaces the previous foundation stiffness k by an equivalent stiffness k_{eq} as,

$$1/k_{eq} = \underset{\text{(top flange)}}{1/k_f} + \underset{\text{(web)}}{1/k_w} \tag{2.23}$$

where k_f = torsional restraint to the top flange

$$k_w = Et^3/4(1-v^2)d^3$$

for an inverted-U frame, k_f can be derived as,

$$k_f = 2(EI)_G /h^2 L$$

where

$(EI)_G$ is the flexural stiffness of an unit strip of
the concrete slab in the transverse direction

h   is the distance between the centroids of the

slab and the bottom flange

L is the distance between the two parallel beams

The governing differential equation was again solved in a non-dimensional form by satisfying the boundary conditions for pin-ended struts, but this time elastic Saint Venant torsional effect was introduced into the problem, that was previously ignored by Svensson. Design tables for eight loading cases were given to obtain the elastic distortional buckling stress σ_{cr}.

For design purpose, Svensson suggested to limit the compressive stress σ_{11} at the bottom flange in line with the approach adopted in Eurocode 3 as

$$\sigma_{11}/f_y = 1/(1+\lambda^4)^{0.5} \qquad (2.24)$$

where λ is defined in Eqn. (2.22)

A computer program has been developed in the present work including the restraining effect of the slab and the 15% of web added to the equivalent column, which can be used to obtain the elastic distortional buckling stress for beams subject to arbitrary moment distribution. In the program Galerkin's method is used to solve equation (2.19) with $k = k_{eq}$ and the eigenvalue routine to find the lowest buckling load is based on reference (91). The results are similar to those obtained by Williams and Jemah.

It should be pointed out that interaction of local and distortional buckling cannot be modelled in a column on elastic foundation type problem. Therefore the above discussions of evaluating the critical buckling stress apply only to slender composite beams, which have low flange B/T ratios, but high span-to-flange width L/B ratios. For compact beams (Class 1 and 2), the elastic critical buckling stresses for distortional buckling are usually well above f_y, so inelastic local buckling of the bottom flange may precede lateral buckling and becomes a governing factor on the beam bending resistance. The elastic critical buckling stress is also underestimated by assuming the boundary conditions at the two ends of the column as pin-ended.

2.4.2.5 Energy method with web distortion

To be consistent with the current design practice for lateral-torsional buckling of steel beams in BS5950 : Part 1 [2], Lawson and Rackham [92] have recently proposed a less conservative method for checking distortional lateral buckling of composite beams in the hogging region to take into account the effect of web distortion modifying the effective slenderness λ_{LT}, defined in the code as,

$$\lambda_{LT} = nuv_t\lambda \qquad (2.25)$$

where

n   is the slenderness correction factor (for shape
     of bending moment diagram)

u   is the buckling parameter (=0.9 for universal
     beams)

v_t is the slenderness factor (torsional effect and
     shear centre, etc)

λ   is the slenderness of the beam length between
     lateral and torsional restraints

This equation is similar to Eqn.(2.8) used in BS5400:Part
3.

In the analysis, the top flange was assumed to be fully
restrained by the concrete slab both laterally and
torsionally, but the torsional stiffness of the slab was
not included. Assuming a half sine wave buckle of L due
to uniform bending moment, it can be shown that using
energy method the slenderness factor v_t is modified to
allow for web distortion as,

$$v_t = \frac{1}{[\ 1 + (\lambda/x)^2/40 + (L/D)^3 I_w L/16 I_y\ ]^{0.5}} \qquad (2.26)$$

where

L is the buckling length

I_w is the second moment of area of the web per
   unit length = $t^3/12$

I_y is the second moment of area of the steel beam
about its minor axis

λ is the slenderness ratio = L/r_y, where r_y is the
radius of gyration of the steel section about its
minor axis

x is the torsional index of the steel section

D is the overall depth of the steel section

Combining eqns (2.25) and (2.26) and differentiating λ_{LT}
with respect to L to obtain the maximum value, it gives,

$$L_{cr} = 3.74 \ I_y^{0.25} \ (D/t)^{0.75} \tag{2.27}$$

Substituting L_{cr} into Eqn. (2.24), it gives,

$$\upsilon_t = 1 / [\ 2 + (\lambda /x)^2 /40\ ]^{0.5}$$

where $\lambda = L_{cr} /r_y$

Ignoring the small term involving the torsional index in
υ_t and substituting the sectional properties for
symmetrical I-sections, the effective slenderness λ_{LT} in
Eqn.(2.23) can be rewritten as,

$$\lambda_{LT} = 6.55 \ nu(T/B)^{0.25} \ (D/t)^{0.75}$$
$$= 5.9 \ n \ (T/B)^{0.25} \ (D/t)^{0.75} \tag{2.28}$$

The slenderness correction factor n is dependent on the
value of L_{cr} obtained from Eqn. (2.27). If L_{cr} is
greater than the length of the hogging moment region, it
is conservative to assume n as 0.77 in Eqn. (2.28), that

corresponds to a linear bending moment diagram over L_{cr}. Otherwise n is to be calculated from the moment ratio β at the location given by L_{cr} from Table 16 of BS5950 : Part 1. Lawson and Rackham suggested that λ_{LT} should be less than 34 and 30 for grade 43 and 50 steel beams respectively, to enable the use of the plastic moment resistance of the section without lateral restraint along the member. Buckling resistance moment is to be obtained following the procedures using λ_{LT} in Eqn. (2.28) as BS5950 : Part 1.

The latest design recommendation [93] for distortional lateral buckling of continuous composite beams in Eurocode 4, which is presently being revised, follows a rather similar approach to that adopted by Lawson. Details of the method are given in Appendix D. This revised method is intended to be consistent with Eurocode 3 (also under revision) in dealing with lateral-torsional buckling of steel beams. In this method the buckling resistance moment of a laterally unrestrained composite beam is determined by its elastic critical buckling moment, M_{cr}, for the whole cross-section in hogging bending. The analytical model, as shown in Fig. 2.11, replaces restraining effects by the concrete slab to the steel beam as continuous horizontal and torsional restraints to the upper flange. The effect of web flexibility is taken into account by modifying the torsional stiffness using the similar approach as in Eqn.

(2.23). A correction factor, C_4, is introduced to allow for the influence of the bending moment distribution along the span under consideration, and this factor is equivalent to the factor n used in BS5950 : Part 1. A slenderness factor χ_{LT} similar to λ_{LT} in Eqn. (2.25), is used to obtain the buckling resistance moment. A simple check for beams not affected by lateral-torsional buckling without direct calculation of χ_{LT} is also provided.

2.7 Experimental work on distortional lateral buckling

Compared to theoretical works, few experimental result
on distortional lateral buckling of composite beams are
available. This is probably because the cost of a
realistic test specimen that models U-frame behaviour in
a continuous composite beam is high, and the testing set-
up and procedures are also more complex than that of a
double cantilever T-beam test.

Takeshi and Wakabayashi [94] have carried out three
experiments to investigate the restraining effect of pre-
cast reinforced concrete slab against lateral buckling of
I-beams. However in the experiments the pre-cast slab
units were discontinuous longitudinally along the beam,
and therefore the reinforced concrete slab did not
contribute any additional strength to the composite
cross-section apart from restraining the top flange
laterally and torsionally. The precast units were
connected to the steel section by bolts of 8 mm in
diameter inside pockets at a spacing of 100 mm centre-to-
centre along the beam. The bolts were welded on the beam
with threads at the top, then tightened up after the
units were laid. Each of the test specimens was
essentially an inverted U-frame, and the beam dimensions
were 200 mm in height, 60 mm in flange width (top and
bottom) and 6 mm in thickness of both flanges and web.
The beams were built-up by welding using 6 mm thick mild

steel plates. The distance between the two parallel beams attached by the slab was 2000 mm and the slab was 50 mm thick. The length of the lateral unrestrained region varied from 2500 mm to 6500 mm subject to hogging bending. Although the slab was quite flexible, it was observed from the tests that lateral displacement and twist of the upper flange were very small. The results indicated that the maximum strength was 8% higher than the plastic moment of resistance for a beam under linear moment gradient between the two lateral restraining points, when the slenderness ratio about the weak axis L/r_y of the steel section is 600; but when the bottom flange was subjected to uniform compression under uniform hogging moment, the maximum strength was lower than the plastic moment in a small amount of less than 7%.

As discussed in the previous section, most of the theoretical research related to the stability problem of plate girders rather than hot-rolled sections. In practice for a majority of buildings and short span bridges (less than 20 m), hot-rolled steel sections, which are mostly in Class 1 and 2, are often used. In the absence of lateral-torsional buckling, these members are allowed to reach the plastic moment of resistance of the composite cross-section. It is therefore beneficial to explore the restraining effect of the slab to the beam using beams of proportions such that distortional lateral buckling does not occur before the attainment of the

plastic moment of resistance. Therefore the most interesting composite beams for research are those having cross-section near the borderline between Class 2 and Class 3, because by definition a Class 3 beam can only be designed up to the first yield moment of resistance. Previous experiments on isolated T-beam double cantilevers usually have very short length, in general less than 2.5 m, but in practice the hogging region in a continuous beam may be longer than that, for example an end span of a continuous beam is subjected to dead load only, and the adjacent span is fully loaded. In some tests [13,14,15,95] distortional lateral buckling has occurred soon after local buckling, and the results are plotted in Fig. 2.12 and 2.13 using two relevant slenderness parameters - web flexibility slenderness k (Eqn. 2.18) and lateral slenderness ratio L_o/r_{cp} in which L_o is the length of the hogging region equal to the length of the cantilever, and r_{cp} is the radius of gyration of the portion of web and bottom flange in compression below the plastic neutral axis about the minor axis of the steel section. The use of these two parameters provides a common basis for the comparison of various results.

Fig. 2.12 shows that for composite beams using hot-rolled sections, the web slenderness k values are in the range from 0.3 to 0.5, which is practical for buildings. The three specimens at the other end of the spectrum tend to

be too shallow and are therefore not normally used to the construction of main and secondary beams. In addition from Fig. 2.13 no composite beams having L_o/r_{cp} ratio above 125 had been tested, until the present series of tests. However this value can be as high as 200 in practice. To provide some experimental backing for the theoretical work four double-cantilever tests of realistic scale, 2 T-beams and 2 inverted-U frames, have been carried out in this project. The true strength of a real beam (point B in Fig. 2.5) can only be obtained from an experiment, and this value is then used for comparison with various theoretical predictions, usually obtained from elastic buckling theory (point A in Fig. 2.5.). The test results, in particular the two inverted-U frames, are useful for the calibration of the existing and proposed design methods.
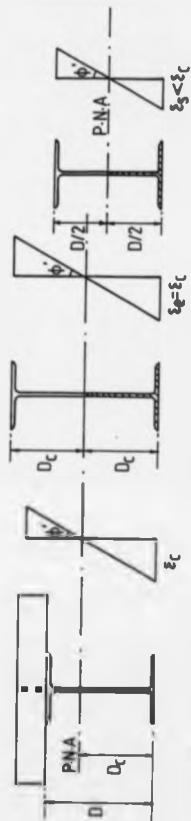
Composite cross-section   Equivalent steel cross-section   Steel cross-section

ϕ = hogging curvature , ε_c, ε_e, ε_s = compressive strains of the bottom fibre

Fig. 2.1 Strain distributions for composite and plain steel sections
in hogging bending
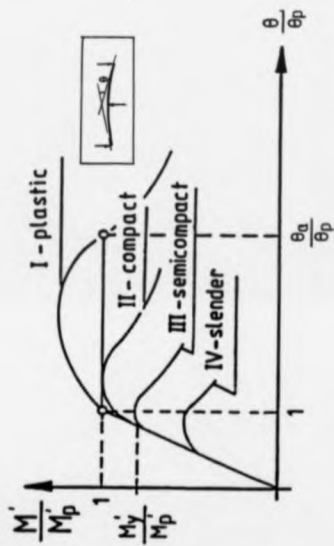
Fig. 2.2 Moment-rotation curves for profiles with different cross-sectional classes

Distortional lateral buckling further away from the support

Due to web distortion   Slab rotation   Pull-out of shear stud

$\delta = \delta_1 + \delta_2 + \delta_3$ and $\delta_1 > \delta_2 > \delta_3$
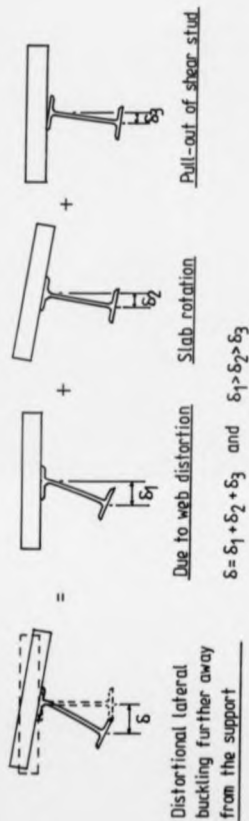
Local buckling near the support

Fig. 2.3   Instability of continuous composite beams in the hogging moment region
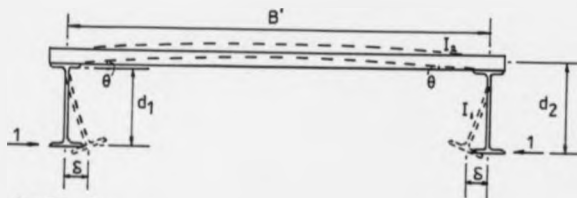
$\delta = \delta_1 + \delta_2$

$\delta_1 = d_1^3 / 3EI_1$ (deformation due to web bending)

$\delta_2 = Bd_2^2 / 2EI_2$ (deformation due to flexure of slab)

INVERTED U-FRAME

$\delta = \delta_1 + \delta_2$
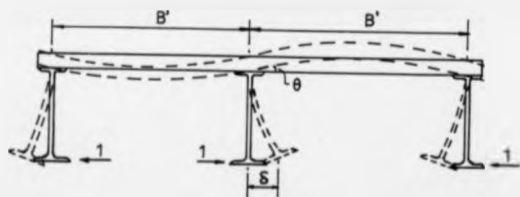
$\delta_1 = d_1^3 / 3EI_1$ (web bending)

$\delta_2 = B'd_2^2 / 3EI_2$ (flexure of slab)

MULTIPLE INVERTED U-FRAME

Fig. 2.4 U-frame action proposed by BS5400:Part 3
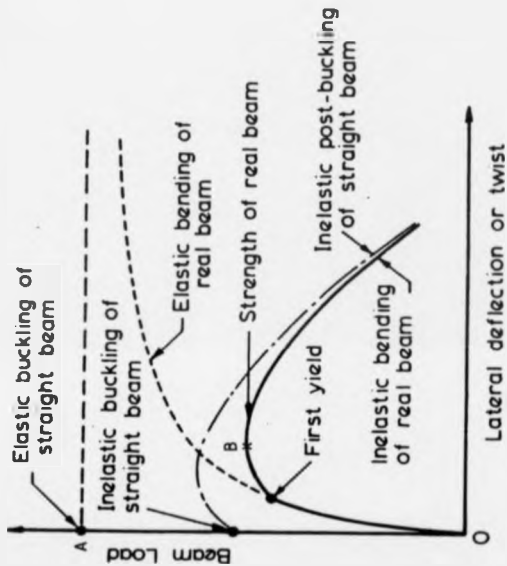
Fig. 2.5 Beam buckling behaviour (adopted from Reference 116)
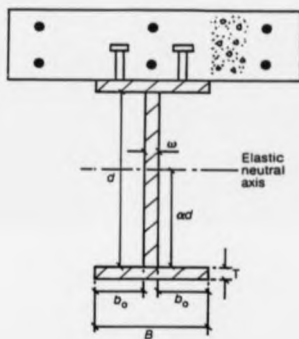
Fig. 2.6 Typical composite cross-section
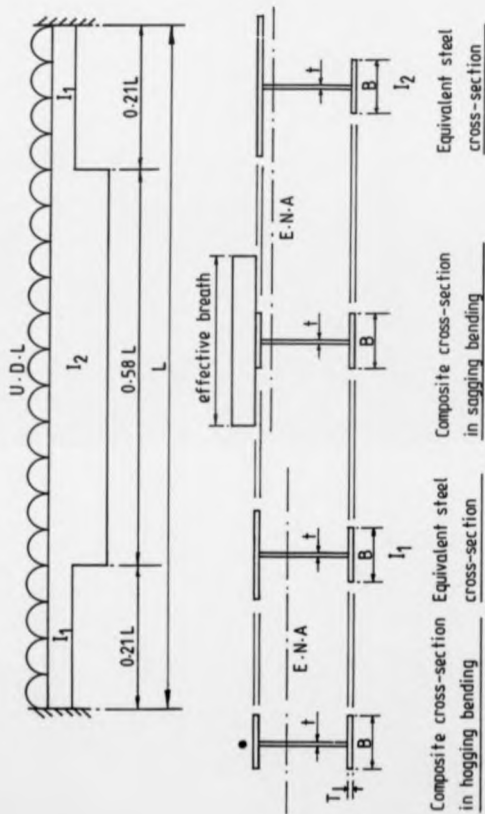
Fig. 2.7 Computer model used by Weston (Reference 77)

Support moment
M'/Mp

- --o--o-- Ref.(5)
- --x--x-- Ref.(77)

$\beta_f = (b_e/T)\sqrt{\sigma_y/355}$ Flange

$\beta_w = (\angle d/w)\sqrt{\sigma_y/355}$ Web

$\sqrt{\beta_f\beta_w}$
Combined slenderness

Symbols refer to Fig. 2·6
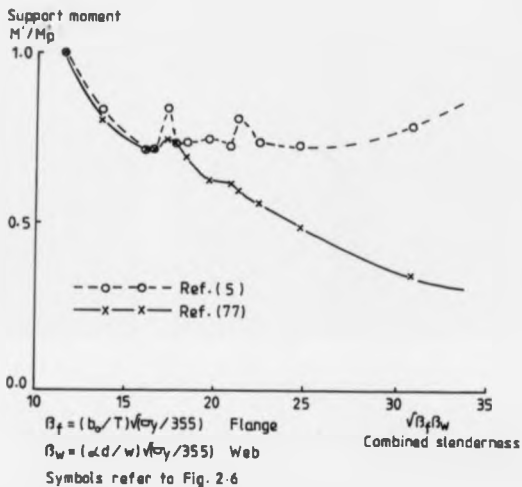
Fig. 2.8 Comparison of predictions between the design methods proposed by Bradford and Johnson (Ref. 5) and Weston (Ref. 77)
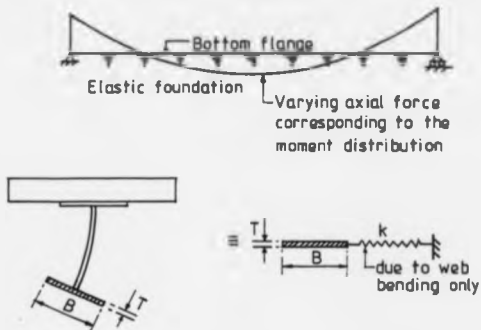
Fig. 2.9 Distortional lateral buckling of the bottom flange modelled as a strut on elastic foundation
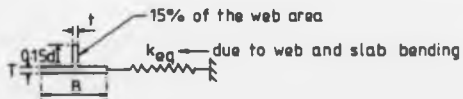
Fig. 2.10 Modified model for the buckling problem of composite beams as a strut on elastic foundation
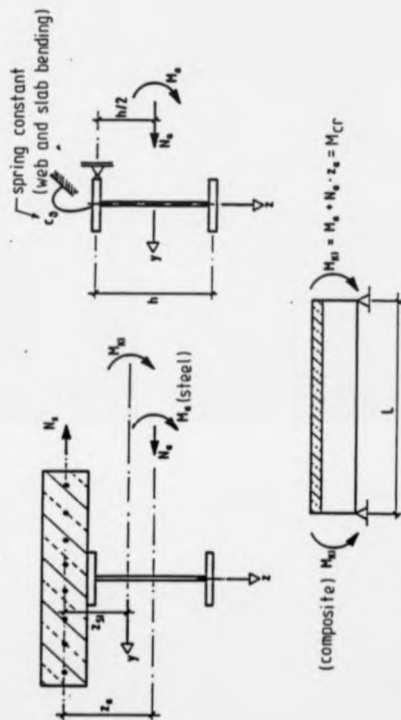
Fig. 2.11 Analytical model used in the draft Eurocode 4 for distortional lateral buckling of composite beams
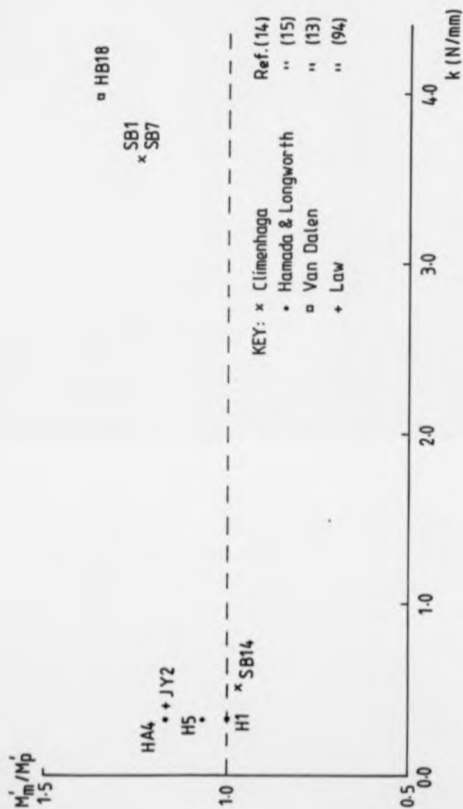
Fig. 2.12 Experimental results of composite double cantilever tests showing distortional lateral buckling plotted against web flexibility
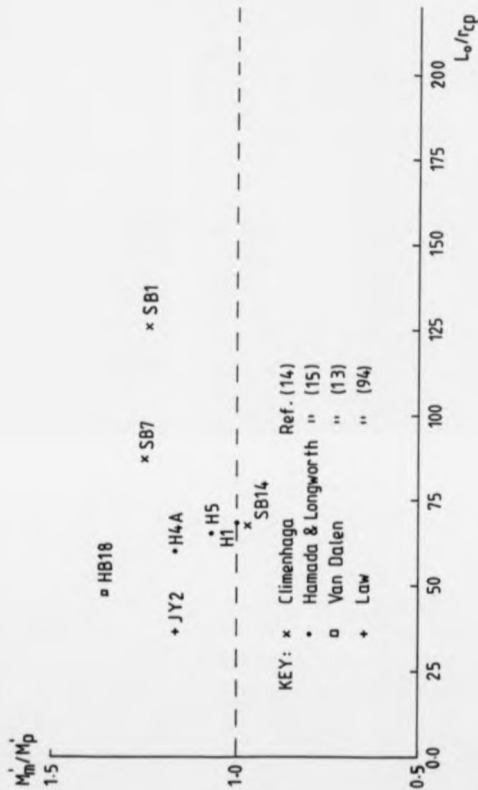
Fig. 2.13 Experimental results of composite double cantilever tests showing distortional lateral buckling plotted against bottom flange strut slenderness

CHAPTER 3
NUMERICAL ANALYSIS OF MOMENT
REDISTRIBUTION IN
CLASS 3 CONTINUOUS COMPOSITE BEAMS

3.1 Introduction

A numerical analysis has been made to assess the amount
of moment redistribution permitted in Class 3 composite
beams in comparison with the limit proposed by the draft
Eurocode 4. A non-linear computer program has been
written in the present study to simulate the behaviour of
two-span beams before and after local buckling at the
internal support, using elasto-plastic moment-curvature
and experimental moment-rotation characteristics. This
chapter describes the treatment of these characteristics
in the program, and presents a mathematical model, which
is based on the compatibility and equilibrium criteria,
for the simulation.

The conditions for a beam to reach its ultimate strength
are defined and incorporated into the program. Finally a
brief description of the numerical technique employed is
given. This chapter should be read in conjunction with
the publication enclosed in Appendix A.

3.2 Material properties

The specimens used in the computer test are divided into two groups - SB and TB series. Grade 50 steel is assumed for all the specimens. The yield stresses of the structural steel for the SB series are based on the measured values for the relevant cantilevers tested by Climenhaga [14], as shown in Table 1 (Appendix A). For the TB series, the yield stresses are taken as 355 N/mm^2. For both series, f_{cu} for the normal-density concrete and f_y for reinforcement are 30 N/mm^2 and 425 N/mm^2 respectively. Details of the stress-strain curves and assumed residual stresses are given in Figures A1 and A2 (Appendix A).

3.3 Elasto-plastic moment-curvature characteristics

The first stage in the computer simulation requires the knowledge of realistic moment-curvature relationships of the composite cross-section in both the hogging and sagging regions. This can be achieved by making the following assumptions:

(1) Plane sections remain plane after bending.

(2) No slip occurs at the steel-concrete interface.

(3) Materials obey the simplified constitutive stress-strain curves given in Section 3.2.

(4) In hogging bending, concrete is assumed to be fully cracked and tension stiffening is ignored.

The procedures for determining the hogging moment-curvature relationship of a composite cross-section are first described. An initial curvature ϕ is first applied to the section (Fig. 3.1) and a trial position $\underline{y}$ for the neutral axis is guessed, which is slightly above the centroid of the steel section. Then the strains ε_ϕ throughout the cross-section can be calculated from,

$$\varepsilon_\phi = \phi \; (\; y - \underline{y} \;) \; + \; \varepsilon_r \qquad (3.1)$$

where

ε_r is the residual strain in the steel section plus the initial strain due to unpropped construction if present.

If the curvature is to be increased by a factor k, equation (3.1) can be rewritten as,

$$\epsilon_\phi = k\phi (y - \underline{y}) + \epsilon_r \qquad (3.2)$$

Then the longitudinal stress σ_s at any position in the steel section and the longitudinal stress σ_{rt} in the reinforcement can be obtained from the material stress-strain curves corresponding to ϵ_ϕ. The out-of-balance axial force in the cross-section corresponding to $\underline{y}$ is calculated from,

$$F(\underline{y}) = \int_{A_s} \sigma_s \, dA_s + \Sigma \sigma_{rt} \, A_{rt} \qquad (3.3)$$

where A_s and A_{rt} are the area of the steel section and the area of the reinforcement respectively.

For pure bending, the out-of-balance axial force must be equal to zero, therefore,

$$F (\underline{y}) = 0 \qquad (3.4)$$

Eqns. (3.3) and (3.4) are combined together and $\underline{y}$ is computed by using the Newton Raphson method [96]. In the program both flanges and the web are each partitioned into 10 equal segments to facilitate the integration in eqn. (3.3) and the modelling of residual stresses. The bending moment corresponding to the curvature $k\phi$ is then obtained from statics as,

$$M' = M' (k\phi)$$

$$= \int_{A_s} y \; \sigma_s \; dA_s \; + \; \sum y_{rt} \; \sigma_{rt} \; A_{rt} \qquad (3.5)$$

where y_{rt} is the distance from the top of the slab to the reinforcing bar with area A_{rt}

The integration in eqn. (3.5) is carried out numerically assuming a linear stress distribution across each segment. The initial curvature ϕ is conveniently taken as 1/8 of that corresponding to the first yield moment based on the elastic theory. By increasing the scale factor k linearly, a full set of hogging moment-curvature relationships $M'- \phi'$ is found.

For the sagging moment-curvature characteristics, the procedures are the same as above except that reinforcement in the slab is ignored and the slab is divided into 8 equal horizontal strips to facilitate the numerical integration in eqns. (3.3) and (3.5). The initial trial value of y is one-tenth of the web depth below the upper flange of the steel section. Similarly a full set of sagging moment-curvature relationships $M - \phi$ is obtained.

3.4 Mathematical model for a two-span continuous beam

Multi-span beams have a higher degree of redundancy, and
the various patterns of imposed loading usually lead to
the provision of more surplus strength than that in two-
span beams of uniform depth. Two-span beams therefore
benefit most from the redistribution of moment, so only
they have been considered in the present study. For a
two-span beam subject to a given system of loads as shown
in Fig. 3 in Appendix A, the bending moment at the
internal support is indeterminate. It can be found by
considering the relationships of moment and curvature,
equilibrium and compatibility conditions. For a guessed
arbitrary support bending moment, the bending moment
diagram is uniquely defined and the corresponding
curvatures in the hogging and sagging regions can be used
to check whether the compatibility conditions of the beam
are satisfied. The beam is assumed to be braced against
lateral buckling and local buckling is assumed to occur
when the support section reaches first yield, that is
$M_c' = M_y'$ (composite). The theoretical models for the
pre-buckling and post-buckling stages are given below.

3.4.1 Pre-local-buckling model

With reference to Fig. 3.2, compatibility equations to
satisfy continuity can be derived for each span as
follows:

Considering the right hand span (symbols shown in the figure are positive),

$$\beta_2 = \int_{L_{02}}^{L_2} \phi \ dx \qquad (3.6)$$

where ϕ is the sagging curvatures corresponding to the bending moment diagram.

$$\beta_2 = \alpha_{C2} + \theta_2' + \alpha_E \qquad (3.7)$$

But

$$\theta_2' = \int_0^{L_{02}} \phi' \ dx \qquad (3.8)$$

where ϕ' is the hogging curvatures corresponding to the bending moment diagram.

Therefore, combining eqns. (3.6) to (3.8), it gives,

$$\alpha_E = \int_{L_{02}}^{L} \phi \ dx \ - \ \int_0^{L_{02}} \phi' dx - \alpha_{C2} \qquad (3.9)$$

The requirement of compatibility for no lack of fit at point E is given by,

$$\delta_2 = \delta_{21} + \delta_{22} + \delta_{23} \qquad (3.10)$$

where

$$\delta_2 = \int_{L_{02}}^{L_2} \phi \ (L_2 - x) \ dx$$

$$\delta_{21} = \alpha_{C2} \ L_{02}$$

$$\delta_{22} = \int_0^{L_{02}} \phi' \ (L_{02} - x) \ dx$$

$$\delta_{23} = (\alpha_{C2} + \theta_2') \ (L_2 - L_{02})$$

Hence,

$$\int_{L_{02}}^{L_2} \phi(L_2-x)\,dx = \alpha_{C2}L_{02} + \int_0^{L_{02}} \phi'(L_{02}-x)\,dx$$
$$+ (\alpha_{C2} + \theta_2')\,(L_2 - L_{02}) \qquad (3.11)$$

After simplification, eqn. (3.11) becomes,

$$\alpha_{C2}L_2 = \int_{L_{02}}^{L_2} \phi(L_2-x)\,dx - \int_0^{L_{02}} \phi'(L_{02}-x)\,dx$$
$$- \theta_2'(L_2 - L_{02}) \qquad (3.12)$$

Substituting θ_2' from eqn. (3.8) in eqn. (3.12), it gives,

$$\alpha_{C2} = [\int_{L_{02}}^{L_2} \phi(L_2-x)\,dx - \int_0^{L_{02}} \phi'(L_2-x)\,dx] / L_2$$
$$(3.13)$$

Equations (3.9) and (3.13) define the beam rotations at the two supports C and E.

Now, considering the left span in Fig.3.2,

$$\beta_2 = \int_{L_{01}}^{L_1} \phi\,dx \qquad (3.14)$$

$$\beta_2 = \theta_1' - \alpha_{C1} + \alpha_A \qquad (3.15)$$

But $\theta_1' = \int_0^{L_{01}} \phi'\,dx \qquad (3.16)$

Hence, combining eqns. (3.14) to (3.16), it gives,

$$\alpha_A = \int_{L_{01}}^{L_1} \phi\,dx - \int_0^{L_{01}} \phi'\,dx + \alpha_{C1} \qquad (3.17)$$

Similarly the requirement of compatibility for no lack of fit at point A is given by,

$$\delta_1 + \delta_{11} = \delta_{12} + \delta_{13} \qquad (3.18)$$

where

$$\delta_1 = \int_{L_{01}}^{L_1} \phi \ (L_1 - x) \ dx$$

$$\delta_{11} = \alpha_{C1} L_{01}$$

$$\delta_{12} = \int_0^{L_{01}} \phi' \ (L_{01} - x) \ dx$$

$$\delta_{13} = (\theta_1' - \alpha_{C1}) \ (L_1 - L_{01})$$

Hence,

$$\int_{L_{01}}^{L_1} \phi \ (L_1 - x) \ dx + \alpha_{C1} L_{01}$$

$$= \int_0^{L_{01}} \phi' \ (L_{01} - x) \ dx + (\theta_1' - \alpha_{C1}) \ (L_1 - L_{01})$$

$$(3.19)$$

Substituting θ_1' from eqn. (3.16) in eqn. (3.19), it gives,

$$\int_{L_{01}}^{L_1} \phi (L_1 - x) \, dx + \alpha_{C1} L_1 = \int_0^{L_{01}} \phi' \ (L_1 - x) \, dx$$

or

$$\alpha_{C1} = [\int_0^{L_{01}} \phi' \ (L_1 - x) \, dx - \int_{L_{01}}^{L_1} \phi \ (L_1 - x) \, dx \ ] \ / \ L_1$$

$$(3.20)$$

Equations (3.17) and (3.9) define the beam rotations at the two end supports A and E.

For continuity of the beam over the internal support, the two beam rotations, α_{C1} and α_{C2}, derived for either span independently from eqns. (3.20) and (3.13), must be equal and this condition is used to find a compatible

moment distribution along the member which is a function
of the values of the support moment and the applied
loads. If the design ultimate loads, w_1 and w_2 in
Fig. 3 in Appendix A, are known, for instance they have
been calculated in accordance with the draft Eurocode 4
in the present work, then they can be referred as a datum
in the iterative process of finding the correct moment
distribution at any given load level.

3.4.2 Post-local-buckling model

When the internal support reaches the first yield moment
M_y', for a Class 3 section local buckling is assumed to
begin. As a result of buckling, the support moment
starts to drop in association with an irreversible
rotation concentrated in the destabilising region. This
was observed in tests of double cantilevers [14], and the
region is of the length about h_a adjacent to the
support, where h_a is the depth of the steel section.
Furthermore local buckling was observed to occur usually
on one side only of a double cantilever, and therefore in
a two-span beam local buckling is assumed to occur in the
span having the less steep hogging moment gradient. Due
to the localised feature, the moment-rotation behaviour
of hogging moment regions of a two-span beam can be
treated as a quasi-double cantilever, and so the
behaviour from these tests is used to predict the post-
buckling characteristics.

After buckling, the total rotations of the two hogging regions θ_1' and θ_2' measured at the corresponding point of contraflexure, as shown in Fig. 3.2, consist of two components, which are the elastic and irreversible rotations, θ_e' and θ_i'. Therefore,

$$\theta_1' = \theta_{e1}' + \theta_{i1}' \qquad (3.21)$$

where

$$\theta_{e1}' = \int_0^{L_{01}} M'/(EI)_{eq} \, dx \ ,$$

in which,

$$(EI)_{eq} = 0.5 \, E_s \, (I_c + I_u),$$

the effective flexural stiffness of a cracked composite section due to elastic unloading (reference (97)) and I_c and I_u are the cracked and uncracked second moments of area of composite cross-section respectively, and I_u is calculated taking E for concrete from the initial slope of the stress-strain curve in Fig. A1, with a material factor $\gamma_m = 1.5$.

Similarly,

$$\theta_2' = \theta_{e2}' + \theta_{i2}' \qquad (3.22)$$

where

$$\theta_{e2}' = \int_0^{L_{02}} M'/(EI)_{eq} \, dx$$

θ_{i1}' and θ_{i2}' are the irreversible rotations assumed to be concentrated at points $h_a/2$ on each side from the internal support.

Substituting θ_1' from eqn. (3.21) in eqn. (3.18), and noting that,

$$\delta_{12} = \int_0^{L_{01}} M'(L_{01}-x)/(EI)_{eq} \, dx$$
$$+ \theta_{i1}' (L_{01} - 0.5h_a)$$

, it gives,

$$\int_{L_{01}}^{L_1} \phi(L_1 - x) \, dx + \alpha_{C1}L_{01}$$

$$= \int_0^{L_{01}} M'(L_{01}-x)/(EI)_{eq} \, dx +$$

$$\theta_{i1}' (L_{01} - 0.5h_a) +$$

$$[\int_0^{L_{01}} M'/(EI)_{eq} \, dx + \theta_{i1}' - \alpha_{C1}] (L_1 - L_{01})$$

$$(3.23)$$

After simplification, eqn. (3.23) becomes,

$$\alpha_{C1} = [\int_0^{L_{01}} M'(L_1-x)/(EI)_{eq} \, dx - \int_{L_{01}}^{L_1} \phi(L_1 - x) \, dx$$
$$+ \theta_{i1}' (L_1 - 0.5h_a)] / L_1 \qquad (3.24)$$

Substituting θ_2' from eqn. (3.22) in eqn. (3.10), and noting that,

$$\delta_{22} = \int_0^{L_{02}} M'(L_{02} - x)/(EI)_{eq} \, dx +$$
$$\theta_{i2}'(L_{02} - 0.5h_a)$$

,it gives,

$$\int_{L_{02}}^{L_2} \phi(L_2 - x) \, dx$$

$$= \alpha_{C2}L_{02} + \int_0^{L_{02}} M'(L_{02} - x)/(EI)_{eq} \, dx +$$

$$\theta_{i2}' (L_{02} - 0.5h_a) +$$

$$(\alpha_{C2} + \int_0^{L_{02}} M'/(EI)_{eq} \, dx + \theta_{i2}') (L_2 - L_{02})$$

$$(3.25)$$

After simplification, eqn. (3.25) becomes,

$$\alpha_{C2} = [\int_{L_{02}}^{L_2} \phi(L_2 - x) \, dx -$$

$$\int_0^{L_{02}} M'(L_2 - x)/(EI)_{eq} \, dx -$$

$$\theta_{i2}' (L_2 - 0.5h_a)] / L_2 \qquad (3.26)$$

Equations (3.24) and (3.26) define the beam rotation at the internal support in the post-buckling range, provided that the two irreversible rotations θ_{i1}' and θ_{i2}' are known. Again for continuity over the support α_{C1} must equal to α_{C2} , and this condition is therefore used to find a compatible moment distribution such that the support moment is redistributed to the mid-spans as the uniformly distributed loads increase.

3.5 Flexural stiffnesses and load arrangements

The design ultimate loads, w_1 and w_2, for a two-span beam as shown in Fig. 3 (Appendix A), are calculated in accordance with draft Eurocode 4. These loads are then used as references in the numerical analysis, and the applied loads are presented by $w_1' = \lambda w_1$ and $w_2' = \lambda w_2$, where, λ is a load factor. Realistic spans L_1 and L_2 (with $L_2 \geqslant L_1$) and appropriate cross-sections are chosen. Cross-sections at the support are in Class 3 and mid-span sections are in Class 1 or 2, as defined in draft Eurocode 4. The 'cracked reinforced' section is assumed to be uniform over the hogging moment region, taken in Eurocode 4 as 15% of the span on each side of the internal support, and the 'uncracked unreinforced' section is used elsewhere.

The calculation of w_1 and w_2 is explained in Section 7 of the published paper (Appendix A). For propped construction, w_2 can be obtained from equilibrium as,

$$w_2 = [2(2M_y - M_y') + 4(M_y^2 - M_y M_y')^{0.5}] / L_2^2$$

(3.27)

where M_y and M_y' are the first yield sagging (+ve) and hogging (-ve) moment of resistances of the composite section respectively

The use of M_y corresponded to a restriction in EC 4 that behaviour at midspan had to be elastic, if redistribution

of moment was to be used at a support. This was intended
to limit the rotation requirement at the support. After
w_2 is known, w_1 is then found from the compatibility
condition that the vertical deflection of the loaded beam
at the internal support must be zero. Since the values
of the flexural stiffnesses, $(EI)_u$ and $(EI)_c$, may vary
for individual specimens, it becomes necessary to derive
a general expression for w_1. Referring to Fig. 3 in
Appendix A, it is convenient to define two parameters α
and β as,

$\alpha = (EI)_c / (EI)_u$

and $\beta / (1- \beta)$ = the ratio of uncracked length to
cracked length for each span.

β is taken as 0.85 in the figure according to the
draft Eurocode 4.

Using the virtual work method, w_1 can be calculated from,

$$w_1 = \{ 1.25M_y' - w_2 L_1 L_2^2/2(L_1+L_2)$$
$$+ w_2 L_1 L_2 [L_2 (\beta^3 + 1/\alpha - \beta^3/\alpha) / 2L_1$$
$$- 3L_2^2 (\beta^4 + 1/\alpha - \beta^4/\alpha)/ 8L_1(L_1+L_2)] /$$
$$(\beta^3 + 1/\alpha - \beta^3/\alpha) \} \times$$
$$\{ 0.5L_1 L_2 - L_1 L_2 [(L_1^2+L_2^2) (4\beta^3$$
$$- 3\beta^4 - 4\beta^3/\alpha + 3\beta^4/\alpha + 1/\alpha) / 8L_1 L_2$$
$$+ 3(\beta^4 + 1/\alpha - \beta^4/\alpha) /8] / (\beta^3 + 1/\alpha - \beta^3/\alpha)$$
$$- L_1 L_2^2/2(L_1+L_2)$$
$$+ L_1 L_2 [L_2 (\beta^3 + 1/\alpha - \beta^3/\alpha) / 2L_1$$
$$- 3L_2^2 (\beta^4 + 1/\alpha - \beta^4/\alpha) / 8L_1(L_1+L_2)] /$$
$$(\beta^3 + 1/\alpha - \beta^3/\alpha) \}^{-1} \qquad (3.28)$$

Equations (3.27) and (3.28) are incorporated in a pre-processor program.

For unpropped construction, M_y' and M_y (Fig. B1, Appendix A) are deduced from two separate loading cases — uniformly distributed dead loads and imposed loads, and consist of two components — steel and composite moment of resistances. They are given as,

$$M_y' = M_s' + M_{cm}' \quad \text{(hogging)} \quad (3.29)$$
$$\text{and} \quad M_y = M_s + M_{cm} \quad \text{(sagging)} \quad (3.30)$$

where suffixes s and cm denote steel and composite sections respectively

Instead of w_2, the maximum imposed load $1.5q_2$ on span L_2 is found by replacing M_y' and M_y in eqn. (3.27) by M_{cm}' and M_{cm} in eqns. (3.29) and (3.30). The load $1.5q_1$ for span L_1 is obtained by elastic analysis as above for w_1 in eqn. (3.28), but w_2 is now replaced by $1.5q_2$ and the first term $1.25M_y'$ related to the amount of redistribution is altered to eliminate the hogging moment caused by the dead loads, as the beam is not composite at that stage, as,

$$1.25M_y' - M_s' = 1.25 \ (M_s' + M_{cm}') - M_s'$$
$$= 0.25M_s' + 1.25M_{cm}'$$

The design loads w_1 and w_2 are then the summation of the dead loads and the imposed loads obtained as above.

3.6 Method of analysis

Based on the mathematical model described in Section (3.4), a FORTRAN program BAULS.F77 has been written to analyse two-span Class 3 continuous composite beams in both the pre-local-buckling and post-local-buckling ranges. Details of the program are described here.

3.6.1 Moment-curvature relationships

For propped construction, the elasto-plastic moment-curvature relationships for the hogging and sagging regions are generated using the method given in Section (3.3), which takes into account material non-linearity and residual stresses.

For unpropped construction, the steel section has previously been subjected to dead loads and therefore ε_r in eqn. (3.1) needs to include the initial strains compatible with the applied moments. However the bending moments along a uniformly loaded two-span steel beam are not uniform, consequently the initial strains may not be the same for different cross-sections, depending on the shape of the bending moment diagram. To overcome this problem, an approximation is made to replace the original moment diagram by initial equivalent constant moments in both the hogging and sagging regions. The error is in strain, not in stress, so it diminishes as yielding

develops, and the uncertainly of residual stresses
(another error) is also a diminishing error at high
strains. These equivalent moments are obtained by
equating the area enclosed by the bending moment diagram
due to dead loads only by rectangular blocks of the same
area in both regions. In the program, for a symmetrical
two-span beam these moments in the hogging and sagging
regions are simply taken as half of the internal support
moment and two-thirds of the maximum sagging moment
respectively. These initial moments create initial
strains across the steel section, which are then combined
with residual strains and strains due to imposed loads in
the composite cross-section in eqn. (3.1), subsequently
the hogging and sagging moment-curvature relationships
are obtained by means of the same numerical technique as
for the case of propped construction.

3.6.2 Details of the computer program

There are two stages in the analysis, pre-local-buckling
and post-local-buckling. A two-span beam specimen is
assumed to be subjected to λw_1 and λw_2 on spans L_1
and L_2 respectively, where w_1 and w_2 are found as
discussed in Section 3.5. From the equilibrium and
continuity conditions, the bending moment at the internal
support can be obtained compatible with the applied loads
using realistic moment-curvature relationships. When the
support moment is less than M_y' , for a Class 3 section

local buckling is assumed not to occur. Therefore
equations (3.13) and (3.20) are used to search for the
correct support moment in relation to the applied loads.
The support moment is iterated in the analysis until the
absolute difference of the two beam rotations α_{C1} and
α_{C2} is less than 0.1mrad using the Newton Raphson
technique. At each iteration, curvatures along the beam
are defined by the bending moment diagram and the
numerical integration of curvatures is carried out using
Simpson's method. In the pre-buckling analysis, the
load factor λ is started off at a convenient value
(usually 0.75) and is then increased monotonically by a
fixed increment (usually 0.01). When the support moment
reaches $M_y{}'$, local buckling is assumed to take place
and the current λ is denoted as λ_b, which is the
buckling load factor giving the serviceability loads of
the beam.

At the onset of local buckling, the bending moment
diagram of the beam is uniquely defined by knowing the
internal support moment $M_y{}'$ and the applied loads $\lambda_b w_1$
and $\lambda_b w_2$. Using the post-buckling analytical model
described in section 3.4.2, an irreversible rotation $\theta_b{}'$
compatible with this moment diagram can be found. First
$\theta_b{}'$ is substituted as $\theta_{11}{}'$ and $\theta_{12}{}'$ in equations (3.24)
and (3.26) respectively; iterative procedures based on
the Newton Raphson method are used to obtain $\theta_b{}'$ such
that the beam rotations α_{C1} and α_{C2} on either side of

the internal support become equal and the tolerance limit
is set to be 0.1 mrad in the program. The angle $2\theta_b'$
concentrated near the internal support is essential to
satisfy the continuity condition that makes compatible
the new curvatures appearing in eqns. (3.24) and (3.26).

In the subsequent post-buckling analysis, the
irreversible rotation θ_i' on the buckled span is
assumed to follow the path of a bi-linear curve as shown
in Fig. C1 in Appendix A. For beams of practical
dimensions, this model compares favourably with the
results of double-cantilever tests as shown in Fig. 2
(Appendix A). In a real Class 3 beam, the hogging moment
of resistance is usually higher than M_y' and the
corresponding irreversible rotations are also higher than
those predicted in Fig.2 (Table A1 in Appendix A).
These provide a margin of safety in the model to avoid
unrealistic redistribution of moments from the internal
support to the mid-spans. Irreversible rotations are
assumed to follow the path PQR for the span with local
buckling and the path PS for the other span in Fig. C1.
At a given support moment, these rotations are TU and TV
in the non-buckling span and the buckling span
respectively and are substituted in eqns. (3.24) and
(3.26) for θ_{i1}' and θ_{i2}', depending on which span is
chosen to be the buckling span. To search for a
compatible solution, in contrast to the pre-buckling
analysis, the support moment M_c' is decreased

monotonically by a fixed amount (usually $0.01M_y'$) and the load factor λ ($> \lambda_b$) is iterated using the Newton Raphson technique until a new λ factor is found such that eqns. (3.24) and (3.26) for the beam rotations at the internal support are satisfied simultaneously with the associated curvatures.   An accelerated iteration scheme is employed to speed up the convergence process and is explained in the next section.   The failure loads $(\lambda = \lambda_f)$ are assumed to be reached when either

(i) M_c' at the internal support drops below $0.6M_y'$,

(ii)   the tensile strain in reinforcing steel exceeds
         0.01,

(iii)   the maximum compressive strain in concrete
         reaches 0.0035,

(iv)   the maximum stress in structural steel reaches
         $1.3\sigma_y$, or

(v)   the iteration for a new load increment fails to
         converge.

Criterion (ii) is to avoid debonding between the concrete and reinforcement, and assumes constant curvatures ϕ_b in the buckled region, so ϕ_b is equal to θ_1' / h_s. Tensile strain in reinforcing steel is then calculated with reference to the elastic neutral axis of the cracked cross-section.   Criteria (iii) and (iv) are monitored by checking the moment-curvature characteristics involved in the integrations in eqns. (3.24) and (3.26).

3.6.3 Accelerated iteration scheme

In the post-buckling range, the support moment M_c' is decreased monotonically by a fixed step. For a given value of M_c', the compatibility requirement is to find a λ factor, which satisfies eqns. (3.24) and (3.26) with the curvatures generated from the bending moment diagram, such that

$$F(\lambda) = |\alpha_{C1} - \alpha_{C2}| \leq \xi \qquad (3.31)$$

where ξ is the tolerance limit of convergence, equal to 0.1 mrad in the program.

The iterative procedures used in the program to find λ are now described as follows:

1) From the previous iteration, a λ factor satisfying eqn. (3.31) is found. The support moment is then decreased by one further step and the previous λ is taken as $\lambda(\text{old})$.

2) Let the increment $\Delta\lambda(\text{old}) = 0.001\lambda(\text{old})$, and so
    $\lambda(\text{new}) = \lambda(\text{old}) + \Delta\lambda(\text{old})$

3) Substituting $\lambda(\text{old})$ and $\lambda(\text{new})$ in eqn.(3.31) separately, two values of F, $F(\text{old})$ and $F(\text{new})$ are obtained. If $F(\text{new}) \leq \xi$, then $\lambda(\text{new})$ is the solution corresponding to the new M_c'. Otherwise it is necessary to update λ in proportion to

the error so as to speed up the convergence process.
By linearisation, an appropriate updated λ should be
$\lambda(new) = \lambda(old) + \Delta\lambda(old).F(old)/[F(old)-F(new)]$
or $\lambda(new) = \lambda(old) + \Delta\lambda(old)$,
and put $\lambda(old) = \lambda(new)$

4) Substituting $\lambda(new)$ in eqn. (3.31), an updated value
of $F(new)$ is obtained. If $F(new) \leq \xi$, the $\lambda(new)$
is the solution for compatibility. Otherwise λ has
to be updated again to cancel the error leading
to convergence. Therefore, by linearisation again
the updated λ becomes
$\lambda(new) = \lambda(old) + \Delta\lambda(old) . [F(new)/F(old)]$
or $\lambda(new) = \lambda(Old) + \Delta\lambda(old)$,
and put $\lambda(old) = \lambda(new)$

5) Substituting $\lambda(new)$ again in eqn. (3.31) to get
$F(new)$, if $F(new) \leq \xi$, $\lambda(new)$ is the answer.
Otherwise iteration has to continue by repeating
steps (3) to (5).

This iteration algorithm is incorporated in a DO loop in
the program and convergence has usually been obtained in
less than 6 cycles.
A flow chart of the program is shown in Fig. 3.3

3.7 Convergence test and program validation

An increase in the number of elements for the numerical
integrations of curvatures gives different values for the
buckling and failure load factors, λ_b and λ_f, as the
approximations become closer to the true results of the
integrals. Typical results from studies of convergence
in relation to the number of elements in the hogging and
sagging regions are shown in Fig. 3.4, in which λ_b and
λ_f for specimen SB42 (Table 3 in Appendix A) are plotted
against $1/(n_h+n_s)$ for $n_h + n_s = 20$, 30, 40 and 50,
where n_h and n_s are the number of elements in the hogging
and sagging regions for each span and $n_h = n_s$. Twenty
elements each for the hogging and sagging regions have
been adopted in the program, and the typical errors as
shown in Fig. 3.4 are 0.4% higher for λ_b and 0.3% higher
for λ_f than the extrapolated values as $n_h + n_s$ tends
to infinity.

Experimental results of two-span composite beams of the
nature simulated by the program are not available, but
the theory and coding of the program can be checked by
comparing between the results obtained from the program
and an elastic analysis. A two-span plain steel beam
with equal spans of 10 m subject to uniformly distributed
loads w has been analysed by the program and by hand
calculation using elastic theory separately, and residual
stresses were ignored. The program gave the bending

moment at the internal support 1.5% higher than that $(0.7M_y')$ from elastic analysis, and the beam rotations at the two ends obtained from eqns. (3.9) and (3.17) in the program agreed closely because from symmetry the beam rotation at the central support must be zero.

Computed results M_y', θ_b', and maximum vertical shear V for five of the SB series of two-span beams are compared in Table 3 (Appendix A) with the results from the tests on double cantilevers with Class 3 cross-sections by Climenhaga [14]. Propped construction was assumed. The values of θ_b' from the analytical model are conservative and compare favourably with the observed results, except specimen SB42 having a shear ratio about 0.2, which is lower than that in practical beams. In a real beam this error is offset by having a hogging moment of resistance higher than M_y' assumed and a λ_s factor well above 1.0 from the numerical analysis.

Fig. 3.1 Moment-curvature relationship of
a composite cross-section

NOTE: All variables shown are +ve

Fig. 3.2 Deflection curve of a two-span beam
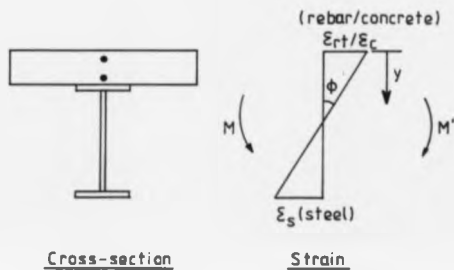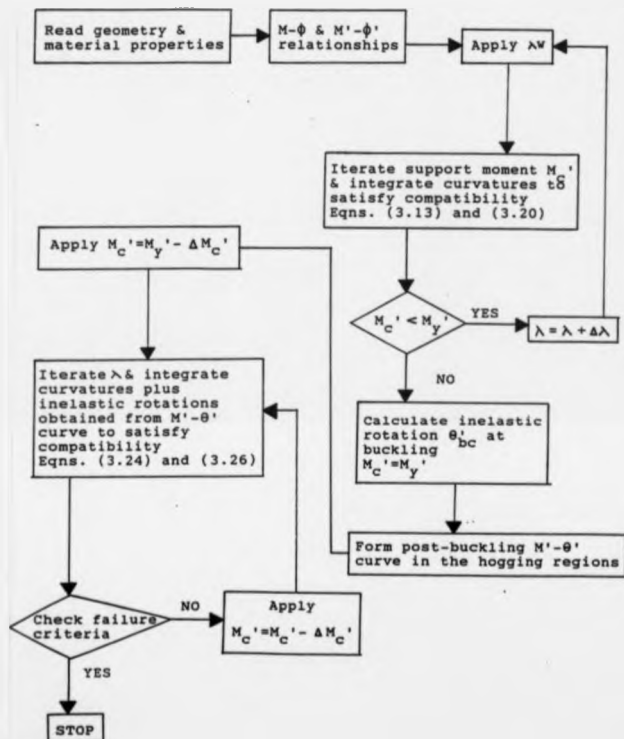
Fig. 3.3 Flow chart for the computer analysis
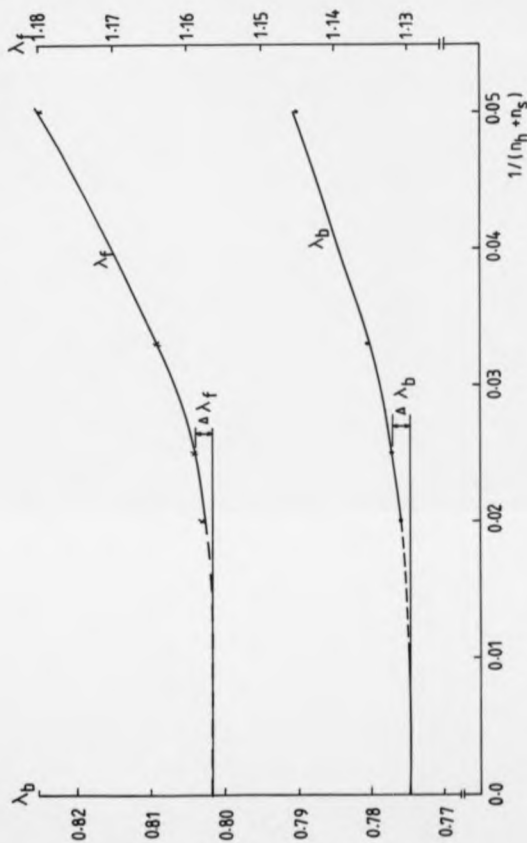
Fig. 3.4 Study of convergence (specimen SB42)

CHAPTER 4

RESULTS OF PARAMETRIC STUDY ON MOMENT REDISTRIBUTION

4.1 Introduction

The draft Eurocode 4 [1] has proposed two design methods
for Class 3 continuous composite beams - methods (a) and
(b). Method (b) is a traditional approach using the
uncracked EI values as flexural stiffnesses for the
entire beam, with plastic moment M_p at midspan after
redistribution, if needed, whilst method (a) is an
innovative method which uses the cracked EI values as
flexural stiffnesses over 15% of the span on each side of
an internal support, and allows 20% redistribution of
support moment to midspans provided that they remain
elastic. Since method (b) is an established method for
global analysis, it is generally accepted to be
conservative and therefore does not require further
investigation. However method (a) seems to be less
conservative because it permits a higher percentage of
moment redistribution. A typical example of the design
of a two-span composite beam given in Appendix B, shows
that method (a) allows the same beam to carry loads 40%
higher than that obtained from method (b). Method (a)
tends to underestimate the support moments as a result of
20% redistribution of moment and correspondingly
overestimate the near mid-span sagging moments in real
continuous composite beams. In the absence of

experimental evidence, an alternative approach to check its safety is by means of computer simulation.

A parametric study has been carried out to investigate the implication of the amount of moment redistribution allowed by method (a), in relation to the real beam behaviour of two-span continuous composite beams, using the computer program described in Chapter 3. Specimens are assumed to be unstiffened except at the central support. The analysis includes the effects of nonlinear material properties, residual stresses and local buckling, but excludes the effects of geometric imperfections, secondary effects such as creep, shrinkage and slip, and distortional lateral buckling of the bottom flange. A wide range of variables affecting the behaviour of a beam in typical commercial and industrial buildings was considered. Ten cross-sections were chosen for the study, of which five were those used in Climenhaga's local buckling tests [14], representing typical behaviour of Class 3 cross-sections in the hogging moment region. This chapter presents the results of the parametric study, which are used in the subsequent discussion regarding the validity of method (a).

4.2 Choice of members for study

4.2.1 Cross-sections

There are four classes of cross-section defined in the draft Eurocode 4 and each class is governed by the limiting slenderness ratios for steel flanges and webs in compression separately. The code does not provide a combined limiting slenderness ratio between the flange and web, so a cross-section will be classified as Class 3 when either the flange or web slenderness ratio exceeds the Class 2 limit but is within the Class 3 limits. In the computer tests the specimens were grouped into two series - SB and TB. Each series has five different cross-sections. For Climenhaga's beams [14] SB4, SB5, SB6, SB10 and SB11, all the flanges and webs belong to Class 2 and Class 3 respectively, and so they are all Class 3 cross-sections. These cross-sections were used in the computer tests for beams of different span ratio in the SB series. Another group of specimens, TB series, comprises fictitious beams using five different cross-sections. The three most slender cross-sections within the Class 3 limits available in British hot-rolled UB sections were chosen to represent TB1 to TB3. Two plated sections, which satisfy both Class 3 flange and web slenderness criteria in the practical range, were chosen for TB4 and TB5.

The properties of cross-sections studied here are given
in Tables 1 and 2 in the published paper (Appendix A).
The notation for properties of cross-sections is also
shown in Fig. 4. The practical range of Class 3 sections
is given by the area ABCD in Fig. 5 (Appendix A). A
scatter of sample points in Fig. 5 gives representative
results for Class 3 sections commonly used in practice.

4.2.2 Choice of spans

Hot-rolled UB sections are usually used for the
construction of Class 3 continuous composite beams, so
only two-span beams of uniform depth have been studied.
Most of these beams for buildings, footbridges and short-
span viaducts have ratios of longer span to overall depth
between 20 and 30, and spans varying between 6 m and 20
m. In addition, under normal circumstances, two-span
beam with very unequal spans would be avoided, therefore
the ratios L_1/L_2 of shorter to longer span were chosen to
range from 0.6 to 1.0. These ranges have been explored
in the beams analysed in Tables 4.1, 4.2 and 4.3. Each
beam number consists of the section number plus an extra
digit. Propped construction was assumed for beams given
in Tables 4.1 and 4.2, but four symmetrical beams in the
TM series were analysed assuming unpropped construction,
as shown in Table 4.3.

4.2.3 Loadings and γ_F factors

The calculation of the applied loads w_1 and w_2 (Fig. 3, Appendix A) is explained in Section 3.5. The partial coefficients γ_F are taken as 1.35 (γ_G) and 1.5 (γ_Q) for dead and imposed loads respectively in accordance with draft Eurocode 4. Therefore in the case of propped construction w_2 will be the ultimate design load, equal to $1.35g_2 + 1.5q_2$, where g_2 and q_2 are the distributed characteristic dead and imposed loads per unit length respectively. But for span 1 the distributed dead and imposed loads per unit length are g_1 and q_1, and it is assumed that w_1 can have any value between $1.0g_1$ and $1.35g_1 + 1.5q_1$. For a uniform two-span beam g_1 is the same as g_2.

For unpropped construction, the design dead load $(1.35g$ with $g = g_1 = g_2)$ is first applied to the steel member alone, acting elastically. The relevant extreme fibre stresses are then deducted from the yield stress σ_y, to obtain the allowable stresses in both hogging and sagging bending for the composite section. Section 3.5 explains the method to obtain the imposed loads $1.5q_1$ and $1.5q_2$. Hence w_1 and w_2 are given as $1.35g_1 + 1.5q_1$ and $1.35g_2 + 1.5q_2$ respectively.

4.2.4 Properties of materials and γ_m factors

For the SB series, the yield stresses of the structural steel (Table 1, Appendix A) are based on the measured values for the relevant cantilevers [14]. For the TB series, σ_y is assumed to be 355 N/mm², the nominal yield stress for Grade 50 steel. The stress-strain curve for structural steel is shown in Fig. A2(a), Appendix A, which is similar to that recommended by Reference (98). Reinforcement is assumed to have a stress-strain curve (Fig.A1(b), Appendix A) as suggested by BS5400 : Part 4 [8], and the partial safety factor γ_m is taken as 1.15. The nominal yield stress of reinforcement f_y is assumed to be 425 N/mm².

For all concrete top flanges, Grade 30/20 OPC concrete with a nominal crushing strength $f_{cu} = 30$ N/mm² is assumed. The stress-strain curve [8] shown in Fig. A1(a) is used, and the partial safety factor γ_m for concrete is taken as 1.5.

In the analyses, the compressive residual stress at the four flange tips for a double-symmetrical I-section is taken as $\sigma_y/2$. The residual stress is assumed to vary linearly from the tip to the junction between the flange and web as shown in Fig. A2(b) (Appendix A), reaching an unknown tensile stress σ_T. Considering the whole web to have an uniform tensile stress at this level, σ_T can be calculated from longitudinal equilibrium.

4.3 Numerical results

4.3.1 Comparisons between cantilevers and two-span beams

Computed results of M_y', θ_b' and maximum vertical shear V for five of the SB series of two-span beams are compared in Table 3 (Appendix A) with the observed results from the tests on double cantilevers with the same cross sections and properties of materials under propped construction. The two sets of results agree closely and detailed discussion is given in Section 4.1 of the published paper[37]. In view of the complexity of predicting an accurate post-buckling $M' - \theta'$ curve, the simplification adopted in this study is believed to give a conservative model of the falling branch of the characteristic $M' - \theta'$ curve.

4.3.2 Two-span beams

Results for the SB and TB series are given in Tables 4.1 and 4.2 respectively. Propped construction was assumed. The four symmetrical beams that gave the lowest values of failure load factor λ_f were further analysed assuming unpropped construction, and their results are given in Table 4.3.

4.4 Analysis and discussion

4.4.1 Load factors λ_b and λ_f

The load factor λ_b at the onset of local buckling, corresponding to the first yield of the bottom fibre, was between 0.77 and 0.79 for all 43 beams with propped construction. Assuming a dead to imposed load ratio equal to 0.5 for a typical floor beam, the serviceability loads are about 69% of the ultimate loads using γ_F factors recommended by draft Eurocode 4. It is clear that local buckling does not occur and shakedown deflection is not a problem at the serviceability limit state. However λ_b was much less than 1.0 and this indicates that, as expected, the attainment of the design ultimate loads relies on there being sufficient post-buckling rotation to shed at least 20% of the peak hogging moment into the adjacent midspan regions. No beam could be found with the failure load factor λ_f less than 1.05, in other words the permission of 20% redistribution of hogging moment is justified. The results also show that λ_f is in general higher for the stockier cross-sections of the SB series, than for the TB series.

4.4.2 Effect of unpropped construction

For a given beam and total load, unpropped construction gives higher stresses in steel and earlier local buckling

as discussed by Yam[99]. The method described in Section 3.5 to obtain w_1 and w_2 for unpropped construction takes into account these higher stresses, and it is consistent with the method of draft Eurocode 4. As a result, the design loads in Table 4.3 are less than that in Table 4.2 for unpropped construction. Since the theoretical carrying capacities of a beam for propped and unpropped construction are different, it is therefore not appropriate to compare the load factors λ_b and λ_f directly for the two cases. A better comparison is to examine the total carrying capacity for each case at the onset of buckling and failure as shown in Table 4.4. Due to the effect of unpropped construction, the reductions in total load at buckling range from 4% to 12% comparing to propped construction, and reductions in total load at failure range from 2.6% to 10%.

Also the values of λ_b and λ_f (Table 4.3) are slightly higher than for propped construction (Table 4.2). The method of draft Eurocode 4 is thus slightly more conservative for unpropped than for propped construction.

4.4.3 Residual stresses

Rotter et al[19] have reported that residual stresses in rolled sections tend to increase curvatures at intermediate load levels by up to 25 per cent; but comparison of results of analyses with or without

residual stresses in Table 4.1 and 4.2 show that they cause only small decreases in λ_f. The largest reductions are 3.5 per cent for the SB series and 9 per cent for the TB series. These indicate that the load factors λ_b and λ_f were obtained by integrating both hogging and sagging curvatures along the beam; the integration was influenced by residual stresses to a lesser extent when compared to the curvatures of a cross-section alone.

4.4.4 Span ratio

There is no obvious relationship between λ_f and the ratio of the two spans (e.g., results TB11, 12, and 13). This is probably because the design loads w_1 and w_2, which satisfy compatibility and equilibrium, are influenced in a complex way by span ratio, as well as having the expected reduction with increasing span. Span ratios below 0.6 have not been studied; but for these, beams of uniform section would rarely be used. Generally the results show that beams of longer spans and with higher span ratio L_1/L_2 tend to give slightly lower values of λ_f. The total length L_1+L_2 has negligible effect (e.g., λ_f is similar for beams TB11 and TB43).

4.4.5 Sensitivity of λ_f to the shape of the falling branch

The values of θ_b' computed in the parametric study are the inelastic rotations at the internal supports when the maximum hogging moment reaches M_y' and the load factor is λ_b. Further increase of load level depends on whether the inelastic rotation available in the falling branch of the $M' - \theta'$ curve can cope with the demand due to an increase of sagging curvatures to satisfy the compatibility requirement. A separate study was made of the sensitivity of the results for λ_f to the shape of this falling branch (Fig. C1, Appendix A). The effect of increasing the inelastic rotation at $0.6M_y'$ from $10\theta_b'$ to $16\theta_b'$ was to increase λ_f by less than 5 per cent in all cases. It is then believed that an appropriate $M' - \theta'$ curve close to the reality is adequate to predict the failure load, and the error is likely to be in the range of ± 5 per cent. The assumed $M' - \theta'$ curves are considered to be appropriate and conservative, in view of this insensitivity.

4.4.6 Combined bending and shear

For ultimate strength in combined bending and shear in Class 3 sections, the draft Eurocode 4 refers to the draft Eurocode 3[87], which deals with the design of steel structures. Experimental results [100, 101] on interaction between bending and shear in composite beams

had shown that shear strengthening was given to the steel section by the concrete slab, and as a result the shear capacity of a composite beam was higher than that of a steel beam alone. So it is not appropriate to use the draft Eurocode 3 method for the checking of interaction between bending and shear as it will certainly be too conservative. The method of BS5400 : Part 3[8], based on tension-field theory[102], is more relevant and less conservative. For composite beams classified as Class 3 according to the draft Eurocode 4, an interaction diagram shown in Fig. 4.1 can be obtained by using Clause 9.9.3 in BS5400 : Part 3. The partial safety factors, γ_m and γ_{f3}, which have to be allowed in BS5400 : Part 3, were both taken to be 1.0 to form the interaction diagram. Fig. 4.1 shows that for Class 3 beams no reduction in $M_y{}'$ need be made until V/V_{pl} exceeds 0.68. On the same diagram the maximum shear ratio found in the parametric study was 0.57 and was plotted at point A. Therefore, for Class 3 beams with uniform cross-section and practical spans, the assumed moment of resistance $M_y{}'$ is unlikely to be affected by the co-existing shear at the internal support.

4.5 Comments on the design method of draft Eurocode 4

In design practice, the applied loads w_1 and w_2 are known initially and the bending moment and shear envelopes are calculated using global elastic analysis for various possible loading cases. The required cross-sections are then chosen such that the extreme-fibre stresses in the steel do not exceed yield when the hogging moment is the maximum obtained from the bending moment envelope. Therefore the actual design loads are usually lower than the values of w_1 and w_2 used in the present study. In addition, a margin of safety is contributed from the possibility for a Class 3 section to have a moment of resistance above M_y'. For beams with uniform cross-section (practical in building structures), any continuous beams other than two-span would be subject to more onerous loading arrangements to obtain the bending moment envelope, and so a stronger section would have been chosen, but the actual loading conditions might not be as severe as those assumed. Ignoring the conservatism discussed above, the computer results have shown that the draft Eurocode 4 method (1985) would be safe (all $\lambda_f > 1$). This can be further checked against any experimental results for the ultimate strength of continuous Class 3 beams that may become available in the future.

A recent technical paper[103] has proposed to revise the amount of redistribution from 20% to 10% using elastic

uncracked analysis in the second draft of Eurocode 4. The effect of this reduction not only improves the safety but also reduces the severity of local buckling in the hogging region at the ultimate limit state. Besides, for beams with uniform cross-section, a stronger section would have been chosen for 10% redistribution of moment instead of 20%, and consequently for the same spans and loading conditions, the amount of deflections would be reduced at the serviceability limit state. It is obvious that 10% redistribution of moment would demand about half of the inelastic rotation in the hogging region to shed the support moment as required by 20% previously. Thus the proportion of hogging moment to be redistributed into mid-spans, which relies on the post-buckling behaviour of the hogging region, is greatly reduced. Generally the new proposal is more conservative and it is very likely that the stress level in mid-spans is very low at service and so it might lose some economy in materials.

4.6 Conclusions

Forty-seven two-span continuous composite beams with Class 3 cross-sections at the internal support, and ten different cross-sections, have been designed for flexural failure at the ultimate limit state by the less conservative of the two methods given in draft Eurocode 4, which allows 20% redistribution of hogging moment using elastic global cracked analysis. These designs correspond to a load factor $\lambda_f = 1$. Spans ranged from 6m to 20m and span ratios from 0.6 to 1.0 have been studied and reported here.

The ultimate strengths of these beams were determined by an inelastic method, without referring to the global analysis, that takes account of the actual stress-strain relationship of materials and also the loss of strength in hogging bending caused by local buckling observed in tests of five double cantilevers with typical Class 3 cross-sections. The values of λ_f for the beams used in the computer simulation ranged from 1.05 to 1.33. The effects of residual stresses and unpropped construction were studied, and were found to have little influence on the ultimate carrying capacity of the beams. For the beams studied the maximum shear ratio V/V_{pl} was 0.57 and it has shown that there is no need to reduce the hogging moment of resistance below M_y' unless V/V_{pl} exceeds 0.68.

For both propped and unpropped construction, local
buckling was found not to occur until well above service
load levels. This was reflected by the values of λ_b,
load factor at local buckling, which ranged from 0.77 to
0.84, except for one value of 0.98, for the beam with the
highest ratio of slab reinforcement $(A_r/b_c h_c = 0.02)$.
In general unpropped construction is slightly more
conservative than propped construction because the design
criterion is to limit the extreme-fibre stresses in the
steel section at yield, no matter which form of
construction is used.

Because of more onerous loading cases for beams having more
than two spans, a stronger uniform section would have been
chosen normally and therefore it is believed that the
present study is a more severe test of the design method
than would be likely to occur in practice. The method
provides an alternative to the over-conservative design
of Class 3 beams that is restricted by the exclusive use
of elastic theory in current practice. The new proposal
of reducing the amount of redistribution from 20% to 10%
in the revised Eurocode 4 is believed to be slightly more
conservative, but it provides some safety to control
excessive deflections and might even avoid local buckling
at the ultimate limit state in a real continuous beam.

Beam	L_1	L_2	w_1	w_2	θ'_b	λ_b	λ_f
	m	m	kN/m	kN/m	mrad		
SB41	10.0	10.0	17.95	24.09	7.56	0.78	1.165
SB42	10.0	12.5	17.18	15.42	8.51	0.78	1.159
SB43	10.0	15.0	16.41	10.71	9.48	0.78	1.156
SB44*	10.0	15.0	16.41	10.71	9.21	0.77	1.166
SB51	10.0	10.0	23.19	30.47	5.99	0.79	1.139
SB52	10.0	12.5	22.19	19.50	6.73	0.79	1.134
SB53	10.0	15.0	21.27	13.54	7.48	0.79	1.131
SB54*	10.0	15.0	21.27	13.54	7.27	0.78	1.150
SB61	10.0	10.0	28.48	37.12	5.27	0.79	1.154
SB62	10.0	12.5	27.40	23.76	5.93	0.79	1.148
SB63	10.0	15.0	26.32	16.50	6.59	0.79	1.146
SB64*	10.0	15.0	26.32	16.50	6.41	0.78	1.157
SB101	10.0	10.0	17.98	23.97	7.77	0.78	1.237
SB102	10.0	12.5	17.23	15.34	8.75	0.78	1.218
SB103	10.0	15.0	16.49	10.65	9.73	0.78	1.203
SB104*	10.0	15.0	16.49	10.65	9.46	0.77	1.210
SB111	10.0	10.0	23.30	29.86	6.42	0.79	1.143
SB112	10.0	12.5	22.48	19.11	7.22	0.79	1.139
SB113	10.0	15.0	21.66	13.27	8.02	0.79	1.136
SB114*	10.0	15.0	21.66	13.27	7.81	0.78	1.177
				Mean values		0.78	1.163

* For these beams, no account was taken of residual stresses

Table 4.1 Computed results for beams of series SB

Beam	L_1	L_2	w_1	w_2	θ'_b	λ_b	λ_f
	m	m	kN/m	kN/m	mrad		
TB11	6.0	10.0	82.15	50.33	4.19	0.79	1.078
TB12	8.0	10.0	51.27	50.33	4.65	0.79	1.069
TB13	10.0	10.0	34.76	50.33	5.13	0.79	1.073
TB14*	10.0	10.0	34.76	50.33	4.97	0.78	1.097
TB15	13.0	15.0	19.86	22.37	7.17	0.79	1.071
TB16	15.0	15.0	15.45	22.37	7.65	0.79	1.073
TB17*	15.0	15.0	15.45	22.37	7.41	0.78	1.097
TB21	10.0	10.0	30.81	40.63	5.35	0.79	1.137
TB22	10.0	12.5	29.58	26.00	6.01	0.79	1.132
TB23	10.0	15.0	28.35	18.06	6.69	0.79	1.129
TB24*	10.0	15.0	28.35	18.06	6.50	0.78	1.196
TB31	10.0	10.0	18.29	26.63	7.48	0.79	1.059
TB32	10.0	12.5	17.25	17.04	8.44	0.79	1.055
TB33	10.0	15.0	16.20	11.84	9.42	0.79	1.052
TB34*	10.0	15.0	16.20	11.84	9.14	0.78	1.155
TB41	15.0	15.0	81.43	98.39	5.65	0.79	1.096
TB42	15.0	18.0	79.73	68.32	6.20	0.79	1.094
TB43	15.0	20.0	78.60	55.34	6.58	0.79	1.092
TB44*	15.0	20.0	78.60	55.34	6.20	0.77	1.088
TB51	12.5	12.5	79.05	94.26	6.17	0.79	1.093
TB52	12.5	15.0	77.53	65.46	6.78	0.79	1.089
TB53	12.5	17.5	76.00	48.10	7.40	0.79	1.086
TB54	12.5	17.5	76.00	48.10	7.19	0.78	1.086
					Mean values	0.79	1.096

* For these beams, no account was taken of residual stresses

Table 4.2 Computed results for beams of series TB

Beam	L_1	L_2	Dead Load	w_1	w_2	λ_b	λ_f
	m	m	kN/m	kN/m	kN/m		
SB51	10.0	10.0	4.57	17.47	26.85	0.84	1.255
TB13	10.0	10.0	9.28	21.01	40.46	0.98	1.334
TB41	15.0	15.0	10.16	74.03	94.46	0.79	1.136
TB51	12.5	12.5	8.19	73.03	91.28	0.80	1.123

<u>Table 4.3</u> Results for unpropped construction

Beam	$\lambda_b (w_1 + w_2)$		$\lambda_f (w_1 + w_2)$	
	kN/m		kN/m	
	Propped	Unpropped	Propped	Unpropped
SB51	42.39	37.23	61.12	55.62
TB13	67.22	60.24	91.30	82.00
TB41	142.06	130.11	197.08	191.40
TB51	136.91	131.45	189.43	184.52

<u>Table 4.4</u> Comparison of load levels between propped and
        unpropped construction
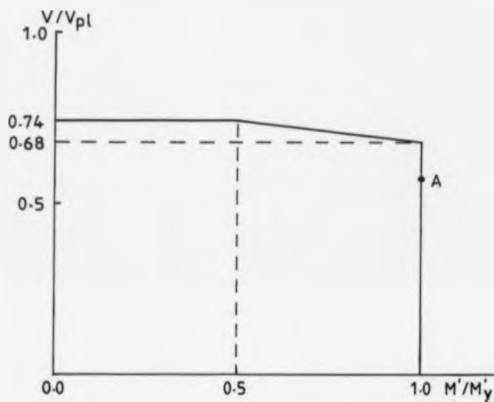
Fig. 4.1 Interaction diagram for combined bending and shear of Class 3 beams (EC4) designed in accordance with BS5400:Part 3

CHAPTER 5

TESTS TO INVESTIGATE
DISTORTIONAL LATERAL BUCKLING - T BEAMS

5.1 Introduction

Instability of the bottom flange in the hogging moment region has caused concern to structural engineers when the slab-beam system is designed as continuous. Previous experimental and theoretical studies[94,86,4,6] have indicated that the restraints provided by the slab against lateral buckling of the bottom flange are considerable. Due to this added structural advantage, not present in plain steel beams, it is widely believed that lateral buckling should not be a major design consideration in continuous unstiffened composite beams with compact proportions, as the web is less flexible. However there have been few relevant large scale tests on composite beams, and so it is impossible to assess the deviations between actual behaviour and theoretical predictions.

Tests are now reported on two composite beams of 'T' cross-section, S2 and U1. In each test, the beam was loaded as a double cantilever which represented the length of a continuous beam subjected to hogging bending between an intermediate support and points of contraflexure. The objectives of the tests were to determine whether the concrete slab could enhance the

overall resistance of the beam against lateral-torsional buckling, when the member was unbraced, and to provide experimental data for the development of a rational design approach to the underlying problem. Test S2 was a pilot test, which was performed to check instrumentation, the bearing system, and testing procedures. This specimen had been used previously[97] in a study of shrinkage-induced curvature in continuous composite beams; it had not reached yield in that test, so could be re-used for the proposed test. The next specimen U1 was designed to represent a typical floor beam in office buildings.

5.2 Choice of specimens

Beam S2 represented a typical floor beam with compact proportions. The slab was cast using the conventional method with the steel member unpropped. This specimen was tested to provide background information for the planning of future tests in this project.

The member length and cross-section of specimen U1 were based on the design of a typical commercial building, assuming a column grid of 6m x 10m. Considering the design of the end span of a 3-span continuous composite secondary beam which is taking the loading of a floor area 3m x 10m, the length of each hogging moment region can be up to 5.1m long in a span subject to dead load only, when a plastic hinge is formed at the penultimate support. This is the basis for choosing a cantilever length of 5.1m long to allow for the moment gradient, that could possibly happen in practice. The model is shown in Fig. 5.1. This arrangement also gives higher vertical shear force on the short side : three times the shear on the long side, because the ratio of span lengths is 1 to 3. So the shear and moment interaction on the short cantilever will be greater when the specimen is approaching its maximum carrying capacity.

Hot-rolled sections are often preferred to plate girders in building construction because of lower cost and better availability. However this eliminates the choice of the

flange slenderness, as most of the commonly used sections are in either Class 1 or 2 in accordance with draft EC4[1]. According to established design methods, a cross-section must be within Class 2, otherwise its full plastic moment of resistance cannot be used , therefore the section of greatest research interest is one with a web slenderness just outside the existing limit for Class 2. This can be achieved by using an appropriate amount of slab reinforcement.

In industry, steel decking is now widely used for floor slab construction, and normally one line of shear connectors is provided by means of either conventional or through deck stud welding technique. Specimen U1 was therefore manufactured following industrial practice as closely as possible, in an attempt to represent a realistic model. The thickness of the concrete slab was kept to the absolute minimum of 90mm for the purpose of casting and to provide space for the shear connectors and reinforcement.

5.3 Details of test specimens

5.3.1 Beam S2

The elevation and cross-section of beam S2 (Grade 43) are shown in Fig. 5.2. The 13x65 mm shear connectors were placed in pairs at 220 mm spacing over lengths AB and DE, and singly at 110 mm, staggered, over length BD. This provided complete shear connection throughout the beam in accordance with the draft EC4[1]. A point load was applied at a distance of 5 m from the central support on each side, leaving a 1 m long extension to simulate the continuity that would be present in a real continuous beam.

5.3.2 Beam U1

The geometry and cross-section of beam U1 are shown in Fig. 5.3. The 900 mm extension at each end is to allow for the effect of continuity. PMF CF46 profiled sheeting, 0.9 mm thick, was used to support the concrete slab, and 1.2 mm thick edge closure channels were employed to form the edges of the slab. One layer of high-yield reinforcing fabric A193 was placed inside the slab. Ready mix concrete grade C25/10 (OPC) was used to construct the concrete slab and the measured slump was 50 mm.

A maximum aggregate size of 10 mm was specified for the mix in order to avoid segregation because of limited space between the fabric and the top of the decking.

TRW Nelson shear connectors, 19 mm diameter and 75 mm LAW, were used. Conventional stud to steel welding was first employed, and holes were made in the decking to fit over the studs. Connectors were placed in every other trough of the decking, so the spacing is 450 mm. This provided complete shear interaction ($N/N_f \gg 1$) throughout the beam in accordance with draft EC4, but it failed to satisfy the requirement that the spacing should not exceed four times the thickness of the slab.

5.4 Construction of test specimens

Existing stiffeners on beam S2 were removed by flame
cutting, and then two pairs of 10 mm thick stiffeners,
120 mm apart, were welded onto the beam on both sides
with respect to the centre line. The beam was supported
on two cross-frames, and held stable by wedging the slab
against four temporary columns, two along each side,
prior to the installation of instrumentation.

The concrete slab of beam U1 was cast with the steel beam
propped. The universal beam was supported on three
equally spaced trestles, and the top flange was made
horizontal by packing the bottom flange with wooden
wedges at the supporting points. Steel decking was then
laid on top of the beam after stud welding. The edges of
the slab were formed by factory-made edge closure
channels 1.2 mm thick. Fourteen 100x100 mm cubes were
made during concreting in accordance with BS1881 : Part
108[104].

5.5 Testing rigs

The general arrangement of the test rig for the S2 test is shown in Fig. 5.2 and Plate 5.1. The loading frames at the two ends were made up of standard structural "Meccano". At the central support load was applied from a hydraulic jack, through a 25 tonne load cell and a cylindrical roller bearing of 50 mm in diameter (Fig. 5.4). The end bearings, shown in Fig. 5.5, are essentially an assembly of a roller slider on top of a spherical ball joint seating (Plate 5.2). This bearing system provides complete freedom in rotations and longitudinal movement, whilst at the central support only vertical jack movement, in-plane beam rotation and twist about the vertical axis of the beam's centre line are allowed. The specimen was free from lateral restraints during the test except at loading points.

The general arrangement of the test rig for the U1 test was similar to S2, but the method of applying external loads was completely different. Since the specimen U1 would be tested as a double cantilever of unequal lengths, therefore instability in the longitudinal direction during testing was a prime concern. Details of the test rig are shown in Figs. 5.3, 5.6, 5.7 and Plate 5.3. In order to keep the beam horizontal at the support it was necessary to apply loading at the two ends by controlling the rate of jacking. Furthermore from a computer analysis and previous experience of testing S2,

it was realised that the available travel of the ram of a single jack, 230 mm, would not be sufficient. As a result a double jack system (Fig. 5.7) was introduced.

Standard structural "Meccano" was used to construct the reaction frames at the two ends. At each end a vertical guide (a channel section bolted onto a cross beam) was also fixed to stop possible lateral movement of the double jack (Plate 5.4). At the central support the beam was carried on a cylindrical bearing keyed into a 25 tonne load cell (Plate 5.5). However the bearing system was inclined laterally about 2° with respect to the horizontal floor in order to match the initial tilting of the bottom flange.

It was anticipated that the specimen might be unstable when it started to unload, therefore adjustable guides were placed close to the top flange (Plate 5.6), but not touching, on both sides at 4 locations to provide additional safety. However in the test the specimen was not restrained laterally other than the loading points throughout the test. The boundary conditions for the U1 test were similar to S2 except that there was no vertical movement at the central support, and the two ends were free.

5.6 Instrumentation

5.6.1 Beam S2

One 25 tonne load cell was used to measure the force at
the internal support, and the end reactions were
calculated from the equilibrium condition. The lateral
movements and transverse rotations of the bottom flange
were measured by using dial gauges and inclinometers
respectively. Their positions are shown in Fig. 5.8.
For the measurement of lateral movement, dial gauges were
mounted on light-weight Dexion frames which were clamped
onto the concrete slab (Plate 5.7). Although this method
was found to be effective, rigid body rotation about a
longitudinal axis could not be detected. A change of
dial-gauge reading indicated transverse bending of the
web or separation between the top steel flange and the
slab, or both.

The beam rotation was measured by using an inclinometer
at positions C1 to C4 shown in Fig. 5.8. In the support
regions, the steel beam was painted with white emulsion
paint in order to detect yielding visually. No strain
measurements were taken in test S2 for two reasons:
first, the specimen had previously been loaded and the
concrete slab was cracked, and second, only knowledge of
overall behaviour was required to assist the planning of
future buckling tests.

5.6.2 Beam U1

Similar to S2, one 25 tonne load cell was used to measure the reaction at the internal support for the U1 test, and the applied forces at the ends were deduced from equilibrium. The same technique as for S2 was used to measure the in-plane and transverse rotations of specimen U1. The monitoring points are shown in Fig. 5.9. Dial gauges were also installed to measure the vertical and lateral movements of the bottom flange, at positions shown in Fig. 5.9.

Fifty TML electrical resistance 10-mm strain gauges were bonded onto the steel beam, and the data was collected using a Schlumberger Orion 3531D data logger. Their positions are shown in Fig. 5.10. Most of the gauges fixed to the web were located in the support region so as to detect local buckling, and were so arranged that longitudinal strains across several cross-sections could be measured as a check on the applied moment gradients in the elastic range. It was anticipated that extensive yielding would occur in regions near the support, and so post-yield YL-10 TML gauges were used, which are capable of measuring strains above 10%. On the bottom flange the strain gauges were installed in pairs such that the mean compressive strains, as well as the corresponding lateral bending strains, could be recorded at specified positions

when lateral buckling of the bottom flange occurred at
high loads.

Similarly three strain gauge pairs were used to monitor
the out-of-plane bending of the web. Table 5.1
summarizes the type of gauges assigned for the purpose
mentioned above.

5.7 Auxiliary tests

5.7.1 Calibrations

Both tests were done using the same 25 tonne Mayes load
cell which was calibrated twice, before and after each
test, using a 3 MN Denison testing machine. Test results
were taken as the average values from the two sets of
calibration graphs.

5.7.2 Material properties

Tensile test pieces were prepared and tested in
accordance with BS18 : 1987[105], from the test samples
obtained in accordance with BS4360 : 1986[106]. Material
testing was carried out using a 25 tonne Dartec tensile
machine. Typical details of the coupon samples and their
positions are shown in Fig. 5.11.

A 12-m long beam was first flame-cut to give a length of
8.6 metres for the U1 specimen, and coupons were then
taken from the scrap end. In order to minimize the
influence of mechanical and flame cutting on the material
properties, samples were chosen at least one metre away
from each end.

High-yield fabric was sampled randomly and six specimens
were taken. Tensile tests using a 10 tonne Monsanto
Extensometer machine were carried out on the samples,
which are cruciform in shape. Concrete cubes were tested

using a 3 MN Dension machine in accordance with BS1881 :
Part 116[107].

5.7.3 Cross-sectional dimensions and imperfections

Cross-sectional dimensions of the steel section of
specimen S2 were reported in Reference (108).
Measurements of the thickness of U1 rolled section were
taken at regular intervals using a micrometer. Six and
eight locations, uniformly spaced, were measured for each
flange and the web respectively. The width and depth of
the cross-section were measured using a vernier caliper
at half metre intervals.

The initial lateral imperfections of the bottom flange
relative to the top flange were measured after the
concrete slab was cast. Before casting, the top steel
flange was made level and a centre line was marked
joining the ends where the web and the top flange
intersect. A "theoretical straight flange edge" was
then located by offsetting uniformly by a distance equal
to half of the average width of the top flange from the
centre line. Lateral imperfections were then referred to
this straight flange edge. An extended plumb line was
dropped from the top flange and the offset of the edge of
the bottom flange from this line gave the imperfection.
Initial tilting of the bottom flange with respect to the
horizontal was measured using an inclinometer.

5.7.4 Residual stress measurements

Residual stress measurements were carried out to specimen U1 using the method of dissection[109,110] on the unwanted cut-off length. A section of 250 mm in length was cut out by sawing from the middle of the parent off-cut, and the positions of the test specimens for stress relief are shown in Fig. 5.12.

5.7.5 Instrumentation check

The strain data were collected using a Schlumberger Orion 3531D data logger. In order to check its accuracy and repeatability, five PL-10 strain gauges were bonded onto an aluminium plate with known material properties fixed in a Hounsfield tensometer and tested using the data logger at different load levels including loading and unloading in a linear manner. The results showed that the strain measurements were accurate to better than ± 0.3%. In addition, four tensile coupons, two with PL-10 and two with YL-10 strain gauges, were tested using the Monsanto extensometer machine, and the strain results were subsequently used to compare with the records stored in the data logger. It was confirmed that the accuracy of ± 0.3% was maintained for TML strain gauges as installed in the test specimens.

5.8 Test procedures

5.8.1 Beam S2

Beam S2 was a symmetrical double cantilever and there was
less concern about its instability in the longitudinal
direction. The test assembly was self-equilibrating with
only one hydraulic jack to be controlled in the test. In
the beginning the jack was pumped to make the central
bearing just touching the underside of the beam, jack
load and end reactions were both zero as the beam was
still at rest, an initial set of readings of dial gauges
and inclinometer points was then taken. There were all
together eight loading and four unloading stages, and at
each stage a full set of instrumentation readings was
recorded. However, due to the jack running out of
travel, it was not possible to trace the falling branch
of the beam's moment-rotation curve. The test took two
working days to complete.

5.8.2 Beam U1

Unlike the S2 test, the loading arrangement of specimen
U1 was not symmetrical and care had to be taken to avoid
possible longitudinal movement of the specimen during
loading. This was done by controlling the jack travel at
each end carefully such that the beam was kept level at
the central support at all times. Continuous monitoring

of the level was carried out by using a precise spirit level, resting on top of two small angle sections perpendicular to the web welded onto the pair of stiffeners (Plate 5.5), and two dial gauges located at the underside of the beam on both sides close to the support.

Initially the jack on the short cantilever was pumped until it touched the bearing, and then all the temporary supports were removed leaving the long span as a free-hanging cantilever. At this moment the internal support was out of level. Jacking on the long cantilever was immediately carried out to restore the level, and the initial set of readings was taken when the beam was steady. The end reaction at the long side was close to zero. Further increase of applied loads was done by alternate pumping of the jacks at the two ends to ensure that the internal support was level as described earlier, and usually jacking was carried out on the short span first. A set of measurements including strains, rotations and displacements was taken at the end of each load stage. When the ram of the bottom jack was completely extended on the long span, the jack was immediately locked and subsequent jacking was continued using the top jack of the double jack system. Balancing the level of the internal support was a slow process and so the whole test required three days to complete.

Location	Strain gauges	Type
LR1	61, 63, 65	
LR2	69, 71, 73	
LR3	83, 85, 87	
LR4	89, 91, 93	
SR1	13, 15, 17	Rosette
SR2	21, 23, 25	
SR3	31, 33, 35	
SR4	37, 39, 41	
L1	49, 51	
L2	53, 55	
L3	57, 59	
S1	1, 3	
S2	5, 7	
S3	9, 11	Pair
T1	81, 95	
W1	77, 87	
W2	79, 93	
W3	29, 41	

<u>Table 5.1</u> U1 strain gauge type and classification
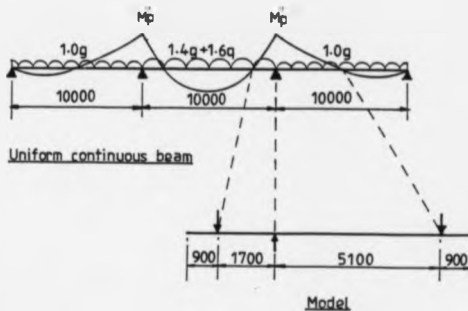
Fig. 5.1 Continuous composite beam modelled as an unsymmetrical double cantilever
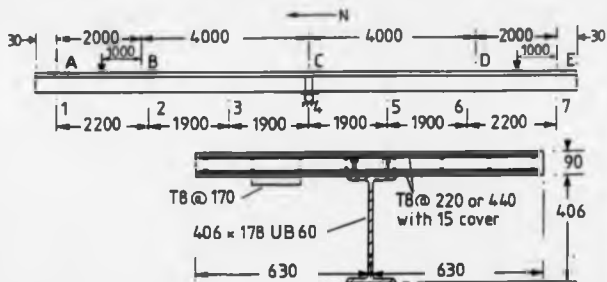
Fig. 5.2 Elevation and cross-section of beam S2

ELEVATION
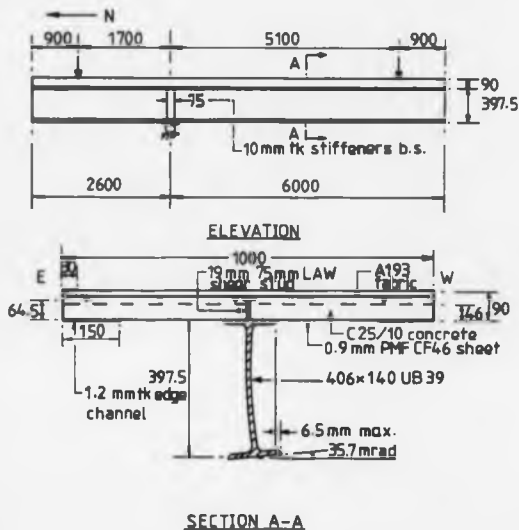
SECTION A-A

Fig. 5.3 Elevation and cross-section of beam U1 and testing arrangement

10mm thk stiffener

cylindrical bearing

100

70

Scale 1:10

CROSS-SECTION

10

10

50

load cell

100

70

Enerpac jack

bearing plate

connecting plates

base plate bolted to strong floor

approx. 560
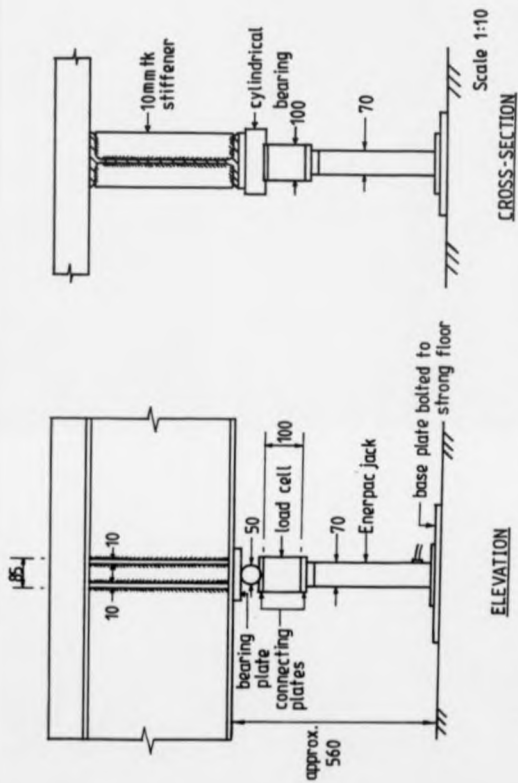
ELEVATION

Fig. 5.4 Central support details of beam S2

200

CROSS-SECTION

Reaction
frame

roller slider
spherical seating
grout

bearing
plate

base
plate

approx.
200

406×178 UB 60

ELEVATION

Scale 1:10
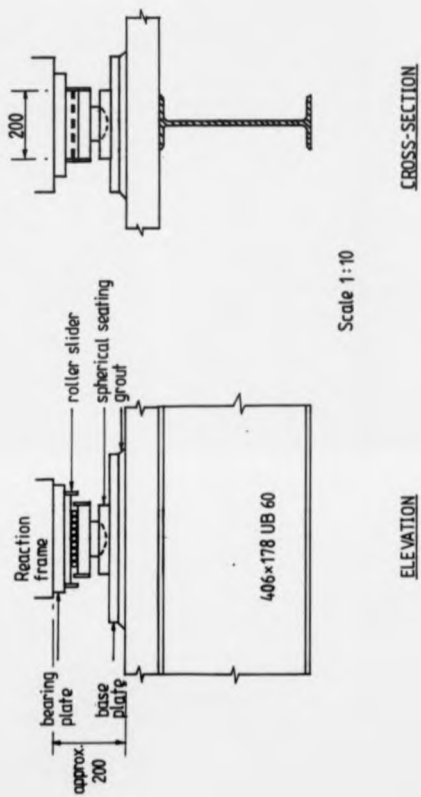
Fig. 5.5 End reaction details of beam S2
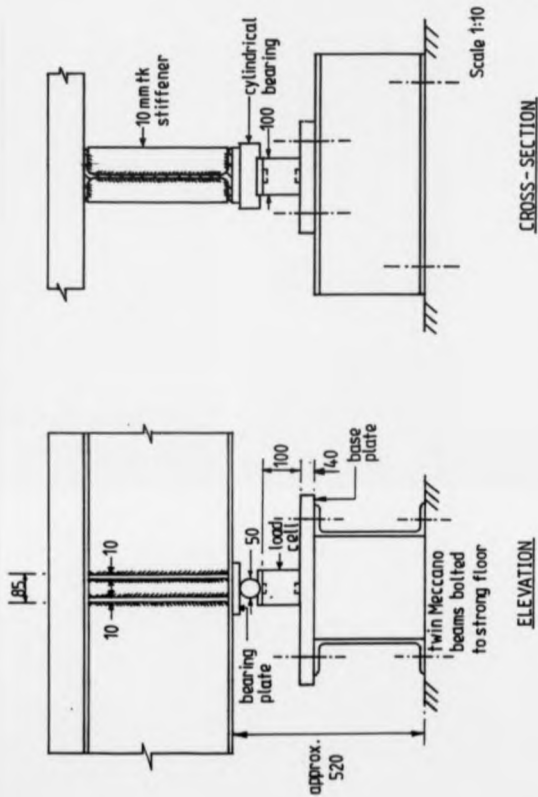
Fig. 5.6 Internal support details of beam U1

CROSS-SECTION

top plate bolted to
reaction frame

connecting cap

twin Enerpac jacks
bolted back-to-back

vertical guide channel
bolted to cross-beam

70

shear key

roller slider

spherical seating

grout

slab

approx. 930

base plate

200

Scale 1:10
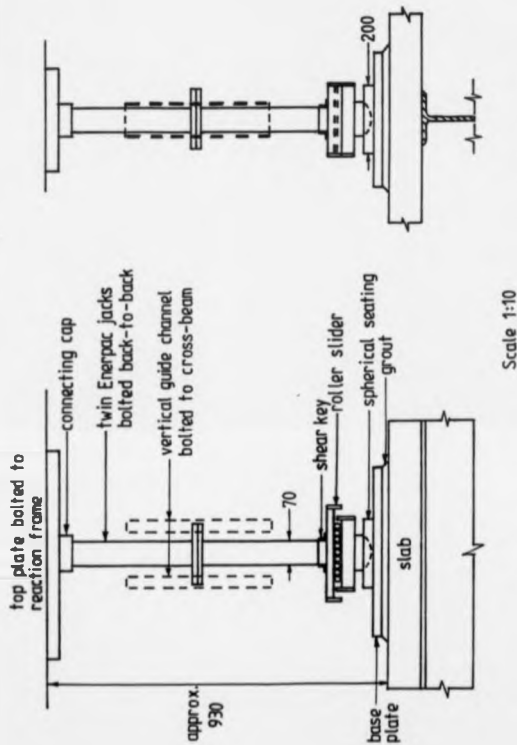
ELEVATION

Fig. 5.7 End reaction details of beam U1

147

KEY:

—▲— lateral displacement gauges

⊥ inclinometer points

C1-C8 concrete flange

S1-S8 steel flange

ELEVATION

PLAN

concrete slab
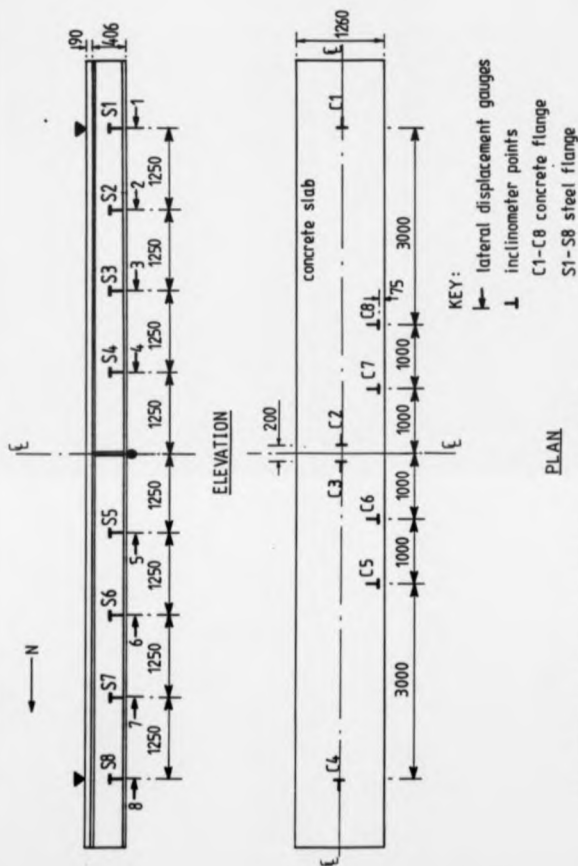
Fig. 5.8 Instrumentation positions for beam S2

Fig. 5.9 Instrumentation positions for beam U1

ELEVATION

BOTTOM FLANGE REFLECTED PLAN
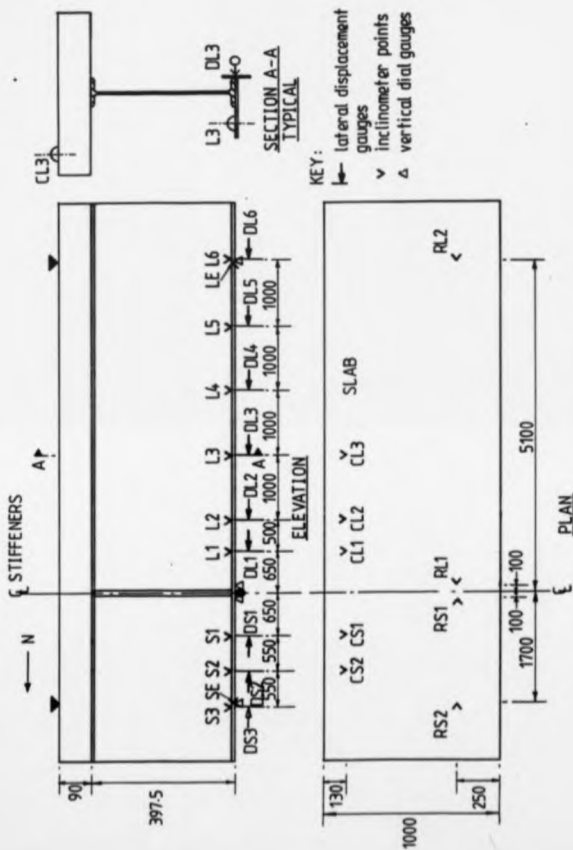
Fig. 5.10 Strain gauge positions for beam U1
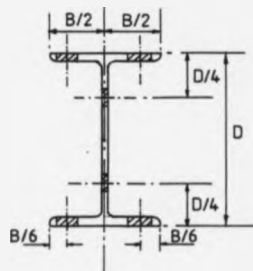
Coupon positions
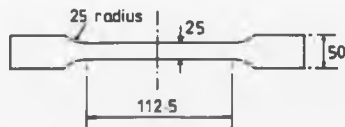
Test specimen

Fig. 5.11 Positions of coupon samples
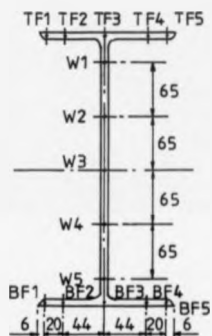
Fig. 5.12 Residual stress sample points for beam U1

Plate 5.1   Test rig for beam S2

Plate 5.2   End bearing for beam S2

Plate 5.3   Test rig for beam U1

Plate 5.4   Double jack system and vertical channel guide in test U1

Plate 5.5   Central support details for beam U1

Plate 5.7   Instrumentation for the
            measurement of lateral
            displacement for beam U1

Plate 5.6   Adjustable edge lateral restraint
            for beam U1

CHAPTER 6

TEST RESULTS OF T BEAMS AND DISCUSSION

6.1 Introduction

The results of both the auxiliary tests and testing are presented in this chapter. The large number of measurements of strains, rotations and displacements precludes the possibility of listing all the results, therefore those results that are relevant to the understanding of the global behaviour of specimens S2 and U1 are selected. For convenience, some results are presented graphically rather than in tables.

Observations from the tests are first described briefly. It was observed that the general patterns of behaviour in the two tests were similar. The final part of this chapter describes the common behaviour and then the features of the individual tests in greater detail.

6.2 Material properties

The yield stresses of the flanges and web for specimen S2 are 255 N/mm^2 and 270 N/mm^2 respectively, as reported in Reference (108). The hot-rolled section was Grade 43. The mean yield stress of the Y8 reinforcing bars is 446 N/mm^2 from four tensile tests. Properties of concrete are given in Table 6.1. Ordinary Portland cement and 20 mm coarse aggregate were used for the concrete. For specimen U1, the hot-rolled section was Grade 50. Coupon results and the strength of the A193 reinforcing fabric are summarised in Tables 6.2 and 6.3 respectively. Cube strengths of the concrete slab are given in Table 6.4. The weight of specimen S2 was 44.7 kN, as reported in Reference (97). The measured unit weight of concrete and steel section for specimen U1 are 23.0 kN/m^3 and 0.38 kN/m respectively.

6.3 Cross-sectional dimensions and imperfections

Mean measured cross-sectional dimensions of specimens S2
and U1 are given in Table 6.5.

The initial lateral imperfections of specimens S2 and U1
are plotted in Figures 6.1 and 6.2 respectively. Apart
from lateral imperfections, there was also uniform
tilting of the bottom flange with respect to the plane of
the web along the beam U1, and the mean measured value is
35 mrad, or 2.0°. However it is still within the rolling
tolerance, 45 mrad, in accordance with BS4 : Part 1[111].
The initial tilting of the bottom flange of S2 was small.

6.4 Residual stresses

A residual stress pattern for the universal beam was obtained for specimen U1 using the method of dissection. The results are given in Table 6.6 and plotted in Fig. 6.3. It was found that the compressive stress at the flange tip was small, as compared with the reported figures in other research publications, and the sign is opposite at the two tips in a flange. The observed stress distribution is similar to that for cold bent members reported by Young in an ECCS guide [112]. Thus it was suspected that the rolled section had been cold-straightened by rotorizing before delivery. In view of such low level of compressive residual stresses at the flange tips, their effect on the buckling of the bottom flange is expected to be small.

6.5 Compactness and beam resistance

The cross-section slenderness ratios were calculated in accordance with three Code of Practice – draft EC4[1], draft BS5950 : Part 3.1[2] and BS5400 : Part 3[8] summarised as in Table 6.7, and the calculations are given in Appendix C. The plastic hogging moments of resistance for beams S2 and U1 are reported in Table 6.8. The shear capacity, V_p , is taken as $f_y d w / \sqrt{3}$. Both the cross-section slenderness and beam resistance are calculated using measured material properties and dimensions. The partial material safety factors γ_m for the structural steel and reinforcing bars are taken as 1.0, that is appropriate for comparisons between test and design values.

6.6 Test results

There were 12 load stages - 8 loading and 4 unloading,
for the test S2. Although the beam was stable after
passing its maximum load, it was not possible to trace
the falling branch of the moment-rotation curve due to
insufficient travel of the hydraulic jack. The moment-
rotation curves for the two spans are shown in Fig. 6.4,
in which the span rotation is defined as the angle
between the tangents at the central support and at the
point of application of the point load. Bending moment
and shear force at the support corresponding to each load
stage are given in Table 6.9. The maximum recorded
bending moment and shear force are 410.8 kNm (M'/M_p' =
1.09) and 90.7 kN (V/V_p = 0.2) respectively.

The lateral deflections of the bottom flange for the
first few load stages were small, and displacements along
the beam for stages 3, 6, and 8 are shown in Fig. 6.1.
The lateral movement of the bottom flange, Δ , is defined
as the horizontal distance displaced from the initial
state to the deformed state of the intersection point
between the web and the bottom flange. The relationship
between the dial-gauge reading and rotations of the
concrete and the steel bottom flanges is shown in Fig.
6.5. The lateral deflections versus support moment at
locations of 2.5 m and 1.25 m from the support on the
long and short spans respectively are also given in Figs.

6.6 and 6.7. The bottom flange rotations plotted against the support moment are shown in Figs. 6.8 and 6.9. The transverse rotations of the concrete flange versus support moment are shown in Fig. 6.10.

There were 24 load stages for the U1 test. Table 6.10 gives results for the support moments and shear forces. It was again not possible to trace the falling branch of the moment-rotation curve because the specimen was unstable after the maximum load had been reached. The moment-rotation curve of the beam is shown in Fig. 6.11. At maximum load, the transverse rotations of both concrete and steel flanges became excessive, and for safety reasons the test was stopped soon after the load began to drop. The maximum hogging moment recorded is 272.6 kNm ($M'/M_p' = 0.9$), which is not included in Table 6.10 because the load dropped so quickly that there was no time to take a set of measurements at this level.

Figures 6.2 and 6.12 to 6.16 show the experimental results related to the lateral displacements and transverse rotations of the beam. The sign convention of the graphs refers to Figs. 5.3 and 6.14. The strain measurements are plotted in Figs. 6.17 to 6.29. For positions of the monitoring points and strain gauges, reference should be made to Figs. 5.9 and 5.10 and Table 5.1 in Chapter 5. The sign convention of the principal plane direction is shown in Fig. 6.21.

6.7 Behaviour of beams during test

The characteristics of specimens S2 and U1 were similar, in the sense that both specimens failed in a lateral-torsional mode of buckling and there was no sign of plastic local buckling in the support regions when the beams reached their maximum load. The yielded regions adjacent to the support were so short that the formation of plastic local buckling was prohibited. However the excessive lateral deflections and twisting of the bottom flange caused additional in-plane bending, and gradually a long-wave elastic buckle of the bottom flange associated with distortion of the web was developed, that was observed in both tests. The half wave length of the elastic buckle was about 2.2 m in both cases. No uplift or failure of shear connections was observed in either test. For S2, although the loading system was symmetrical in respect of the internal support, the observed displacements and rotations were generally higher on the southern span, where the long-wave buckle was formed, than on the northern span. This distinctive feature is illustrated clearly by comparing the two moment-rotation curves (Fig. 6.4) for the two cantilever spans. The transverse rotations of the concrete flange were observed to be small, in general less than 3 mrad, until the bottom flange began to yield. After yielding had occurred in the bottom flange, the rotations of both the concrete slab and the bottom flange began to

accelerate, and then increased in a faster rate in the
southern span, when the beam was approaching its ultimate
strength.   In the meantime, rotations of the concrete
slab in the northern span reversed their direction.

In the U1 test the concrete slab on both spans rotated in
the same direction transversely throughout the test.
Despite its distorted appearance the specimen was quite
stable when carrying the applied load, and it was not
necessary to provide any lateral restraints.   The
specimen eventually failed as a result of lateral-
torsional buckling (Plate 6.1).   Cracks on the concrete
surface were spaced at multiples of 200 mm which is
roughly the spacing of the wire mesh, and were closer
within the half of the cantilever span near the support
on both sides.   The maximum crack width was about 1 mm.
It was observed that a long-wave local buckle on the
bottom flange of the long span had just developed at
ultimate load due to in-plane bending and twisting.
There was also evidence that not only the bottom flange
but also the concrete slab had a tendency to curve in the
horizontal plane, as its flexural stiffness fell as a
result of cracking. There was no fracture of reinforcing
bars in this test.

6.8 Accuracy of results

The reaction at the support was taken as the mean value from two sets of calibration graphs, before and after the test. Since the reaction was known and the beam was self-equilibrating, the two end applied forces were calculated from static conditions. Linear regression analysis on the calibration results of the load cell showed a variation as much as ±2% of the applied load and the results were repeatable. Another error of about 1% may be resulted due to the system eccentricities and errors in incorrect dimensions of the two cantilevers, because of the assumption that they remain constant in length throughout the test. The overall error of the results should not exceed 4%, although the combined effect between the calibration results and system eccentricities is complicated.

Other instrumentation errors are discussed in Chapter 9.

6.9 Discussion of test results

There are a number of common features exhibited in the
two tests such as the initial deflection pattern of the
bottom flange, web distortion and mode of failure. It
was interesting to note that the lateral movements and
transverse rotations of the bottom flange followed the
directions of the initial imperfections at early load
stages (Figs. 6.1 and 6.2). This phenomenon is similar
to the effect of imperfections on the buckling behaviour
of struts[10,12].

It can be seen from Figures 6.8 to 6.10 (S2), and Figures
6.14 to 6.16 (U1) that the rotations of the bottom flange
are much higher than those of the concrete flange
especially when the beam is approaching its maximum
bending resistance. Nakamura et al[94] concluded from
their experiment that for a steel beam braced by slabs,
some web distortion would inevitably take place , and
hence cause a reduction in the torsional rigidity of the
member. The test results of specimens S1 and U1 indicate
that the web distortion is significant, and when
associated with increasing lateral displacements, it
might decrease the load carrying capacity of the beam and
prevent strain hardening of the material from taking
place.

Both specimens lost their bending resistance due to lateral-torsional buckling, because the lateral movements and transverse rotations of the bottom flange increased rapidly, when the beam was approaching its ultimate strength.

The test S1 was more stable than U1, probably because it was a symmetrical double cantilever. The torsional effects induced by the external forces at each end balanced out at the central support, and the bottom flange buckled eventually in a classical 'S' shape mode. Without further research, the torsional properties of the composite cross-section can be calculated following the recommendations by Heins[113]. The 1 m overhang at each end tends to provide assistance in reducing the amount of lateral movements of the bottom flange, by keeping the two ends more or less stationary, because the bottom flange was not free to warp at the loading point.

In the test, the bottom flange is subjected to non-uniform torsion as shown in Figs. 6.8 and 6.9. Due to the flexibility of the web, the amount of twisting occurring in the bottom flange is much higher than that in the concrete top flange (Fig. 6.10). On the southern span, buckling causes greater twisting of the concrete slab than in that on the northern span. When the beam is approaching its maximum strength, the transverse rotations of the concrete flange on the northern side

change direction, that is similar to the 'snap-through'
phenomenon that occurs in many elastic buckling
problems[12,114]. Lateral torsional buckling in isolated
composite T-beams is a rather complex subject and needs
further research. Without better understanding of the
behaviour of such beams, they should never be built
unbraced.

Similar to S1, specimen U1 behaved like a cantilever
rather than a floor-beam system, and the boundary
conditions do not allow the bending stiffness of the
concrete slab to restrict the lateral movement of the
bottom flange. The torsional stiffness of the concrete
flange can in principle do so, but it is less effective.
It is obvious that the initial imperfections dictated the
directions of the lateral displacements of the bottom
flange at early load stages as shown in Fig. 6.2. In
addition the tilting of the support by 2° imposed
favourable boundary conditions for the bottom flange to
deflect in a symmetrical rather than an anti-symmetrical
mode as in S2. To complicate the behaviour further, the
applied load positions at the two ends were fixed
laterally, and as the beam deflected and rotated, the two
end reactions caused a destabilising torque, relative to
the shear centre at each end, especially at high load.
The test thus created an unsafe model in comparison with
a true floor beam. The results are therefore on the safe
side. The results from specimen U1 can be assumed to

give a lower bound to the response of composite beams of
similar cross-section subjected to a 5.1 m long moment
gradient.

Most of the lateral displacements occurred after the
bottom flange near the support began to yield (Figs. 6.12
and 6.13). Due to the fact that the torsional stiffness
of the concrete flange is much greater than that of the
web and the bottom flange, Figs. 6.13 and 6.14 show that
the distortion of the cross-section is considerable.
Close to the end reaction, twisting of the bottom flange
diminishes, as shown in Fig 6.16. Apparently the
destabilised region is confined within about 2.5 m
adjacent to the internal support on both sides.

The strain measurements for the bottom flange (Figs. 6.17
and 6.18) show clearly the in-plane bending as a result
of internal stresses. It is also evident from the strain
measurements for the web (Fig. 6.19) that distortion of
the web is considerable on both spans especially when the
bottom flange and part of the web begin to yield. The
web out-of-plane bending strains were small when the
support moment is below first yield, but gradually
increased at a much faster rate until the beam lost its
bending stiffness. The results from two vertical strain
gauges on the web, no. 93 and 41, shown in Figs. 6.22 and
6.28 respectively, give further evidence that U1 failed
as a result of distortional lateral buckling. When

M'/M_p' is above 0.7, the vertical strains in the web increase rapidly. Distortion of the web is due mainly to the combined effect of three factors - flexibility of the web itself, relaxation of the boundary conditions due to yielding and equilibrium of internal stresses consistent with the global displacements and forces (kinematic condition). So the classical non-distortional buckling theory is not applicable to an isolated composite T-beam with a flexible web, even when it is in Class 2.

From Fig. 6.2, it can be seen that the unstable region was confined to within 2 metres of the central support (on both sides), and the beam U1 was still able to reach 0.9 Mp', which is higher than that for a steel beam alone. The higher shear in the short span, $V/V_p = 0.26$, did not cause the web to buckle. This gives further evidence that the interaction between local and lateral buckling was slight. The resistances of the T-beams S2 and U1 were predicted by the method of Clause 4.3 of BS5950 : Part 1[2]. The effective length was taken as 0.9L, even though the loading had a destabilising effect. It was assumed that both flanges were laterally restrained at the support, but the top flange only at the free ends. Cracked and uncracked composite cross-sections were used to evaluate the flexural and torsional properties respectively. The method gave M_d'/M_p' as 0.94 and 0.54 for the two beams respectively, whereas the test values, M_m'/M_p', were 1.07 and 0.88.

6.10 Conclusions

Specimens S1 and U1 do not represent a true composite multi-beam floor or deck system, but they are conservative models for real systems under the same moment gradients. Both beams lost their bending resistance as a result of lateral-torsional buckling with considerable web distortion. The initial imperfections influenced the load-deformation history, especially at early load stages, in such a way that movements and rotations of the bottom flange followed the same direction as the imperfections initially.

Strain, lateral movement and transverse rotation measurements showed that distortion of the web for both specimens is large especially after the support section passed its first yield hogging moment of resistance. In general the overall load-deformation behaviour can be described in two stages - pre-yielding and post-yielding. When the support section was below first yield, the rate of increase with loading of deformations such as strains, lateral movements and rotations was small. After the support section reached its first yield moment, the rate of increase in deformations began to accelerate and grew rapidly as the beam was approaching failure. The effect of web distortion must be allowed for when predicting the buckling strength for composite beams with a slender web. The results indicated that for a composite T-beam the St.

Venant torsional stiffness of the composite cross-section alone was not adequate to prevent significant twisting of the concrete flange and to restrain the bottom flange against lateral displacement; therefore U-frame action is more relevant to the problem.

	150 mm cube	200 x 100 mm cylinder	
Age days	compression strength, N/mm^2	split tensile strength, N/mm^2	Young's modulus kN/mm^2
28	42.6	3.44	27.0
89	47.5	3.36	-

Table 6.1 Properties of concrete for beam S2

Coupon position	f_y N/mm^2	f_u N/mm^2	E kN/mm^2
TF7	391.0	525.0	223
TF8	403.0	527.0	194
TW4	433.0	550.0	203
BW3	427.0	541.0	212
BF5	396.4	519.5	196
BF6	398.0	523.0	205

Table 6.2 Tensile test results for the specimen U1

Cross-section area mm^2	f_y N/mm^2	f_u at 7500 $\mu\varepsilon$ N/mm^2	E_r kN/mm^2
36.05	610.0	640.0	194.0

Table 6.3 Tensile test results for high-yield A193 fabric

Grade	Measured slump mm	Age days	fcu N/mm^2	No. of 100 mm cubes	Remarks
C25/10	50.0	3	14.8	2	
		7	22.9	2	
		14	27.7	2	
		28	30.1	2	
		38	34.1	2	7 days after U1 test
		87	35.3	4	end of U2 test

Table 6.4 Properties of concrete for beams U1 and U2

Specimen	Breadth B (mm)	Depth D (mm)	Thickness Top flange t_{tf} (mm)	Bottom flange f_{bf} (mm)	Web t_w (mm)
S2	177.8	406.4	12.80	12.80	7.80
U1	140.0	397.5	7.88	7.99	6.68

Table 6.5 Cross-sectional dimensions of specimens S2 and U1

Position	Residual stress N/mm²
TF1	14.27
TF2	-29.10
TF3	244.70
TF4	5.20
TF5	-18.60
W1	-28.42
W2	-99.47
W3	-124.50
W4	-118.72
W5	-53.00
BF1	36.46
BF2	34.10
BF3	233.10
BF4	20.80
BF5	-21.60

Sign convention : -ve for compressive stress

Table 6.6 Residual stress measurements for the specimen U1

	S2		U1	
Code	Web	Bottom flange	Web	Bottom flange
EC4	2	1	3	3
BS5950	1	1	2	3
BS5400	2	2	3	3

Table 6.7 Classification of cross-section for specimens S2 and U1

Specimen	First yield moment $M_y{}'$ (kNm)	Plastic moment $M_p{}'$ (kNm)	Shear capacity V_p (kN)
S2	291.9	378.5	463.0
U1, U2A, U2B	241.4	302.5	624.8

Table 6.8 Beam resistances of specimens S2, U1 and U2

Loading stages	Support moment M' (kNm)	$M'/M_p{}'$	Shear V (kN)	V/V_p
0	10.0	0.00	0.0	0.00
1	69.3	0.18	22.4	0.05
2	105.8	0.28	29.7	0.08
3	182.3	0.48	45.0	0.10
4	255.0	0.67	59.5	0.13
5	314.8	0.83	71.5	0.15
6	351.0	0.93	78.7	0.17
7	393.5	1.04	87.2	0.19
8	405.5	1.07	89.6	0.19
9	379.0	1.00	84.3	0.18
10	317.8	0.84	72.1	0.16
11	206.7	0.55	49.8	0.11
12	71.3	0.19	22.8	0.05

Table 6.9 S2 test results

Loading stages	Support moment M' (kNm)	M'/M_p'	Shear force on short span V (kN)	V/V_p
1	57.0	0.19	34.8	0.06
2	56.0	0.19	34.2	0.05
3	69.5	0.23	42.4	0.08
4	91.5	0.30	55.1	0.09
5	87.0	0.29	52.4	0.08
6	107.4	0.36	64.4	0.10
7	133.8	0.44	80.0	0.13
8	149.6	0.49	89.3	0.14
9	162.9	0.54	97.1	0.16
10	173.9	0.57	103.6	0.17
11	184.7	0.61	109.9	0.18
12	194.3	0.64	115.6	0.19
13	205.5	0.68	122.1	0.20
14	217.1	0.72	129.0	0.21
15	209.5	0.69	124.5	0.20
16	224.9	0.74	133.6	0.21
17	230.0	0.76	136.6	0.22
18	236.5	0.78	140.4	0.22
19	244.0	0.81	144.8	0.23
20	249.6	0.83	148.1	0.24
21	255.3	0.84	151.5	0.24
22	260.0	0.86	154.2	0.25
23	263.6	0.87	156.3	0.25
24	266.0	0.88	157.7	0.25

<u>Table 6.10</u>   U1 test results

Fig. 6.1 Lateral displacements of the bottom flange of beam S2

KEY:

Curve	M'/M'_p	Initial imperfections
1	0.48	
2	0.93	
3	1.07	
4		

Fig. 6.2 Lateral displacements of the bottom flange of beam U1

KEY:

Curve	M'/M'p Initial imperfections
1	0.44
2	0.57
3	0.74
4	0.88
5	

LAT. DISP.(mm) δ

LENGTH (m)

N
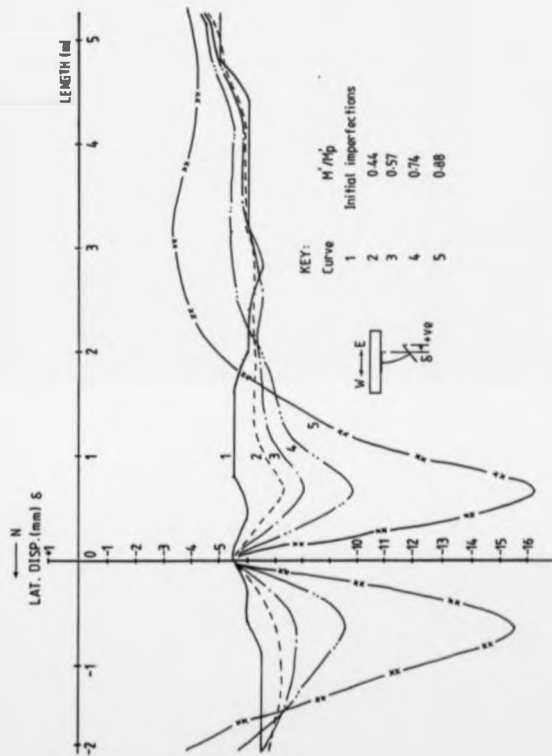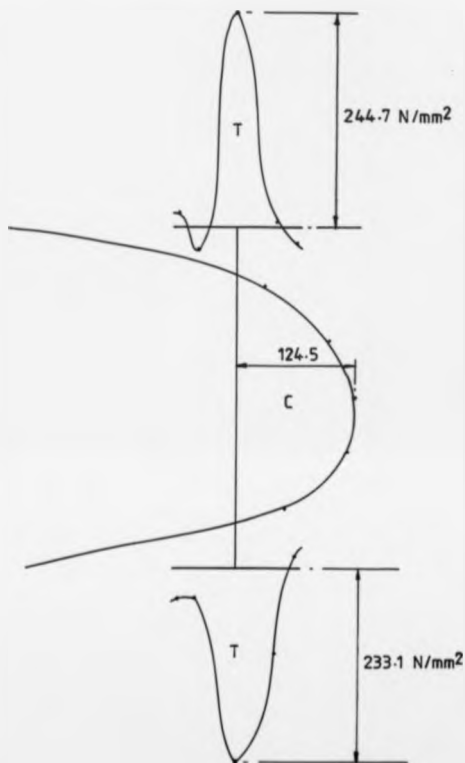
Fig. 6.3 Residual stress pattern of beam U1
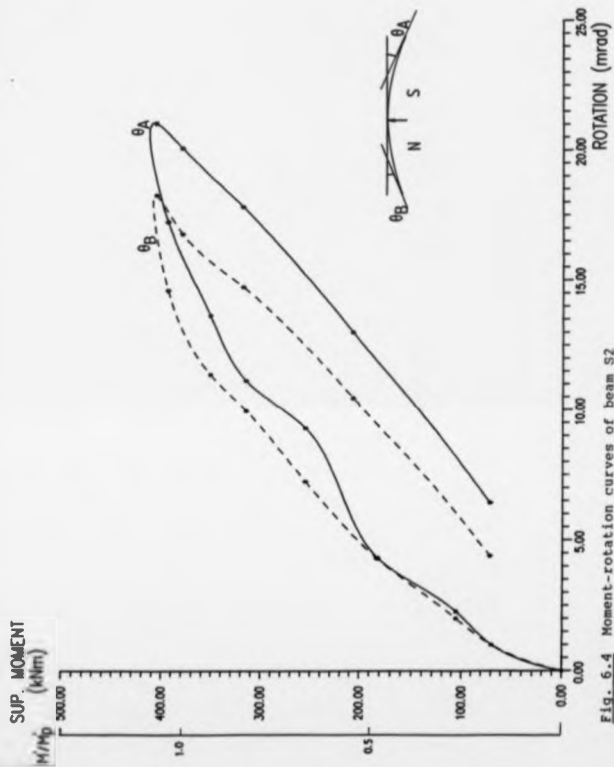
Fig. 6.4 Moment-rotation curves of beam S2

From geometry,
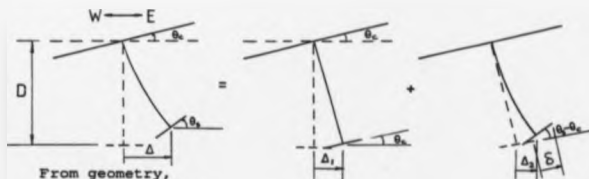
$$\Delta_1 = D \sin \theta_c$$

$$\Delta_2 = B/2 \left[1 - \cos (\theta_s - \theta_c) \right] + \delta$$

$$\Delta = \Delta_1 + \Delta_2$$

where

θ_c = rotation of the concrete flange, anti-clockwise +ve

θ_s = rotation of the bottom flange, anti-clockwise +ve

Δ_1 = lateral displacement due to rigid body rotation, eastward +ve

Δ_2 = lateral displacement due to web distortion, eastward +ve

δ = dial gauge reading, eastward +ve

B = bottom flange width

D = overall depth of the beam

Δ = lateral displacement defined in the test, eastward +ve

Fig. 6.5 Relationship between the lateral displacement measurement and rotation of the bottom flange for beams S2 and U1
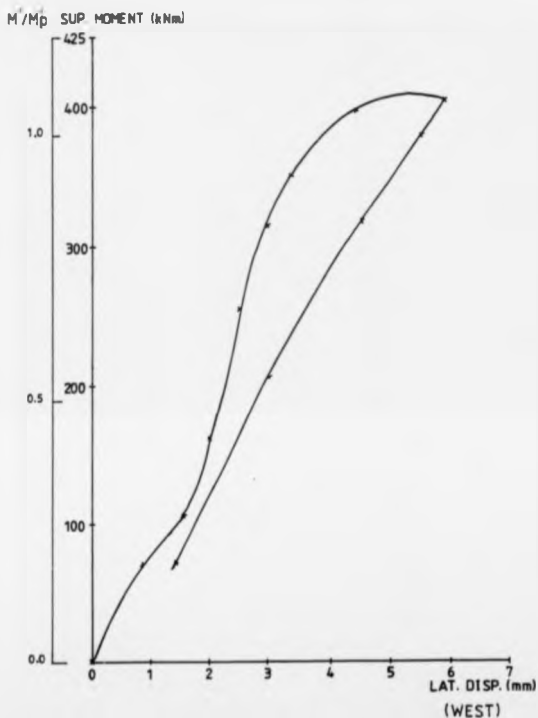
Fig. 6.6 Lateral displacement of the bottom flange
of beam S2 at monitoring point 3 in Fig. 5.8
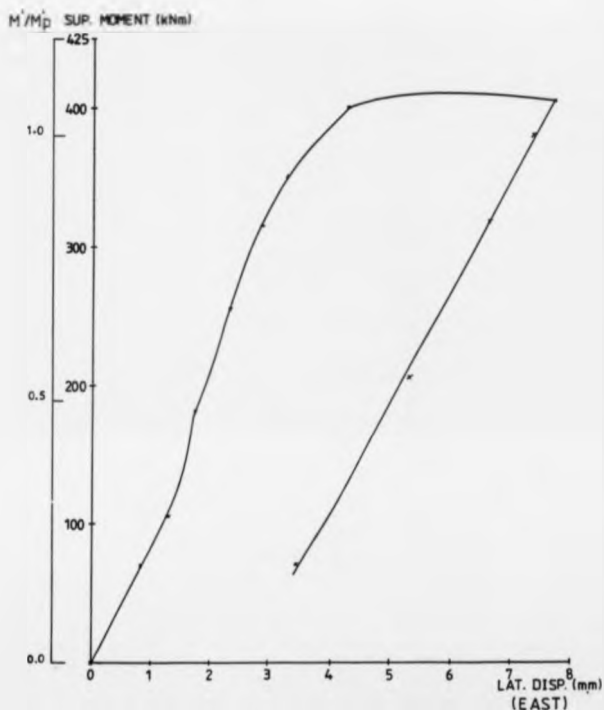
Fig. 6.7 Lateral displacement of the bottom flange of beam S2 at monitoring point 5 in Fig. 5.8
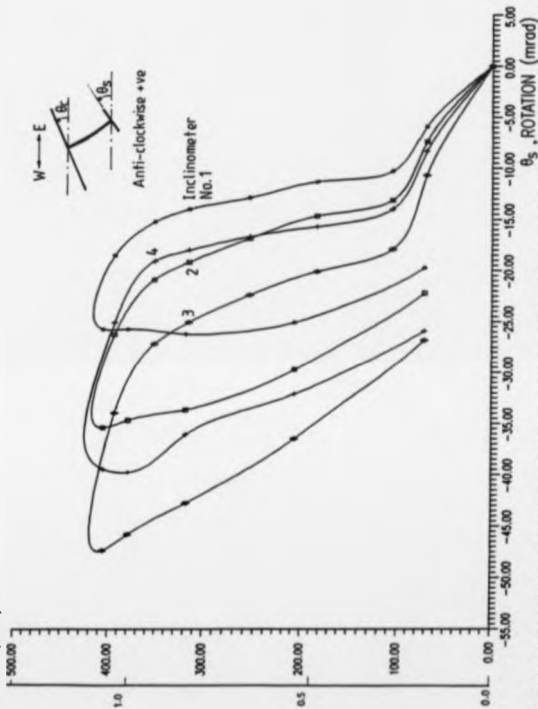
Fig. 6.8 Support moment versus bottom flange transverse rotations for beam S2 (south side)
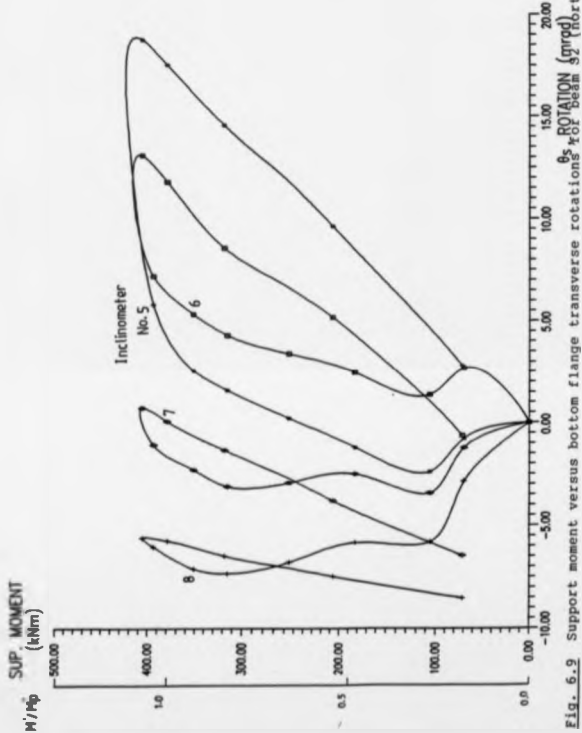
Fig. 6.9 Support moment versus bottom flange transverse rotations of beam 32 (north side)

187
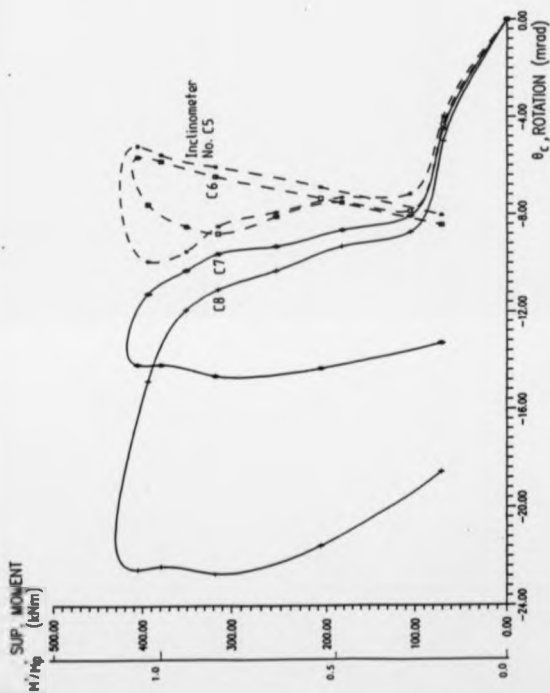
Fig. 6.10 Support moment versus concrete flange transverse rotations for beam S2
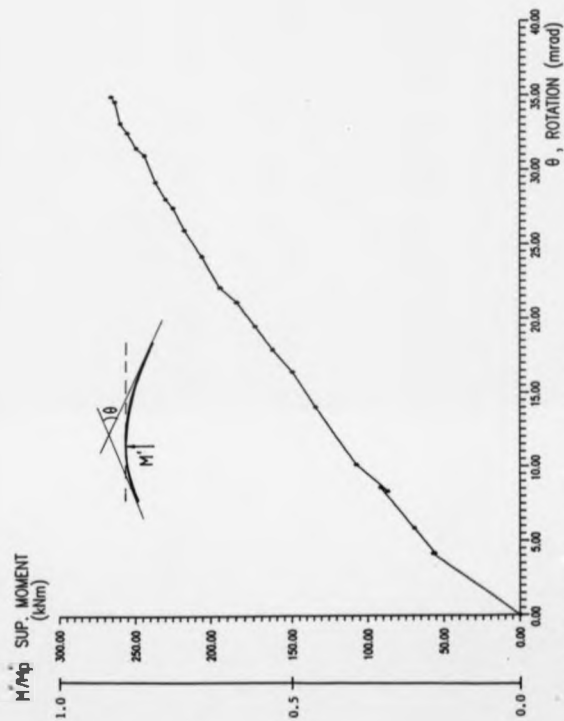
Fig. 6.11 Moment-rotation curve of beam U1

189
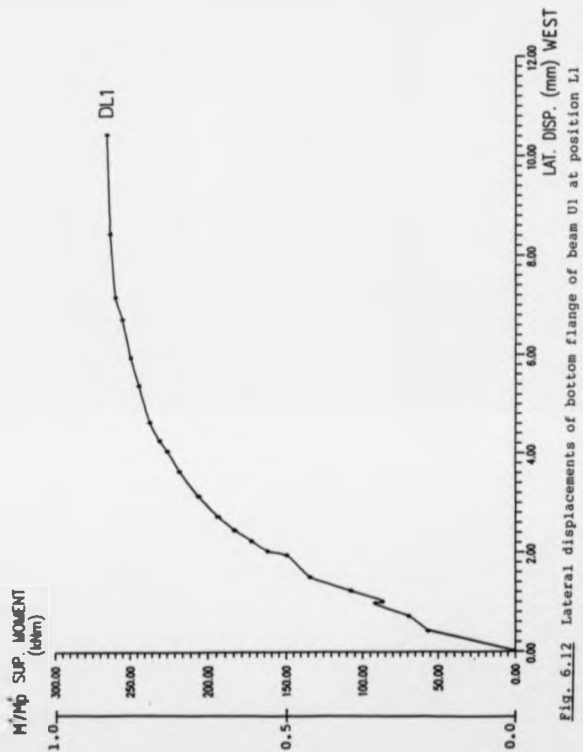
Fig. 6.12 Lateral displacements of bottom flange of beam U1 at position L1

190
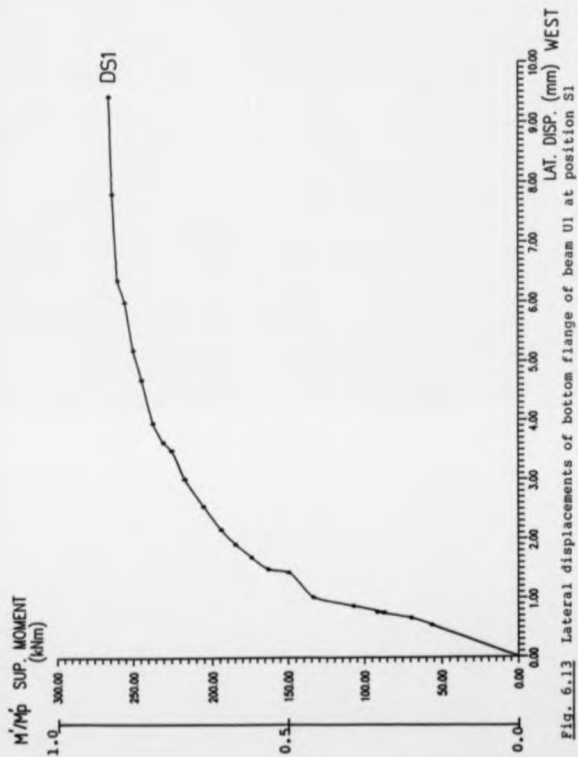
Fig. 6.13 Lateral displacements of bottom flange of beam U1 at position S1

191
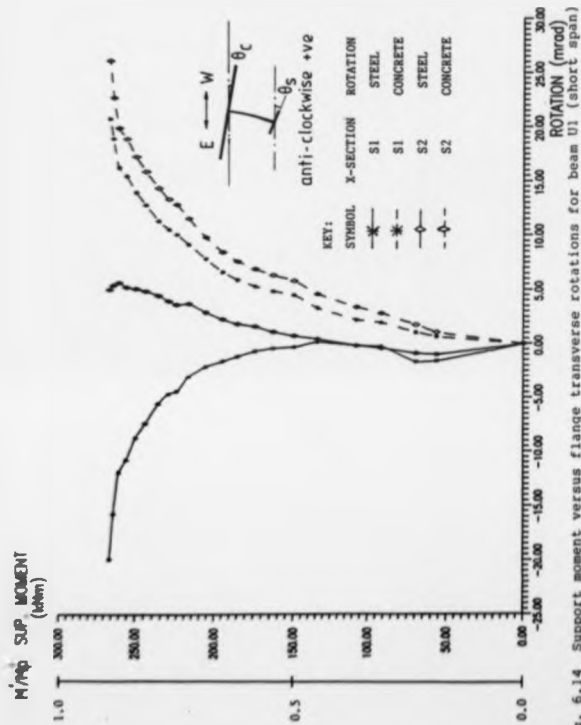
Fig. 6.14 Support moment versus flange transverse rotations for beam U1 (short span)

192

Fig. 6.15 Support moment versus flange transverse rotations for beam U1 (long span)

Fig. 6.16 Support moment versus bottom flange transverse rotations for beam U1 (long span)
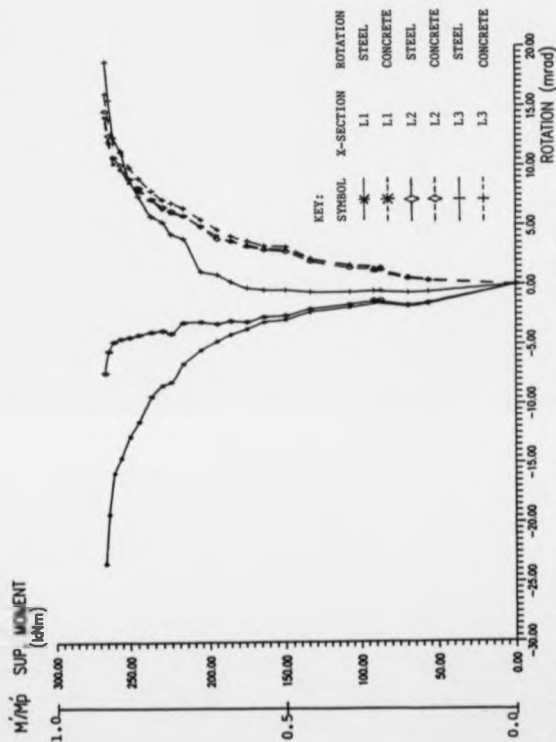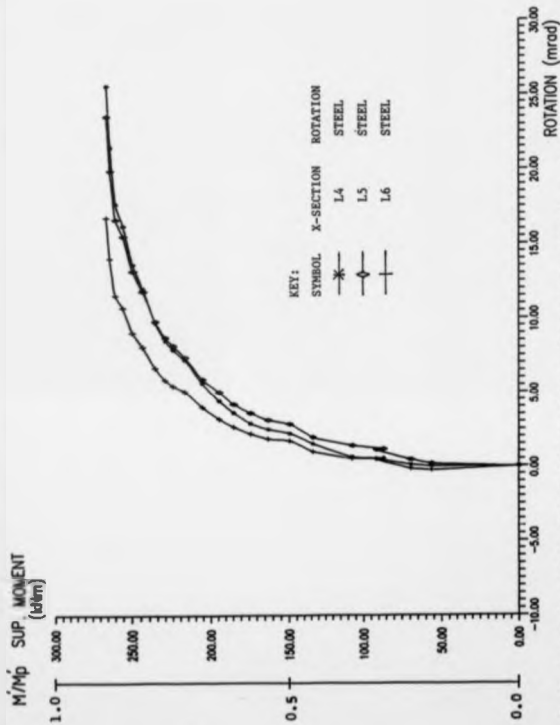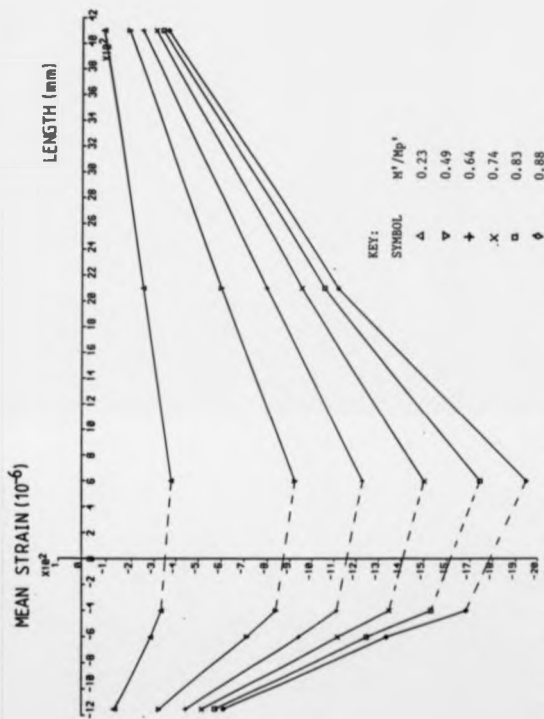
Fig. 6.17 Compressive strains of the bottom flange along the beam for beam U1
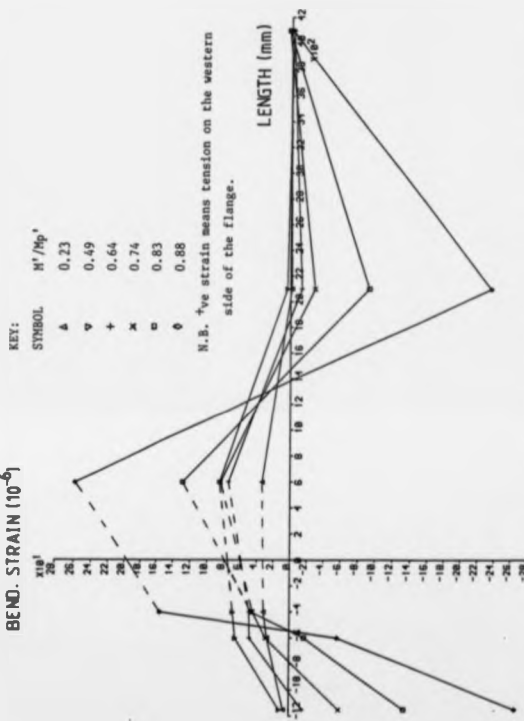
Fig. 6.18 In-plane bending strains of the bottom flange along the beam for beam U1
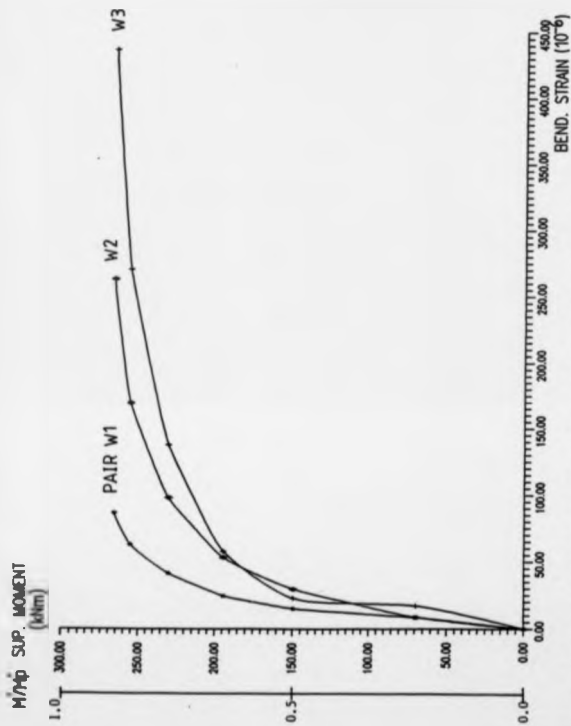
Fig. 6.19 Out-of-plane bending strains of the web for beam U1
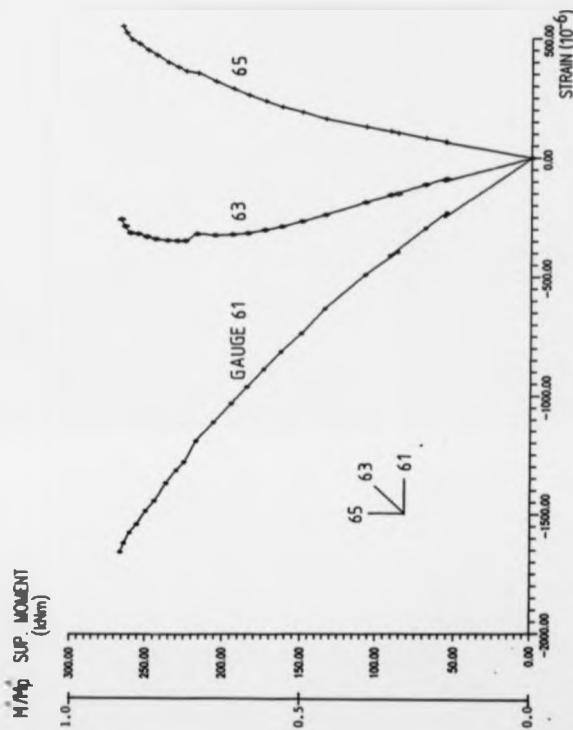
Fig. 6.20 Strains of rosette LR1 for beam U1

198
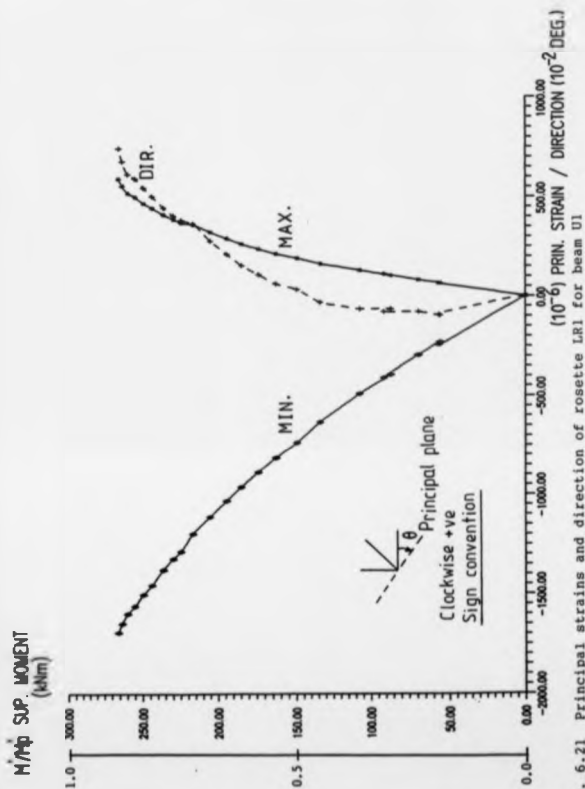
Fig. 6.21 Principal strains and direction of rosette LR1 for beam U1
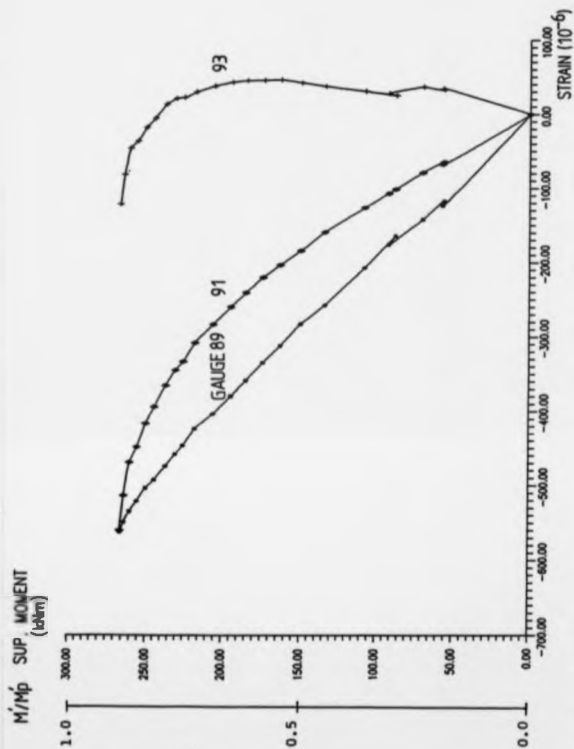
Fig. 6.22 Strains of rosette LR4 for beam U1
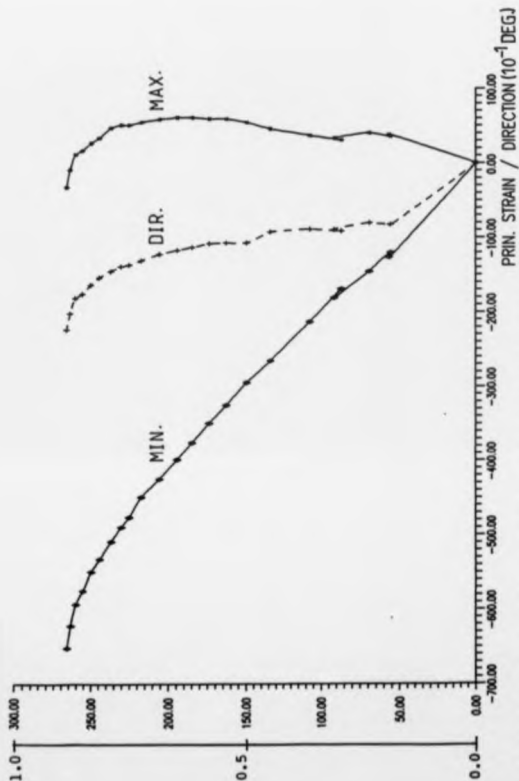
Fig. 6.23 Principal strains and direction of rosette LR4 for beam U1
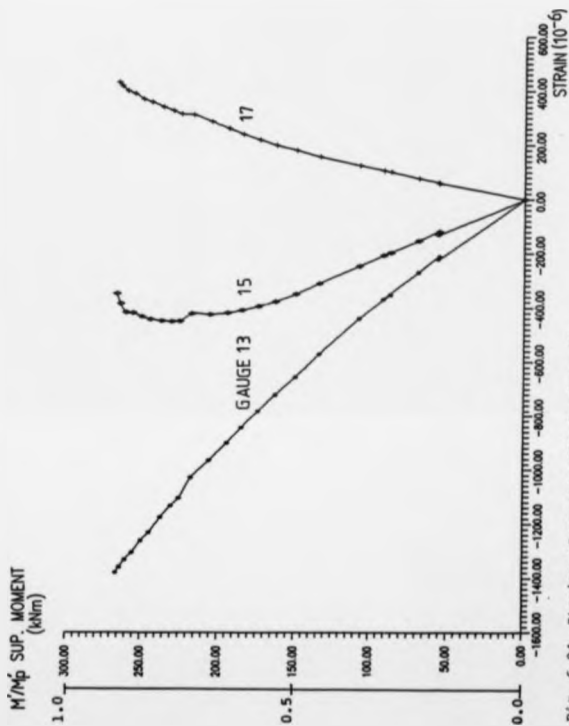
Fig. 6.24 Strains of rosette SR1 for beam U1
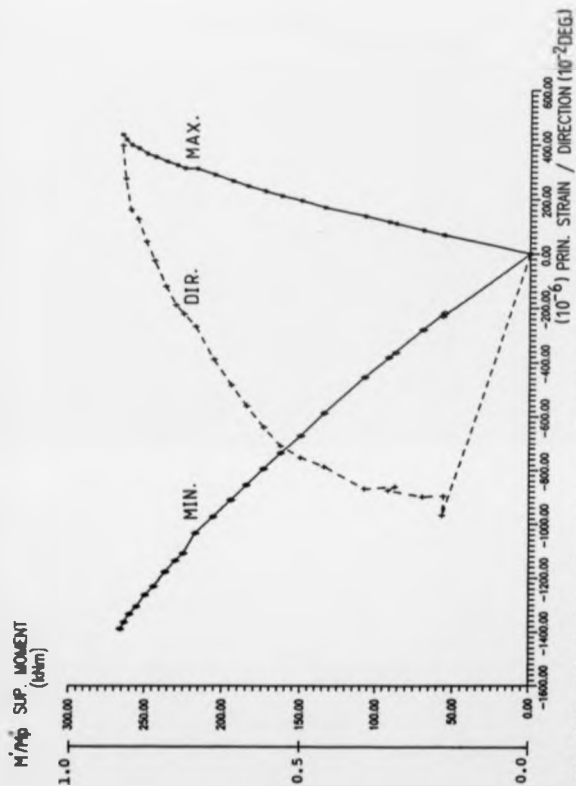
Fig. 6.25 Principal strains and direction of rosette SR1 for beam U1
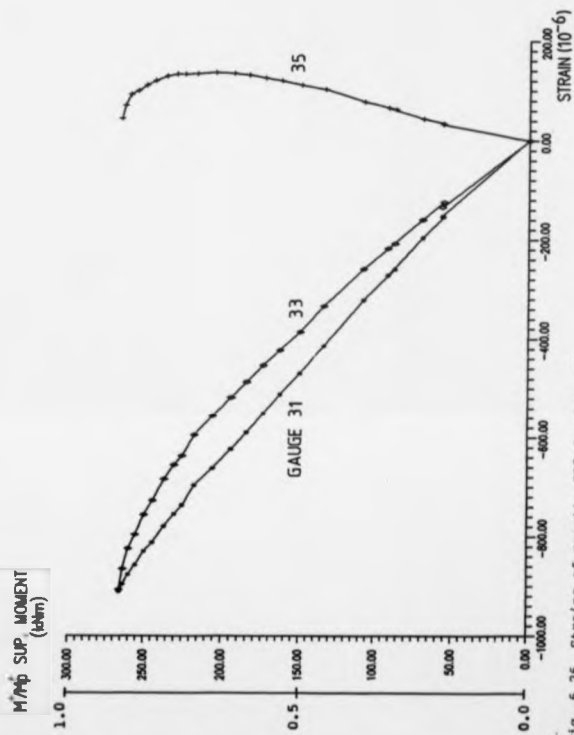
Fig. 6.26 Strains of rosette SR3 for beam U1
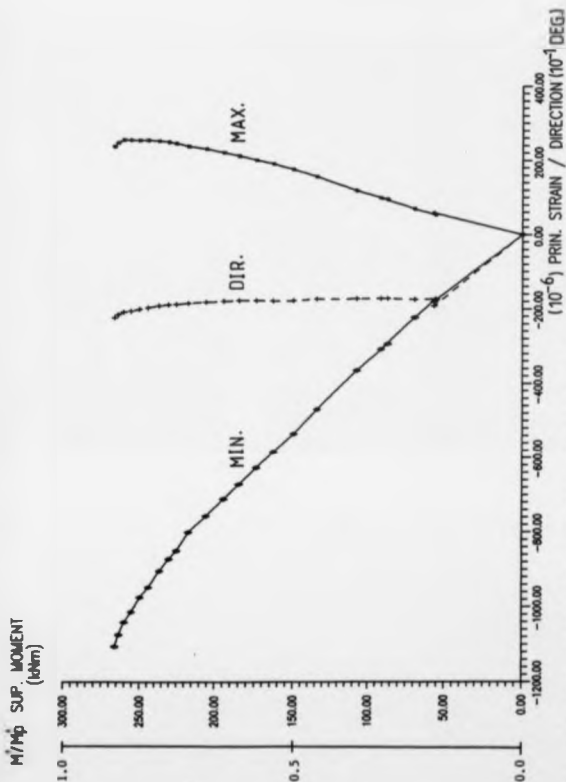
Fig. 6.27 Principal strains and direction of rosette SR1 for beam U1

204

Fig. 6.28 Strains of rosette SR4 for beam U1
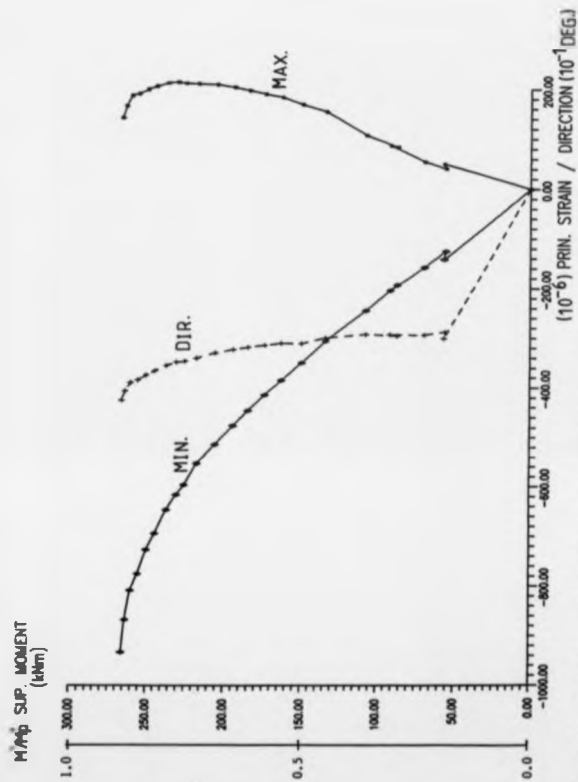
Fig. 6.29 Principal strains and direction of rosette SR4 for beam U1
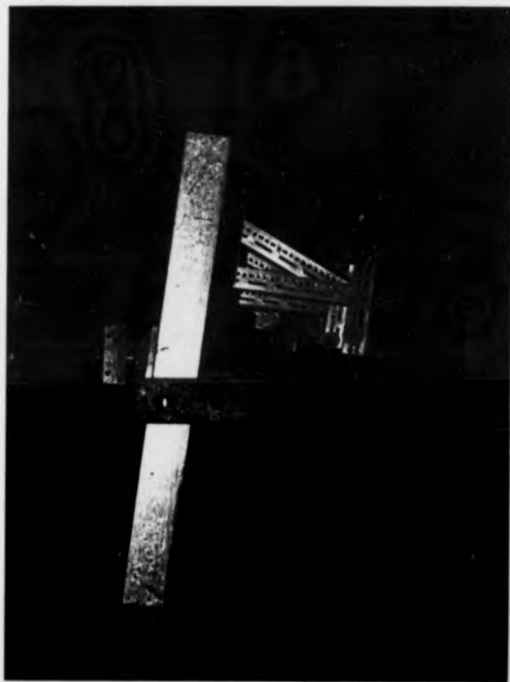
Plate 6.1   Failure of specimen U1

CHAPTER 7

TESTS TO INVESTIGATE DISTORTIONAL
LATERAL BUCKLING - INVERTED U-BEAMS

7.1 Introduction

From the results of tests S2 and U1, it is evident that
the boundary conditions do not allow the concrete slab,
which will certainly help to stabilise the steel beam in
a real floor-beam structure, to restrain the bottom
flange against lateral movement, as much as it would be
in a real structure. As a result, tests S2 and U1 may
produce conservative results. In order to further
investigate the restraining effect of the slab against
lateral buckling of the steel bottom flange, it was
necessary to conduct large scale inverted U-frame tests.
Two tests on inverted U-frame double cantilevers, U2 and
U3, were then carried out. Each steel beam represents an
edge beam in a multi-beam floor or deck system, which is
more vulnerable to lateral instability than internal
ones.

Common rolled sections were used for the specimens and
the cross-section classification was made just outside
Class 2 (EC4) by controlling the amount of longitudinal
reinforcement in the slab. A composite slab (with steel
decking) and a normal R.C. slab were used for specimens
U2 and U3, respectively. In addition to all the features

present in the U2 test, the U3 test incorporated a line loading applied on one side of the double cantilever, which simulated live loading on a floor. This arrangement was purposely set up to investigate whether beam stability would be impaired by transverse bending of the slab due to the presence of live loading.

7.2 Choice of specimens

specimen U2 was essentially a twin inverted L-beam .
Each inverted L-beam was identical to the specimen U1,
same hot-rolled steel section and amount of reinforcement
in the slab, apart from the positioning of the steel
section in relation to the slab. In order to simulate U-
frame action and to achieve realistic flexural bending
stiffness of the slab, the steel section was shifted
closer to the edge of the slab rather than right at the
middle in the case of specimen U1.

Test specimen U3 was similar to U2 but there were two
layers of longitudinal reinforcement in the slab and the
serial size of the steel section was different. It was
chosen to represent composite multi-beams in highway
bridges or viaducts rather than in buildings. For a
continuous bridge of uniform depth, critical hogging
moments usually occur when an HB vehicle straddles the
first internal support. The points of contraflexure are
located at a distance about 0.21 x span from the support
resulting in fairly steep hogging moment gradients.
Highway-bridge structures using universal beam (UB)
rolled sections seldom have spans above 20 m because of
economic reason. The hogging moment region of U3 was
therefore made slightly shorter (4.2 m) to be in line
with practice.

7.3 Details of test specimens

7.3.1 Specimen U2

The U2 specimen was divided into two inverted L-beams namely U2A and U2B. Geometry and dimensions of the specimen are shown in Figs. 7.1 and 7.2. Specimens U1 and U2 were constructed at the same time using the same batch of materials and concrete, and so their properties would be very similar. Shear connectors were placed in every other trough of the decking, but through deck stud welding technique was used in favour of the conventional method as employed for U1. Light horizontal and diagonal internal bracings were provided in two planes of the two central supports as shown in Fig. 7.2, to prevent lateral movement and tilting of each beam, but not to restrain rotation in plan, about a vertical axis (Plate 7.1).

7.3.2 Specimen U3

Similar to U2, the specimen U3 was also divided into two inverted L-beams namely U3A and U3B. Geometry and dimensions of the specimen are shown in Figs. 7.3 and 7.4. Two layers of steel mesh (top and bottom) were used to construct the slab. Slab reinforcement details are shown in Fig. 7.5. An additional layer of transverse bottom bars (Y8) was placed to increase the bending

resistance of the slab. It was provided to resist the sagging bending of the slab caused by the line loading.

Provision of shear connection was similar to U2 by using TRW Nelson shear studs, 75 mm LAW and 19 mm in diameter. Spacing of studs was made to 400 mm to avoid clashing with the reinforcement. Complete shear interaction was provided in accordance with the draft EC4 (360%).

Horizontal and diagonal internal bracings were provided in one plane only at the two central supports as shown in Fig. 7.4. The bracings were installed on the side where line loading was applied.

The orientation of the two steel beams was chosen to allow the initial imperfections to enhance the lateral movements of the two bottom flanges in the test. On the side with slab central loads, the initial lateral imperfections of the bottom flange for both beams near the support region were outwards with reference to the centre line of each steel member. When the slab was in sagging bending, it caused further outward movements of the two bottom flanges.

7.4 Construction of test specimens

Stiffeners for all the steel girders at the support and extension bars for monitoring transverse rotations were first welded in the laboratory. Strain gauges were then bonded onto the girders.

Propped construction was used for both beams U2 and U3. For U2, setting out was first carried out to the final positions of the twin beams, and then followed by laying profiled sheeting across the beams. The edges of the slab were formed by factory made edge closure channels which were held vertical by means of 50 mm x 1.2 mm thick restraint straps riveted to both the channel itself and the base of the decking. The twin beams were supported by four temporary cross-frames, and in turn supported the decking. Timber shuttering was used to construct the U3 concrete slab. All temporary works were dismantled 7 days after casting.

Stud welding was done by using the Nelson series 6000 (TR2400) dual gun system. Through deck and conventional stud welding were done to U2 and U3 respectively. Performance tests were carried out before welding to ensure reliability and workmanship in accordance with TRW Nelson's recommendations.

Concrete cubes were prepared and tested in accordance with BS1881 Part 108 and Part 116 respectively. Twelve 100 x 100 mm cubes were taken for specimens U1 and U2 because they were cast using the same delivery of concrete, and ten 150 x 150 mm cubes were prepared for U3. All cubes were cured under damp hessian for 24 hours, then transferred to a curing tank until they were crushed. After casting damp hessian was used to cover the entire slab and remained there for 7 days to complete the curing process. Inclinometer points were fixed after the curing was completed.

7.5 Testing rigs

Two portal reaction frames built up from standard structural "Meccano" were erected at each end of the beam U2. The rig is shown in Figs. 7.6 and 7.7 and Plate 7.2 . Bearing details at the southern end were similar to those in the S2 test shown in Fig. 5.5. The load was applied to each beam at the support through a double jack system, previously used for the U1 test, which consisted of two 20 tonne capacity Enerpac hydraulic jacks bolted together back-to-back. Special details and connecting parts were designed to attach each double jack to a 25 tonne load cell and a cylindrical roller bearing (Fig. 7.6). Guide rails were also provided to prevent lateral movement of the jack during loading (Plate 7.3). Thus the boundary conditions at the support only allowed vertical movement of the jack , longitudinal movement and horizontal in-plane rotations of the beam.

At the northern end of U2 two 50 tonne load cells, one for each beam, were used to obtain the reaction forces. Each load cell was placed on top of a roller slider integrated with a spherical ball joint seating as shown in Fig. 7.7. The bearing details at the southern end were similar to the north but without load cells. The spherical ball joint provided four degrees of freedom - three rotations and the longitudinal movement of the slab.

Details of the rig for the U3 test are shown in Figs. 7.8 to 7.11 and Plate 7.4. Central support details were similar to those in the U1 test shown in Fig. 5.6. In addition to the two reaction cross-frames at the end of the specimen, two portal frames were erected on the southern side, where the line loading was applied. The line loading was represented by eight equally spaced point loads, 500 mm apart, and consisted of two identical loading systems shown in Figs. 7.10 and 7.11 and Plate 7.5. A cross girder was used to transfer the jack forces from the two primary spreader beams to the strong floor. The loads were applied to the specimen through four double jack systems, one at each corner, and two jacks, on at each primary spreader beam. The double jack systems were identical to those used in the U1 test.

Different from U2, the central supports of U3 were made stationary, and the reaction forces were measured by two 25 tonne load cells each with a cylindrical roller bearing above it. At the northern end two 50 tonne load cells, one for each girder, were used to obtain the reaction forces, and served as a check on the global loading, using the equilibrium condition. The central slab loads were applied by two hydraulic jacks connected together using one pump through the two spreader beams. Two 10 tonne load cells were used to measure the reaction at each jack. The typical spherical ball joint seating

was placed between the jack and the spreader beam to
allow for longitudinal movement and rotations of the
slab.   Despite the presence of slab central loads and
different loading procedures the boundary conditions at
the central supports and the ends were identical to U2.

7.6 Instrumentation

7.6.1 Specimen U2

Two 25-tonne and two 50-tonne load cells were used to measure the reactions at four points out of the total of six. The strain gauge positions are shown in Figs. 7.12 and 7.13. 22 No.. and 28 No. TML strain gauges were installed on beams U2A and U2B respectively, and near the supports post-yield YL-10 gauges were used, capable of measuring strains above 10%. The gauges were located on the webs and the bottom flanges in such a way that they could detect not only the mean compressive or tensile strains, but also the bending strains as a result of possible lateral bending at high loads.

The in-plane beam rotations and transverse rotations of the concrete slab and bottom flanges were measured by using a demountable inclinometer at the positions shown in Figs. 7.14 and 7.16.

The vertical movements of the two central supports were measured by using four dial gauges located 90 mm away from the centre line of each beam on either side at the underside of the bottom flange. The lateral movements of the two bottom flanges were monitored at the positions shown in Figs. 7.15 and 7.16. Two theodolites were set up, each along one side of the specimen, and the lateral

movements of the bottom flanges were measured from the offset with reference to an initial datum line. The offset was obtained by reading a steel ruler, adopting the conventional levelling technique to obtain the shortest distance from a point by means of forward and backward motion.

7.6.2 Specimen U3

Six load cells (two 25T, two 50T and two 10T) were used to measure the reactions at six points out of the total of eight. The load cell readings gave the external forces at each load stage and also served as a check on the accuracy of the load cells, using the equilibrium condition. 22 No. and 20 No. TML strain gauges were installed in pairs on beams U3A and U3B respectively, and the arrangement is shown in Fig. 7.17 and 7.18.

The rest of the instrumentation for rotations and lateral movements were similar to the U2 test. The monitoring points are shown in Figs. 7.19 and 7.20. There were no dial gauges at the supports, but instead four dial gauges, one at each corner below the jacking point, were installed to monitor the vertical movements. Furthermore six dial gauges were fixed 1100 mm from the supports on either side of the specimen, to detect any possible separations between the slab and the steel beam at high loads.

7.7 Auxiliary tests

7.7.1 Material properties

Coupon samples were cut from the universal beams and tested in a 25-tonne Dartec tensile machine in accordance with BS18. U2 coupons were taken from two segments, one for each steel beam, flame cut at one end after the test was completed, and so there were no samples taken from the top flange. In the elastic region, strain was measured by means of a Sandner extensometer of gauge length 25 mm and sensitivity ±2.5%. Above yield the stress-strain relationship was obtained by measuring the elongation of the sample in a stroke operation. All data were logged to a micro-computer and the material properties were calculated automatically.

High-yield fabric and reinforcing bars were sampled randomly and six of each were taken. Tensile tests were subsequently performed on samples using a 10-tonne Monsanto Extensometer machine and the material properties were taken as the average from six tests.

Concrete cubes were tested using a 3MN Denison machine. Tests were carried out at regular intervals after concreting the slab, to decide a suitable date for the inverted U-frame test. For the U3 test, in which the

concrete strength was important in the prediction of the ultimate strength of the slab, three cubes were crushed during the second day of the test.

7.7.2 Cross-sectional dimensions and imperfections

Measurements of the thickness of rolled sections were taken at regular intervals using a micrometer. Six and eight locations were measured for each flange and the web respectively.

Initial imperfections of the bottom flange with reference to the top flange were measured using the same method adopted for the U1 specimen. The tilting of the bottom flange for each universal beam was further measured using an inclinometer.

7.7.3 Instrumentation check

The strain data were collected using a Schlumberger Orion 3531D data logger. In order to check its accuracy and repeatability, five strain gauges were bonded onto an aluminium plate fixed in a Hounsfield tensometer and tested using the data logger at different load levels in a linear manner. The results showed that the strain measurements were accurate to better than ±0.3%. In addition four tensile coupons, two with PL-10 and two with YL-10 strain gauges, were tested using the Monsanto

extensometer machine, and the strain results were subsequently used to compare with the records stored in the data logger. It was again confirmed that the accuracy of ±0.3% was maintained for TML strain gauges as installed in the specimens.

The surveying technique adopted to measure the lateral movements of the bottom flange was checked by repeated observations. At the beginning of the test, the initial readings were taken twice by two operatives independently, and the results were then compared to check the accuracy and repeatability. The accuracy was found to be better than 0.5 mm since the sight line was less than 14 metres. One operative was in charge of reading the theodolites for a whole test so that systematic error could be cancelled out since the increments were of main interest but not the absolute values.

The inclinometer used in the test has a sensitivity of 0.333 x 10-3 radians per division.

7.8 Test procedures

7.8.1 Specimen U2

The twin-beams were symmetrical double cantilevers which gave less difficulty with the beam rotation at the support; but it was important to keep the vertical support movement of both beams the same, or rather as close as possible, at each load stage, otherwise transverse bending of the concrete slab would have occurred, then the longitudinal stress distribution across the cross-section would have been non-uniform. This was undesirable because the shear lag effect may also become significant. To avoid this, the vertical jack travel for each beam was carefully controlled during loading by means of dial gauges, and the difference in level of U2A and U2B at the support was kept less than 1 mm at each load stage. Two sensitive spirit levels were employed to check any sign of out of level transversely and longitudinally at the supports. The method was successful and the differential level was found to be less than 1 mm for all load stages except stage 6, which was 2 mm out because of human error, and it was immediately rectified by bringing the two beams level again at stage 7. The rest of the testing was smooth and the whole test took four days to complete.

7.8.2 Specimen U3

U3 test was a complicated test not only because of the concern for beam instability, but also due to difficulties in controlling the many external forces during the testing - there were altogether 14 load and reaction points acting on the specimen. The main aim was to maintain the line loading on the southern side high enough to just reach the bending resistance of the slab at the final load stages, and to see whether the deterioration of slab flexural stiffness would affect the lateral stability of the steel bottom flanges. It was therefore necessary to know all the reactions exactly at any load stage. This was achieved by feeding data from load cells into a micro-computer which was programmed to give updated reaction forces calculated from equilibrium. With the instant computerised results the forces on the line loading were closely monitored to ensure that the strength of the slab was not exceeded.

The loading system was simplified as shown in Fig. 7.21. In the test, jacks 1,2,5 and 6 were individual and independent but jacks 3 and 4, which powered 8 No. of point loads representing the line loading, were connected to a single hydraulic pump via a T junction socket. A dial gauge was installed at each corner at the underside of the bottom flange directly below the jacking point. The testing procedure was as follows :

1) When the support hogging moments were below first
    yield, jacks 1, 2, 3 and 4 (Fig. 7.21) were pumped
    simultaneously until jacks 3 and 4 reaching 60 % of
    their maximum loads. The loads on jacks 1 and 2
    were prevented from falling to zero by controlling
    the pumping rate of jacks 3 and 4 as necessary.
    Differential movement of jacks 1 and 2 was kept to a
    minimum with the help of dial gauge readings during
    pumping.

2) The beam levels at the two supports were now out of
    level because jacking had been done on one side
    only. Jacks 5 and 6 were then pumped downwards to
    restore the level at the supports. Again
    differential movement of jacks 5 and 6 was kept to
    a minimum, close to zero if possible. In the
    meantime, checks were made to ensure that jack
    forces at 3 and 4 were about 80% of their ultimate
    loads. Sometimes it was necessary to repeat step 1
    and to follow up pumping jacks 5 and 6 several times
    in small increments to obtain the right balance.

3) When the desirable load level was reached, lateral
    movements, rotation and strain measurements were
    taken. Steps 1 to 3 were repeated for the next
    higher load level until the support moment were
    above first yield.

4) Jacks 1 and 2 were then pumped simultaneously to
    increase the hogging bending. As a result, loads
    fell at points 3 and 4. Loads at 3 and 4 were then
    increased to about 80% of their maximum values.

5) Jacks 5 and 6 were pumped to restore the beam levels
    at the internal supports, meanwhile load levels at 3
    and 4 were closely monitored, making sure that they
    were between 90% and 100% of the maximum load. If
    the loads at 3 and 4 were too high, forces on jacks
    1 and 2 were increased to reduce the surplus. It
    was necessary to apply the loading in small
    increments and to adjust the travels of all the
    jacks in due course to obtain the right balance.
    Above yield, a large amount of jack travel
    corresponded to a small increase in support hogging
    moments. The loading was therefore a very slow
    process.

6) When the load was close to the desirable level,
    jacks 3 and 4 were further pumped in order to
    maintain the slab load as close as possible to the
    design ultimate load.   Once the twin-beams
    stabilised, lateral movements, rotation and strain
    measurements were then taken.

7) Steps 4 - 6 were repeated until the beam became
    unstable.

In general the testing method was successful but it was found difficult to maintain the slab loading at a specified value due to creep, concrete cracking and the overall equilibrium. However it was possible to control the slab loading within a small defined range. The test took five day to complete.
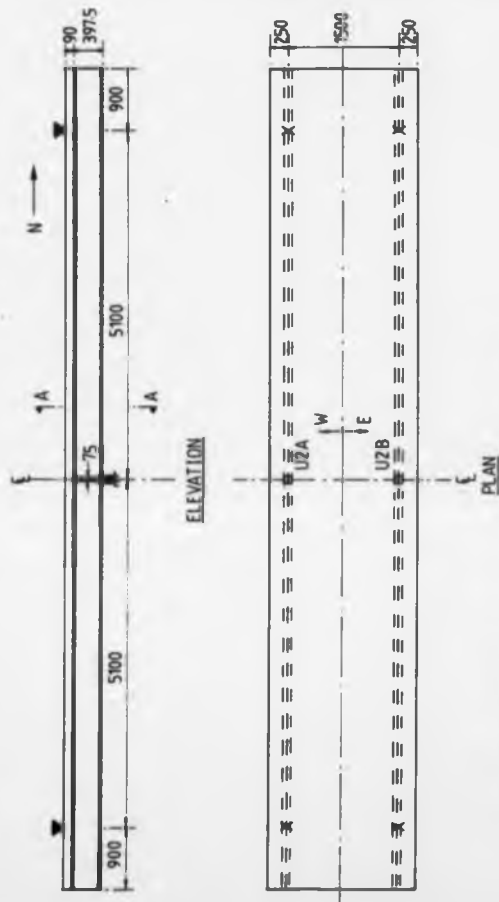
Fig. 7.1 Geometry of the inverted U-frame specimen U2
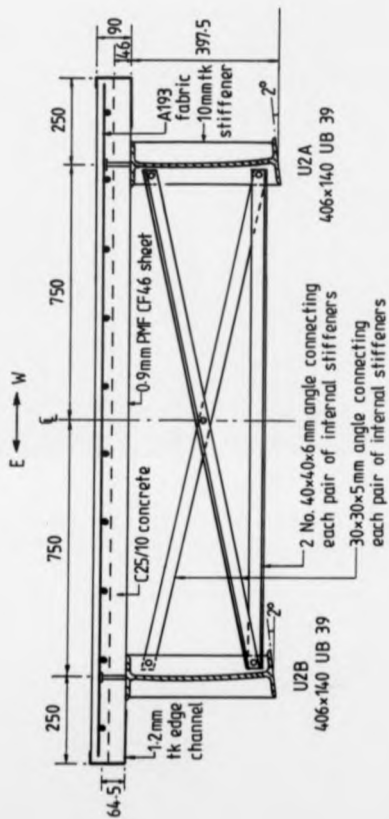
Fig. 7.2 Cross-section of specimen U2

SECTION A-A

E ——▶ W

90
46
397.5

A193 fabric
10 mm tk stiffener

U2A
406×140 UB 39

250

750

0.9 mm PMF CF46 sheet

2 No. 40×40×6 mm angle connecting
each pair of internal stiffeners

30×30×5 mm angle connecting
each pair of internal stiffeners

C25/10 concrete

750

250

1.2 mm tk edge channel

U2B
406×140 UB 39

64.5
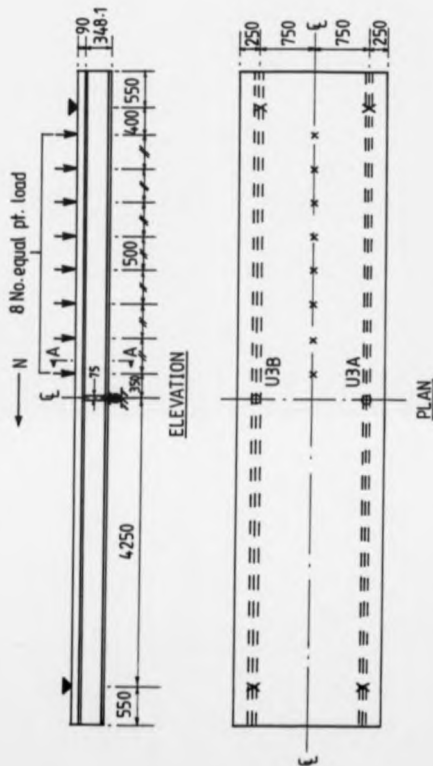
Fig. 7.3 Geometry of the inverted U-frame specimen U3
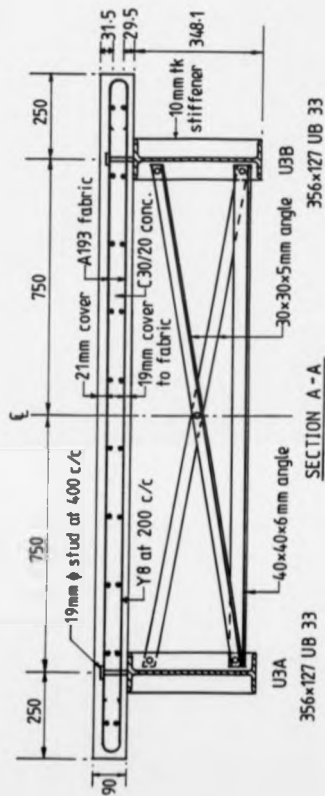
Fig. 7.4 Cross-section of specimen U3

Labels within the figure:

31·5
29·5
348·1
250
750
250
90
750

19mm ⌀ stud at 400 c/c
21mm cover — A193 fabric
19mm cover — C30/20 conc.
to fabric
10mm lk stiffener
Y8 at 200 c/c
40×40×6mm angle
30×30×5mm angle

U3A
356×127 UB 33

U3B
356×127 UB 33
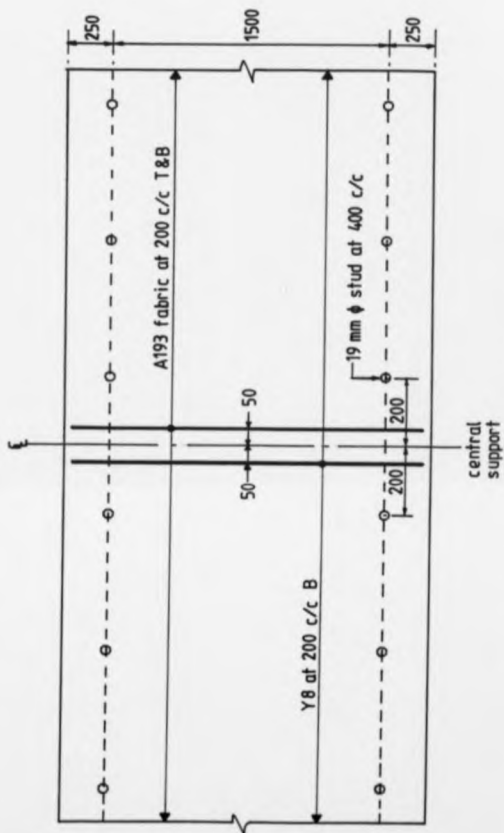
SECTION A-A

Fig. 7.5 Slab reinforcement details of specimen U3

10 mm tk stiffener
cylindrical bearing
70
100

CROSS-SECTION

406×140 UB 39
load cell
100
bearing plate
connecting plates
10
85
10
50
70

twin Enerpac jacks bolted back-to-back
vertical guide channel bolted to cross-beam

base plate bolted to strong floor

connecting cap

ELEVATION

approx. 940
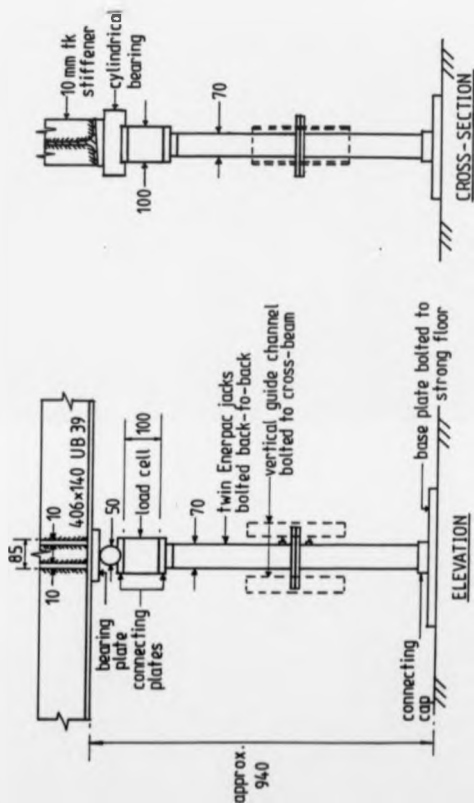
Fig. 7.6 Central support details of specimen U2

CROSS-SECTION

ELEVATION

reaction frame
bearing plate
load cell
shear key
roller slider
spherical seating
grout

connecting plate

base plate

approx. 440

200

200

406×140 UB 39
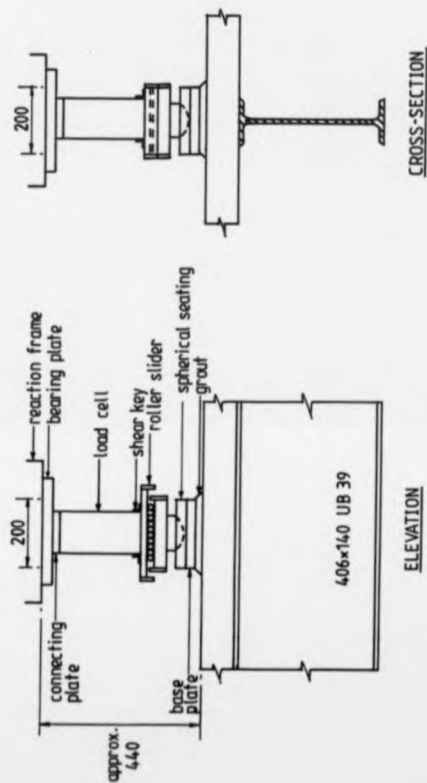
Fig. 7.7 Bearing details at the northern end of specimen U2

Fig. 7.8 Bearing details at the northern end of specimen U3

ELEVATION

top plate bolted to reaction frame

connecting cap

twin Enerpac jacks
bolted back-to-back

vertical guide channel
bolted to cross-beam

connecting plate

load cell

shear key
roller slider

spherical seating
grout

356x127 UB 33

base
plate

approx.
1170

70

120

200

CROSS-SECTION

200

top plate bolted to reaction frame

connecting cap

twin Enerpac jacks bolted back-to-back

vertical guide channel bolted to cross-beam

shear key

roller slider

spherical seating

grout

slab

base plate

approx. 930

70

200

ELEVATION

CROSS-SECTION

Scale 1:10

Fig. 7.9 Bearing details at the southern end of specimen U3
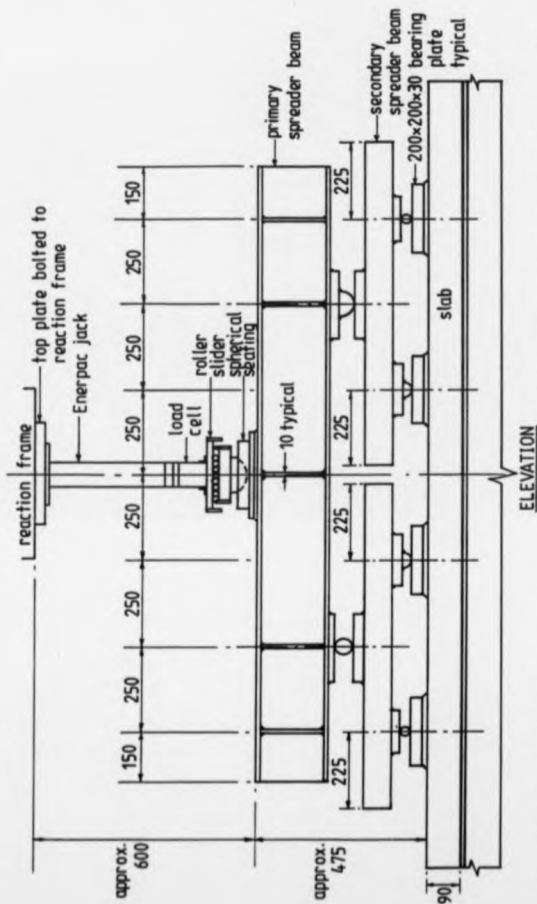
Fig. 7.10 Loading system for the simulation of uniformly distributed loads in test U3
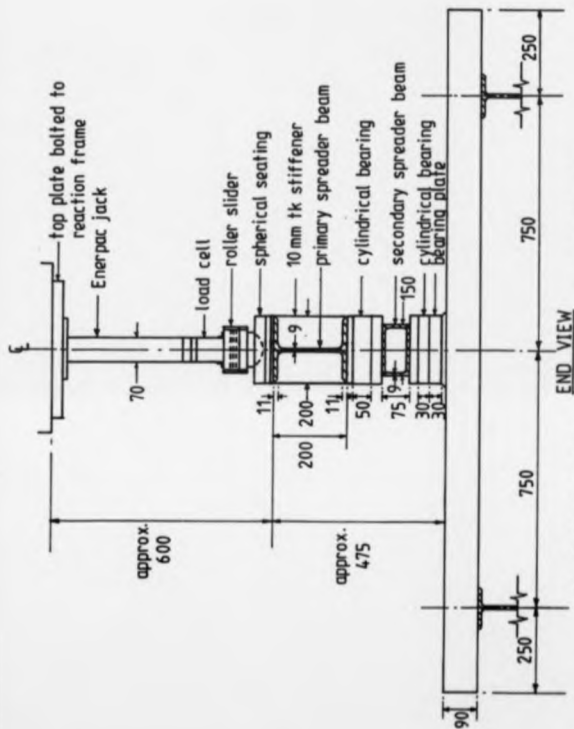
Fig. 7.11 End view of the line loading in test U3

Labels (top to bottom on the loading apparatus):
- top plate bolted to reaction frame
- Enerpac jack
- load cell
- roller slider
- spherical seating
- 10 mm tk stiffener
- primary spreader beam
- cylindrical bearing
- secondary spreader beam
- cylindrical bearing
- bearing plate

Dimensions:
- approx. 600
- 70
- 11 1/4
- 200
- 11 1/4
- 9
- 50
- 75 9
- 30
- 30
- 150
- approx. 475
- 250
- 750
- 750
- 250
- 90

END VIEW

239
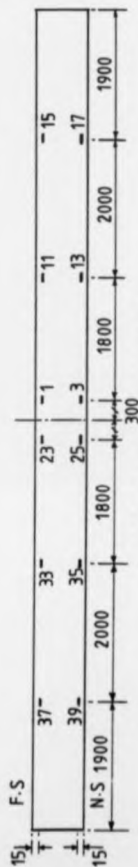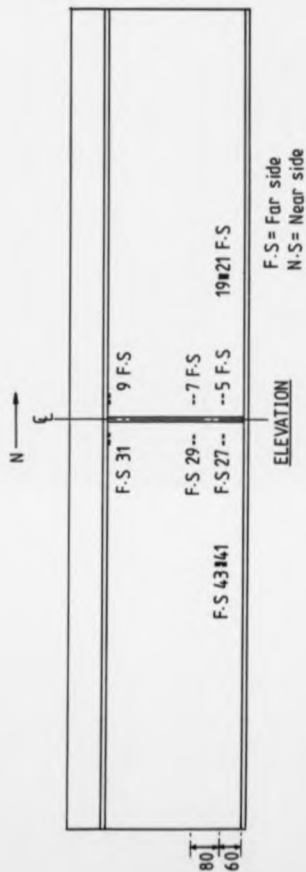
Fig. 7.12 Location of strain gauges for beam U2A

240
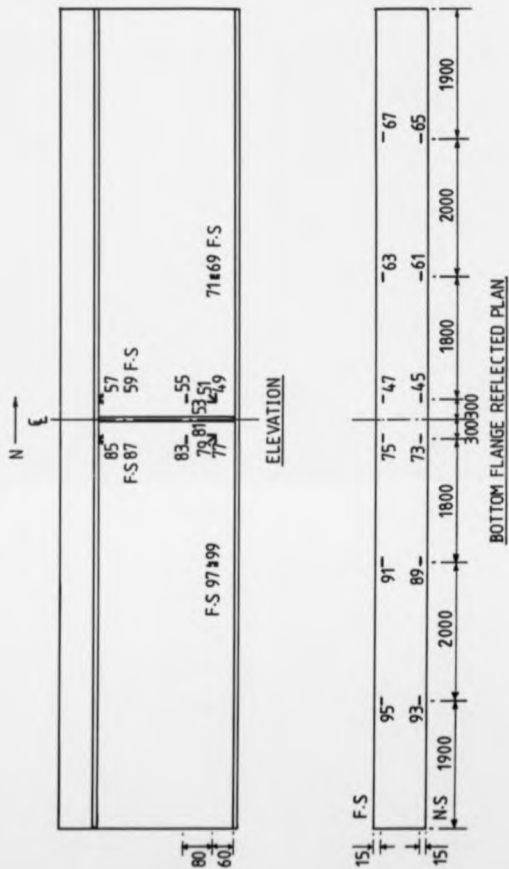
Fig. 7.13 Location of strain gauges for beam U2B
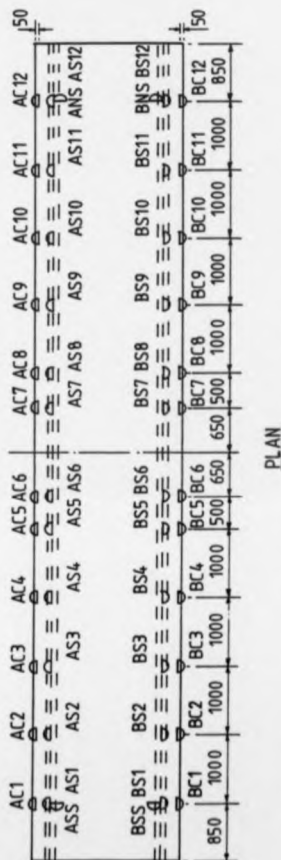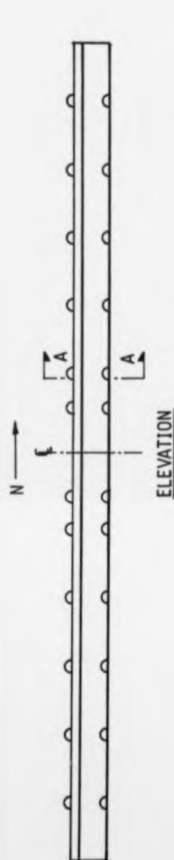
Fig. 7.14 Monitoring points for transverse rotations of the flanges for specimen U2

242
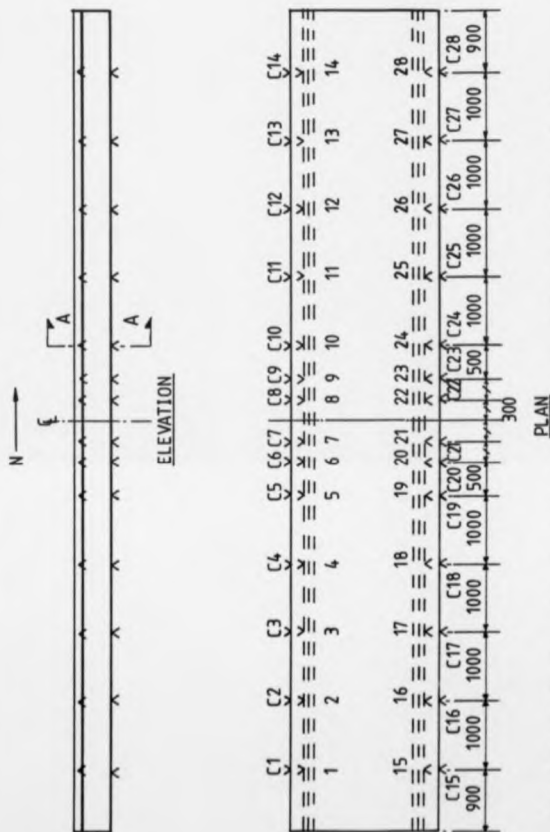
Fig. 7.15 Monitoring points for lateral displacements of the flanges for specimen U2
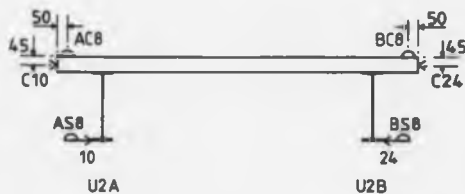
SECTION A-A
TYPICAL

Fig. 7.16 Positions of instrumentation for
specimen U2

BOTTOM FLANGE REFLECTED PLAN

Fig. 7.17 Location of strain gauges for beam U3A
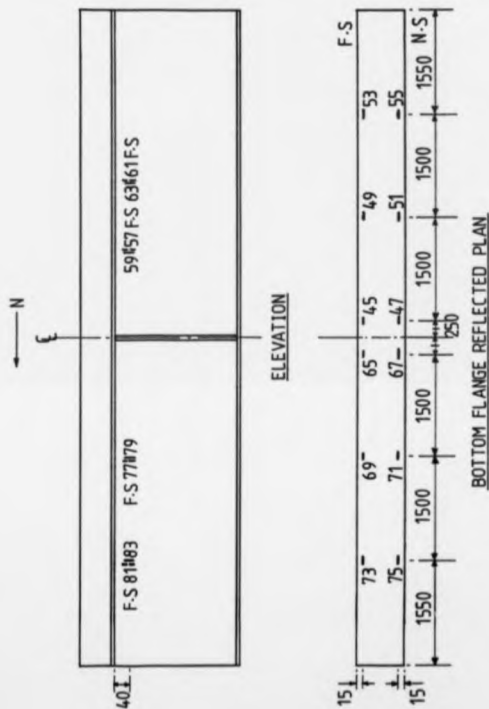
Fig. 7.18 Location of strain gauges for beam U3B
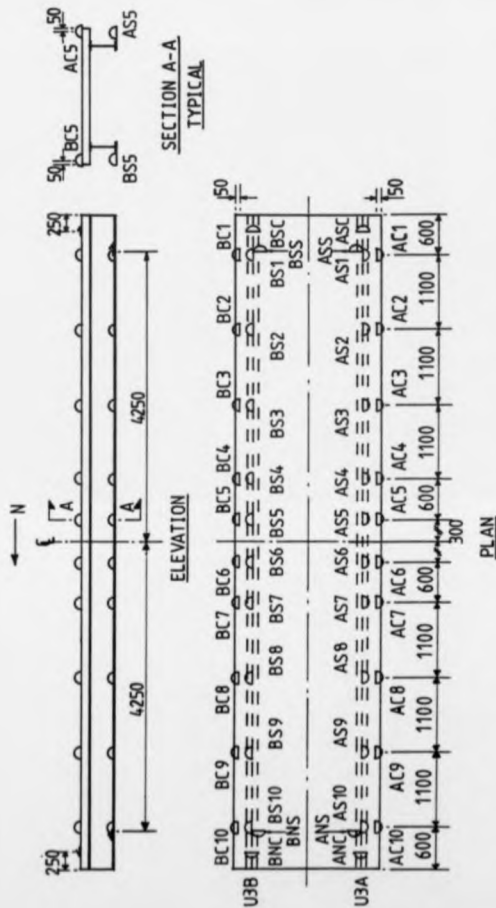
Fig. 7.19 Monitoring points for transverse rotations of the flanges for specimen U3

Fig. 7.20 Monitoring points for lateral displacements of the flanges for specimen U3
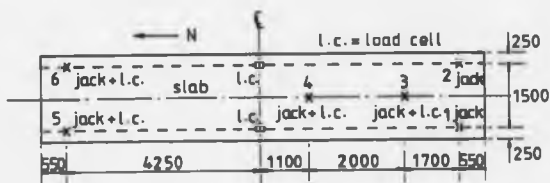
Fig. 7.21 Loading arrangement of test U3

Plate 7.1 Diagonal bracings at the supports for specimen U2

Plate 7.2 Test rig for specimen U2
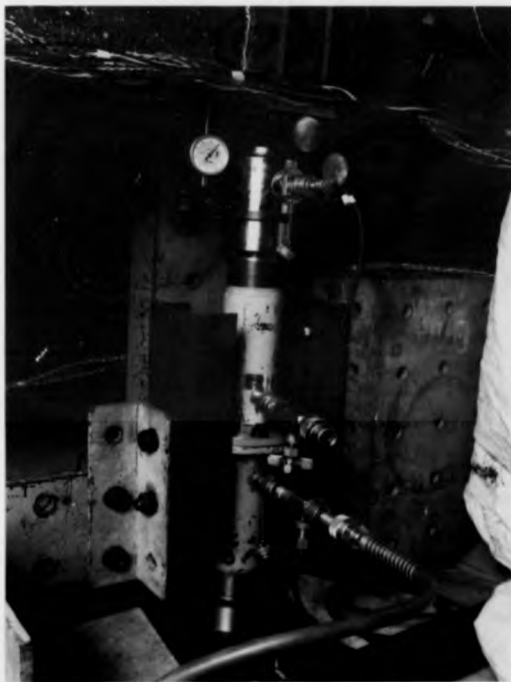
Plate 7.3 Vertical guide rails to prevent
lateral jack movement for specimen U2

Plate 7.4 Test rig for specimen U3

Plate 7.5 End view of test rig for specimen U3

Plate 7.6 Line loading set-up for specimen U3

CHAPTER 8
RESULTS OF INVERTED U-BEAM TESTS

8.1 Introduction

In this chapter the results from the auxiliary tests and
the two inverted U-frame double cantilever tests are
presented. It is impossible to give here all of the
extensive strain and rotation data recorded in the tests,
so only essential values and those that represent
significant changes in behaviour have been selected.
These results are the basis for the discussions on the
general behaviour of the specimens in the following
chapter. Observations from the tests are also described
briefly.

8.2 Material properties

These are summarised in Tables 8.1 to 8.3. No coupon
samples were taken from the top flange of the universal
beams for the U2 specimen. The strength will be similar
to U1 since they are of the same serial size and
delivered in the same batch.

The A193 reinforcing fabric used in U2 and U3 tests was
the same as in U1; the strength is given in Chapter 6.
Properties of the 8-mm diameter bars are given in Table
8.2. Specimens U1 and U2 were cast at the same time.
The cube strengths are reported in Chapter 6, and those
for specimen U3 are given in Table 8.3. The measured
unit weight of grade 30/20 concrete is 23.0 kN/m^3, which
is the average of 10 cube samples.

8.3 Cross-sectional dimensions and initial imperfections

Dimensions of the universal beams of the specimens U2 and
U3 are given in Table 8.4. The measured unit weights of
the rolled sections for beams U2 and U3 are 0.38 and 0.31
kN/m respectively.

Similar to specimen U1, there were worse initial
imperfections to the bottom flanges of specimen U2 not
only in lateral displacements but also tilting with
respect to the plane of the web. The tilting is nearly
uniform along both beams, U2A and U2B. The mean measured
value is 35.0 mrad. To accommodate such large initial
tilt, it was necessary to use bearing plates with 2° of
taper, one on each beam of U2, to level off the bottom
flange above the central roller so that the jack force
could be applied vertically and uniformly to the
specimen. The initial lateral imperfections of specimens
U2 and U3 are plotted in Figs. 8.1 and 8.2 respectively.
The initial tilting of the bottom flanges of specimen U3
was negligible.

8.4 Residual stresses

It is believed that the residual stress pattern of U2A
and U2B was very similar to specimen U1, as they were in
the same batch.   For high yield rolled sections, the
compressive stresses at the flange tips are normally
small, less than 25 N/mm^2 in most cases[115]. Compared
to the high yield strength of the material, the effect of
residual stresses on the instability of the bottom flange
hence becomes insignificant. Although yielding may start
a little earlier and the member tends to deflect more,
the overall behaviour is affected very little by residual
stresses in comparison to other factors.   So it was
decided not to carry out residual stress measurements for
specimen U3.

8.5 Compactness and beam resistance

The cross-section slenderness of specimen U2 is the same
as U1, reported in Chapter 5. This is because the size
of the rolled section and amount of reinforcement are
identical for beams U1, U2A and U2B. The cross-section
slenderness of specimen U3 was also calculated in
accordance with EC4[1], BS5950 Part 3.1[2] and BS5400
Part 3[8], as given in Table 8.5; calculations are given
in Appendix C.

The differences in dimensions and material strengths are
very small between specimens U1 and U2, therefore for
simplicity the shear, first yield and plastic hogging
moment resistances are taken as the same as those for U1.

From Table 8.3 the variations in dimensions between U3A
and U3B are small - the greatest difference of 2.8% for
the web. But there are slightly higher discrepancies in
yield strength between them, and Table 8.1 shows that the
difference can be as much as 5%. However the coupon
results may not provide accurate predictions to the yield
strengths for the member as a whole, because the number
of samples is insufficient. Since both beams were from
the same batch under the same manufacturing process, it
can be assumed that they are of the same strength. An
estimate of the maximum error implied by this assumption
is less than 3%. The results of the beam resistances are

summarized in Table 8.6. In the calculation the flanges
and web are separated, and their yield stresses are taken
as the mean values derived from Table 8.1. All material
partial safety factors γ_m are taken to be 1.0 The
bending resistances of the U2 and U3 slab in sagging,
M_{max} (Table 8.8), were calculated to be 12.8 and 12.7 kNm
per metre width respectively. In the calculations, the
BS8110 values of γ_m for steel and concrete are implicitly
included, and f_{cu} and f_y are measured values; the
method used is the simplified stress block method as per
BS8110. As for an inverted U- frame action, the flexural
stiffness per metre width of the slab was calculated to
be 318 and 181 kNm/rad for U2 and U3 respectively, using
a steel/concrete modular ratio of 7.

8.6 Experimental results

The test results for U2 and U3 are summarised in Tables
8.7 and 8.8 respectively. The concurrent values of the
eight equal point loads and the end reaction for each
beam in the U3 test, which define the moment gradient at
the southern span, are given in Table 8.9. The moment-
rotation curves are plotted in Figs. 8.3 and 8.4. The
vertical support movement versus the support moment for
specimen U2 is shown in Fig. 8.5.

Other results are presented in three groups - lateral
movement of the bottom flange, transverse rotations about
longitudinal axes and strain measurements. The sign
conventions for the graphs for specimens U2 and U3 are
shown in Figs. 8.6 and 8.7 respectively, and the previous
figures in Chapter 7 should be referred to for the
positions of instrumentation. The origin of all the U2
graphs corresponds to the initial state of the specimen,
in which the support moment was nearly zero as the
specimen was propped at the beginning of the test.
However the origin of all the U3 graphs corresponds to a
different initial state, in which the specimen was
subjected to its self-weight, including the weight of
spreaders, rockers and load cells, acting as a double
cantilever, when the test began. For the plots of bottom
flange lateral movement along the members of U2 and U3,
the x-axis (y=0) is only a datum line, which indicates

that the lateral movements are zero at the beginning of
the test. For imperfections and their directions,
reference should be made to Figs. 8.1 and 8.2. The
results of the U2 test are given in Figs. 8.8 to 8.11,
for lateral movements, Figs. 8.12 to 8.17, for transverse
rotations, and Fig. 8.18 to 8.25, for strain
measurements. For the U3 test, Figs 8.26 to 8.28, 8.29
to 8.36 and 8.37 to 8.42 are shown for lateral movements,
transverse rotations and strain measurements
respectively.

The lateral displacements of the concrete slab in the U2
test were small, in general less than 2.5 mm except at
position C16 (Fig. 7.15), where the maximum value was 3.5
mm at high loads. Before local buckling had occurred,
the lateral movements of the concrete slab in the U3 test
were small too, in general less than 2 mm, however
lateral buckling of the bottom flanges caused an overall
twisting of the specimen about the vertical axes of the
two central supports at the end of the test. The lateral
movements of the slab are plotted in Fig. 8.43, which
shows a clear sign of rigid body rotation as the slab is
too rigid to be bent transversely, when the bottom flange
of each beam buckled into a S-shape.

8.7 Behaviour of beams during test

The behaviour in the two tests was similar, even though
there was a line loading on one side of specimen U3. The
bending resistances of both specimens fell soon after
local buckles became visible in the central support
regions. Local buckling started around stage 12 and 10
for the U2 and U3 test respectively (Figs. 8.3 and 8.4).
As discussed earlier in Chapter 6, the bottom flange is
much more flexible to lateral bending caused by induced
internal stresses as compared to the composite top
flange. For both specimens, coupled with increasing
lateral movements of the bottom flanges, local buckling
caused the support moment to drop at a much faster rate
than that, when no interaction between local and lateral
buckling was taking place. In Fig. 8.3, the rapid
decline of the falling branch after stage 14 was due to a
fracture of reinforcing fabric (4 bars, 2 at each edge)
inside the U2 slab, that occurred at the position of the
central crack (Plate 8.1). Fracture of reinforcement did
not occur in the U3 test, hence the two falling branches
in Fig. 8.4 are smooth. Both tests were stopped when
there was excessive twisting about a vertical axis at the
support. At the end of each test, each bottom flange was
deformed and deflected in a typical S-shape curve (Figs.
8.8, 8.9 and 8.26), which is similar to lateral buckling
of continuous unrestrained steel beams.

The U2 test was very stable as compared to the previous U1 test. There were 16 load stages. Local buckling was seen on the southern side of both beams immediately after stage 12. The half-wavelength in both cases was about 300 mm and the amplitude of the buckle was approximately 30 mm at the end of the test (Plate 8.2). Local buckling of U2A was found very near the central support (Plate 8.3), but it occurred at a distance 500 mm from the support for U2B (Plate 8.4). The transverse curvatures of the concrete slab were small, but the lateral movements of the bottom flange relative to the top flange were considerable and easily detected visually, especially for U2B (Plate 8.5). This is the buckling mode associated particularly with composite beams commonly described as distortional.

Initial cracks formed in the slab above the central supports after load stage 3, and cracks propagated above almost every crest of the metal decking, as the support bending moment became higher (Plate 8.1). Before the test was terminated, there was a central crack of 10 mm wide across the slab, and due to this localised effect of strain distribution in the reinforcing fabric, the two outer longitudinal bars fractured between stages 13 and 14. At high loads, there was some separation between the metal decking and tip flange in the support region, but there was no spalling to the slab. The bracings at the

supports showed no deformation after the test was terminated.

There were 13 load stages in the U3 test. Extensive yielding was observed from flaking of the brittle coating on the web before local buckles were developed. Local buckling occurred on the northern and southern sides in the support region after stage 11 for U3A and U3B respectively. The half-wavelength in both beams was about 240 mm and the amplitude of the buckle was approximately 20 mm. Local buckling in U3A (Plate 8.6) was less severe than in U3B (Plate 8.7), probably because the web had buckled to a lesser extent. There was no visual separation between the top flange and concrete slab for both beams in the support region throughout the test.

Cracks started to form after load stage 3 and at the end of the test there was a central crack 3.5 mm wide across the slab directly above the two supports. The rest of the cracks were fine ones, except that the two adjacent to the central crack on either side were as wide as 1 mm (Plate 8.8). On the northern side of the cantilever, spacing of cracks was closer near the supports over one third of the span, but became wider in the middle third of the span; there was no crack in the last third of the span. In general the spacing of cracks was a multiple of the spacing of transverse bars inside the slab, which is

200 mm. On the southern side of the cantilever where the line loading was acting, the crack pattern was slightly different. Cracks did not occur under the patch loads, but instead formed between them (Plate 8.8). There was no crack found in the second half of the span near the end. As on to the southern side, the spacing of cracks was a multiple of 200 mm. Due to transverse bending, there were few longitudinal cracks at the bottom of the slab underneath the line loading, but there was no longitudinal crack at the top, indicating that the concrete had not reached its crushing strength. Fracture of reinforcing fabric did not occur in this test.

Location		0.2% proof stress N/mm²	Ultimate stress, f_u N/mm²	E kN/mm²
	Top flange	–	–	–
U2A	Web	424.5	537.5	202.0
	Bottom flange	396.5	524.0	201.5
	Top flange	–	–	–
U2B	Web	424.5	538.5	206.0
	Bottom flange	396.5	521.5	209.0
	Top flange	429.5	569.5	209.0
U3A	Web	448.5	573.5	212.5
	Bottom flange	432.0	576.0	205.0
	Top flange	432.5	560.5	204.5
U3B	Web	425.0	552.5	199.5
	Bottom flange	416.0	560.5	196.5

<u>Table 8.1</u> Structural steel properties of specimens U2 and U3

cross-section area, A_s (mm²)	0.2% Proof stress, f_y (N/mm²)	Tensile strength, f_u (N/mm²)	E (kN/mm2)
52.0	498.0	577.0	202.0

<u>Table 8.2</u> Material properties of 8 mm high-yield bars

Concrete grade	Cement type	Slump (mm)	Duration (day)	Cube strength 150 mm f_{cu} (N/mm^2)
C30/20	OPC	50	3	15.6
			7	24.2
			14	27.9
			28	31.6
			48	34.5

Table 8.3   Compressive strength of ready-mix concrete for U3 specimen

Beam No.	Nominal Size	Dimensions (mm)					
		D	WT	WB	TF	BF	TW
U2A	406x140 UB39	396.0	140.1	140.0	7.84	7.92	6.66
U2B	ditto	398.0	140.0	140.2	7.83	7.92	6.59
U3A	356x127 UB33	348.1	123.4	123.2	7.42	7.71	6.53
U3B	ditto	348.1	124.3	124.3	7.82	7.64	6.72

Table 8.4   U2 and U3 universal beam dimensions (mm)

Beam	Location	EC4	BS5950 Pt.3.1	BS5400 Pt.3
U3A	Flange	Class 3	Class 3	Class 3
	Web	Class 3	Class 2	Class 3
U3B	Flange	Class 3	Class 3	Class 3
	Web	Class 3	Class 2	Class 3

Note: calculations are based on measured dimensions and
material strengths.

<u>Table 8.5</u> U3 Cross-section classification

Beam	Beam resistances (composite)		
	M_Y' (kNm)	M_R' (kNm)	V_R (kN)
U3A/U3B	211.3	270.1	553.8

<u>Table 8.6</u> Beam resistances of specimen U3

Stage	U2A M' (kNm)	U2A M'/Mp'	U2A V (kN)	U2A V/Vp	U2B M' (kNm)	U2B M'/Mp'	U2B V (kN)	U2B V/Vp
0	0.0	0.00	0.0	0.00	0.0	0.00	0.0	0.00
1	47.2	0.16	14.4	0.02	47.5	0.16	14.4	0.02
2	58.3	0.19	16.5	0.03	52.8	0.17	15.5	0.02
3	78.4	0.26	19.6	0.03	75.4	0.25	19.9	0.03
4	96.9	0.32	24.1	0.04	97.2	0.32	24.2	0.04
5	123.0	0.41	29.2	0.05	130.6	0.43	30.7	0.05
6	160.0	0.53	36.5	0.06	143.8	0.48	33.3	0.07
7	198.3	0.66	44.0	0.07	206.5	0.68	45.5	0.08
8	230.0	0.76	50.2	0.08	237.1	0.78	51.6	0.09
9	249.7	0.83	54.1	0.09	256.9	0.85	55.5	0.10
10	271.3	0.90	58.3	0.09	281.4	0.93	60.3	0.10
11	290.0	0.96	62.0	0.10	299.4	0.99	63.8	0.11
12	301.5	1.00	64.2	0.10	311.3	1.03	66.1	0.11
13	299.9	0.99	63.9	0.10	314.7	1.04	66.8	0.11
14	269.2	0.89	57.9	0.09	310.0	1.02	65.9	0.11
15	236.9	0.78	51.6	0.08	245.0	0.81	53.2	0.09
16	228.4	0.76	49.9	0.08	223.2	0.74	48.9	0.08

Note : M_p' = 302.5 kNm   and V_p = 624.8 kN
       (See Chapter 6)

Max M'(U2A) = 312.7 kNm corresponding to M'/M_p' = 1.03
    M'(U2B) = 320.1 kNm corresponding to M'/M_p' = 1.06

Table 8.7 U2 test results

Stage	Slab M_g/M_{max}	U3A M' (kNm)	U3A M'/M_p'	U3A V (kN)	U3A V/V_p	U3B M' (kNm)	U3B M'/M_p'	U3B V (kN)	U3B V/V_p
0	0.05	43.19	0.16	16.76	0.03	43.42	0.16	16.94	0.03
1	0.19	62.24	0.23	27.66	0.05	69.43	0.26	28.88	0.05
2	0.29	90.55	0.34	37.57	0.07	99.33	0.37	39.62	0.07
3	0.33	108.97	0.40	43.68	0.08	116.24	0.43	45.28	0.08
4	0.61	131.33	0.49	58.59	0.11	140.94	0.52	61.37	0.11
5	0.68	165.53	0.61	69.51	0.13	173.45	0.64	71.18	0.13
6	0.70	193.15	0.72	76.06	0.14	200.76	0.74	77.53	0.14
7	0.76	208.94	0.77	82.27	0.15	220.26	0.81	84.18	0.15
8	0.87	228.67	0.85	89.88	0.16	237.17	0.88	92.27	0.17
9	0.96	253.66	0.94	98.92	0.18	261.87	0.97	100.07	0.18
10	0.97	265.50	0.98	102.04	0.18	272.27	1.01	103.27	0.19
11	0.96	278.65	1.03	102.92	0.19	256.67	0.95	103.10	0.19
12	0.96	258.92	0.96	97.80	0.18	234.57	0.87	97.40	0.18
13	0.98	244.45	0.91	95.73	0.17	208.56	0.77	91.66	0.16

Table 8.8 U3 test results

Stage	Slab point load on each beam (kN)	U3A end reaction (kN)	U3B end reaction (kN)
0	0.4	1.6	1.7
1	1.9	0.5	1.7
2	2.9	2.9	4.9
3	3.2	6.1	7.7
4	5.7	1.3	4.1
5	6.4	6.7	8.4
6	6.4	13.0	14.5
7	7.1	13.9	15.8
8	8.1	13.7	16.1
9	8.6	17.1	18.3
10	8.9	19.6	20.8
11	8.7	21.9	22.1
12	8.7	16.4	16.0
13	9.1	11.6	7.7

Table 8.9   U3 concurrent values of external loads on the southern span
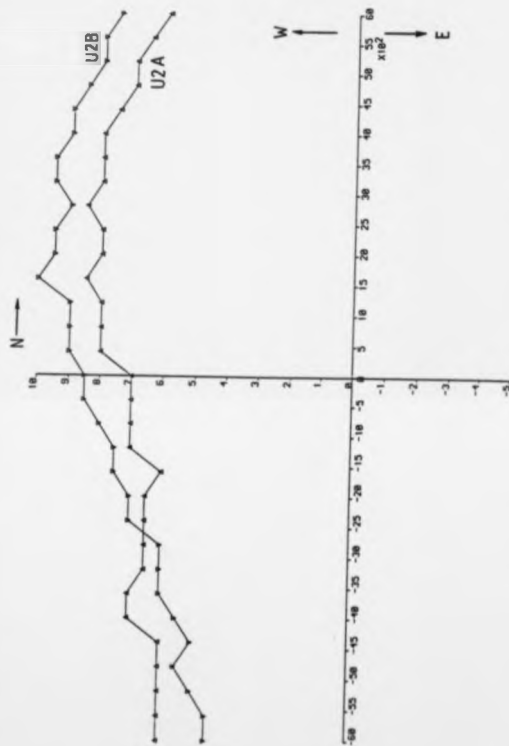
Fig. 8.1   Initial lateral imperfections of the bottom flanges for specimen U2

Fig. 8.2 Initial lateral imperfections for specimen U3
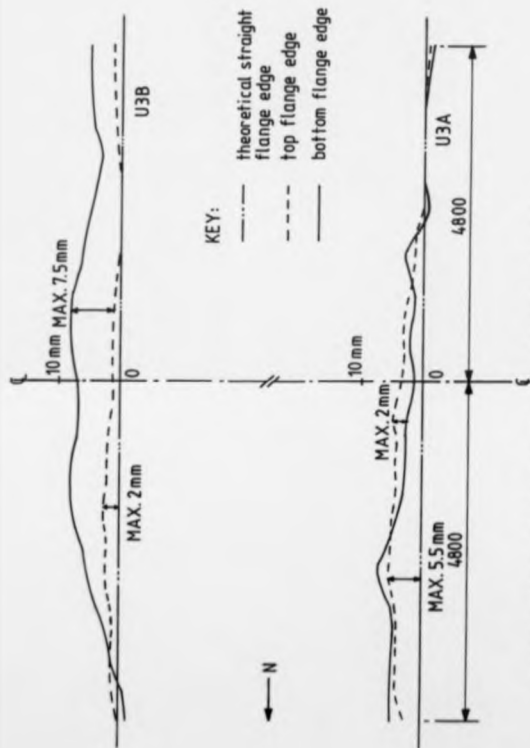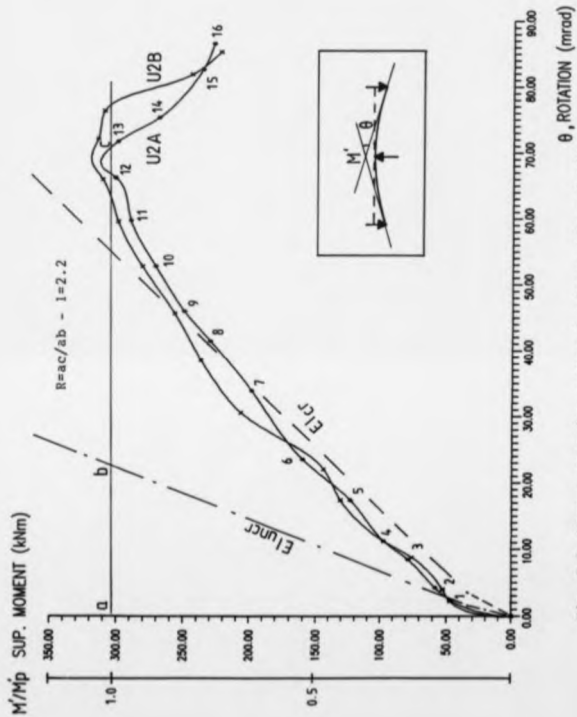
Fig. 8.3 Moment-rotation curves for beams U2A and U2B
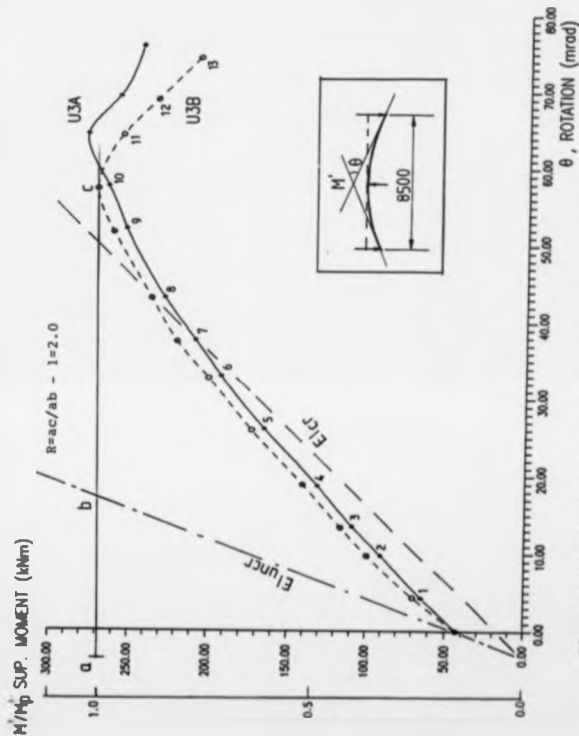
Fig. 8.4 Moment-rotation curves for beams U3A and U3B
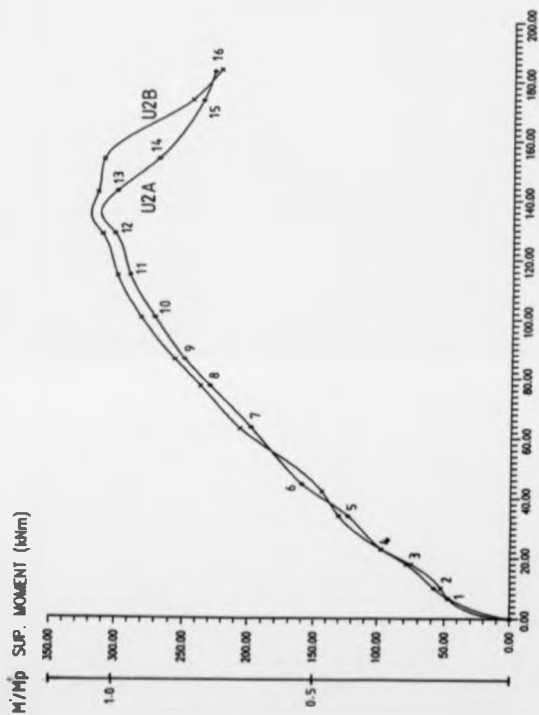
Fig. 8.5 Support moment versus vertical support movement for beams U2A and U2B
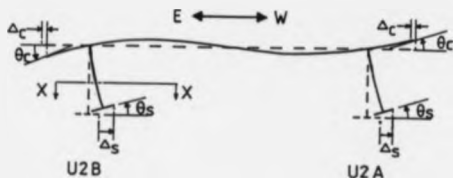
i) θ_c and θ_s are the transverse rotation of the concrete and bottom flanges respectively, anti-clockwise +ve.

ii) Δ_c and Δ_s are the lateral displacement of the concrete and bottom flanges respectively, westward +ve.

Section X - X   Strain diagram
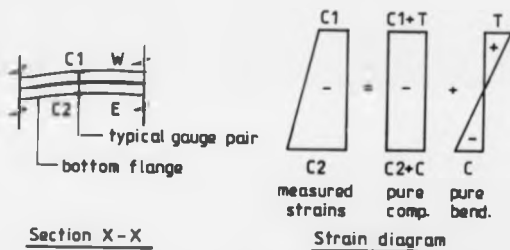
iii) Longitudinal strain for the bottom flange, compressive -ve.
iv) For pure bending strain, west side in tension +ve.

Fig. 8.5 Sign convention for U2 test

i) θ_c and θ_s are the transverse rotation of the concrete and bottom flanges respectively, anti-clockwise +ve.

ii) Δ_c and Δ_s are the lateral displacement of the concrete and bottom flanges respectively, eastward +ve.

Section X-X

Strain diagram
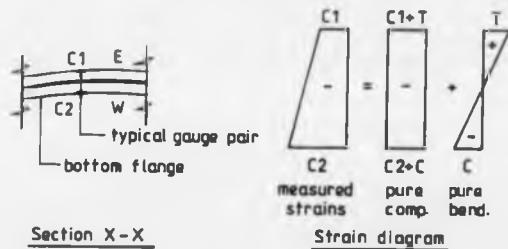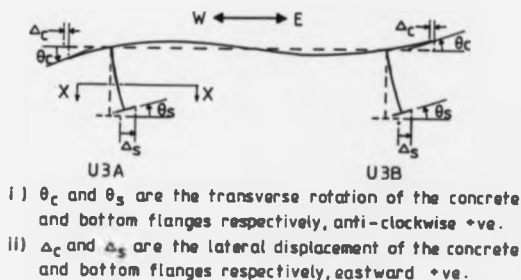
iii) Longitudinal strain for the bottom flange, compressive -ve.

iv) For pure bending strain, east side in tension +ve.

Fig. 8.7 Sign convention for U3 test
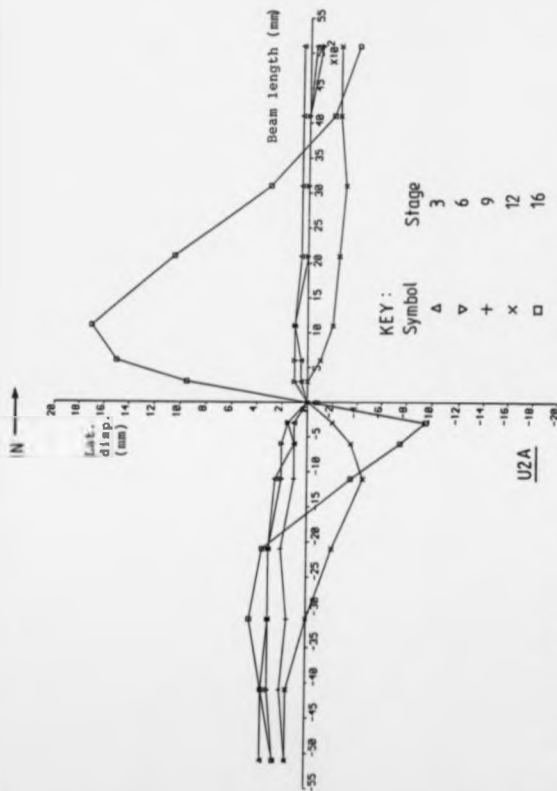
Fig. 8.8 Lateral displacements of bottom flange along beam U2A
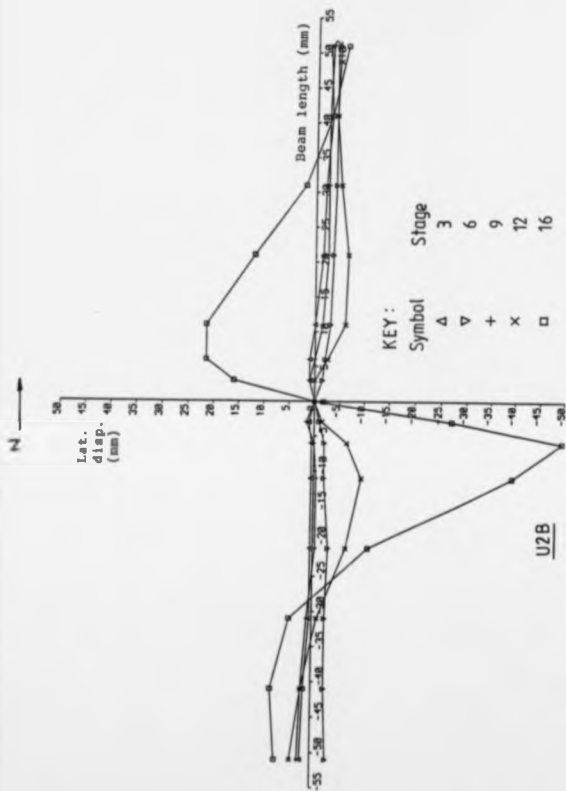
Fig. 8.9 Lateral displacements of bottom flange along beam U2B
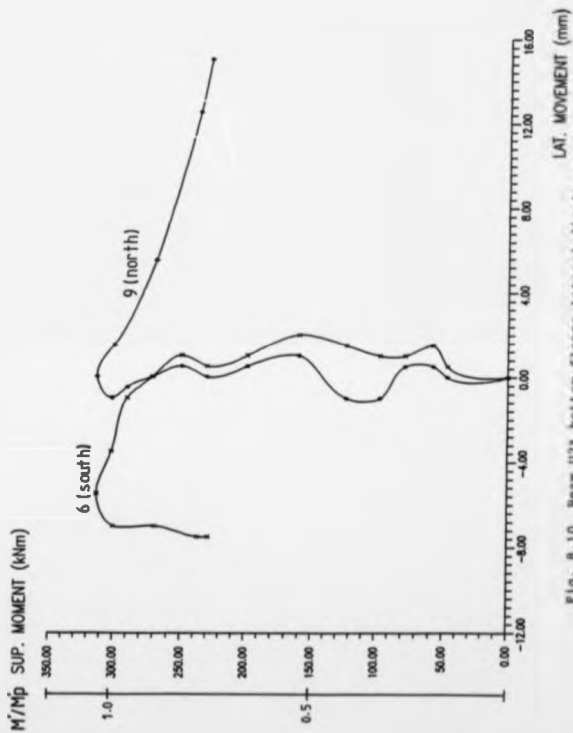
Fig. 8.10 Beam U2A bottom flange lateral displacements
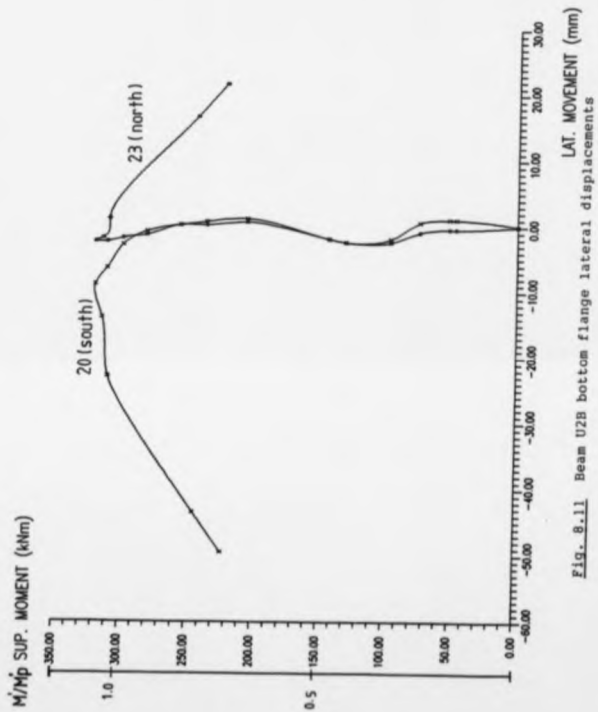
Fig. 8.11 Beam U2B bottom flange lateral displacements
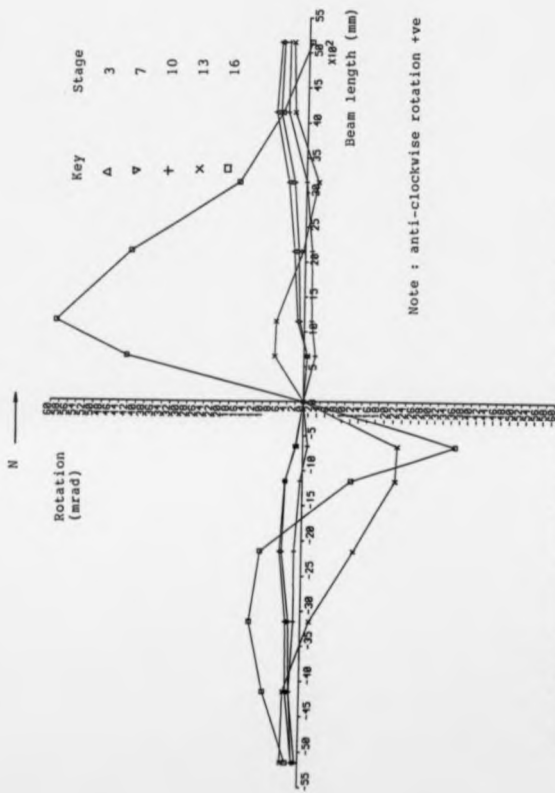
Fig. 8.12 Transverse rotations of bottom flange along beam U2A
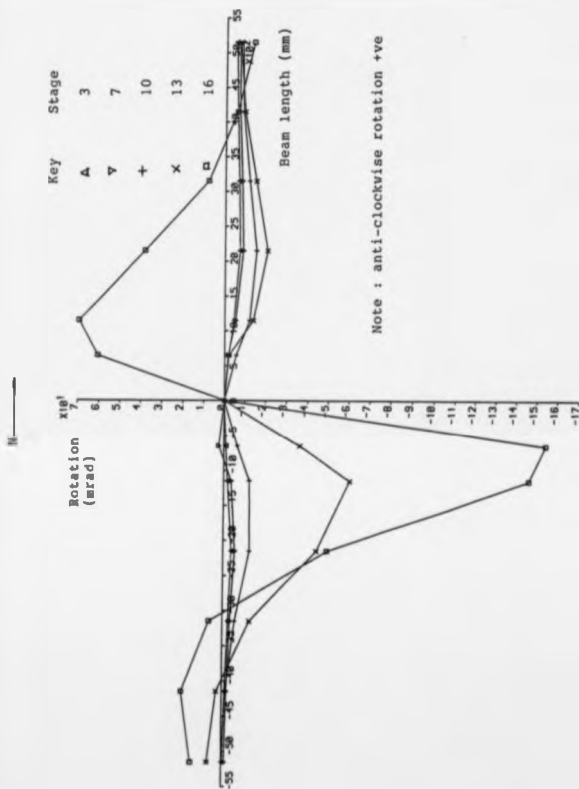
Fig. 8.13 Transverse rotations of bottom flange along beam U2B
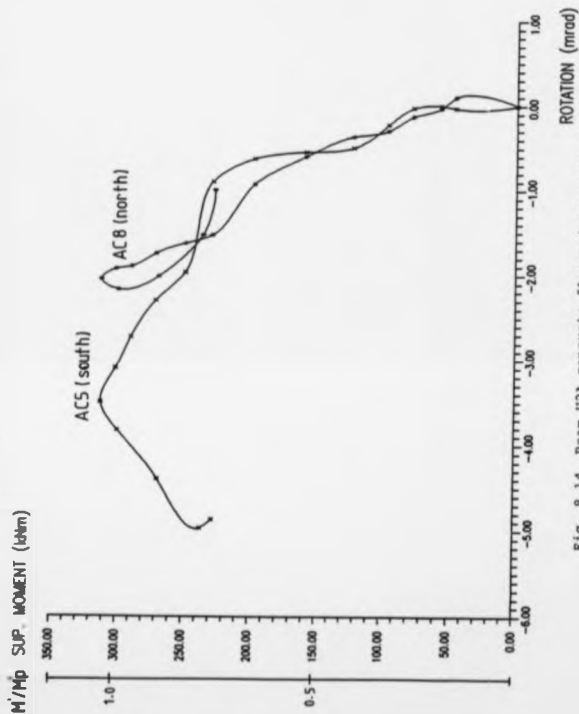
Fig. 8.14 Beam U2A concrete flange transverse rotations
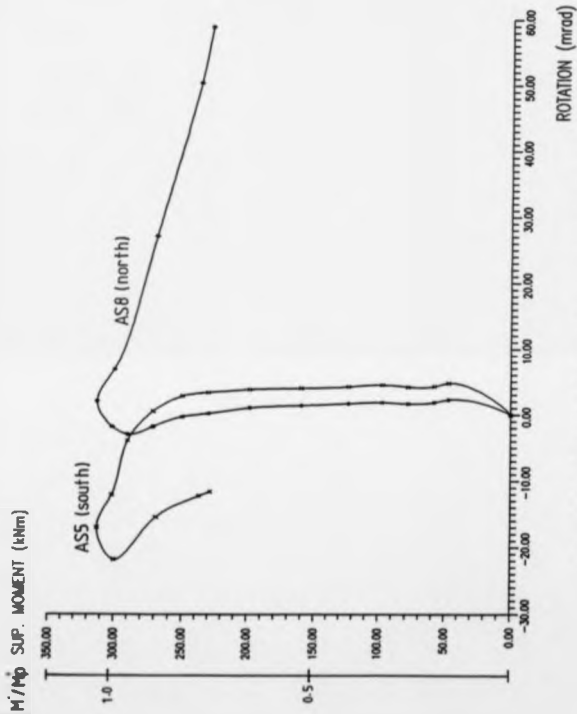
Fig. 8.15 Beam U2A bottom flange transverse rotations

288
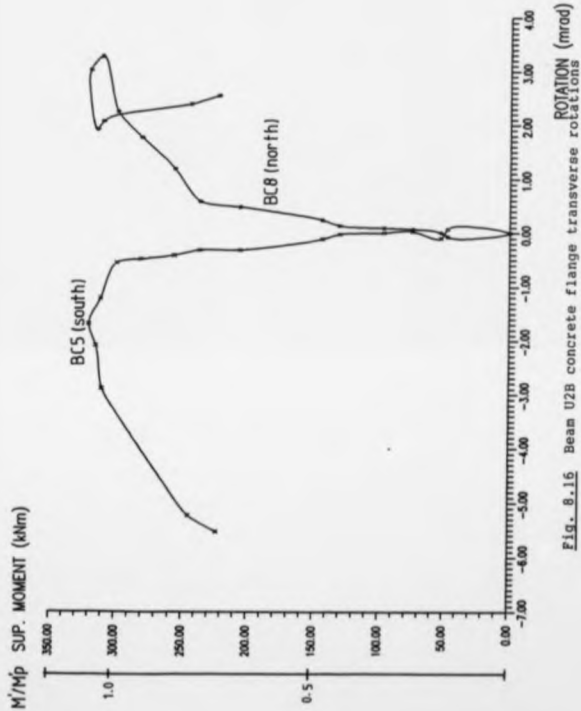
Fig. 8.16 Beam U2B concrete flange transverse rotations
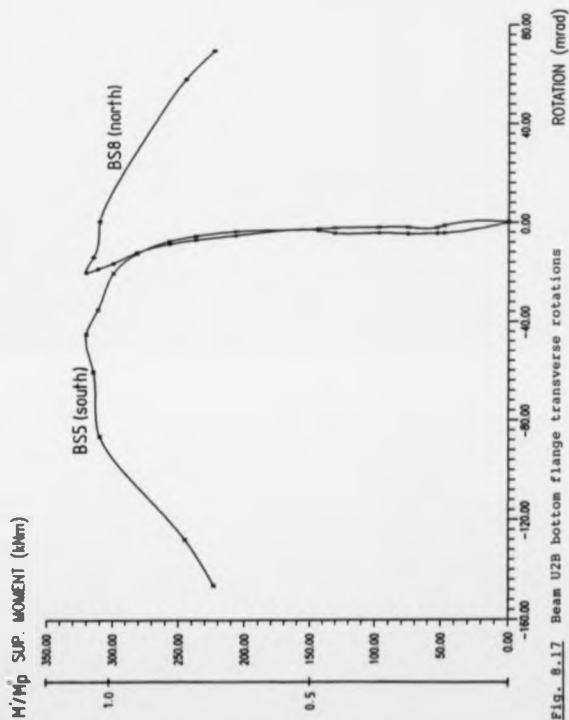
Fig. 8.17 Beam U2B bottom flange transverse rotations
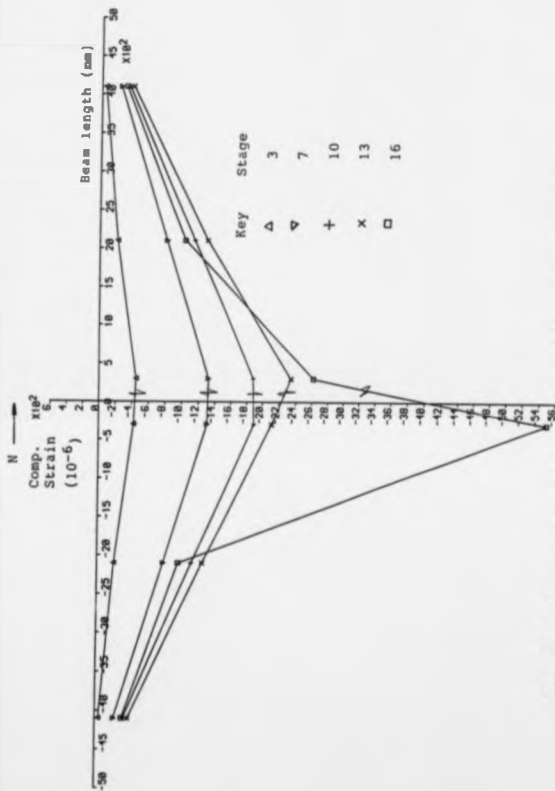
Fig. 8.18 Compressive strains of bottom flange along beam U2A
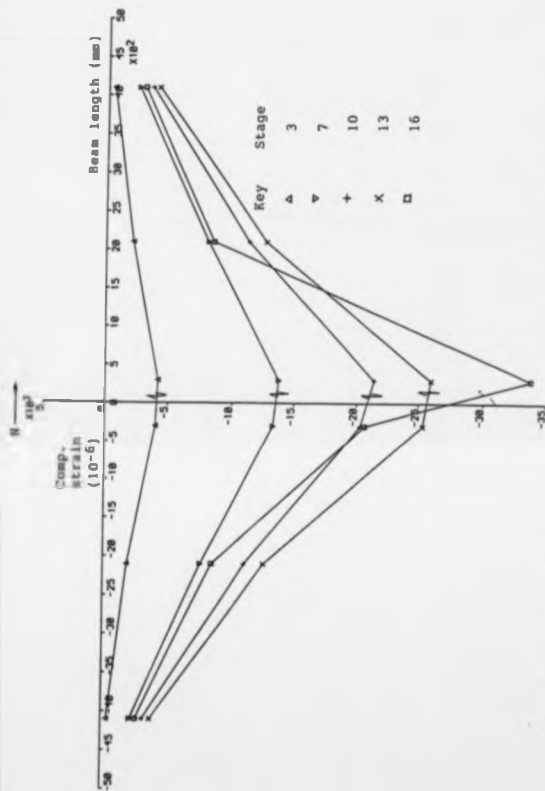
Fig. 8.19 Compressive strains of bottom flange along beam U2B
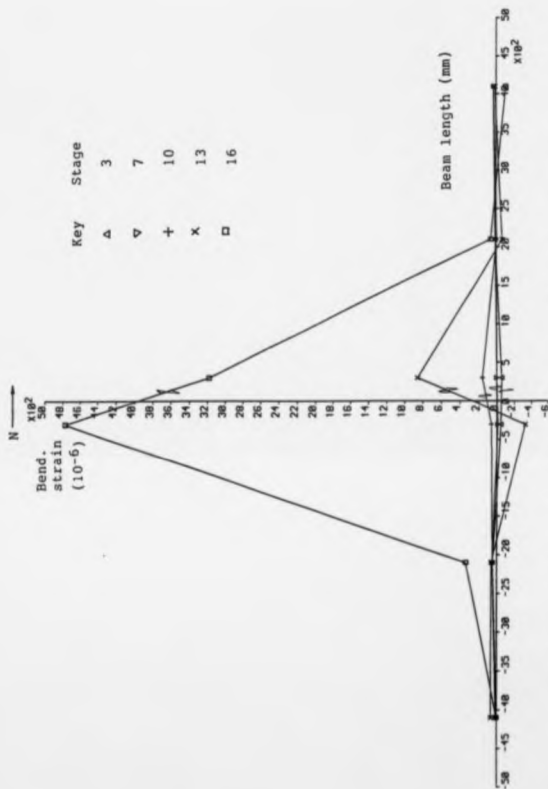
Fig. 8.20 In-plane bending strains of bottom flange along beam U2A

292
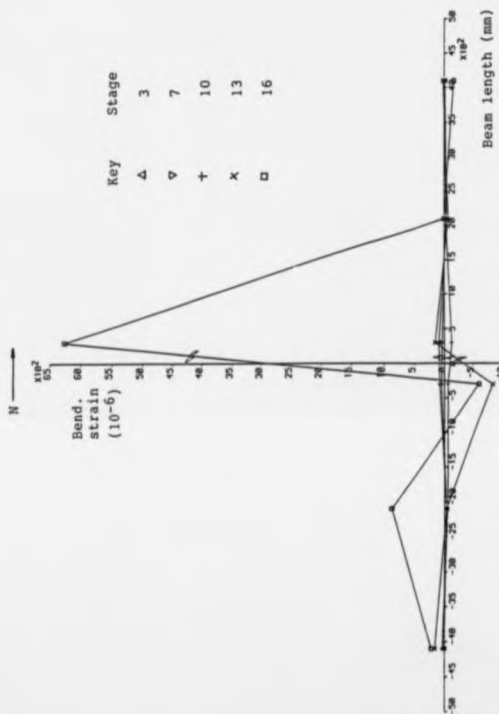
Fig. 8.21 In-plane bending strains of bottom flange along beam U2B
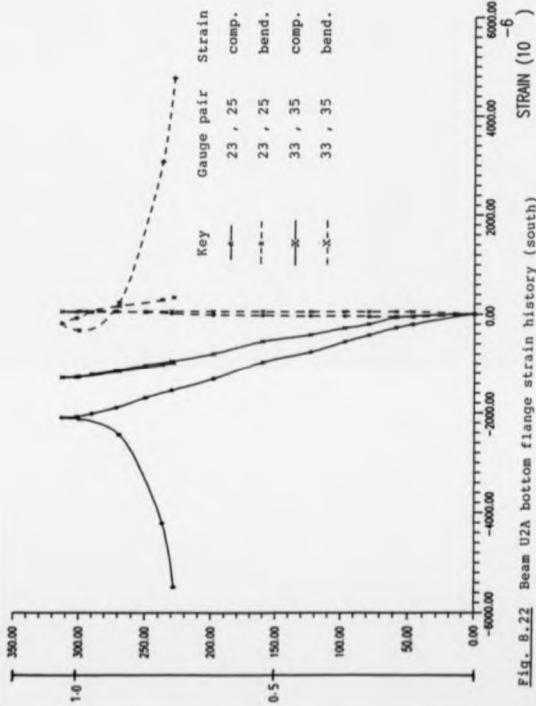
Fig. 8.22 Beam U2A bottom flange strain history (south)
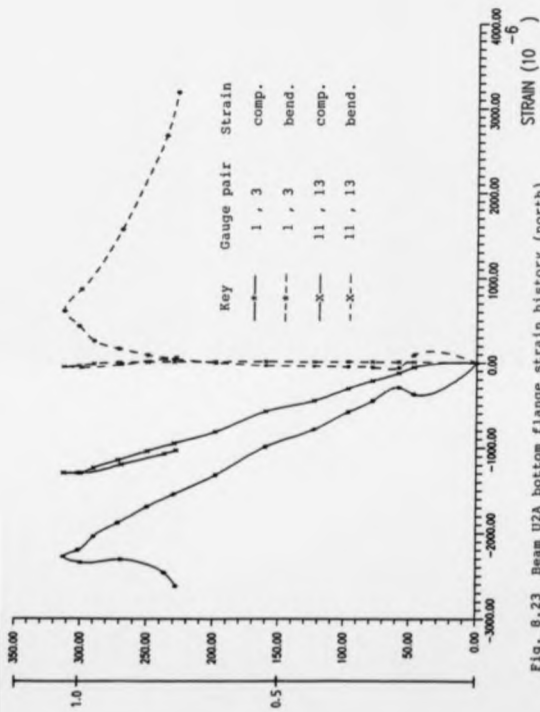
Fig. 8.23 Beam U2A bottom flange strain history (north)
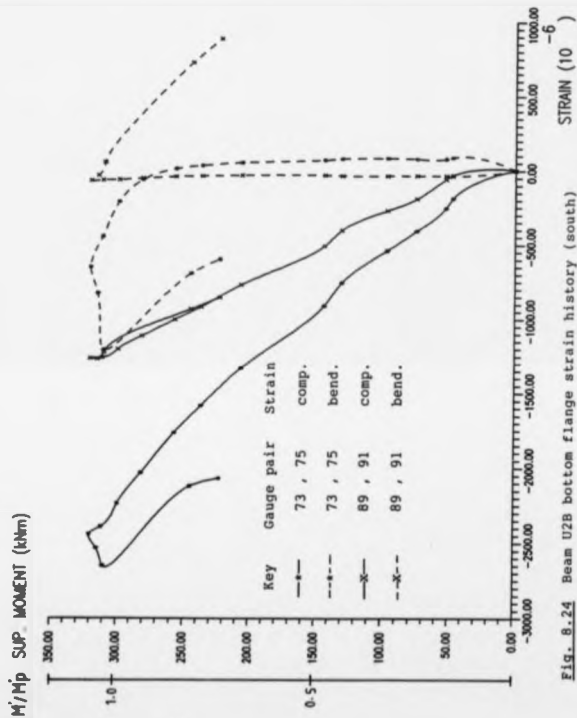
Fig. 8.24 Beam U2B bottom flange strain history (south)

Key	Gauge pair	Strain
——■——	73 , 75	comp.
——■——	73 , 75	bend.
——×——	89 , 91	comp.
——×——	89 , 91	bend.

M'/Mp SUP. MOMENT (kNm)

STRAIN (10^{-6})

Fig. 8.25 Beam U2B bottom flange strain history (north)

Key	Gauge pair	Strain
—+—	45 , 47	comp.
—+—	45 , 47	bend.
—×—	61 , 63	comp.
—×—	61 , 63	bend.

M'/Mp SUF. MOMENT (kNm)

STRAIN (10^{-6})
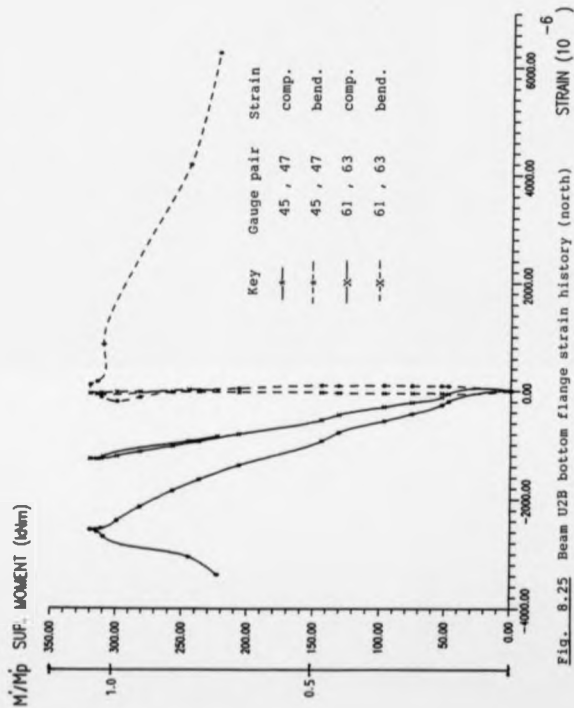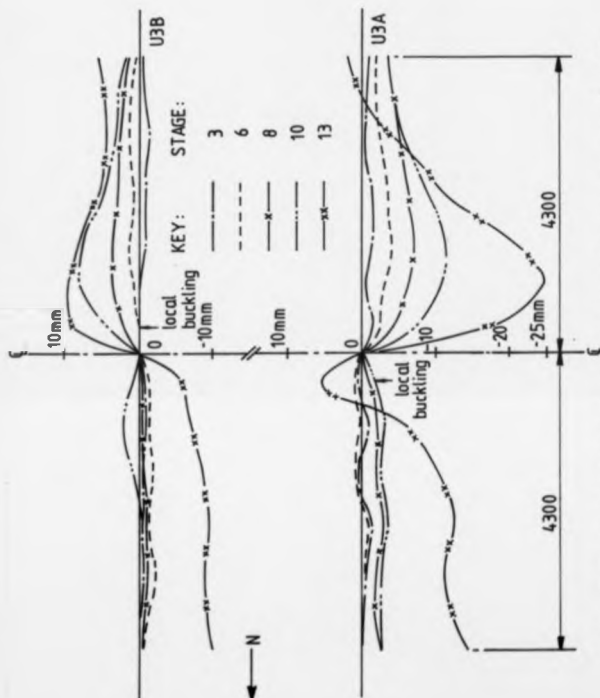
Fig. 8.26 Lateral displacements of bottom flanges along specimen U3

299

SUP. MOMENT (kNm)

Key   Monitoring pt.
       (see Fig. 7.20)
         5
         6
         7
         9

Fig. 8.27 Support moment versus bottom flange lateral
           displacement for beam U3A

LATERAL MOVET (mm)

SUP. MOMENT (kNm)

LATERAL MOVE'T (mm)

Key	Monitoring Pt. (see Fig. 7.20)
•	17
○	18
□	19
△	21

Fig. 8.28 Support moment versus bottom flange lateral displacement for beam U3B

300

301
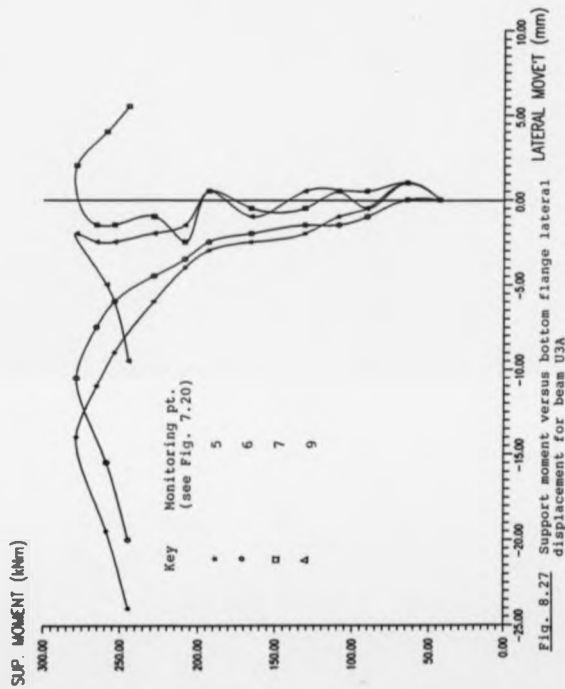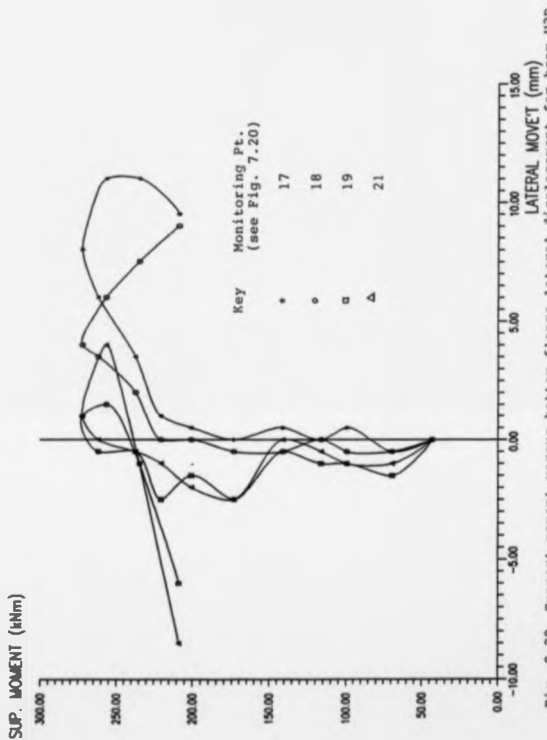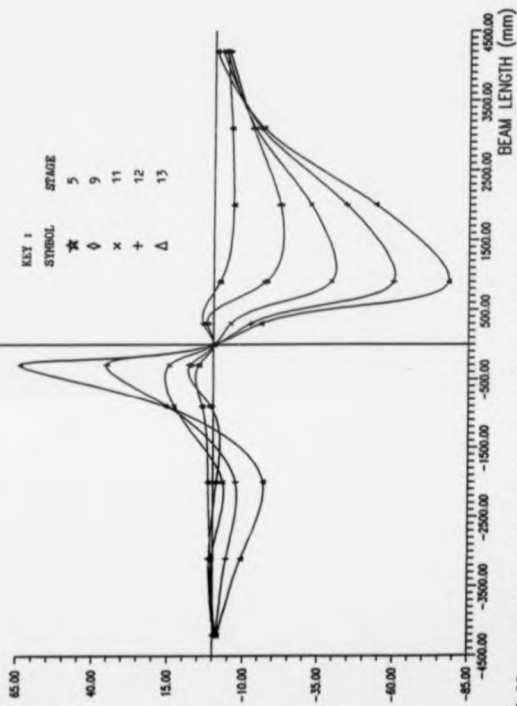
Fig. 8.29   Beam U3A - variation of transverse rotation of the bottom flange along the member
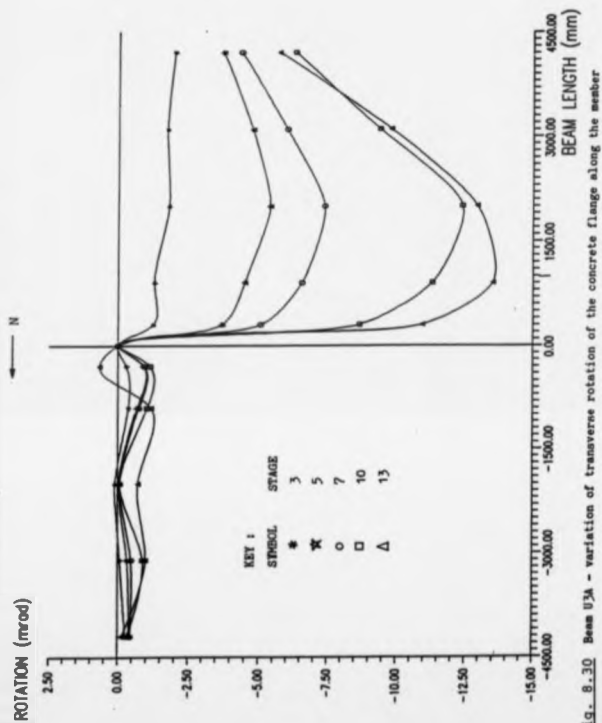
Fig. 8.30 Beam U3A - variation of transverse rotation of the concrete flange along the member
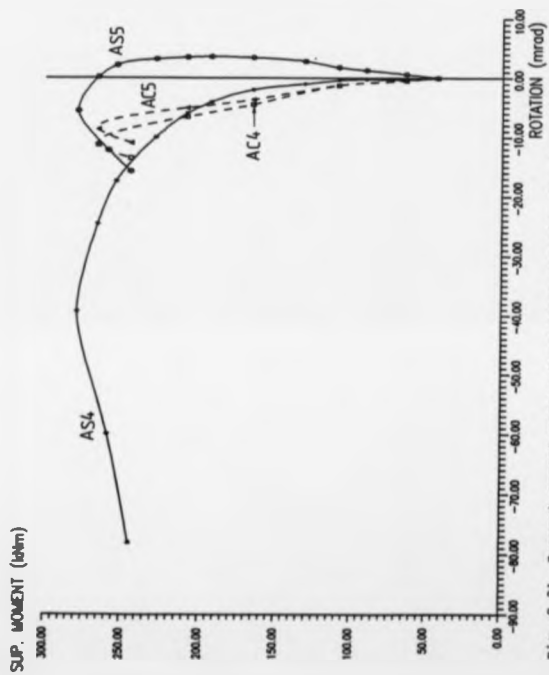
Fig. 8.31 Support moment versus transverse rotation for beam U3A (south)

Fig. 8.32 Support moment versus transverse rotation for beam U3A (north)

Fig. 8.33 Beam U5B - variation of transverse rotation of the bottom flange along the member

ROTATION (mrad)

KEY :

SYMBOL	STAGE
✳	3
★	5
○	7
□	10
△	13

BEAM LENGTH (mm)
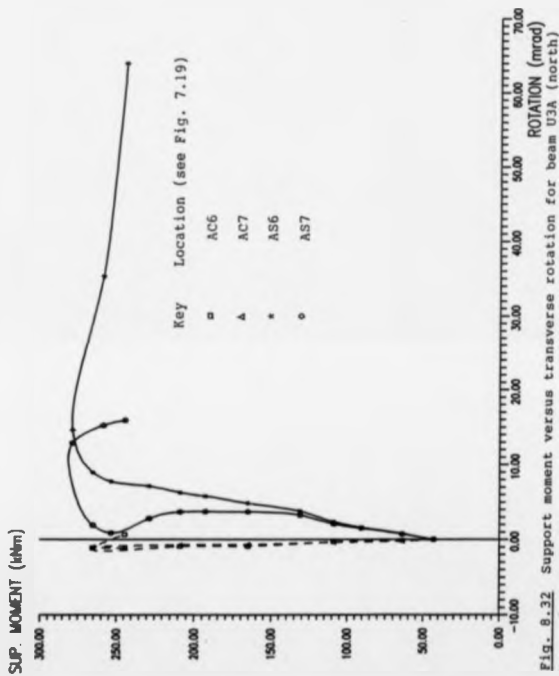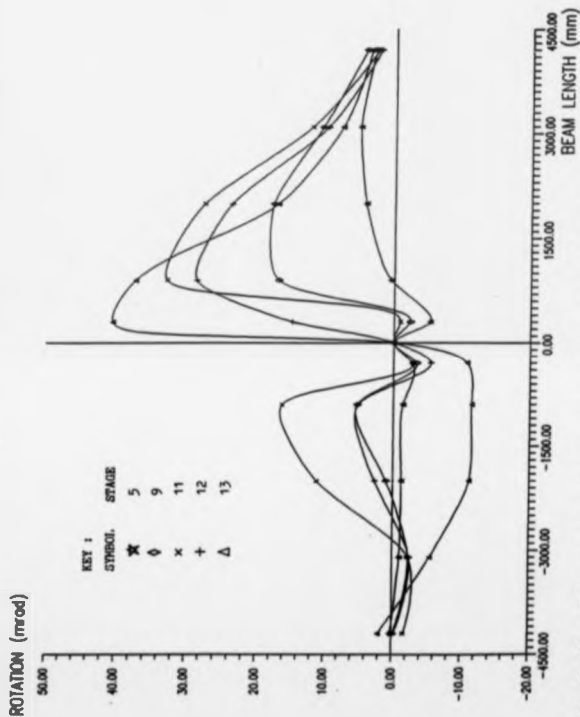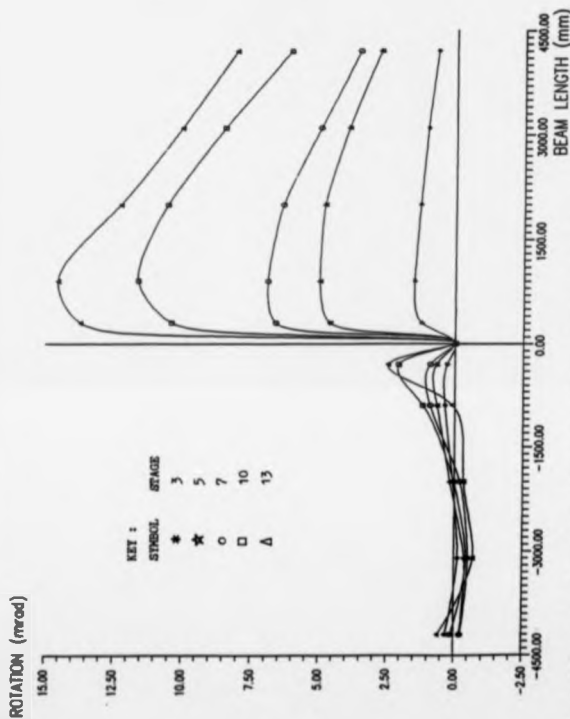
Fig. 8.34   Beam U38 - variation of transverse rotation of the concrete flange along the member
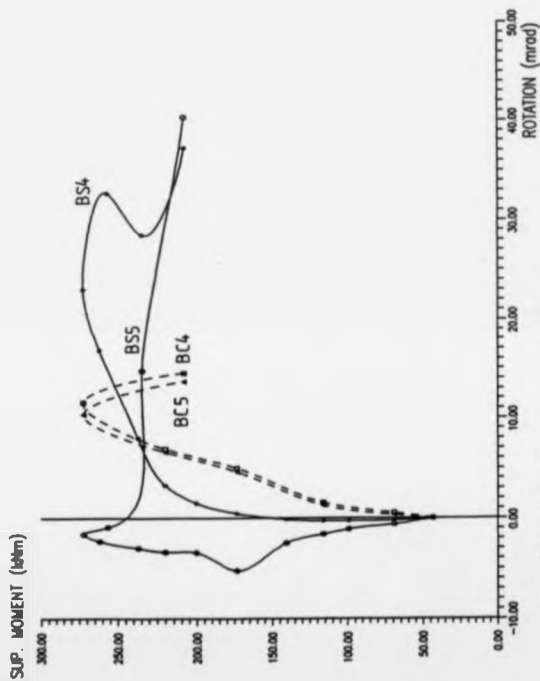
Fig. 8.35 Support moment versus transverse rotation for Beam U3B (south)
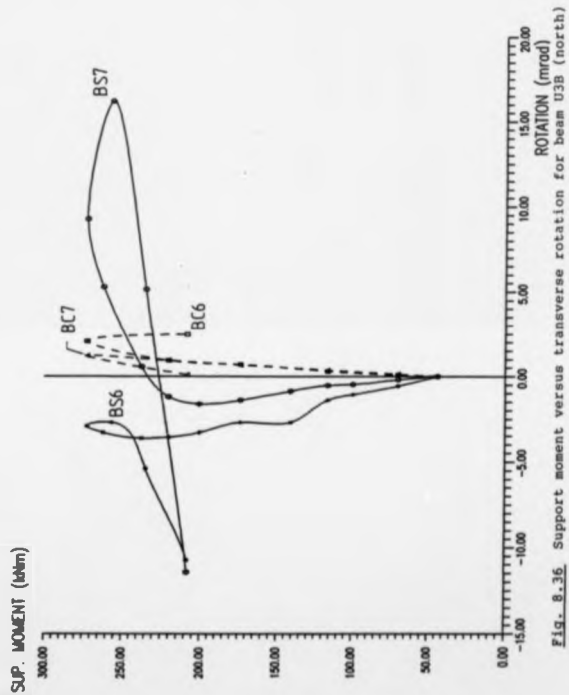
Fig. 8.36 Support moment versus transverse rotation for beam U3B (north)
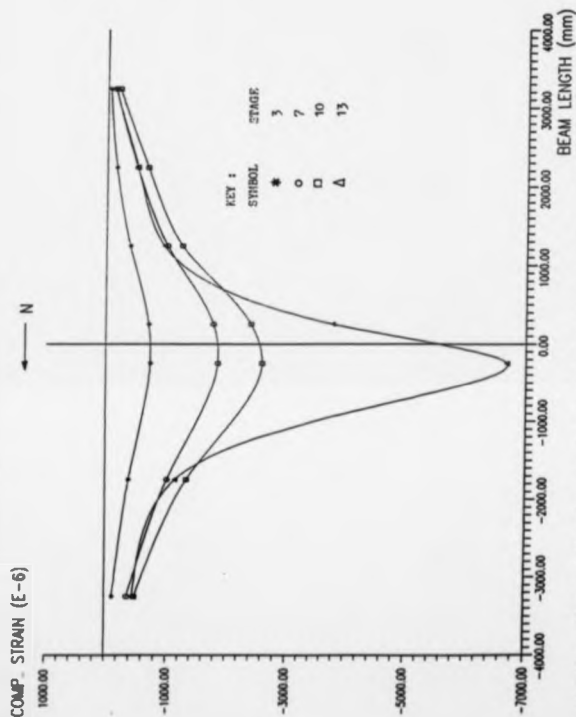
Fig. 8.37 Beam U3A - variation of compressive strain of the bottom flange along the member
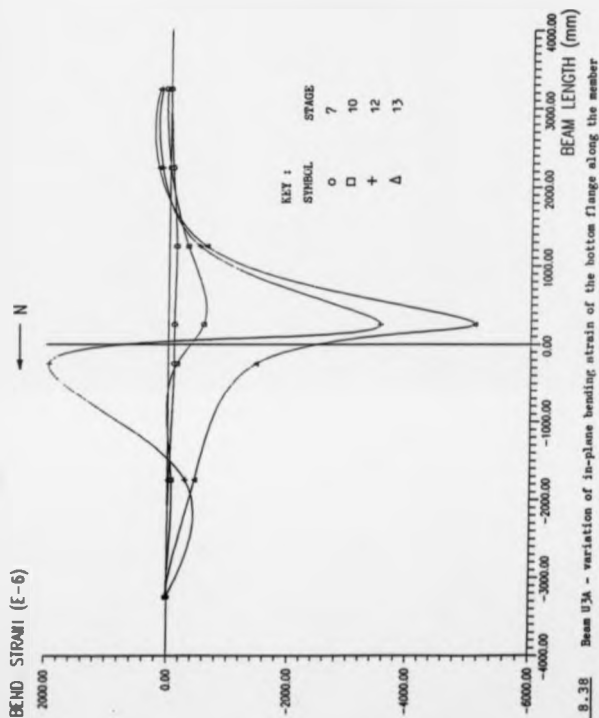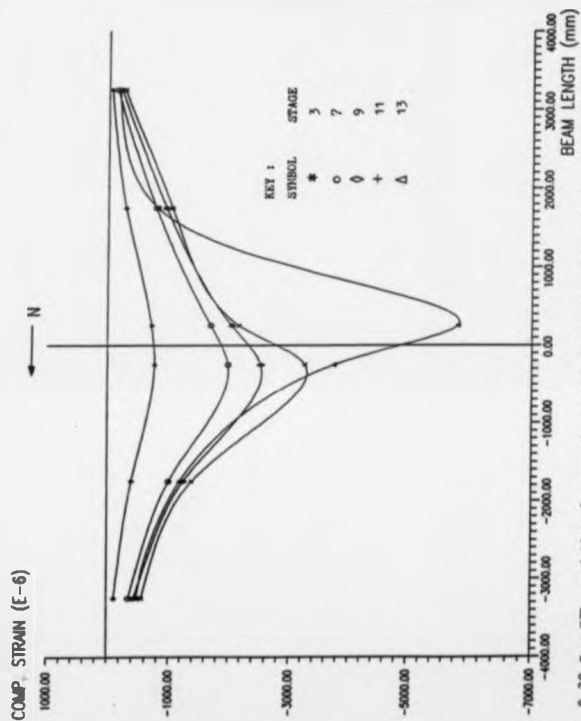
310

Fig. 8.38   Beam U3A - variation of in-plane bending strain of the bottom flange along the member

Fig. 8.39 Beam U3B - variation of compressive strain of the bottom flange along the member

312
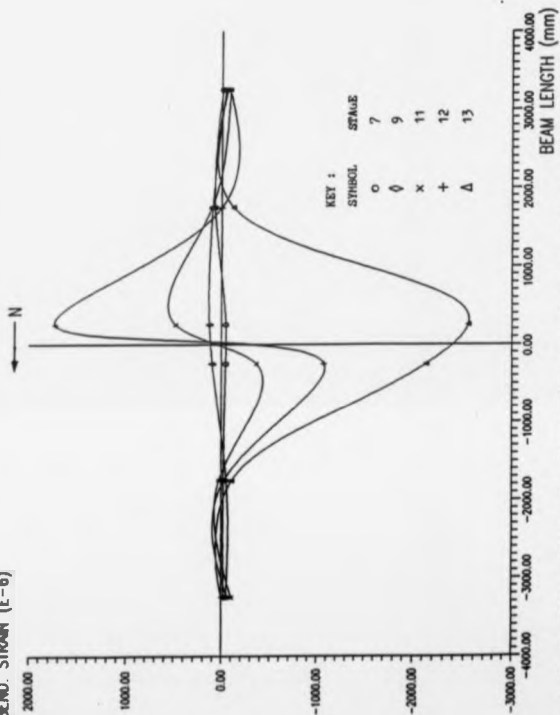
Fig. 8.40 Beam U38 – variation of in-plane bending strain of the bottom flange along the member
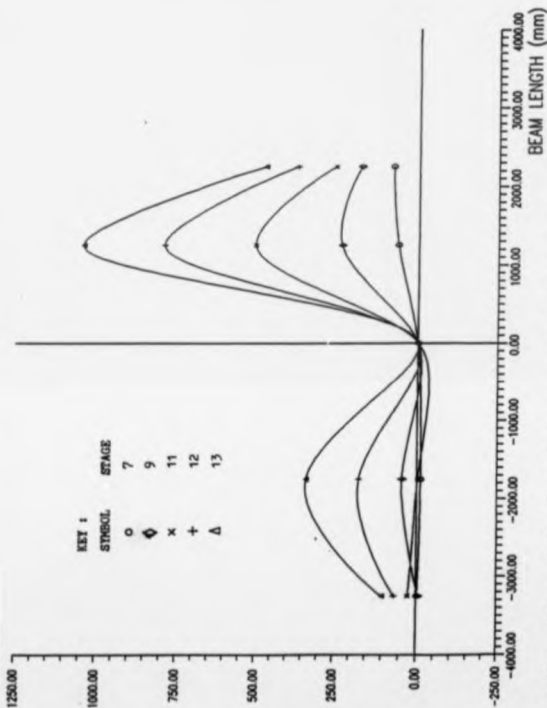
Fig. 8.41 Beam U3A - variation of out-of-plane bending strain of the web along the member

314
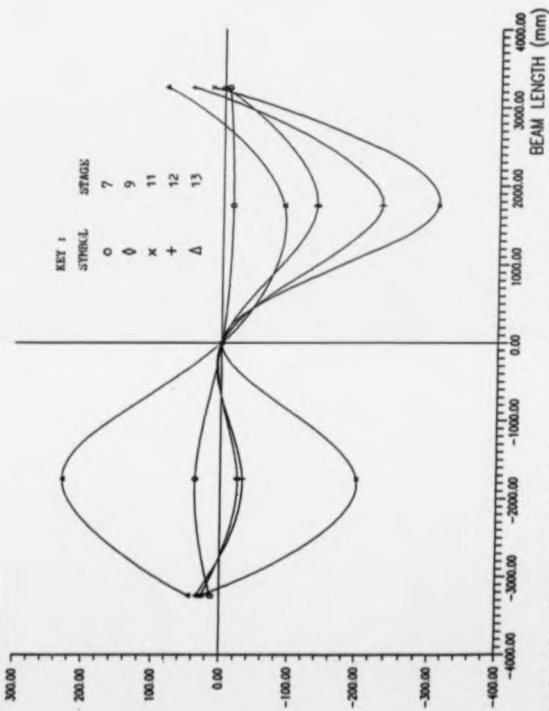
Fig. 8.42 Beam U3B - variation of out-of-plane bending strain of the web along the member
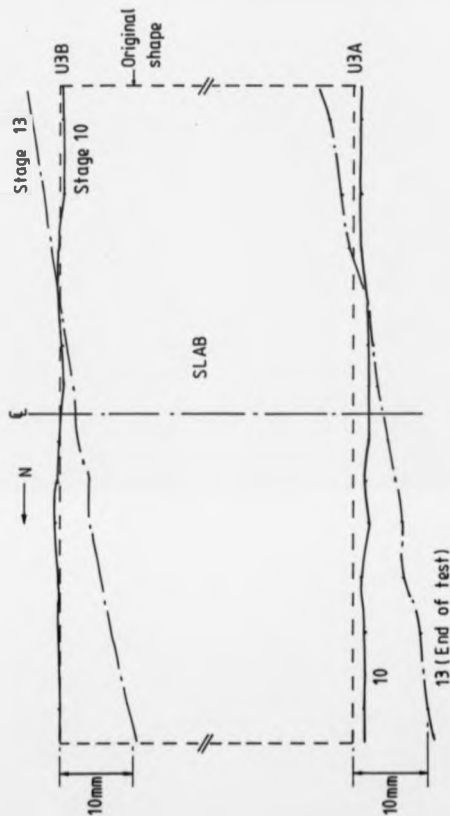
Fig. 8.43 Lateral movement of concrete slab for specimen U3

Plate 8.1 Crack pattern in concrete slab for specimen U2

Plate 8.2   Wavelength and amplitude of the local
            buckle for beam U2A

Plate 8.3   Local buckling in beam U2A

Plate 8.4 Local buckling in beam U2B

Plate 8.5 Interaction of local and lateral
buckling in beam U2B

Plate 8.6 Local buckling in beam U3A

Plate 8.7 Local buckling in beam U3B

Plate 8.8 Crack pattern in concrete slab for specimen U3

CHAPTER 9

ANALYSIS AND DISCUSSION OF

THE INVERTED U-BEAM TESTS

9.1 Introduction

The experimental results of the two inverted U-beam tests have been given in the previous Chapter, and the following sections contain a discussion on the experimental errors, followed by an analysis of the results, in particular, in relation to the effect of buckling on the strength of the specimens. Firstly the general behaviour of both tests and common features are discussed in greater detail. Comparisons are made between the U1 and U2 specimens in terms of their load-displacement behaviour. The distinctive features in each test are then summarized and conclusions are drawn.

9.2 Accuracy of results

9.2.1 Accuracy of experimental measurements

All load cells were calibrated twice, before and after
each test, and the final results were taken as the mean
of the values from these two sets of calibration graphs.
This gives better accuracy than using one set of graphs
alone.   Linear regression analysis on the calibration
results showed that the loads could vary as much as ±2%
with respect to the best fitted straight line.   In
addition the inaccurate alignment of the bearings,
resulting in unequal lever arms, was another source of
error.   In calculating the values of support moments
using the static conditions, there are small errors in
the assumptions. For instance, in the U3 test the line
loading might not be uniformly distributed on the twin-
beams,   U3A   and   U3B,   and   the   specimen   shortened
horizontally as a result of large vertical deflections.

For the U2 test, the load cell results and static checks
agree within 3%. The reported support moments and shear
forces are based on the recorded load cell measurements
and the maximum error due to calibration errors and
system eccentricities is believed to be within ±4%.

For the U3 test, the load cell results and static checks
agree within 3% before local buckling, but discrepancies

increased to 4% after local buckling as the presence of line loading complicated the system in terms of the spread of external loads. In the calculations of the applied sagging moment and static checks, the line loading is resolved into two rows as shown in Fig. 9.1, in order to similar better the actual structural response during the test, and this assumption is found to be satisfactory from comparing the results between load cells and static predictions at the initial three load stages. With regard to the overall accuracy, the possible error should not exceed 5%.

Strains were measured by electrical resistance strain gauges and recorded by using a Schlumberger 3531D data logger. The manufacturer claimed that the error is better than 0.15%. A separate check showed that the repetitive error is less than 0.5%. However, at high yield the measurements might not be as accurate as in the elastic region due to the fact that the bonding agent could have some non-linear material response itself. This situation occurs at locations with high strains, near the internal supports, where local buckling has developed. In view of the magnitudes recorded, these strain measurement errors should not have effects on the general trend of the beam behaviour, and therefore are not so important for the test. It must be remembered that the strain is being measured over a short gauge length, and is thus only a sample of behaviour in a

region of interest. In a region having high disturbance
such as the occurrence of local buckling, neighbouring
strains could sometimes vary a great deal. Under these
circumstances it is better to study the deformation
behaviour over the entire region than to concentrate on
strain levels at particular points.

Measurements of rotations and displacements are also
important. The inclinometer used in the tests is an
extremely sensitive device and gives an accuracy of
measurement up to 0.001 mrad. In view of this
sensitivity, the errors in rotation measurements are
assumed to be negligible. There are two major sources of
error in the measurement of lateral displacements :
parallax and the measuring scale ruler being out of
level. It is believed that the errors have an average of
about 0.5 mm and rarely exceed 1 mm. Although the
measurements are by no means as accurate as those
obtained by dial gauges or transducers, however they are
accurate enough for the purpose of these tests.

9.2.2 Accuracy of calculations on the plastic moment of
resistance

Errors in the calculated values of M_p' are mainly caused
by inaccurate measurements of section dimensions and
yield stresses. Although the thickness of the web and
flanges can be measured quite accurately, it is very

difficult to estimate the areas of the root fillets. With regard to yield stresses, there are 3% variations across the web and each flange, and thus the errors are reduced to 1.5%, when mean values, shown in Table 8.1, are used in the calculations. It is estimated that the calculated values of M_p' are unlikely to be in error exceeding 4% with respect to the true values.

8.3 Strain softening behaviour

8.3.1 Moment-rotation characteristic

The moment-rotation curves of the two tests shown in Figs. 8.3 and 8.4 have similar features. At low load (M' < $0.2M_y'$) both curves follow the elastic uncracked stiffness line, and then lie between the elastic uncracked and cracked stiffness lines because of tension stiffening, until the support moment was above M_y'. The change of the trend in the loading branches occurs around stages 8 and 7 for U2 and U3 tests respectively. For all the four beams, the load began to drop soon after local buckling had taken place in the support region, and the rate of unloading was faster than that of loading. Fracture of four longitudinal wires of the reinforcing fabric, two on each side near the edge, at the support around stage 14, caused a sudden drop of the load applied to the U2 specimen, and an abrupt change of slope in the unloading branch for U2B. There were two layers of longitudinal reinforcement in the U3 specimen, but one layer in the U2 specimen. Since both specimens had the same slab thickness of 90 mm, the plastic neutral axis was therefore further away from the slab in U2 than that in U3. As a result, for the same curvature, the tensile strain in the reinforcement is higher in U2 than in U3. The welded joints in fabric could be quite brittle, perhaps this is the reason why fracture of fabric

occurred in the U2 test. It was not clear in the test whether the fractures were at or near the welded joints, and this needs further investigation.

In Fig. 8.4, U3B has steeper falling branch than U3A, and it appears that the local buckle, which occurred on the span with slab loading, interacted with lateral buckling, magnified by the distributed loads, causing the bending resistance to drop at a faster rate. From the observations in this test, it is therefore important to take account of the adverse effect of imposed loads on the slab for laterally unrestrained beams, when the unloading branch is relied on to redistribute moments in a design method.

9.3.2 Load-displacement relationship

Similar to the results of previous tests on T-beams, a common feature appeared in the U-beam tests. The initial lateral movements of the bottom flanges took place in the same direction as the imperfections until the support moments were above yield. In test U2, at early stages lateral deflections of the two bottom flanges were in the same direction as the imperfections, but rather small (Figs. 8.1, 8.8 and 8.9). Lateral movements started to grow at a faster rate when the material in the support region began to yield (Figs. 8.10 and 8.11). This is because, as a result of yielding, there was a relaxation

of restraint to the bottom flange at the internal support with respect to lateral bending. This can be visualised as the formation of two plastic hinges, on each side of both beams adjacent to the support. Local buckling occurred eventually on the southern side of both beams, and subsequently initiated a further growth of lateral movements at a faster rate as shown in Figs. 8.10 and 8.11. The loss of bending resistance seems due to a combination of lateral and local buckling of the bottom flange, as Figs. 8.10 and 8.11 show that lateral displacements on the southern side were already growing from stage 9. However, judging from the magnitude of the lateral movements recorded, the reduction in lever arm and the corresponding changes in longitudinal strains would be small, and hence their effect on the beam's bending resistance becomes less significant. Nor does it occur at the cross-section of maximum moment. For a cross-section to unload, there must be a reversal of stresses and local buckling is doing exactly that [3,117].

In test U2, it is considered that the growing lateral displacements of the bottom flange before local buckling did not cause the initial loss of bending stiffness, but was responsible subsequently for the sharp fall-off of load carrying capacity. This is undesirable if a continuous beam is designed to rely on large rotation capacity to shed the hogging moments at the internal supports into midspans, while maintaining a high level of

moment resistance in hogging bending. The U2B local buckle was more severe than in U2A, and hence caused higher lateral movements to the U2B bottom flange. As a result of local buckling, the phenomenon of "snap through", which is essentially a bifurcation, was observed in the test on the northern side for both beams (Figs. 8.8 to 8.11).

In test U3, despite having a central slab line loading on one side of the specimen, the load-lateral deflection relationship followed a similar pattern as that in test U2. Due to the presence of the line loading, the lateral deflections of the two bottom flanges on the southern side were much higher than those on the northern side; also, they deflected outwards away from the specimen on the southern side (Fig. 8.26). This was because the line loading, as expected, caused the slab to sag, and as a result of that the two steel beams rotated in an opposite manner giving the outward movements. It was interesting to note that the lateral movements on beam U3A were slightly higher than those on beam U3B, and this was probably due to the influence of initial imperfections (see stage 3 in Fig. 8.26 and the shape of initial imperfections in Fig. 8.2). Similar to U2, Figs. 8.27 and 8.28 show that there were three stages in the load-deflection relationship - pre-yielding, post-yielding and post local buckling. Lateral deflections began to grow at a faster rate when the two beams had reached their

first yield hogging moment of resistance. These deflections caused additional compressive strains on one side of the bottom flange, and encouraged local buckling to develop earlier than it would have in a laterally restrained bottom flange. Subsequently local buckling occurred causing a decline of bending resistance for each beam, and interacted further with lateral buckling to continue the fall-off of loads as shown in Figs. 8.26 to 8.28. This was more prominent on the southern side. "Snap through" occurred on the northern side for both beams (Fig. 8.26).

Comparing the results of U2 and U3, apparently the slab line loading on U3 did not have adverse effect on the lateral stability of the bottom flanges, at least for the sizes, geometry and moment gradients tested. Also the results indicated that lateral deflections of the bottom flanges prior to local buckling did not reduce the specimens' bending resistance significantly, nevertheless subsequent interaction between local and lateral buckling was detrimental, in that the specimens were unable to maintain a plateau for the moment-rotation characteristic. From observations, the susceptibility to instability in the hogging regions for inverted-U beams depends mainly on the flexural rigidity of the slab, shear connection, and web and on the bottom flange slenderness. For a deep plated girder with narrow bottom flange and unstiffened web, the web will not be

sufficient to restrain the bottom flange laterally, and under this circumstance the lateral deflections become important and may cause the beam to fail at a lower load in a mode of distortional lateral buckling to the steel cross-section.

9.3.3 Transverse rotations of flanges

Unlike the specimen U1, there were less transverse rotations of the concrete slab in U2 because of U-frame action. Moreover previous torsional effects in U1 changed to become a bending effect for the U2 slab. The magnitude of the transverse rotations of the slab were rather small (Figs. 8.14 and 8.16), and their direction followed the bottom flanges closely (Figs. 8.15 and 8.17). Up to stage 10, the transverse rotations of the bottom flanges were small too as shown in Figs. 8.12 and 8.13. This indicated that the web was capable of transferring to the bottom flange the positional restraints to the top flange provided by the slab, when the steel section close to the support was still elastic. Plasticity was gradually spreading near the support until the yielded length was adequate for the formation of a local buckle. The transverse rotations of the two bottom flanges increased rapidly and the pattern changed significantly afterwards, corresponding to an abrupt change of cross-section geometry due to an interaction

between local and lateral buckling. The rotation behaviour was consistent with that of lateral deflection.

Similar behaviour was exhibited in the U3 test except that much higher transverse rotations of the concrete and the two bottom flanges occurred on the southern side than on the northern side associated with slab loading (Figs. 8.29, 8.30, 8.33 and 8.34). Up to stage 8 there were little rotations of the bottom flanges apart from those caused by slab loading. Figs. 8.31, 8.32, 8.35 and 8.36 show that bending occurred to the slab, in particular on the southern side, but twisting of the slab about the longitudinal axis was small (dotted lines in the figures). However the bottom flanges were much more flexible and there was co-existence of twisting and warping as they rotated and deflected sideways non-uniformly at high loads. Around stage 10 the transverse rotations of the bottom flanges began to increase rapidly, coupled with growth of lateral deflections, as a result of local buckling, but their influence on the slab had been small. Further interaction between local and lateral buckling of the bottom flanges enhanced the growth of transverse rotations as well as lateral movements, resulting in a reduction of the specimen's ability to carry loads. This affected both sides of the specimen, not just on the side with slab loading. The results seem to show that the concrete slab did not have much response to local buckling (Figs. 8.31, 8.32, 8.35

and 8.36), and only the bottom flanges were being disturbed and mobilized. The slab provided stiff rotational restraint to the top flange, even when heavily loaded at its midspan. Apparently the destabilizing moments resulting from bottom flange instability were not large enough to make the slab unstable.

8.3.4 Strain measurements

In general strain measurements were consistent with the lateral movement and transverse rotation measurements in the two tests. In test U2 Figs. 8.18 and 8.19 show that beam U2B had slightly higher compressive strains along the bottom flanges than those in U2A at each load stage, and this explains why the recorded support moments were also higher as shown in Fig. 8.3. The strain measurements also gave a clear indication of the effect of buckling. From the bending strains shown in Figs. 8.20 to 8.25, it was evident that lateral in-plane bending of the bottom flanges was very slight before stage 10, and became significant as the load increased. A rapid increase in bending strains at later stages was again due to interaction of local and lateral buckling of the bottom flange. However Figs. 8.20 and 8.21 seem to illustrate that the destabilized region extended for only about 2.5 m from the central support on each side, rather than being the whole length of the cantilever, as commonly assumed. In fact the extension of the beam by

900 mm beyond the end reactions helped to pull back lateral deflections and to keep the bottom flanges more or less stationary towards the ends of the specimen.

In test U3, Figs. 8.37 and 8.39 show that the compressive strains of the two bottom flanges on the southern side associated with slab loading were lower than those on the northern side, otherwise the behaviour would be identical to the U2 specimen. It was interesting to note that local buckling did not occur on the same side of the specimen, but developed on the northern and southern sides for U3A and U3B respectively. Although the northern side was subjected to a more adverse hogging moment gradient, which was linear rather than parabolic, the half-wave length of a plastic local buckle is relatively short, and therefore the small difference in moment gradients on the two sides over the support had little influence on which side the buckle would be formed. From Figs. 8.38 and 8.39, there seems to have been little in-plane lateral bending of the bottom flanges up to stage 9; but once local buckling occurred at stage 10, rapid increase in in-plane lateral bending took place. Web distortion followed a similar pattern as the in-plane lateral bending of the bottom flanges (Figs. 8.41 and 8.42). Apparently the destabilizing region affected by local and lateral buckling extended for only about 2.0 m from the central support on each side of both beams as shown in Figs. 8.38 and 8.40.

9.4 Discussion

Specimens U2 and U3 are appropriate for the modelling of
composite beams in commercial multi-storey buildings and
short span bridges, but the flexural stiffness of the U2
slab would be 75% higher than the value found in practice
for standard composite building floor. These stiffnesses
tend to be low as compared to bridge structures, so that
the restraining effect on the bottom flanges from the
slab is less favourable in the tests than in practice.
The slenderness ratios of the web, d/t, ignoring fillets,
are 57.5 and 50.4, and hogging length/flange width ratios
are 36.4 and 34.2, for U2 and U3 respectively. To take
into account the effect of moment gradient, it is
appropriate to examine the values of two strut
slendernesses for the bottom flange alone, which are the
ratios of cantilever length/r_y and beam span/r_y, assuming
the hogging region corresponds to a length of 0.21 x
span, where r_y is the radius of gyration of the bottom
flange with respect to the section's minor axis. These
ratios are 126 and 600 for U2, and 118 and 562 for U3.
These figures were deliberately chosen to be close to the
lower end of the practical range for Class 2 composite
beams in buildings. According to the design chart
published by Weston et al[6], both specimens would fail
at lower loads, 75% and 78% of the ultimate moment of
resistance for U2 and U3 respectively (Table 10.1), as a
result of lateral buckling of the bottom flange. However

the results showed that lateral buckling became significant only after local buckling had occurred. It was evident from the tests that the decline of resistance for both specimens was due to an interaction of local and lateral buckling of the bottom flanges over a region of approximately 2.5 m on either side of the support.

Lateral bracing effect by the concrete slab to the bottom flanges was adequate, when the cross-section at the internal support was still elastic, for the flexural stiffnesses derived from the web and slab used in specimens U2 and U3. The test results are useful for the checking of conceptual models. With closely spaced shear connectors (spacing ≤ 450 mm), the flexibility of the U-frame using hot-rolled steel sections can be estimated considering the slab-joist joint as "rigid", that is appropriate because the web is rather flexible. The concrete slab can be assumed to restrain the rotation of the steel top flange partially according to its bending stiffness, and to provide complete lateral restraint. The strength of both specimens was slightly above the plastic moment, which was calculated using measured material properties, and so this means that strain hardening had not yet developed in the tests. This is probably because the cross-section was less stocky, causing local buckling, to occur at a lower strain level, and consequently, buckling reduced the beam's bending

resistance. From the results of test U3, it is recommended that the minimum value of the slab flexural stiffness per unit metre (EI/L), where L is the distance between two parallel beams, should be at least 180 kNm/rad to prevent excessive lateral deflections of the bottom flange before the occurrence of local buckling, for a Class 2 edge beam in a building designed as composite. This figure can be reduced to 120 kNm/rad for an internal beam with slab cast over on both sides.

Bode and Uth [23] suggested from their tests that the longitudinal reinforcement in general should not be taken into account in calculations of the plastic moment of resistance M_p' due to the possibility of premature fracture of reinforcing bars. They also gave design guidances whether strength of reinforcement can be used as follows :

a) For deformed bars with $\phi > 8$ mm,
    $x / h \leq 0.50$

b) For wire mesh with $\phi \leq 8$ mm

    $x / h \leq 0.25$

    where x and h are defined in Fig. 9.2.

In test U2, fracture of the wire mesh occurred soon after reaching plastic moment, M_p' (composite), at the support, and the x/h ratio was calculated to be 0.53 for wire mesh with ϕ = 7mm. It seems that Bode and Uth's criteria on prevention of premature fracture of rebars are conservative and restrictive. It is important to distinguish two design situations: (A) If large rotation capacity is required such as in the case of using plastic hinge theory, it would be better to ignore the contribution in strength from the rebars completely, unless they are ductile. (B) If a beam is being designed on the basis of an elastic moment diagram, it would be uneconomical to ignore the contribution in strength from the rebars. Bode and Uth' criteria are applicable to the former case. In view of the fact that wire mesh has non-uniform strain distribution and is brittle, less ductile at the grid joints than in the mid-length between them, it would be safer to neglect its contribution in strength, especially for Class 2 beams with high demand of rotation capacity in the hogging region.

From the test results it appears that it is not necessary to reduce the ultimate bending moment of resistance below M_p' for Class 2 beams in buildings, if the rotation capacity is not a prime concern in a design, even when the beam is laterally unbraced. But lateral restraint to the bottom flange at the supports is essential. It can

be achieved by means of ties[92] or specially designed connections. The pull-out strength of the shear connectors has to be checked and this is not usually a governing factor in design.

In building structures, it would be beneficial to explore the applicability of plastic design using beams with Class 2 cross-section and unbraced laterally. Bode and Uth[23] suggested that plastic hinge analysis can be used even in case of Class 2 members, if reduced cross-sections are taken into account to compensate for the reduction in strength due to local buckling. In their analysis, they ignored the effect of slab loading and lateral buckling of the bottom flange. From the U3 test results, it is evident that the slab loading coupled with local buckling caused the bottom flange to deflect laterally at an increasing rate, meanwhile the support moment was dropping. This is undesirable for moment redistribution because the unloading branch of the moment-rotation curve became too steep. Also it is rather difficult to justify how much reduction to the bending resistance should be made in order to satisfy the rotation capacity required for the purpose of plastic design. From experimental observations, at high rotations the support became unstable and had a tendency to twist about a vertical axis, and so in practice either the columns or cross-beams supporting the beam would be subjected to the same destabilisation. It is therefore

suggested that the unloading branch of the moment-rotation curve for Class 2 laterally unbraced beams should not be relied on to redistribute moments from the hogging to sagging regions. If plastic hinge design must be used, a remedy is to restrain the bottom flange laterally at about 1 m from the support and this could just consist of additional vertical stiffeners. In addition the maximum moment of resistance should be reduced as suggested by Bode and Uth. In other words, interaction between local and lateral buckling of the bottom flange in critical cross-sections should be avoided. The buckling strength affected by local buckling only can therefore be obtained reasonably accurate by using numerical analysis [16].

In the design of bridge girders, elastic global analyses and moment envelopes (influence lines etc.) are normally used. It seldom requires large rotation capacity in a hogging region, even when compact members (Class 2) are used in bridge decks. For the vast majority of practical configurations for girders subjected to moment gradients, lateral buckling of the bottom flange would not occur until local buckling has started in the critical cross-sections. Under this circumstance, an economical design would be to allow the hogging moment of resistance to reach a certain level, such that it is slightly lower than the level at which local buckling would have occurred. Further research is required to identify the

range of composite beams, in which distortional lateral
buckling of the bottom flange does not occur prior to
local buckling.   Then a design method can be developed in
terms of the local buckling strength of a member.

9.5 Conclusions

At early load stages lateral deflections of the bottom
flanges followed closely the shape of initial lateral
imperfections, but the magnitudes were small, when both
specimens were still elastic. The ultimate strength of
each of the four beams in specimens U2 and U3 is governed
by a complex interaction between local and distortional
lateral buckling, strongly influenced by initial lateral
imperfections of the bottom flange. The load-deformation
relationship can be generalised into 3 stages : (1)
elastic, little deformation, (2) pre-local-buckling with
some yielding, a gradual increase of deformation, and (3)
post-local-buckling, a rapid increase of deformation.

Test results showed that further decline in bending resistance after
reaching the maximum for both specimens was due to a
combination of local and distortional lateral buckling of
the bottom flange.   The experimental results, in
particular U3, showed that lateral deflections of the
bottom flanges were an integral feature of the behaviour
even at low load levels; but the magnitudes recorded
before local buckling seem unlikely to affect the bending
resistance significantly.   The slab loading on the U3
specimen caused higher lateral deflections and transverse
rotations to the bottom flanges on the loaded side than
on the other, and this could possibly cause local
buckling to start at a lower load level.   It was

interesting to note that local buckling occurred on the loaded side for U3B rather than on the other side with steeper moment gradient. The ultimate moments of resistance for both specimens were slightly above their plastic bending resistances. The inability of the beams to reach higher resistances (effect of strain hardening) seems to be due to the proportions of their cross-sections, and not at all to the length of the laterally unbraced hogging region.

Lateral deflections and transverse rotations of the concrete slab for both specimens were small throughout the tests, and for the geometry and sizes of beams tested it shows that the restraining effect of the slab to the bottom flange through the web was high enough to reduce excessive lateral deflections prior to local buckling of the bottom flange. With closely spaced shear connectors (spacing $\leq$ 450 mm), the slab-joist joint can be considered as rigid. The concrete flange can be assumed to provide complete lateral restraint to the steel top flange, and also partial rotational restraint about a longitudinal axis depending on its bending stiffness.

As compared with single T-beams the effect of inverted-U frame action enhanced considerably the stability of unbraced continuous composite beams. Therefore it is recommended to use the theoretical prediction of the ultimate strength of these beams rather than isolated T-

beam model with complete lateral and rotational restraints to the steel top flange. But at the internal support it is necessary to provide lateral restraint to eliminate the possibility of flange lateral deflection, such that an S-shape buckling mode is enforced.

Fracture of the reinforcing fabric occurred in the U2 specimen soon after local buckling began and led to a sudden drop of bending resistance. If large rotation capacity in the hogging region is required to shed bending moment, it is recommended not to take into account the contribution from reinforcing fabric inside the slab in calculating the plastic hogging moment of resistance, Mp'. Premature fracture of reinforcing fabric tends to be more acute when metal decking is used to construct the slab. Bode and Uth's criteria [23] on the prevention of premature fracture of reinforcement seem to be a little restrictive, especially in a situation when the unloading branch of the moment-rotation curve is not used in moment redistribution. Further research is required on this subject.
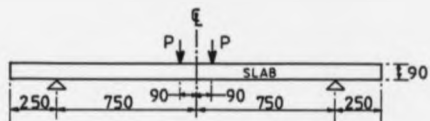
Fig. 9.1 Idealization of the positions of reaction
on U3 slab for the line loading
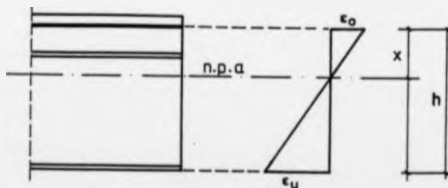
Fig. 9.2 Strain distribution across a composite
cross-section

CHAPTER 10
DESIGN RECOMMENDATIONS FOR
DISTORTIONAL LATERAL BUCKLING

10.1 Introduction

In this chapter comparisons are made between the experimental results of the tests on distortional lateral buckling and the predictions from various design methods described in Chapter 2. The appropriateness of each method is discussed with respect to the real beam behaviour. There are several factors which strongly influence the ultimate hogging moment of resistance for continuous composite beams using hot-rolled I-sections susceptible to distortional lateral buckling, or rather interaction between inelastic local buckling and lateral buckling of the compression flange. Each factor is considered separately for the purposes of developing a simple design method for Class 1 and 2 unbraced composite beams. Finally, based on the experimental results and other evidence, a simple method, which identifies the type of composite beams not vulnerable to distortional lateral buckling, is proposed.

10.2 Comparisons between the test results and predictions from various design methods

As discussed in Chapter 2, a generally accepted method of dealing with distortional lateral buckling in the hogging region for continuous composite beams is not presently available. As far as this instability behaviour is concerned, the two inverted-U beam tests are more representative and relevant than the single T-beam tests, therefore their results are compared with predictions from some of the existing methods proposed by different research workers. Comparisons have been made with respect to the following five design methods.

1. BS5400 : Part 3 (Ref. 8)

2. Bradford and Johnson (Ref. 5)

3. Weston and Nethercot (Ref. 6)

4. Lawson (Ref. 92)

5. Proposed Eurocode 4 (Ref. 93)

The first three methods are related to the design of composite beams with more slender cross-section (Class 3) such as plate girders, but they do not preclude the design of compact beams. The last two methods are

developed in conjunction with the drafting of design rules for composite building structures, and they will probably be incorporated into the final versions of BS5950 and Eurocode 4. It is understood that these two methods are more relevant for the design of composite beams using hot-rolled I-sections, although it has not been specifically mentioned. The test results and predictions are summarised in Table 10.1. Weston's method requires the input of the span length, so in the calculation a span/overall beam depth ratio equal to 25 is assumed, that is commonly found in practice.

To examine the results in Table 10.1, it is necessary to identify the most important slenderness parameters influencing the ultimate strength in the tests. These include the web depth-to-thickness ratio d/t, the web flexural stiffness k, the compression flange width-to-thickness ratio B/T and the modified lateral slenderness ratio L_o/r_{cp} defined in section (2.7) in Chapter 2, where L_o is the length between the support and the point of contraflexure, and r_{cp} is the radius of gyration of the portion of the beam in compression below the plastic neutral axis, and are summarised in Table 10.2. Transverse bending stiffness of the slab also affects the lateral instability because it determines the degree of rotational restraint provided by the slab to the steel section. The U2 slab, which is composite with steel

decking, is stiffer than U3, and the ratio between the
two flexural rigidities is calculated to be 1.75.

As compared with specimen U2, U3 has a stiffer web and
was subjected to a less severe moment distribution,
parabolic due to slab loading, rather than a linear
moment gradient. It would be expected to have an
ultimate strength of U3 normalised to the plastic moment
of resistance higher than U2. Table 10.2 shows that the
webs in U3 are almost 50% stiffer than those in U2, and
the lateral slenderness ratios are however of similar
values. Yet the test results indicated that both
specimens reached an ultimate moment of resistance
slightly higher than the plastic moment (measured
material strengths are used), and the strength of U3 was
marginally lower than U2 in contrast to the expectation
($M_m'/M_p' = 1.03$ and 1.01 for U2 and U3 respectively). So
the apparent drop of moment resistance in U3 is somewhat
influenced by having a less rigid slab than U2, slab
central loading and inelastic local buckling.

From Table 10.1, it is evident that BS5400 is unduly
conservative by a factor of 3. This is because the
bottom flange is not uniformly compressed as assumed in
the model. Bradford and Johnson method gives consistent
predictions for both specimens by a factor of about 1.4,and
this is probably due to the fact that the slenderness
ratios of both specimens are close to those examined in

their parametric study. If the lateral slenderness ration L_o/r_{cp} becomes greater, this method will probably produce unsafe results, since this ratio, which is dependent on the moment gradient and the shape of the bottom flange, does not appear in its formulation. For continuous composite beams using hot-rolled steel section with span less than 15 m, the method should be conservative. Similar conclusion has been made by Weston and Nethercot[6].

The Weston method seems to give good predictions, but in the calculations a span-to-overall depth ratio equal to 25 is assumed. With this ratio, the length of the hogging region corresponding to the fixed-ended beam model (approximately 0.2 x span) is much shorter than the cantilever length in the test, 47% and 52% of the cantilever length for specimens U2 and U3 respectively. If a span of a fixed-ended beam, corresponding to the hogging moment region at both ends modelled in either of the tests, is used, the method becomes very conservative due to the fact that the predicted moment resistance decreases as the span increases. This reveals a defect in the method because it uses the span L as a design parameter, but ignores any variation of the moment diagram other than the case derived from a uniformly loaded fixed-ended beam. For instance, it may be unsafe for an end span with rather long hogging region on one side only.

Among the two more general methods, draft Eurocode 4 gives more consistent and better predictions than the Lawson method. These two methods are based on the same principle , using energy method and taking into account the restraining effect by the slab to the steel section, but the latter uses a very simple model, in which the bottom flange in hogging bending is assumed to buckle in a half sine wave, and the top flange is fully restrained by the concrete slab. The critical buckling moment is then obtained by optimizing the length of the buckle. Theoretically draft Eurocode 4 is superior to the Lawson method because the critical moment is obtained from a buckling analysis for the beam as a whole, not just the hogging region. The Lawson method is therefore more conservative as a result of using a less restrictive buckling mode. In terms of consistency and versatility, draft Eurocode 4 seems to be the best overall method.

10.3 Flexural rigidity of the slab

Except the Eurocode 4 method, all theoretical studies on
distortional lateral buckling assume the slab is
torsionally very stiff longitudinally. It is certainly
true in most bridge structures, but in buildings it might
not be so. From the observations of test U3, it was
found that lateral displacements of the bottom flange
began to grow, especially on the side with slab loading,
prior to local buckling, although the magnitude was
small. These displacements were caused jointly by the
flexibility of the web and transverse bending of the
slab. For hot-rolled I-sections, the flexibility of the
web is fixed by the serial size, thus it is beyond the
control of a designer. To eliminate excessive lateral
displacement of the bottom flange caused by the slab, it
is important to ensure that the flexural stiffness of the
slab, EI/a, where a is the spacing between the steel
members in an inverted-U frame, is above a critical
value. This value is suggested to be 180 kNm/rad per a
metre strip judging from the results of test U3. The
flexural stiffness of any slab can be calculated as
follows:

i) Calculate the position of the elastic neutral axis,
    assuming concrete in tension is cracked referring to
    Fig. 10.1 .

$$A_T (x - c) + 0.5 b x^2 = A_B (d_s - x) \qquad (10.1)$$

ii) Calculate the second moment of area after x is solved from eqn. (10.1)

$$I_s = A_B (d_s - x)^2 + A_T (x-c)^2 + bx^3/3 \quad (10.2)$$

iii) The flexural stiffness of the slab is given as,

$$k_{slab} = E_s I_s/a \quad (10.3)$$

In buildings, top steel is usually not required for the floor slab in sagging bending and the neutral axis depth x is seldom less than 0.4 d_s for economic reason. Assuming a nominal amount of bottom steel, $A_B = 193$ mm^2/m, and a short term modular ratio $\alpha_e = 7$, equation (10.2) reduces to,

$$I_s = (69.5 + 3 d_s) d_s^2 \quad (10.4)$$

Conservatively, if d_s is greater than 70 mm, eqn. (10.4) becomes,

$$I_s = 280 d_s^2 \quad (10.5)$$

Combining eqns. (10.3) and (10.5), it gives

$$E_s \, I_s \, / \, a = 280 \, E_s \, d_s^2 \, / \, a \; \geq \; 180 \times 10^6,$$

therefore conservatively,

$$E_s \, d_s^2 \, / \, a \; \geq \; 650 \qquad\qquad (10.6)$$

where

E_s is the modulus of elasticity of the
reinforcement in $kNmm^{-2}$

d_s is the effective depth of the slab for sagging
in the direction normal to the span of the beam
in mm

a   is the spacing between the steel members in an
inverted-U frame in mm

Equation (10.6) is suitable for an outer beam in a floor-
multi-beam system, but becomes too conservative for an
inner beam interconnected by two-inverted-U frames. It
is suggested to adjust the limit in eqn. (10.6) by a
factor of 2/3, which is based on the relative stiffness
of the two cases shown in Fig. 2.4.

Therefore, the requirement is,

$$E_s \, d_s{}^2 \, / \, a_1 \; \geq \; 450 \qquad\qquad (10.7)$$

where a_1 is the greater of the two parallel distances be
tween the beam and the two adjacent beams normal to the
span in mm.

In cases where a composite slab is used, the cross-
sectional area of the steel decking can be treated as
bottom steel reinforcement, provided that the ribs are
perpendicular to the span of the beam and continuous.
The flexural stiffness of the slab should be calculated
using eqns. (10.1) to (10.3) and k_{slab} is not allowed to
be less than 180 kNm/rad. In addition no reduction is
made to this limit for an inner beam as discontinuity of
the decking may occur for multi-bay floor construction.

10.4 Flexibility of the web

In order to stabilise the compression bottom flange, it is vital to ensure that the flexural stiffness of the web is sufficiently high to prevent excessive lateral displacements of the bottom flange prior to local buckling. Ultimate capacities of the beams in the present tests are plotted in Fig. 10.2 as a function of web stiffness k N/mm, defined in eqn. (2.18), in addition to the existing experimental results. Nearly all beams have M_m'/M_p' value higher than 1.0 except beams SB14 and U1, but SB14 was subject to high shear ratio $V/V_p = 0.4$ and U1 was a 5.1 m long isolated T-beam cantilever. By comparing the results of tests U1 and U2, it is evident that the U-frame action has enhanced the ultimate moment of resistance of the beam by more than 10%. Fig. 10.2 also shows that when k lies between 0.3 to 0.5, which is the practical range for hot-rolled I-sections, the strength of the beams is still higher than the plastic moment of resistance. Therefore for a beam to reach its plastic moment it is not advisable to have a web stiffness k less than 0.3 N/mm. Substituting this limit into eqn. (2.18), the web depth-to-thickness ratio is given as,

$$E t^3 / 4 (1-\nu^2) d^3 \geq 0.3,$$

for $E = 205$ kNmm^{-2} and $\upsilon = 0.3$,

$$d \, / \, t \; \leq \; 57 \qquad\qquad (10.8)$$

where d is the depth of the web between the flanges

t is the web thickness

Equation (10.8) applies to both grade 43 and 50 steel sections.

10.5 Modified lateral slenderness

The buckling resistance of a composite beam against distortional lateral buckling in the hogging region depends on many factors such as the length of the hogging region, the geometry of the cross-section and the position of the plastic neutral axis. Table 10.1 shows that the closest prediction is still 21% lower than the test result, and both specimens U2 and U3 have bending resistance higher than the plastic moment. This means there is a scope for improvement, perhaps for a certain class of beams it is possible to design up to their plastic moment of resistance without making a separate check on lateral instability. The present test results are plotted in addition to the existing results in Fig. 10.3 using the modified lateral slenderness ratio L_o/r_{cp}, which is an appropriate design parameter for lateral buckling previously defined in Section 2.7 in Chapter 2. It is found that the ultimate strength of U2, which is an inverted-U frame, is marginally higher than the plastic moment with a L_o/r_{cp} ratio equal to about 190. This suggests that it would be unsafe for beams to have the plastic moment capacity in a design with a modified lateral slenderness ratio higher than this value.

The following condition can be obtained by limiting the L_o/r_{cp} ratio equal to 190 and substituting the

geometrical properties of the cross-section into the ratio. Symbols and dimensions are defined in Fig. 10.4.

$$r_{cp}^2 \; = \; I_c \; / \; A_c$$

$$= \; [TB^3 + \alpha'dt^3] \; / \; [12 \; (TB+\alpha'dt)]$$

or

$$1 \; / \; r_{cp}^2 \; = \; [12 \; (TB+\alpha'dt)] \; / \; [TB^3 + \alpha'dt^3]$$

for B >> t,

$$1 \; / \; r_{cp}^2 \; = \; 12 \; (1+\alpha'dt/TB) \; / \; B^2 \qquad (10.9)$$

If $\quad L_o \; / \; r_{cp} \; \leq \; 190$

then $L_o^2 \; / \; r_{cp}^2 \; \leq \; 36100$ $\qquad\qquad$ (10.10)

Let $0.5L \; / \; L_o \; = \; \beta$, where L is the span of the beam between lateral restraints and L_o is the distance between the support and the point of contraflexure; for an internal span L_o should be taken as the greater of the two distances on either side. In practice, β is usually greater than 1.0. Therefore, eqn. (10.10) becomes,

$$L^2 \; / \; (4\beta^2 \; r_{cp}^2) \; \leq \; 36100 \qquad\qquad (10.11)$$

Substituting τ_{cp} from eqn. (10.9) into eqn. (10.11), it gives,

$$(L^2/B^2)(1 + \alpha'dt/TB) \leq 12033 \ \beta^2$$

or conservatively,

$$1.0 + \alpha'(d/B)(t/T) \leq 12000 \ \beta^2 \ (B/L)^2 \qquad (10.12)$$

where $\alpha'=$ the proportion of the web in compression below
           the plastic neutral axis

  $\beta = L/2L_0$ obtained from the moment distribution
         along the beam

Conservatively, β can be taken as 1.0, then eqn, (10.12) becomes,

$$1.0 + \alpha'(d/B)(t/T) \leq 12000 \ (B/L)^2 \qquad (10.13)$$

To serve as a check, the geometrical properties of specimen U3 are substituted in eqn. (10.12) as follows:

  $\alpha' = 0.62$
  $d = 332.8$ mm
  $t = 6.6$ mm
  $B = 124.0$ mm
  $T = 7.65$ mm
  $\beta = 1.0$

Hence,

$$1.0 + 0.62 \ (332.8/124)(6.6/7.65) \ \leq \ 12000(124/L)^2$$

or $\quad$ L $\leq$ 8704 mm

This means that the beam can reach its plastic hogging moment of resistance without lateral restraints to the bottom flange, if the unbraced length is less than 8.7m . Equation (10.12) is based on very limited test data, and so needs more validation against more test results when they are available, especially for beams with high shear ratio V/V_p about 0.5. There will be a margin of safety about 10% if the plastic hogging moment of resistance is based on the nominal material strengths rather than the measured strengths assumed in the simplified method.

Overall depth of U3, h, is 438 mm, so the span/depth ratio is 8704/438 = 20, which is within the range of normal practice to control deflections at the serviceability limit state. Apparently equation (10.13) is applicable in practice.

10.6 Other design considerations

To provide continuous lateral restraint to the upper
flange, it is necessary to check that the pull-out
strength of the shear connectors is not exceeded as a
result of lateral buckling of the bottom flange. This
criterion is not usually critical in building structures
when the longitudinal spacing of the studs is less than
four times the slab thickness and a sufficient number of
studs are provided in accordance with draft Eurocode 4,
and are placed uniformly along the beam and symmetrically
with respect to the plane of the web.

Kemp[30] identified that for Class 2 sections the maximum
redistribution of moments of 30% from the support to the
mid-spans based on an elastic uncracked analysis
corresponds to a required rotation capacity of 1.6
(eqn.(2.1)). The minimum available rotation capacities
for specimens U2 and U3 are estimated to be 2.2 and 2.0
respectively as shown in Figs. 8.3 and 8.4. Apparently
the present slenderness limits for Class 2 cross-sections
in Eurocode 4 are justified from the test results, even
for unbraced members. Although fracture of reinforcing
mesh may occur at high rotation, the test results suggest
that there is no need to ignore the contribution of the
mesh in the calculation of the plastic moment of
resistance for Class 2 beams. However for Class 1
sections to be employed in plastic design the maximum

redistribution of moments is over 40%, which requires a rotation capacity of more than 3. At such high level of rotation, corresponding to high hogging curvatures reinforcing mesh placed in the slab would have fractured. In view of the research by Bode and Uth[23], it is recommended not to include the contribution of any reinforcing fabric in the calculation of the plastic moment for Class 1 cross-sections. Also, by reducing the level of the design moment resistance, the rotation capacity of the beam can be improved significantly, which provides an extra margin of safety in shedding the support moments. Interaction between shear and moment in the hogging moment region has not been studied and high shear might affect the ultimate moment of resistance.

10.7 Tentative design method

Based on the previous discussions, a simple check without
direct calculation method is now proposed, for the design
of Class 1 and 2 continuous composite beams using grade
43 or 50 hot-rolled I-section at the ultimate limit state
in buildings, without lateral bracing except at the
supports. The steps are as follows:

1) The provision of shear connectors is calculated in
accordance with draft Eurocode 4 for full interaction and
the longitudinal spacing of the studs does not exceed
four times the slab thickness. Studs are placed
uniformly along the member and symmetrically with respect
to the plane of the web, either one row in the middle or
two rows with a transverse spacing at least half the
width of the upper flange.

2) The flexural rigidity of the slab has to satisfy
equation (10.6) for an inverted-U frame or equation
(10.7) for multiple inverted-U frames. For composite
slabs, the cross-sectional area of the steel decking can
be treated as bottom reinforcement where appropriate.
The flexural rigidity is then calculated using eqns.
(10.1) to (10.3) and should not be less than 180 kNm/rad
per metre strip.

3)   The web slenderness has to satisfy equation (10.8).

4)   The lateral slenderness of the bottom flange has to satisfy equation (10.12).

5)   For Class 1 sections, the contribution of any reinforcing fabric in the slab to the moment of resistance is ignored.

6)   The hogging moment of resistance of the beam can be taken as the plastic moment, M_p', which is calculated using nominal material properties and including the usual material safety γ_m factors. No reduction in design moment M_p' need be made if the design shear force V is less than $0.2V_p$.

10.8 Conclusions

Calibration of the test results of the two U-frame
specimens against various existing design methods shows
that the predictions are conservative ranging from 31% to
79% of the maximum bending resistance obtained in the
tests. Weston and the new Eurocode methods give the best
predictions in comparison with the test results, however
the former method will be more conservative if the
span/overall depth ratio is higher than 25, which is
assumed in the calculation.

The present classification system for Class 2 sections in
the draft Eurocode 4[1] is justified, although the loss
in moment resistance in these tests is not solely due to
local buckling near an internal support, but rather as a
result of interaction between local and distortional
lateral buckling. The test results also confirm that it
is safe to increase the Eurocode 4 web slenderness
(d_b/t_f) limit from 33 to 39 for Class 2 sections.

Because of the high demand of rotation capacity required
in a plastic analysis for Class 1 sections, it is
recommended not to include the contribution of any
reinforcing fabric in the slab in calculating the hogging
moment of resistance as premature fracture may occur at
large curvatures. However the test results suggest that
for Class 2 section this limitation may not be necessary,

since the available rotation capacity is found to be sufficient as demonstrated in the two inverted-U frame tests.

On the basis of available experimental results and other evidence , a tentative simple design method is proposed for the purpose of identifying Class 1 and Class 2 unbraced and unstiffened continuous composite beams using grade 43 or 50 hot-rolled steel I-sections, for which distortional lateral buckling either would not occur or would have very little effect on the ultimate bending resistance at the ultimate limit state. For those members, the ultimate strength can be taken as the plastic hogging moment of resistance using nominal material strengths together with their partial safety factors.

Method	U2				U3			
	M_D^*	M_D^*/M_p^*	U2A M_m^*/M_D^* (M_D^*/M_m^*)	U2B M_m^*/M_D^* (M_D^*/M_m^*)	M_D^*	M_D^*/M_p^*	U3A M_m^*/M_D^* (M_D^*/M_m^*)	U3B M_m^*/M_D^* (M_D^*/M_m^*)
1	100.0	0.33	3.13 (0.32)	3.20 (0.31)	89.2	0.33	3.12 (0.32)	3.05 (0.33)
2	221.0	0.73	1.41 (0.71)	1.45 (0.69)	199.7	0.74	1.40 (0.71)	1.36 (0.74)
3	236.9	0.78	1.32 (0.76)	1.35 (0.74)	215.8	0.80	1.29 (0.77)	1.26 (0.79)
4	218.4	0.72	1.43 (0.70)	1.47 (0.68)	199.0	0.73	1.40 (0.71)	1.37 (0.73)
5	245.0	0.81	1.28 (0.78)	1.31 (0.76)	210.0	0.78	1.33 (0.75)	1.30 (0.77)

1) BS5400

2) Bradford and Johnson

3) Weston and Nethercot

4) Lawson

5) Rolk, EC4

Table 10.1 Comparisons between the test results and theoretical predictions

	Web	Web flexibility	flange	lateral slenderness
	d/t	k (N/mm)	B/T	L_o/r_{cp}
U2A	57.1	0.30	17.7	189.4
U2B	58.0	0.29	17.7	189.4
U3A	51.0	0.42	16.0	184.8
U3B	49.5	0.46	16.3	184.8

<u>Table 10.2</u> Slenderness parameters for U2 and U3 specimens
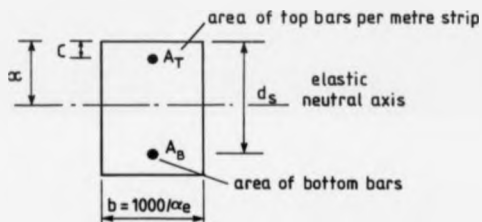
Fig. 10.1 Transformed cross-section of
reinforced concrete slab
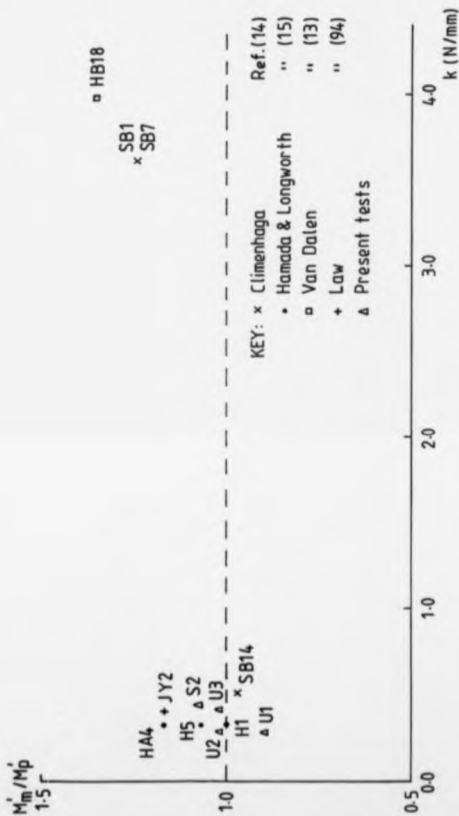
Fig. 10.2 Experimental results versus web flexibility
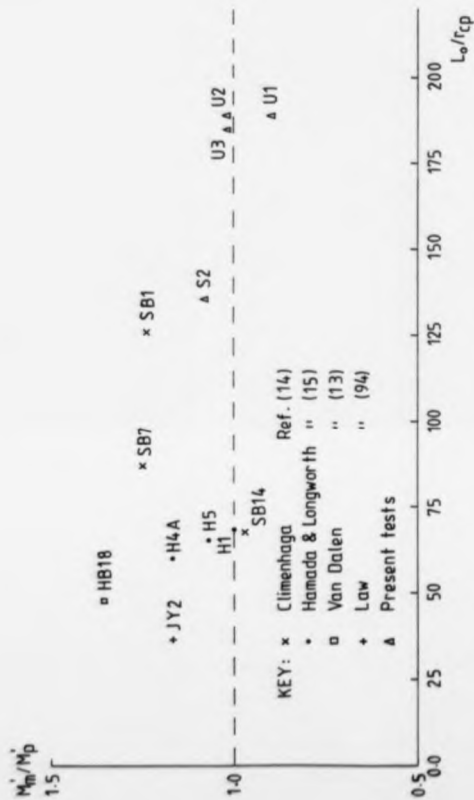
Fig. 10.3 Experimental results versus bottom flange strut slenderness
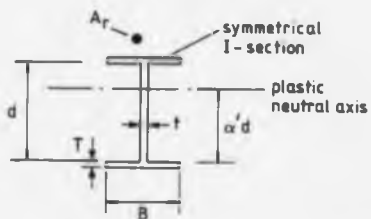
Fig. 10.4 Cracked composite cross-section in hogging bending

REFERENCES

1. Eurocode No.4, Common unified rules for composite
    steel and concrete structure, draft, Commission of
    the European Communities, 1985.

2. BS5950 : Structural use of steel work in building -
    Part 1 : Code of practice for design in simple and
                continuous construction : hot-rolled
                sections, 1985
    Part 3.1:Code of practice for design of composite
                beams, draft, Issue 8, Sept. 1988
    British Standards Institution, London.

3. Climenhaga, J.J. and Johnson, R.P., Local buckling
    in continuous composite beams, The structural
    Engineer, 50, Sept. 1972, pp.367-374.

4. Johnson, R.P. and Bradford, M.A., Distortional
    lateral buckling of unstiffened composite bridge
    girders, Proc. Conf. Instability and Plastic
    Collapse of Steel Structures, ed. L.J. Morris,
    Granada, 1983, pp.569-580.

5. Bradford, M.A. and Johnson, R.P., Inelastic buckling
    of composite bridge girders near internal supports,
    Proc. Instn. Civ. Engrs., Part 2, 83, March 1987,
    pp.143-159.

6. Weston, G. and Nethercot, D.A., Continuous composite
    bridge beams - stability of the steel compression
    flange in hogging bending, stability of Plate and
    Shell Structures, ed. P. Dubas and D. Vandepitte,
    European Convention for Constructional Steelwork,
    1987, pp.47-52.

7. Johnson, R.P. and Hope-Gill,M.C., Applicability of
    simple plastic theory to continuous composite beams,
    Proc. Instn. Civ. Engrs., Part 2, 61, March 1976,
    pp.127-143.

8. BS5400 : Steel, concrete and composite bridges -
    Part 3 : Design of steel bridges, 1982
    Part 4 : Design of concrete bridges, 1984
    Part 5 : Design of composite bridges, 1979
    British Standards Institution, London.

9. Background document for Chapter 5 of draft Eurocode
    3, the b/t ratios controlling the applicability of
    analysis models in Eurocode 3, Eurocode 3 editorial
    group, Commission of European Communities, April
    1989.

10. Bleich, F., Buckling strength of metal structures,
    Engineering societies monographs, McGraw Hill, 1952.

11. Bulson, P.S., Local stability and strength of structural section of thin-walled structures, ed. by Chilver A.H., Part II, Chapter 2, Chatto and Windus Ltd., 1967.

12. Allen, H.G. and Bulson, P.S., Background to buckling, McGraw Hill, London, 1980.

13. Van Dalen, K., Composite action at the supports of continuous beams, PhD thesis, University of Cambridge, 1967.

14. Climenhaga, J.J., Local buckling in composite beams, PhD thesis, University of Cambridge, 1970.

15. Hamada, S. and Longworth, J., Buckling of composite beams in negative bending, Journal of structural division, ASCE., Vol.100, No.ST11, 1974, pp.2205-2222.

16. Bradford, M.A., Local buckling analysis of composite beams, Trans. Instn. Engrs, Australia, 4, CE28, 1986, pp.312-317

17. Hope Gill M.C. and Johnson R.P., Tests on three three-span continuous composite beams, Proc. Instn. Civ. Engrs., Part 2, 61, 1976, pp.367-381.

18. Ansourian, P., Experiments on continuous composite
    beams, Proc. Instn. Civ. Engrs., Part 2, 73, 1982,
    pp.25-51.

19. Rotter, J.M. and Ansourian, P., Cross-section
    behaviour and ductility in composite beams, Proc.
    Instn. Civ. Engrs., Part 2, 67, June 1979, pp.453-
    474.

20. Ansourian, P., Plastic rotation of composite beams,
    Journal of Struct. Div., ASCE, Vol.108, No.ST3,
    March 1982, pp.643-659.

21. Ansourian, P., The behaviour and design of composite
    beams, Proc. of the ninth Australasian Conference on
    the Mechanics of Structures and Materials, Aug.1984,
    pp.220-225.

22. Kemp, A.R., Quantifying ductility in continuous
    composite beams, Proc. of the Engineering Foundation
    Conference on Composite Construction in Steel and
    Concrete, ASCE, ed. by C.D. Buckner and I.M. Viest,
    Henniker, New Hampshire, June 1987, pp.107-121.

23. Bode, H., and Uth, H., Plastic design of composite beams with special regard to negative moment regions, Proc. of Int. Conf. on Steel Structures (recent research advances and their application to design), Vol.2, ed. by N. Harding, Yugoslavia, Sept. 1986, pp.649-655.

24. Richtlinien für die Bemessung und Ausführung von Stahlverbundträgern, Ausgabe März 1981, Ergänzende Bestimmungen zu den Richtlinien, Fassung März 1984.

25. Eurocode 3, Common unified rules of practice for steel structure, 2nd draft, Commission of European Communities, 1989.

26. Smith, D.G.E., and Johnson, R.P., Commentary on the 1985 draft of Eurocode 4, Building Research Establishment Report, Watford, England, 1986.

27. Johnson, R.P., Continuous composite beams for buildings, Steel in Buildings, IABSE-ECCS Symposium Report, Luxembourg, 1985, pp.195-202.

28. Brett, P.R., Nethercot, D.A. and Owens, G.W., Continuous construction in steel for roofs and composite floors, The Struct. Engr., Vol. 65A, No.10, Oct. 1987, pp.355-368.

29. Discussion on the paper 'Continuous construction in steel for roofs and composite floors' by Brett, P.R., Nethercot, D.A. and Owens, G.W., The Struct. Engr., Vol.66, No.14, July 1988, pp.216-227.

30. Kemp, A.R., Comparison between Eurocodes 3 and 4 of classification for local buckling of Class 1 and 2 sections, Technical paper J91, Editorial panel for Eurocode 4, Sept. 1989. (unpublished)

31. Barnard, P.R. and Johnson, R.P., Plastic behaviour of continuous composite beams, Proc. Instn. Civ. Engrs., Vol. 32, Oct. 1965, pp.180-197.

32. Barnard, P.R. and Johnson, R.P., Ultimate strength of composite beams, Proc. Instn. Civ. Engrs., Vol.32, Oct. 1965, pp.161-179.

33. Barnard, P.R., On the collapse of composite beams, PhD thesis, University of Cambridge, 1963.

34. Yam, L.C.P. and Chapman, J.C., The inelastic behaviour of simply-supported composite beams, Proc. Instn. Civ. Engrs., Vol.41, Dec. 1968, pp.651-683.

35. Hope-Gill, M.C., The ultimate strength of continuous composite beams, PhD thesis, University of Cambridge, 1974.

36. Hope-Gill, M.C., Redistribution in composite beams, The Struct. Engr., Vol.57B, No.1, March 1979, pp.7-10.

37. Johnson, R.P. and Fan, C.K.R., Strength of continuous composite beams designed to Eurocode 4, Proc. IABSE, May 1988, pp.33-44.

38. Kirby, P.A. and Nethercot, D.A., Design for structural stability, CONSTRADO Monograph, Granada, 1979.

39. Nethercot, D.A. and Rockey, K.C., A unified approach to the elastic lateral buckling of beams, The Struct. Engr., No.7, Vol.49, July 1971, pp.321-330.

40. Clark, J.W. and Hill, H.N., Lateral buckling of beams, Journal of Struct. Div., ASCE, Vol.86, No.ST7, July 1960, pp.175-195.

41. Nethercot, D.A. and Rockey, K.C., Lateral buckling of beams with mixed end conditions, The Struct. Engr., No.4, Vol.51, April 1973, pp.133-138.

42. Lay, M.G. and Galambos, T.V., Inelastic beams under moment gradient, Journal of the Struct. Div., ASCE, Vol. 93, ST1, Feb. 1967, pp.381-399.

43. Nethercot, D.A., Inelastic buckling of steel beams under non-uniform moment, The Struct. Engr., Vol.53, No.2, Feb. 1975, pp.73-78.

44. Nethercot, D.A. and Trahair, N.S., Inelastic lateral buckling of determinate beams, Journal of the Struct. Div., ASCE, Vol.102, No.ST4, April 1976, pp.701-717.

45. Kitipornchai, S. and Trahair, N.S., Buckling of inelastic I-beams under moment gradient, Journal of the Struct. Div., ASCE, Vol.101, No.ST5, May 1975, pp.991-1004.

46. Kitipornchai, S. and Trahair, N.S., Inelastic buckling of simply supported steel I-beams, Journal of the Struct. Div., ASCE, Vol.101, No. ST7, July 1975, pp.1333-1347.

47. Salvadori, M.G., Lateral buckling of beams of rectangular cross-section under bending and shear, Proc. 1st U.S. Nat. Congr. of Applied Mechanics, 1951, p.403.

48. Trahair, N.S., Elastic stability of continuous beams, Journal of the Struct. Div., ASCE, Vol.95, No.ST5, June 1969, pp.1295-1312.

49. Nethercot, D.A. and Trahair, N.S., Lateral buckling
    approximations for elastic beams, The Struct. Engr.,
    No.6, Vol.54, June 1976, pp.197-204.

50. Poowannachaikul, T. and Trahair, N.S., Inelastic
    buckling of continuous I-beams, Civil Eng.
    Transactions, the Instn. of Engrs., Australia, Vol.
    CE18, Part 2, 1976, pp.134-139.

51. Singh, K.P., Ultimate behaviour of laterally
    supported beams, PhD thesis, University of
    Manchester, Oct. 1969.

52. Lawson, R.M. and Nethercot, D.A., Lateral stability
    of I-beams restrained by profiled sheeting, The
    Struct. Engr., Vol. 63B, No.1, March 1985, pp.1-8.

53. Horne, M.R., Shakir-Khalil, H. and Akhtar, S., The
    stability of tapered and haunched beams, Proc.
    Instn. Civ. Engrs., Part 2, 67, Sept. 1979, pp.677-
    694.

54. Nethercot, D.A. and Trahair, N.S., Design of
    diaphragm braced I-beams, Journal of Struct. Div.,
    ASCE, 101, No.ST10, Oct. 1975, pp.2045-2061.

55. Nakamura, T., Strength and deformability of H-shaped steel beams and lateral bracing requirements, Journal Construct. Steel Research, 9, 1988, pp.217-228.

56. Timoshenko, S.P. and Gere, J.M., Theory of elastic stability, 3rd edition, McGraw Hill, New York, 1970.

57. Bradford, M.A., Buckling of beams with flexible cross-sections, PhD thesis, University of Sydney, May 1983.

58. Nylander, H., Drehungsvorgange und gebundene Kippung bei geraden, doppeltsymetrischen I-Tragern, Ingeniors Vetenskaps Akoctemien Handlinger, 174, Stockholm, 1943.

59. Zienkiewicz, O.C., The finite method in engineering science, McGraw Mill, London, 1971.

60. Cheung, Y.K., Finite strip method in structural analysis, Pergamon Press Inc., Oxford, 1976.

61. Rajasekaran, S. and Murray, D.W., Coupled local buckling in wide-flange beam-columns, Journal of Struct. Div., ASCE, Vol.99, No.ST6, June 1973, pp.1003-1023.

62. Johnson, C.P. and Will, K.M., Beam buckling by finite element procedure, Journal of Struct. Div., ASCE, Vol.100, No.St3, March 1974, pp.669-685.

63. Akay, H.U., Johnson, C.P. and Will, K.M., Lateral and local buckling of beams and frames, Journal of Struct. Div., ASCE, Vol.103, No.ST9, Sept. 1977, pp.1821-1832.

64. Hancock, G.J., Local, distortional and lateral buckling of I-beams, Journal of Struct. Div., ASCE, Vol.104, No.ST11, Nov. 1978, pp.1787-1798.

65. Plank, R.J. and Wittrick, W.H., Buckling under combined loading of thin flat-walled structures by a complex finite strip method, International journal for Numerical Methods in Engineering, Vol.8, 1974, pp.323-339.

66. Hancock, G.J., Bradford, M.A. and Trahair, N.S., Web distortion and flexural-torsional buckling, Journal of Struct. Div., ASCE, Vol.106, No.St7, July 1980, pp.1557-1571.

67. Bradford, M.A. and Trahair, N.S., Distortional buckling of I-beams, Journal of Struct. Div., ASCE, Vol. 107, No.ST2, 1981, pp.355-370.

68. Bradford, M.A. and Trahair, N.S., Distortional
     buckling of thin-web beams columns, Engineering
     Structures, Vol. 4, No.1, 1982, pp.2-10.

69. Wang, S.T. and Yeh, S.S., Post-local-buckling
     behaviour of continuous beams, Journal of Struct.
     Div., ASCE, Vol. 100, No.ST6, 1974, pp.1169-1187.

70. Wang, S.T. and Jaa, S.T., Stiffness analysis of
     locally buckled thin-walled continuous beams,
     International Journal Computers and Structures,
     Vol. 5, No.1, 1975, pp.81-93.

71. Wang, S.T. and Wright, R.S., Torsional-flexural
     buckling of locally buckled beams and columns, Proc.
     of the International Colloquium on Stability of
     Structures under Static and Dynamic Loads,
     Structural Stability Research Council/ASCE, May
     1977, pp.587-608.

72. Wang, S.T., Yost, M.L. and Tien, Y.L., Lateral
     buckling of locally buckled beams using finite
     element techniques, International Journal Computers
     and Structures, Vol.7, No.7, 1977, pp.469-475.

73. Coric, B. and Roberts, T.M., Influence of cross-
    section distortion on the behaviour of slender plate
    girders, Proc. Conf. on Instability and Plastic
    Collapse of Steel Structures, Granada, London, 1983.

74. Dowling, P.J., Mears, T.F., Owens, G.W. and Raven
    G.K., A development in the automated design and
    fabrication of portal framed industrial buildings,
    The Structural Engr., Vol.60A, No.10, Oct. 1982,
    pp.311-319

75. Bradford, M.A., Inelastic distortional buckling of
    I-beams, Journal Computers and Structures, Vol.24,
    No.6, 1986, pp.923-933.

76. Dowling, P.J., Owens, G.W. and Chung, K.F.,
    Stability of tapered frames, Structural Stability
    Research Council, Proc. Annual Technical Session,
    1985, pp.379-395.

77. Weston, G., Lateral buckling in diaphragm-braced
    beams and continuous composite bridge girders, PhD
    thesis, Dept. of Civil and Struct. Engineering,
    University of Sheffield, 1987.

78. Horne, M.R. and Ajmani, J.L., Design of columns
    restrained by side-rails, The Struct. Engr., No.8,
    Vol. 49, Aug. 1971, pp.339-345.

79. Johnson, R.P. and Buckby, R.J., Composite structures of steel and concrete, Vol.2 : Bridges, 2nd edition, Collins, London, 1986.

80. Chatterjee, S., New features in the design of beams, Proc. Symposium on BS5400 : Part 3, the Institution of Structural Engineers, Jan. 1980.

81. Kapur, K.K. and Hartz, B.J., Stability of plates using the finite element method, Journal of the Engineering Mechanics Division, ASCE, Vol.92, No.EM2, April 1966, pp.177-195.

82. Crisfield, M.A., Large-deflection elasto-plastic buckling analysis of plates using finite elements, Report LR593, TRRL, 1973.

83. Crisfield, M.A., Large-deflection elasto-plastic buckling analysis of eccentrically stiffened plates using finite elements, Report 725, TRRL, 1976.

84. Dept. of the environment, Inquiry into the basis of design and method of erection of steel box girder bridges, Report of the Committee - Appendix 1, Interim design and workmanship rules, Parts 1 to 4, H.M. Stationery Office, 1973.

85. Crisfield, M.A., Ivanov's yield criterion for thin plates and shells using finite elements, Report 919, TRRL, 1979.

86. Svensson, S.E., Lateral buckling of beams analysed as elastically supported columns subject to a varying axial force, Journal Construction Steel Research, 5, 1985, pp.179-193.

87. Eurocode 3, Common unified rules of practice for steel structures, 1st draft, Commission of the European Communities, Nov. 1983.

88. William, F.H. and Jemah, A.K., Buckling curves for elastically supported columns with varying axial force to predict lateral buckling of beams, Journal Constr. Steel Res., 7(2), 1987, pp.133-147.

89. Wittrick, W.H. and Williams, F.W., Buckling and vibration of anisotropic or isotropic plate assemblies under combined loadings, Int. J. Mech. Sci., 16, 1974, pp.209-239.

90. Goltermann, P. and Svensson, S.E., Lateral distortional buckling : predicting elastic critical stress, Journal of Struct. Div., ASCE, Vol.114, No.7, July 1988, pp.1606-1625.

91. Hancock, G.J., Eigenvalue routines for structural
    buckling and vibration analysis on microcomputers,
    Proc. the Ninth Australasian Conference on the
    Mechanics of Structures and Materials, Sydney, 1984,
    pp.136-141.

92. Lawson, R.M. and Rackham, J.W., Design of haunched
    composite beams in buildings, Steel Construction
    Institute, Aug. 1989.

93. Editorial panel for Eurocode 4, Paper J98,
    Lateral-torsional buckling of composite beams for
    buildings, Nov. 1989. (unpublished)

94. Nakamura, T. and Wakabayashi, M., Lateral buckling
    of steel beams with reinforced concrete slab, Proc.
    Pacific Structural Steel Conference, Auckland, New
    Zealand, 1986, pp.395-406.

95. Law, C.L.C., Planar no-sway frames with semi-rigid
    beam-to-column joints, PhD thesis, University of
    Warwick, Oct. 1983.

96. Ralston, A. and Rabinowitz, P., A first course in
    numerical analysis, 2nd edition, McGraw Hill, New
    York, 1978.

97. Johnson, R.P., Shrinkage-induced curvature in composite beams with a cracked concrete flange, The Struct. Engineer, Vol.65B, No.4, Dec. 1987, pp.72-77.

98. ECCS -Technical Committee 8 - Structural stability, Ultimate limit state calculation of sway frames with rigid joints, Report No. 33, European Convention for Constructional Steelwork, Brussels, 1984.

99. Yam, L.C.P., Design of composite steel-concrete structures, Surrey University Press, London, 1981.

100. Willmington, R.T., Vertical shear in composite beams, PhD thesis, University of Cambridge, 1969.

101. Allison, R.W., et al, Tension-field action in composite plate girders, Proc. Instn. Civ. Engrs., Part 2, _73_, June 1982, pp.255-276.

102. Evans, H.R., et al, The collapse behaviour of plate girders subjected to shear and bending, Proceedings P-18/78, Periodica 4/1978, IABSE, 1978, pp.1-20.

103. Technical paper J69, Redistribution of moments at ultimate limit states in structures for buildings, Editorial panel for Eurocode 4, May 1989. (unpublished)

104. BS1881 : Part 108, Method of making test cubes from fresh concrete, British Standards Institution, 1983.

105. BS18, Tensile testing of metals (including aerospace materials), British Standards Institution, 1983.

106. BS4360, Weldable structural steels, British Standards Institution, 1986.

107. BS1881 : Part 116, Method for determination of compressive strength of concrete cubes, British Standards Institution, 1983.

108. Johnson, R.P., Limitations to the use of partial shear connection in composite beams, Research Report CE21, Dept. of Engineering, University of Warwick, August 1986.

109. Huber, A.W., Residual strain measurement, Fritz. Eng. Lab. Report No. 220A.17, Lehigh University, Bethlehem, Penn., March 1955.

110. Young B.W., Residual stresses in hot-rolled sections, Dept. of Engineering, Technical Report No. CUED/C-struct/TR.8(1971), University of Cambridge, 1971.

111. BS4 : Part 1, Structural steel sections -
     specification for hot-rolled sections, British
     Standards Institution, 1980.

112. Manual on stability of steel structures, 2nd
     edition, ECCS, June 1976, p.44.

113. Heins, C.P. and Kuo, J.T.C., Composite beams in
     torsion, Journal of Struct. Div., ASCE, Vol. 98,
     No.ST5, May 1972, pp.1105-1117.

114. Thompson, J.M.T. and Hunt, G.W., A general theory of
     elastic stability, Wiley, London, 1973.

115. Young, B.W., Residual stresses in hot-rolled
     members, Proc. Int. Colloq. Column Strength, IABSE,
     Zurich, 1972, pp.25-38.

116. Trahair, N.S., Lateral buckling design of steel
     beam, Proc. the Ninth Australasian Conference on
     the Mechanics of Structures and Materials, Sydney,
     August 1984, P. 6.

117. Lay, M.G., Flange local buckling in wide-flange
     shapes, Journal of Struct. Div., ASCE, Vol. 91, No.
     ST6, Dec. 1965, pp. 95-116.

APPENDICES

IABSE PROCEEDINGS P-125/88

MÉMOIRES AIPC
IVBH ABHANDLUNGEN

*Strength of Continuous
Composite Beams
Designed to Eurocode 4
R. P. Johnson, C. K. R. Fan*

Strength of Continuous Composite Beams Designed to Eurocode 4

Résistance des poutres mixtes acier-béton continues,
calculée selon l'Eurocode 4

Tragfähigkeit von durchlaufenden Stahl-Beton-Verbundträgern,
berechnet nach Eurocode 4

Roger Paul JOHNSON
Prof. of Civil Engineering
University of Warwick
Coventry, UK

R.P. Johnson was educated at Cambridge University. After six years in industry he began research on composite structures in 1959. He is a member of IABSE Working Commission 2, and of the Editorial Group for Eurocode 4 on Composite Structures.

C.K. Roger FAN
Research Student
University of Warwick
Coventry, UK

C. K. R. Fan graduated from City University (London) in 1982. After gaining three years' experience in the construction industry, he went to Imperial College, London, for postgraduate study and was awarded an M.Sc. in structural steel design in 1986.

SUMMARY
The 1985 draft of Eurocode 4 gave a new method for the design of continuous composite beams with semi-compact (Class 3) sections at internal supports, that allows limited redistribution of moments. The validity of this method is examined for ultimate and serviceability limit states, by means of a parametric study based on test data on the post-local-buckling behaviour of cantilevers. It is concluded that the method is safe and economical for beams of uniform section, used in buildings.

RÉSUMÉ
Le projet 1985 de l'Eurocode 4 présente une nouvelle méthode pour le calcul des poutres mixtes continues à section semi-compacte (classe 3), autorisant une redistribution limitée des moments sur appuis intermédiaires. La validité de la méthode est examinée aux états limites de service et de ruine, au moyen d'une étude paramétrique basée sur les résultats d'essais relatifs au comportement postcritique de poutres-console. Il est montré que la méthode est sûre et économique pour des poutres de section constante utilisées dans le bâtiment.

ZUSAMMENFASSUNG
Der Entwurf 1985 des Eurocodes 4 schlägt eine neue Methode für die Berechnung durchlaufender Verbundträger mit halb-kompaktem Querschnitt (Klasse 3) über den Zwischenauflager vor, welche eine begrenzte Momentenumlagerung zulässt. Der Gültigkeitsbereich dieser Methode wird für die Grenzzustände der Tragsicherheit und der Gebrauchstauglichkeit geprüft, und zwar durch eine Parameterstudie basierend auf Versuchsresultaten von Kragarmträgern mit überkritischem Beulverhalten. Es wird gezeigt, dass die Methode für Träger des Hochbaus mit konstantem Querschnitt sicher und wirtschaftlich sind.

1.   INTRODUCTION

For the longer spans of continuous composite beams in buildings, it is common to use rolled or built-up steel I- or H-sections that are semi-compact at internal supports. These are sections that can reach the yield moment in hogging bending, M'_y, but lose strength due to local buckling before much plasticity or local rotation can develop.

In design to draft Eurocode 4 [1] these beams are in Class 3 and have web and compression flange slenderness that lie within the limits shown in Figure 5. Design methods for Class 3 steel beams at the ultimate limit state require elastic analyses of the structure and of the Class 3 cross sections. This is over-restrictive for composite beams, which are usually in Class 1 or 2 at midspan, because M'_y is much less than the plastic resistance at midspan, M_p, whereas elastic global analysis gives support moments that exceed the midspan moments.

The less conservative of the two design methods for Class 3 beams given in clause 4.4.3.2 of the draft EC4 (Appendix D) therefore allows up to 20 per cent redistribution of hogging moments determined by elastic analysis, in the belief that local buckling, if it occurs, can be relied on to shed at least this amount of bending moment before collapse occurs. The midspan regions are required to remain elastic (which is rarely a constraint in practice), because any inelastic curvature would increase the demand on the limited rotation capacity available near the internal supports.

The objective of the work reported here was to check on the safety of this method, using the limited test data on the post-local-buckling behaviour of cantilevers with sections in Class 3. It was assumed that complete shear connection was provided, and that lateral buckling did not occur. The 43 beams studied were each of uniform section, and ten cross-sections were used. The results are believed to be applicable to beams that have composite floor slabs and/or lightweight-aggregate concrete, as well as to conventional T- and L-beams.

The disparity between the design moments given by elastic global analysis and design resistances of sections is normally greater in a two-span beam than in those continuous over three or more spans. The various patterns of imposed loading lead to the provision of more surplus strength in multi-span beams, and they have a higher degree of redundancy. Two-span beams benefit most from the exploitation of inelastic behaviour, so only they have been studied. The spans ranged from 6m to 20m, and the ratios of the two span lengths from 0.6 to 1.0. Loading was taken as uniformly-distributed over each span, but allowance was made for different intensities on the two spans.

There has been much research related to the design of continuous composite beams of compact section (Class 1 or 2), and a little on slender (Class 4) cross-sections [2]. Very little work has been done on Class 3 beams [3,4,5], probably because the complex interaction of flange and web local buckling affects the rotation capacity in hogging bending, and this effect is difficult to assess analytically. Climenhaga and Johnson [5] found from double-cantilever tests that specimens with Class 3 cross sections have a distinct type of behaviour. Rotation due to local buckling occurs only near the support, and the buckling extends over a length roughly equal to the depth of the steel section. Due to this localised feature, the moment-rotation behaviour of hogging moment regions of a continuous beam can be predicted from the results of double-cantilever tests.
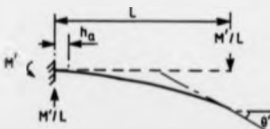
Fig. 1 M' - θ' relationship for a cantilever

2.   OUTLINE OF THE METHOD OF ANALYSIS

(1) From tests on composite or steel cantilevers with point loads M'/L (Figure 1), curves are available (e.g., Figure 2) that relate the end slope θ' to the hogging bending moment at the support, M'.

It is assumed that θ' is the sum of an elastic rotation ($M'\theta'_e/M'_y$ in Figure

2], that can be found by integrating curvatures along the member, and an irreversible rotation θ'_1 that occurs only in a region of length b_o adjacent to the support, where b_o is the overall depth of the steel member. The rotation θ'_1, due mainly to local buckling of the steel compression flange and/or web, is assumed to be the function of M'/M'_y and θ'_{bc} shown in Figure 2, and to occur at distance $b_o/2$ from the support.

(2) For a uniform composite or steel cantilever of any given length and cross section, the curve NP and values of M'_y, θ'_c, and θ'_{bc} are predicted, using realistic stress-strain curves for the materials and allowing for residual stresses in the steel section. The shape assumed for the falling branch, PQR in Figure 2, gives a close but conservative fit to the falling branches observed in the five tests studied. Details of these procedures are given in Appendix A.
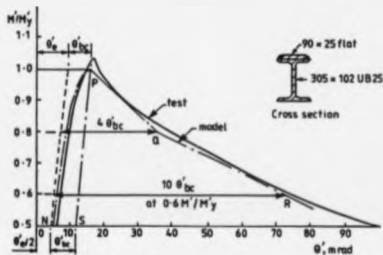
Fig. 2 Moment-rotation model compared with result of test on specimen SB4 [5] for a cantilever

(3) At an internal support of a continuous beam, the member is either stiffened, or interrupted by a column. There will be less redistribution of moments to midspan regions when local buckling occurs on one side only of the support, rather than on both sides. After M'_y has been reached at an internal support, the irreversible rotation is therefore assumed to remain constant (line PS in Figure 2) on the side with the steeper moment gradient, and to follow lines PQR on the other side.

Unlike a cantilever, a two-span continuous beam on point supports can rotate at the internal support, and the length of the hogging moment region reduces as redistribution of moments occurs. The rotation θ'_{bc} then has to be calculated in a different way, explained below and in Appendix C; so for continuous beams the symbol θ'_{bc} is replaced by θ'_b.

First, realistic spans L_1 and L_2 (with $L_2 \geq L_1$) and appropriate cross sections are chosen. The 'uncracked unreinforced' section for the beam is uniform over the whole length. The 'cracked reinforced' section is uniform over the hogging moment region, where the steel section is in Class 3 (semi-compact) as defined in draft Eurocode 4. All midspan sections are in Class 1 or Class 2.
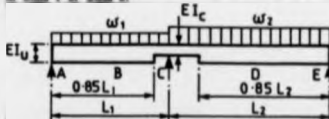
Fig. 3 Loading condition and flexural stiffness of a two-span beam

(4) The design ultimate loads, w_1 and w_2, are uniformly distributed, as shown in Figure 3. They are the maximum loads per unit length for which the beam could have been designed in accordance with the method of Appendix D.

The calculation of w_1 and w_2 is explained in Appendix B.

For span 1, the distributed characteristic dead and imposed loads per unit length are g_1 and q_1. It is assumed that w_1 can have any value between $1.0g_1$ and $1.35g_1 + 1.5q_1$, so the factors γ_F in the Eurocodes are expected to give a similar or lower range of loads. The range for span 2 is similar; g_2 is taken as equal to g_1, but q_2 may differ from q_1.

The designs are usually governed by the bending moments at first yield at cross-sections C (because a Class 3 section) and D (because the method excludes inelastic behaviour in midspan regions).

(5) The beam is now assumed to be subjected to loads λw_1 and λw_2, where λ increases gradually. Using analytical models based on research, and without reference to Eurocode 4, two values of λ are calculated (Appendix C):

    (i) λ_b, at which the bending moment at support C reaches M'_y, and at which local buckling is assumed to occur; and

    (ii) λ_f, at which "failure" (defined in Appendix C) occurs.

(6) The design method is assumed to be satisfactory, for the beam considered, if

    (i) λ_b is high enough for local buckling not to occur at serviceability load levels, and

    (ii) λ_f exceeds 1.0.

Fig. 4   Typical cross-section

Key: × SB series; + TB series
$\varepsilon = (235/\sigma_y)^{1/2}$

Fig. 5   Limiting slendernesses for cross-section to Eurocode 4

3.   CHOICE OF MEMBERS FOR STUDY

3.1 Cross sections

The notation for properties of cross sections is shown in Figure 4. For all sections, $y_1 = 30$mm and $y_2 = b_c = 30$mm. Rolled sections are replaced by three equivalent rectangles. The depth of web in compression, αd, was calculated (following draft Eurocode 4) using the elastic neutral axis. This method is under review; so is the specified maximum web slenderness for a Class 3 section ($\alpha d/w < 33\varepsilon$, where $\varepsilon = (235/\sigma_y)^{1/2}$, σ_y in N/mm² units) used here. The upper limit for a Class 3 web depends on the shear stress, but is unlikely to exceed 60ε. The current limits for webs and for compression flanges of rolled sections are shown in Figure 5. The practical range of Class 3 sections is given by the smaller area ABCDE.

The sections studied here (Tables 1 and 2) are two of the SB series tested by Climenhaga [5] and five (TB series) chosen to include the most slender hot-rolled beam sections that typically have Class 3 webs.

Section	b_o	t	w	d	b_o/t	od/w	σ_y	b_c	h_c	A_r	$10^{-6}I_c$	$10^{-6}I_u$
	mm	mm	mm	mm			N/mm²	mm	mm	mm²	mm⁴	mm⁴
SB4	103.5	7.34	6.0	298.5	14.1	34.5	386	1000	120	1200	91	196
SB5	127.5	8.56	6.0	334.3	14.9	39.8	343	1500	120	1836	155	309
SB6	141.2	8.43	6.2	385.8	16.7	42.7	340	1500	120	1818	214	423
SB10	103.5	7.34	6.0	298.5	14.1	33.0	386	1000	120	960	85	196
SB11	127.5	8.56	6.0	334.1	14.9	35.1	343	1500	120	954	127	308

Table 1 Properties of cross-sections SB

Section	b_o	t	w	d	b_o/t	od/w	σ_y	b_c	h_c	A_r	$10^{-6}I_c$	$10^{-6}I_u$
	mm	mm	mm	mm			N/mm²	mm	mm	mm²	mm⁴	mm⁴
TB1	171.0	9.7	6.9	332.6	17.6	44.9	355	2500	150	516	336	516
TB2	141.8	8.6	6.3	380.1	16.5	43.2	355	2500	120	2250	226	454
TB3	146.1	8.6	6.1	234.3	17.0	32.4	355	2500	120	3000	105	206
TB4	350.0	15.0	10.0	650.0	23.3	40.0	355	2500	150	3750	1927	3669
TB5	315.0	15.0	10.0	500.0	21.0	29.6	355	2500	120	2400	950	1900

Table 2 Properties of cross-sections TB

3.2 Spans

Most continuous two-span Class 3 beams for buildings and footbridges have ratios of longer span to overall depth between 20 and 30, and spans between 6m and 20m. These ranges are explored in the 43 beams analysed, in which the ratios L_1/L_2 of shorter to longer span range from 0.6 to 1.0.

3.3 Materials

For the SB series, the yield stresses of the structural steel (Table 1) are based on the measured values for the relevant cantilever [5]. For the TB series, $\sigma_y = 355$ N/mm². For both series, f_y for reinforcement is 425 N/mm² and f_{cu} for the normal-density concrete is 30 N/mm². Details of the stress-strain curves and assumed residual stresses are given in Figures A1 and A2 (Appendix A).

Beam	L_1	L_2	Comp. M'_y	Obs. M'_m	Comp. θ'_b	Obs. θ'_{bc}	Comp. V/V_{pl}	Obs. V/V_{pl}
	m	m	kNm	kNm	mrad	mrad		
SB42	10.0	12.5	163.9	166.9	8.5	7.0	0.22	0.21
SB52	10.0	12.5	215.0	218.1	6.7	7.0	0.29	0.28
SB62	10.0	12.5	260.0	291.5	5.9	6.0	0.29	0.31
SB101	10.0	10.0	158.8	174.0	7.8	8.0	0.28	0.33
SB111	10.0	10.0	198.1	212.1	6.4	8.0	0.35	0.40

Table 3 Comparison between observed and computed results

Beam	L_1	L_2	Dead Load	w_1	w_2	λ_b	λ_f
	m	m	kN/m	kN/m	kN/m		
SB51	10.0	10.0	4.57	17.47	26.85	0.84	1.255
TB13	10.0	10.0	9.28	21.01	40.46	0.98	1.334
TB41	15.0	15.0	10.16	74.03	94.46	0.79	1.136
TB31	12.5	12.5	9.19	73.03	91.28	0.80	1.123

Table 4 Results for unpropped construction

4. RESULTS OF PARAMETRIC STUDY

4.1 Comparisons between cantilevers and two-span beams

Computed results M'_y, θ'_b, and maximum vertical shear V for five of the SB series of two-span beams are compared in Table 3 with the observed results from the tests on double cantilevers with the same cross sections and properties of materials. Propped construction was assumed.

The ratios V/V_{pl}, where $V_{pl} = \sigma_y dw/\sqrt{3}$, show that the effects of shear on flexural behaviour were negligible. The close agreement between θ'_b and θ'_{bc} shows that differences between their

methods of computation had negligible effect. At $V/V_{pl} = 0.2$ the computed value is slightly higher; at $V/V_{pl} = 0.3$ it agrees closely; at $V/V_{pl} = 0.4$ it is lower than the observed value, and so gives a more conservative model of the falling branch of the $M'-\theta'$ curve as V/V_{pl} increases. The observed maximum moments exceeded M'_y by between 1 and 12 per cent, so providing for most beams a further margin of safety.

4.2 Effect of unpropped construction

The four beams with two equal spans that gave the lowest values of λ_f (1.14, 1.07, 1.10, and 1.09) were also analysed using unpropped construction, with the results given in Table 4.

5. ANALYSIS AND DISCUSSION OF RESULTS FOR BEAMS

5.1 Load factors λ_b and λ_f

The load factor λ_b at the onset of local buckling was between 0.77 and 0.79 for all 43 beams with propped construction. This shows that local buckling does not occur until well above the design serviceability loads; and that, as expected, the attainment of the design ultimate loads relies on there being sufficient post–buckling rotation to shed at least 20 per cent of the peak hogging bending moment into the adjacent midspan regions. The results also show that the load factor at failure, λ_f, is in general higher for the stockier cross–sections of the SB series (range 1.13 to 1.24, with mean value 1.16), than for the TB series (range 1.05 to 1.20 with mean value 1.10). No beam could be found with λ_f < 1.05.

5.2 Residual Stresses

Rotter has reported [6] that residual stresses in rolled sections tend to increase curvatures at intermediate load levels by up to 25 per cent; but comparison of results of analyses with and without residual stresses showed that they cause only small decreases in λ_f. The largest reductions were 3.5 per cent for the SB series and 9 per cent for the TB series.

5.3 Span ratio

There was no obvious relationship between λ_f and the ratio between the two spans. This is probably because the design loads w_1 and w_2 are influenced in a complex way by span ratio, as well as having the expected reduction with increasing span. The total length $L_1 + L_2$ has negligible effect; similar values of λ_f were obtained for two beams in the TB series with total lengths of 16m and 35m. Span ratios below 0.6 have not been studied; but for these, beams of uniform section would rarely be used.

5.4 Unpropped construction

For a given beam and total load, unpropped construction gives higher stresses in steel and earlier local buckling as discussed by Yam [7]. The method of draft Eurocode 4 takes account of these higher stresses. They are allowed for here (Appendix B) in the calculation of w_1 and w_2, giving values (Table 4) which are lower than for propped construction. The computed buckling and failure loads are also lower (by 4 to 12 per cent and 2.6 to 10 per cent, respectively), but the values λ_b and λ_f, which are the ratios of these loads to w_1 and w_2, are slightly higher than for propped construction. The method of EC4 is thus slightly more conservative for unpropped than for propped construction.

5.5 Sensitivity of λ_f to the slopes of the falling branch

The values of θ'_b computed here are the inelastic rotations at the internal supports when the maximum moment reaches M'_y and the load factor is λ_b. Further increase of load level depends on the steepness of the falling branch of the $M'-\theta'$ curve. A separate study was made of the sensitivity of the results for λ_f to the shape of this falling branch (Figure 2). The effect of increasing the inelastic rotation at $0.6 \ M'_y$ from $10\theta'_b$ to $16\theta'_b$ was to increase λ_f by less than 5 per cent in all cases. The assumed $M'-\theta'$ curves are considered to be sufficiently conservative, in view of this insensitivity.

5.6 Combined bending and shear

For ultimate strength in combined bending and shear in Class 3 sections, draft Eurocode 4 refers to Eurocode 3. This is certainly too conservative for composite sections in hogging bending [2]. The method of BS 5400:Part 3 [8], based on tension-field theory, is more appropriate. For the beams in this study it shows that no reduction in M'_y need be made until V/V_{pl} exceeds 0.68. The highest ratio found in these beams, as designed for flexure to Eurocode 4, was 0.57.

5.7 Comments on the design method of draft Eurocode 4

In design practice, instead of calculating the load-carrying capacity of a beam with known cross-sections, the required cross-sections are chosen such that the extreme-fibre stresses in the steel do not exceed yield under various possible loading cases. Usually, the actual design loads are lower than the loads w_1 and w_2 used here, because in practice the ratio w_1/w_2 is known initially. Furthermore, is it possible for a class 3 cross-section to have a moment of resistance above M'_y.

These are further reasons why the present study is a more severe test of the design method than would be likely to occur in practice.

6. CONCLUSIONS

Forty-three two-span continuous composite beams with semi-compact sections at the internal support, and ten different cross sections, have been designed for flexural failure at the ultimate limit state by the less conservative of the two methods given in draft Eurocode 4. These designs corresponded to a load factor $\lambda_f = 1$. Spans ranged from 6m to 20m and span ratios from 0.6 to 1.0.

The ultimate strengths of these beams were determined by an inelastic method that takes account of the loss of strength in hogging bending caused by local buckling, determined from laboratory tests on five double cantilevers. The effects of residual stresses and unpropped construction were studied, and were found to have little influence on values of λ_f for the beams, which ranged from 1.03 to 1.33.

For both propped and unpropped construction, local buckling was found not to occur until well above service load levels. The 47 values of λ_b were all between 0.77 and 0.84, except for one value of 0.98, for one of the beams with the highest ratio of slab reinforcement ($A_s/b_c h_c = 0.02$).

This new method from draft Eurocode 4 was found to be both safe and economical for design for the ultimate limit state, and to reflect the real behaviour of two-span beams. For beams of more than two spans, it is believed to be slightly more conservative. The method provides an alternative to the over-conservative design of Class 3 beams that results from the exclusive use (in current practice) of elastic theory.

7. APPENDICES

A. Prediction of $M'-\phi'$ curves for 2B series of tests on cantilevers

The stress-strain curves used for concrete and reinforcement (Figure A1) were as given in Reference 8. The curve for structural steel (Figure A2(a)) is similar to that used in Reference 9, but modified to be more appropriate for the yield strengths given in Tables 1 and 2.

The cantilevers were similar in section to that shown in Figure 2, with a welded plate simulating the reinforcement and the cracked concrete slab. The residual stresses in the steel section were assumed to be as shown in Figure A2(b), with a compressive stress of $\sigma_r/2$ at the tips of the flanges. The effect of the welds was neglected, being remote from the region that buckled.

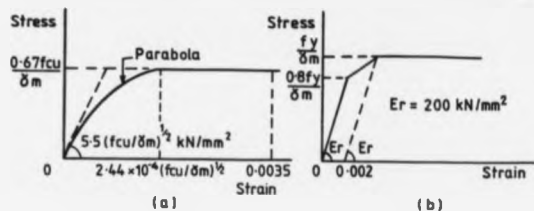The values M'_y and ϕ'_e (Figure 2) were found by conventional linear-elastic theory.

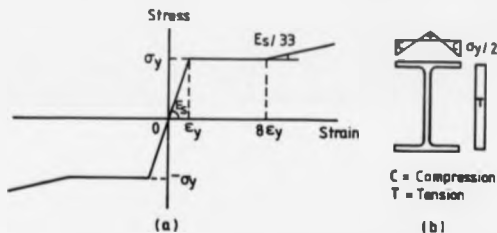Fig. A1 Stress–strain curves; (a) concrete; (b) reinforcement

Fig. A2 Structural steel material properties (a) stress–strain curve; (b) residual stress pattern

Thus,

$$P'_b = M'_y L/2E_s I_c$$

where L is the length of the cantilever, I_c is the second moment of area of the "cracked reinforced" composite section, and $E_s = 205$ kN/mm².

The curve NP (Figure 2) was computed from first principles, assuming plane sections remain plane. The rotation ϕ'_{bc} is that due to yielding caused by residual stresses and, for true composite sections, to the reduced stiffness of reinforcement at stresses exceeding $0.8 f_y/\gamma_m$ (Figure A.1(b)). No account was taken of tension stiffening.

Specimen No.	δ'_1/δ'_{bc} at:		Slenderness:	
	0.8 M'$_y$	0.6 M'$_y$	b_o/t	cd/u
SB4	4.8	13.2	14.1	34.9
SB5	3.8	11.5	14.9	39.8
SB6	3.7	11.7	16.7	42.7
SB10	4.0	11.1	14.1	33.0
SB11	5.7	14.3	14.9	35.1

Table A1 Observed rotation ratios

The resulting $M'-\delta'$ curves (NPQR in Figure 2) were checked by comparing the predicted inelastic rotation ratios δ'_1/δ'_{bc} (4.0 at 0.8M'$_y$ and 10.0 at 0.6M'$_y$) with the observed ratios (Table A1). The value 10 is always conservative (i.e., it underestimates the inelastic rotation) and the value 4 is a good approximation. The discrepancies indicate that there is no simple relationship between δ'_1/δ'_{bc} and the slenderness of the bottom flange or the web.

B. Calculation of design ultimate loads w_1 and w_2 in accordance with method (a) of clause 4.4.3.2 of draft Eurocode 4

The method specifies linear elastic analysis only, except that up to 20 per cent of the peak hogging moments may be redistributed to adjacent midspan regions. For a two-span beam, flexural stiffnesses are as in Figure 3, where I_2 and I_{11} relate to the cracked reinforced and uncracked composite sections respectively. The limiting bending resistances are M'$_y$ (hogging) and M$_y$ (sagging), and $L_2 > L_1$. For short-term loading, the modular ratio is taken as 7.5 in the calculation of M$_y$. Initially, propped construction is assumed.

Maximum loading on the right span is considered first. After redistribution, it is assumed to cause moments M'$_y$ at C and M$_y$ at D (Figure B1 curve 1). Equilibrium then gives the value of load w_2. Before redistribution, the bending moment at C is 1.25 M'$_y$ and the elastic curvatures along CDE are known (Figure B1 curve 2). The maximum loading on span AC, w_1, is then found from the condition that the curvatures along ABC are such that the deflection of point C relative to line AE is zero. It is then checked that M$_B < M_y$. Any higher loading on AC would increase M' at C. It is then checked that with the minimum possible loading on AC, and without redistribution, the moment at D is not excessive. Moment–shear interaction is discussed in Section 5.6.

For unpropped construction, the design dead load (1.35g, with g=g$_1$=g$_2$) is first applied to the steel member alone, acting elastically. The relevant extreme fibre stresses are then deducted from the yield stress σ_y, to obtain the allowable stresses in both hogging and sagging bending for the composite section. The imposed load 1.5q$_2$ is then found, as above, for span L$_2$, using composite section properties and equilibrium. The load 1.5q$_1$ for span L$_1$ is found by elastic analysis of the two-span composite member, as above for w_1.
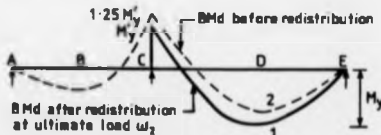

Fig. B1 Redistribution of support moment

C   Calculation of λ_b, θ'_b and λ_f for two-span beam

The geometry, materials, and loads w_1 and w_2 are known. The stress-strain curves and residual stresses are as in Appendix A, except that γ_m is taken as 1.5 for concrete in compression and 1.15 for reinforcement. Slip is neglected.

The method for λ_b is iterative, as follows.

(1) Guess λ (lower than the expected λ_b). The loads λw_1 and λw_2 are thus known.

(2) Guess the moment at support C, M'_c, so all moments are known.

(3) Compute all curvatures, and adjust M'_c until a compatible solution is found.

(4) Compare M'_c with M'_y, modify λ, and iterate until a solution is found with $M'_c = M'_y$.

This solution gives λ_b, and a distribution of moments and curvatures along the beam that includes the effects of cracking of concrete and some local yielding.

The irreversible components of these curvatures occur mainly near the internal support, where stresses in steel and reinforcement are much higher than elsewhere. They will now be represented by two concentrated rotations θ'_b at points $h_w/2$ on each side of support C, determined for load level λ_b, as follows.

The curvatures in sagging regions are unaltered, but in hogging regions a new set is found, neglecting residual stresses and assuming linear-elastic behaviour with stiffness $(E_s(I_c+I_w))$, where I_c is calculated taking E for concrete from the initial slope of the stress-strain curve in Figure A1, with $\gamma_m = 1.5$. The angle $2\theta'_b$ is given by the concentrated rotation at or near point C that makes these new curvatures compatible.

The load factor at failure, λ_f, is found by iterative calculations similar to those for λ_b, but allowing for local buckling in span CB and elastic unloading in the hogging region of span AC. As λ increases above λ_b, the initial guessed value for M'_c is reduced below M'_y, and two concentrated rotations are included in the compatibility checks. When the moment at C is M'_g, Figure C1, these rotations are TU in the non-buckling span and TV in the buckling span.
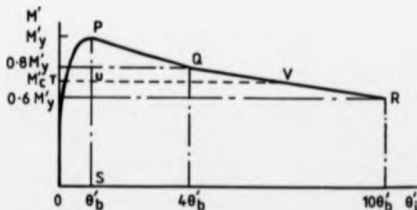

Fig. C1   Irreversible rotations

The failure load ($\lambda = \lambda_f$) is assumed to be reached when either

(i) M'_c drops below $0.6M'_y$.

(ii)   the maximum compressive strain in concrete reaches 0.0035,

(iii)   the maximum stress in structural steel reaches $1.3 \sigma_y$, or

(iv)   the iteration for a new load increment fails to converge.

D. Extract from clause 4.4.3.2 of draft Eurocode 4, related to design of beams with sections in Class 3

Method (a): Flexural stiffnesses are taken as the cracked values, as defined in 4.4.4.2, over 15% of the span on each side of an internal support, and as the uncracked values elsewhere. The resulting bending moment at each internal support (except those adjacent to cantilevers) may optionally be reduced by up to 20%, and corresponding increases made to the sagging bending moments elsewhere.

NOTATION

A_r total area of longitudinal reinforcement

b_c, h_c breadth and depth of concrete slab (Figure 4)

b_o, d, h_a, t, w dimensions of steel section (Figure 4)

f_{cu} characteristic cube strength of concrete

f_y nominal yield stress of reinforcement

I_c, I_u cracked and uncracked second moments of area of composite cross-section

M' hogging bending moment at an internal support

M'_m peak hogging moment in cantilever tests

M_p, M_y plastic and first yield sagging moments of resistance

M_y' first yield hogging moment of resistance

V, V_{pl} maximum shear force and shear capacity

w_1, w_2 design loads (Figure 3)

L_1, L_2 span lengths of a two-span beam (Figure 3)

αd depth of web in compression (elastic theory)

γ_m partial safety factor for a material

θ' total rotation at the end of a cantilever or at a point of contraflexure

θ'_b irreversible rotation of a quasi-cantilever in a continuous beam when $M' = M'_y$

θ'_{bc} irreversible rotation of a cantilever when $M' = M'_y$ (Figure 2)

θ'_e elastic rotation (Figure 2)

λ_b, λ_f buckling and failure load factors

σ_y nominal yield stress of structural steel

REFERENCES

1. EUROCODE No. 4, Common unified rules for composite steel and concrete structures, draft, Commission of the European Communities, 1985.

2. ALLISON R.W., et al, Tension-field action in composite plate girders, Proc.Instn.Civ.Engrs., Part 2, 73, 255-276, June 1982.

3. HOLTZ N.M. and KULAK G.L., Web slenderness limits of non-compact beams, Structural Engineering Report No. 51, Dept. of Civ. Engrg., University of Alberta, Aug. 1975.

4. NASH D.S. and KULAK G.L., Web slenderness limits for non-compact beam-columns, Structural Engineering Report No. 53, Dept. of Civ. Engrg., University of Alberta, Mar. 1976.

5. CLIMENHAGA J.J. and JOHNSON R.P., Local buckling in continuous composite beams, The Structural Engineer, Vol. 50, No. 9, 367-374, Sept. 1972.

6. ROTTER J.M. and ANSOURIAN P., Cross-section behaviour and ductility in composite beams, Proc.Instn.Civ.Engrs., Part 2, 67, 453-474, June 1979.

7. YAM L.C.P., Design of composite steel-concrete structures, Surrey University Press, London, 1981.

8. BS5400 : Steel, concrete and composite bridges - Part 3 : Design of steel bridges, 1982; Part 4 : Design of concrete bridges; 1984; British Standards Institution, London.

9. ECCS - Technical Committee 8 - Structural Stability, Ultimate limit state calculation of sway frames with rigid joints, Report No. 33, European Convention for Constructional Steelwork, Brussels, 1984.
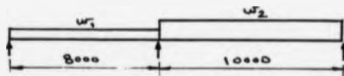
APPENDIX B

DESIGN EXAMPLES : TWO-SPAN CONTINUOUS COMPOSITE BEAMS

TRY 356 X 171 X 45 KG/M UB
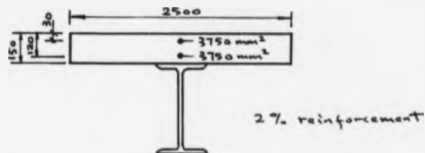
f_{cu} = 30/1.5 = 20N/mm^2
f_y = 355N/mm^2 (Grade 50, Fe 510)
f_r = 425/1.15 = 370N/mm^2
E_s = 205kN/mm^2
M_y = - 373.02 kNm (1st yield hogging)
M_y = 456.39 kNm (1st yield sagging)
M_p = 609.82 kNm (plastic sagging)
α = $\dfrac{(EI)\ cracked}{(EI)\ uncracked}$ = 0.65

(i)   UNEQUAL SPANS

Method (a)

For the given cross section, EC4 method (a) gives:

W_1 = 51.27 kN/m
W_2 = 50.33 kN/m

Loading combinations at ULS:

W max = $1.35Q_k + 1.5G_k$
W min = $1.0Q_k$
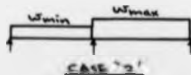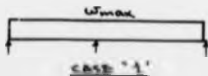
Based on the results of global analysis with W max = 50 kN/m, the corresponding bending moment diagrams are:
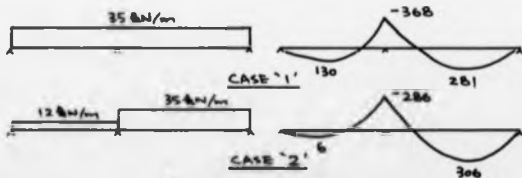

CASE '1'

CASE '2'
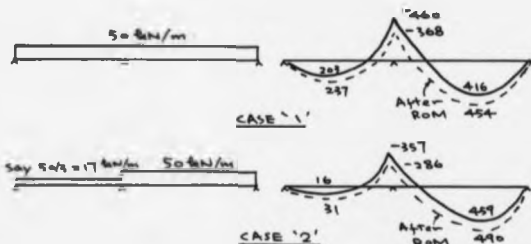
'CRACKED' ANALYSIS

Method (b)

For the given cross section, EC4 method (b) gives:

$W_1 = - 17.78$ kN/m (unrealistic)
$W_2 = + 62.82$ kN/m

Based on the results of global analysis with W max = 35 kN/m, the corresponding bending moment diagrams are:

CASE '1'

CASE '2'

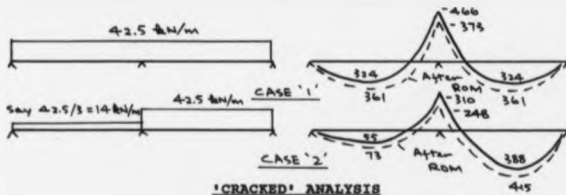'UNCRACKED' ANALYSIS

(ii)   EQUAL SPANS

Method (a)

For the given cross section, EC4 method (a) gives:

$$W_1 = 34.76 \text{ kN/m}$$
$$W_2^* = 50.33 \text{ kN/m}$$

Based on the results of global analysis with W max = 42.5 kN/m, the corresponding bending moment diagrams are:

'CRACKED' ANALYSIS

Method (b)

For the given cross section, EC4 method (b) gives:

$$W_1 = -3.14 \text{ kN/m} \quad \text{(unrealistic)}$$
$$W_2^* = +62.82 \text{ kN/m}$$

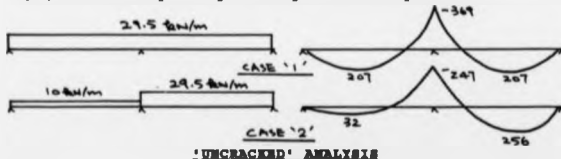Based on the results of global analysis with W max = 29.5 kN/m, the corresponding bending moment diagrams are:

'UNCRACKED' ANALYSIS

SUMMARY

	Two unequal spans beam		Two equal spans beams	
	Theoretical Max Load (kN/m)	Allowable Max. Factored Load (kN/m)	Theoretical Max. Load (kN/m)	Allowable Max. Factored Load (kN/m)
Method (a)	50.3	50.0	50.3	42.5
Method (b)	62.8	35.0	62.8	29.5

REMARK

For these particular examples, method (a) allows the beam to carry a loading 40% more than the value of method (b).

APPENDIX C

Classification of cross-section

Beam S1

(i)   DRAFT EUROCODE 4

Flange :

$\epsilon = (235/255)^{0.5} = 0.96$

Slenderness ratio, $b_o/t = 177.8/12.8$
$= 13.89$

$13.89/\epsilon = 14.47 \qquad 16$ (class 1 limit)

Therefore the flange is in Class 1.

Web:

$\epsilon = (235/270)^{0.5} = 0.933$

Distance between fillets, $b = 380.8 - 10.2 \times 2$
$= 360.4$

$\alpha b = 360.4/2 + 85.1 = 265.3$
$\alpha = 265.3/360.4 = 0.736$
$b/t = 360.4/7.8 = 46.2$

Class 2 web limit is expected to increase from
$33\epsilon/\alpha$ to $39\epsilon/\alpha$, the latter is therefore used here.

$39\epsilon/\alpha = 39 \times 0.933/0.736 = 49.44 < 46.2$

Therefore, the web is in class 2.

(ii)   DRAFT BS 5950: PART 3.1

Flange:

$\epsilon = (275/255)^{0.5} = 1.038$

$b/T = (177.8 \times 0.5)/12.8$
      $= 6.945$

Class 1 (plastic) limit $= 8.5\epsilon$
                        $= 8.5 \times 1.038$
                        $= 8.823 > 6.945$

Therefore, the flange is in class 1

Web:

According to Clause 3.13, refer to Fig. 2a for a
section with plastic or compact compression flange.

$\epsilon = (275/270)^{0.5} = 1.01$
$r = (Y_c - Y_t)/d$
  $= 85.1 \times 2/360.4$
  $= 0.472$
$d/t = 360.4/7.8 = 46.2$

Class 1 web limit $= 64\epsilon/(1 + 0.6r)$
                  $= 64 \times 1.01/(1 + 0.6 \times 0.472)$
                  $= 50.4 > 46.2$

Therefore, the web is in class 1.

(iii)   BS 5400: PART 3

According to Clause 9.3.7, calculations are
referred to the elastic neutral axis.

Flange:

$b_{fo} \not> t_{fo} \ (355/\sigma_{yf})^{0.5}$ compact criterion

$b_{fo} = (177.8 - 7.8)/2 = 10.2$
      $= 74.8$

$t_{fo} = 12.8$

$7 \times 12.8 \times (355/255)^{0.5} = 105.7 > 74.8$

Therefore, the flange is compact (Class 2)

Web:

$ab \not> 28 \, t_w \, (355/\sigma_{yw})^{0.5}$ compact criterion
$ab = 227 - 12.8 - 10.2$
     $= 204$

$t_w = 7.8$

$28 \times 7.8 \times (355/270)^{0.5} = 250.4 > 204$

Therefore, the web is compact (Class 2)

Beams U1, U2A and U2B

The variation in dimensions and properties between U1, U2A and U2B is small, and for simplicity the calculations of the slenderness ratios are based on the mean values of the three beams.

t_f (top flange)   = 7.85mm

t_w (web)   = 6.64mm

t_f (bottom flange) = 7.94mm

Overall depth D = 397.2mm

$f_{yf} = 396.9$ N/mm^2

$f_{fw} = 427.3$ N/mm^2

(i)   DRAFT EUROCODE 4
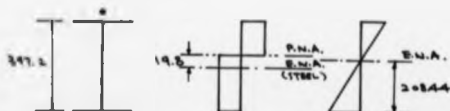
Flange:

$\epsilon = (235/396.9)^{0.5} = 0.77$

Slenderness ratio, bo/t = 140/7.94 = 17.63

$17.63/0.77 = 22.9 > 20$ but < 30

Therefore, the flange is in Class 3.

Web:

$\epsilon = (235/427.3)^{0.5} = 0.74$

Distance between fillets, b = 381.4 - 10.2 x 2
$\qquad = 361$

ab = 361/2 + 19.8 = 200.3
α = 200.3/361 = 0.555
b/t = 361/6.04 = 54.37

$39\epsilon/\alpha$ = 29 x 0.74/0.55
$\qquad$ = 52 < 54.37

Therefore, the web is in Class 3.

Remark: the web is close to the boundary
$\qquad$ between Class 2 and 3.

(ii) DRAFT BS 5950: PART 3.1

Flange:

$\epsilon = (275/396.9)^{0.5} = 0.832$

b/T = (140 x 0.5)/7.94
$\qquad = 8.816$

Class 2 (compact) limit = 9.5ϵ
$\qquad\qquad\qquad\qquad$ = 9.5 x 0.832
$\qquad\qquad\qquad\qquad$ = 7.904 < 8.816

Class 3 (semi-compact) limit = 15ϵ
$\qquad\qquad\qquad\qquad$ = 15 x 0.832
$\qquad\qquad\qquad\qquad$ = 12.48 > 8.816

Therefore, the flange is in Class 3.

Web:

According to Clause 3.13, refer to figure 2b for a
section with semi-compact compression flange.

$\epsilon = (275/427.3) = 0.802$
$r = (f_1 - f_2)/2 Py$
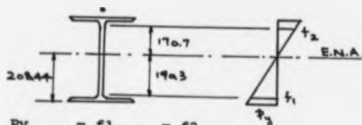
$$\frac{Py}{208.44} = \frac{f1}{190.3} = \frac{f2}{170.7}$$

or $f_1 = \frac{190.3}{208.44}$ Py

and $f_2 = \frac{170.7}{208.44}$ Py

$r = (190.3 - 170.7)/(208.44 \times 2)$

$= 0.047$

$d/t = 361/6.64 = 54.37$

Class 2 web limit $= 80\epsilon/(1 + r)$

$= 80 \times 0.802/(1 + 0.047)$

$= 61.28 > 54.37$

Therefore, the web is in Class 2.

(iii)   BS 5400: PART 3

Flange:

$b_{fo} \not> 7\ t_{fo}(355/\sigma_{yf})^{0.5}$ compact criterion

$b_{fo} = (140 - 6.64)/2 - 10.2$

$= 56.48$

$t_{fo} = 7.94$

$7 \times 7.94 \times (355/396.9)^{0.5} = 52.56 < 56.48$

Therefore, the flange is slender (Class 3).

Web:

$ab \not> 28\ tw\ (355/\sigma_{yw})^{0.5}$ compact criterion
$ab = 208.44 - 7.94 - 10.2$
$= 190.3$

$$t_w = 6.64$$

$$28 \times 6.64 \times (355/427.3)^{0.5} = 169.46 < 190.3$$

Therefore, the web is slender (Class 3).

BEAMS U3A AND U3B

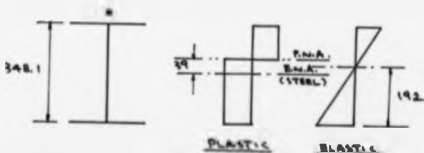Assume both beams have mean values as follows:-

t_f (bottom angle) = 7.65mm

b_o (bottom flange) = 124mm

t_w (web) = 6.6mm

Overall depth D = 348.1mm

$f_{yf} = f_{yw} = 437N/mm^2$ (U3A)

(i)   DRAFT EUROCODE 4

Flange:

$\epsilon = (235/437)^{0.5} = 0.733$

Slenderness ratio, $b_o/t = 124/7.65 = 16.21$

$16.21/\epsilon = 22.1 > 20$ (Class 2 limit)

Therefore, the flange is in Class 3.

Web:

$\epsilon = (235/437)^{0.5} = 0.733$

Distance between fillets, $b = 348.1 - 7.65 \times 2 - 10.2 \times 2$
$$= 312.4$$

$\alpha b = 312.4/2 + 39 = 195.2$

$\alpha = 195.2/312.4 = 0.625$

$b/t = 312.4/6.6 = 47.33$

Class 2 limit, $39\epsilon/\alpha = 39 \times 0.733/0.625 = 45.74 < 47.33$

Therefore, the web is also in Class 3.

(ii)   DRAFT BS 5950: PART 3.1

Flange:

$\epsilon = (275/437)^{0.5} = 0.793$

$b/T = (124 \times 0.5)/7.65$

$\quad = 8.1$

Class 2 limit $= 9.5\epsilon = 9.5 \times 0.793$

$\qquad\qquad = 7.53 < 8.1$

Class 3 limit $= 15\epsilon$

$\qquad\qquad = 15 \times 0.793$

$\qquad\qquad = 11.9 < 8.1$

Therefore, the flange is in Class 3 (non compact)

Web:

$Y_G = 174$

$d = 312.4$

$f_t = 138.4$

$r = (Y_G - Y_t)/d = (174 - 138.4)/312.4$

$\qquad\qquad = 0.114$
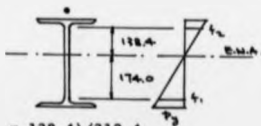
Class 2 web limit = $80\epsilon/(1 + r)$

$= 80 \times 0.793/(1 + 0.114)$

$= 56.95$

$d/t = 312.4/6.6 = 47.33 < 56.95$

Therefore, the web is in Class 2 (compact)

(iii)   BS 5400: PART 3

Flange:

Compact limit = $7 (355/f_{yf})^{0.5}$

$b_{fo}/t_{fo} = (124/2 - 6.6/2 - 10.2)/7.65$

$= 6.34$

$7 \times (355/437)^{0.5} = 6.31 < 6.34$

Therefore, the flange is in Class 3 (non compact), but just outside Class 2.

Web:

$ab \not> 28 \, t_w \, (355/f_{fw})^{0.5}$ compact criterion

$ab = 174$

$28 \times 6.6 \, (355/437)^{0.5} = 166.56 < 174$

Therefore, the web is in Class 3 (non compact)

APPENDIX D

4.6 LATERAL-TORSIONAL BUCKLING OF COMPOSITE BEAMS FOR BUILDINGS

4.6.1 General

(1) A steel flange that is attached to a concrete or composite slab by shear connection in accordance with Chapter 6 may be assumed to be laterally stable, provided that the overall width of the slab is not less than the depth of the steel member.

(2) All other steel flanges in compression shall be checked for lateral stability.

(3) When checking for lateral stability, the bending moment at any cross section shall be taken as the sum of the moment applied to the composite member and the moment applied to its structural steel component.

4.6.2 Check without direct calculation

(1) *A continuous beam or a beam in a frame that is composite throughout its length may be designed without additional lateral bracing when the following conditions are satisfied. [Note. Rules for cantilevers to be added].*

   (a) *The top flange of the steel member is attached to a reinforced concrete or composite slab by headed stud shear connectors in accordance with Chapter 6.*

   (b) *The longitudinal spacing of the studs or rows of studs, p_x, is such that*

$$\frac{p_x}{b} < \frac{f_u}{f_y} \left(\frac{d}{t}\right)^2$$

   where   d   is the diameter of the studs,
   b   and   t   are as shown in Fig. 4.7,
   f_u is the ultimate tensile strength of the studs,
   f_y is the yield strength of the steel member.

   (c) *The same slab is also attached to another steel member approximately parallel to the one considered, to form an inverted-U frame.*

   (d) *If the slab is composite, it spans between the two steel members of the inverted-U frame considered.*

   (e) *Whether the slab is simply-supported or continuous at the steel member considered, fully anchored top reinforcement, with a strength of at least half [?] that of the bottom reinforcement or steel sheeting required to resist bending at midspan of the slab, extends over the length AB shown in Fig. 4.7.*

   (f) *At each support of the steel member, its bottom flange is laterally restrained and its web is stiffened. Elsewhere, the web is unstiffened.*

   (g) *The bending stiffness of the slab is such that*

   $E_{cm} d_s \geq a E_a/210$ for a solid slab and
   $E_{cm} I_s \geq a E_a d_s^3/2520$ for a composite slab
   where E_{cm} and E_a are moduli of elasticity, given in Chapter 3,
   a   is the spacing of the steel members (Fig. 4.7),
   d_s is the mean of the effective depths of the slab for sagging and hogging bending in the direction normal to the span of the beam, and
   I_s is the second moment of area per unit width of the composite slab, assumed to be uncracked and unreinforced.

(h)   The steel member is an IPE section to Euronorm 19-57 or an HE section to Euronorm 53-62 or another hot-rolled section of similar shape.

(i)   If the steel member is partly encased in concrete in accordance with ... [7], its depth   h   does not exceed 1000 mm and its design yield strength does not exceed 360 N/mm².

(j)   If the steel member is not partly encased, its depth   h   is in accordance with Table 4.3.

Table 4.3   Maximum depth h (mm) of steel member for which clause 4.6.2. is applicable

Steel member	Design yield strength of structural steel not exceeding:	
	240 N/mm²	360 N/mm²
IPE or similar	no limitation	≤ 400
HE or similar	≤ 800	≤ 600

4.6.3   Buckling resistance moment

(1)   The buckling resistance moment of a laterally unrestrained beam shall be taken as

$$M_{b.Rd} = \beta_W X_{LT} M_{p\ell.Rd}$$

where

β_W =   1 for a Class 1 or Class 2 cross-section,

β_W = $M_{e.Rd}/M_{p\ell.Rd}$ for a Class 3 or Class 4 cross-section,

X_{LT} is the reduction factor for lateral-torsional buckling,

$M_{p\ell.Rd}$ is the plastic resistance moment given by 4.4.1.2 or 4.4.1.3,

$M_{e.Rd}$ is the elastic resistance to bending given by 4.4.1.4.

(2)   Values of x_{LT} for the appropriate slenderness $\bar{\lambda}_{LT}$ may be obtained from
       Table 5.7 in Eurocode 3, using:
            column a for rolled sections
            column c for welded beams,
       or may be determined from

$$x_{LT} = \left[\varphi_{LT} + (\varphi_{LT}^2 - \bar{\lambda}_{LT}^2)\right]^{-\frac{1}{2}}$$

       where

$$\varphi_{LT} = 0.5\left[1 + \alpha_{LT}(\bar{\lambda}_{LT} - 0.2) + \bar{\lambda}_{LT}^2\right]$$

       and $\alpha_{LT} = 0.21$ for rolled sections
              $\alpha_{LT} = 0.49$ for welded beams.

(3)   The value of $\bar{\lambda}_{LT}$ may be determined from

       $\bar{\lambda}_{LT} = (M_{p\ell}/M_{cr})^{\frac{1}{2}}$ for a Class 1 or Class 2 cross-section,

       $\bar{\lambda}_{LT} = (M_e/M_{cr})^{\frac{1}{2}}$ for a Class 3 or Class 4 cross-section,

       where

              $M_{p\ell}$ is the value of $M_{p\ell.Rd}$ when the γ_M factors γ_a, γ_c
                   and γ_s are taken as 1.0.
              M_e is the value of $M_{e.Rd}$ when the γ_M factors
                   γ_a, γ_c and γ_s are taken as 1.0.
              M_{cr} is the elastic critical moment for lateral-torsional
                   buckling.

(4)   A simplified method for the calculation of $\bar{\lambda}_{LT}$ and information for the
       calculation of M_{cr} are given in Annex B.

(5)   Where the slenderness $\bar{\lambda}_{LT} < 0.4$, no allowance for lateral-torsional buckling
       is necessary.

4.7   WEB CRIPPLING

4.7.1   General

(1)   The principles of clause 5.7 of EC3 are applicable to non-composite steel
       flanges of composite beams, and to the adjacent part of the web.

(2)   *The application rules of clause 5.7 of EC3 are applicable to non-composite
       steel flanges of composite beams and the adjacent part of the web.*

4.7.2   Effective web in Class 2

*As an internal support of a beam designed using an effective web in class 2
(in accordance with 4.3.3.2(2)), transverse stiffening should be provided unless
it can be shown that the unstiffened web has sufficient resistance to web
crippling.*

[Drafting note. This replaces a previous clause 4.7 on plate girders, which has
been incorporated into clause 4.4.2, "Vertical shear"]

4.8   COMPOSITE COLUMNS   [Please refer to a separate document]

Editorial Panel for Eurocode 4   Technical Paper J100

28th November 1989

Annex B - Lateral-torsional buckling

This first draft is based on papers R38, R46, J88, and the draft clause 4.6 in paper J98.   It will be extended to include cantilevers and asymmetrical steel I-sections.

ANNEX B.   LATERAL-TORSIONAL BUCKLING

B.1   CONTINUOUS INVERTED-U FRAME

B.1.1   Elastic critical moment

(1)   *This clause is applicable to a composite beam with continuity at one or both ends, that satisfies conditions (a) to (f) of 4.6.2(1).   The steel member should be a symmetrical rolled or welded I-section, uniform throughout the span considered.*

(2)   *The elastic critical hogging moment M_{cr} at an internal support may be taken as*

$$M_{cr} = k_c C_4 \sqrt{(k_w E_a I_{az})},$$

which is calculated using the following properties of the effective cross-section for hogging bending:

A *is the area of the equivalent composite section, as defined in 4.2.3(1), neglecting concrete in tension;*

I_y *is the second moment of area of the composite section of area A;*

A_a *and E_a are the area and elastic modulus of the structural steel section;*

I_{ay} *and I_{az} are second moments of area of the structural steel section about its centre of area;*

$i_x^2 = (I_{ay} + I_{az})/A_a;$

z_{ac} *is the distance between the centres of area of the steel member and the slab, which may be taken as*

$$z_{ac} = (h + h_s)/2;$$

$z_n = AI_{ay}/[A_a z_{ac}(A - A_a)];$

$$k_c = \cfrac{I_y}{I_{ay}\left[1 + \cfrac{h_f^2/4 + i_x^2}{h_f z_n}\right]} ;$$

and other symbols are defined in Fig. B.1.

- 1 -

(3) *For uncased and partially encased beams,*

$$k_w = E_a i_w{}^3/4h_f.$$

(4) *For beams partly encased in concrete in accordance with 4....,*

$$k_w = \frac{k_{wc}}{1 + k_{wc}/k_s}$$

where $k_s = E_{cm} \, d_s{}^3/5a$ *for internal beams*

$k_s = E_{cm} d_s{}^3/10a$ *for L-beams*

$$k_{wc} = \frac{E_a(t_w/h)b^3}{4[1 + 4v(t_w/b)]}$$

E_{cm} *is the elastic modulus for concrete, given in 3.1.4.1;*

d_s *is the mean of the effective depths of the slab for sagging and hogging bending in the direction normal to the span of the beam;*

(5) *The factor C_4 allows for the influence of the bending moment distribution along the span considered, and is given in Fig. B.2. [To be added]. [Drafting note: C_4 replaces k/v in paper R38].*

B.1.2 Slenderness ratio

(1) *For uncased beams that satisfy the conditions of B.1.1(1), the slenderness ratio $\overline{\lambda}_{LT}$ for a Class 1 or Class 2 cross-section may conservatively be taken as*

$$\overline{\lambda}_{LT} = \left[1 + \frac{t_w h}{4bt_f} \right] \left[2 v \left(-\frac{f_y}{k_s C_4} \right)^{\frac{1}{2}} \left(\frac{h_f}{t_w} \right)^{\frac{1}{2}} \left(\frac{t_f}{b} \right)^{\frac{3}{2}} \right]^{\frac{1}{4}}$$

where f_y is the yield strength of the structural steel, and the other symbols are defined in B.1.1 or Fig. B.1.

(2) *For a cross-section in Class 3 or Class 4, the value given in (1) should be multiplied by $(M_c/M_{pl})^{\frac{1}{4}}$, in accordance with 4.6.3(3).*
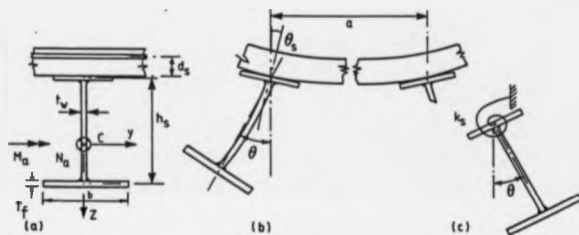
Fig. B.1 Notation, and buckling mode for design to draft Eurocode 4

THE BRITISH LIBRARY DOCUMENT SUPPLY CENTRE

TITLE   BUCKLING IN CONTINUOUS COMPOSITE BEAMS

AUTHOR   Chun Keung Roger Fan

INSTITUTION
and DATE

University of Warwick 1990